TLE PAGE

1. Report No.	2. Government Accession No.	
FHWA/TX-86/06+353-3F		

4. Title and Subtitle	5. Report Date
AN EXAMINATION OF EARTH SLOPE FAILURES IN TEXAS	November 1984
	6. Performing Organization Code
7. Author(s)	8. Performing Organization Report No.
Peter A. Stauffer and Stephen G. Wright	Research Report 353-3F
9. Performing Organization Name and Address	10. Work Unit No.
Center for Transportation Research The University of Texas at Austin Austin, Texas 78712-1075	11. Contract or Grant No. Research Study 3-8-83-353
	13. Type of Report and Period Covered
12. Sponsoring Agency Name and Address Texas State Department of Highways and Public Transportation; Transportation Planning Division P. O. Box 5051 Austin, Texas 78763	Final
	14. Sponsoring Agency Code

15. Supplementary Notes

Study conducted in cooperation with the U. S. Department of Transportation, Federal Highway Administration
Research Study Title: "Stability Evaluation for Earth Slopes"

16. Abstract

Slope stability problems encountered by the Texas State Department of Highways and Public Transportation have been identified and examined. Problems have been encountered with cut and natural slopes, embankment foundations, and the embankment slopes themselves. The most frequent problems encountered occur with the embankment side slopes themselves and occur in embankments constructed of soils having liquid limits generally exceeding 50. Slope failures typically occur in such embankments a number of years after construction and involve relatively shallow slides. Effective stress ("drained") shear strength parameters were back-calculated from the observed slides and compared with corresponding laboratory values. The laboratory strengths were significantly higher than the back-calculated values and suggest that conventional laboratory tests and procedures may be inappropriate for use in design.

17. Key Words	18. Distribution Statement
slope stability, problems, cut slopes, natural slopes, embankment foundations, embankments	No restrictions. This document is available to the public through the National Technical Information Service, Springfield, Virginia 22161.

19. Security Classif. (of this report)	20. Security Classif. (of this page)	21. No. of Pages	22. Price
Unclassified	Unclassified		

Form DOT F 1700.7 (8-69)

AN EXAMINATION OF EARTH SLOPE FAILURES IN TEXAS

by

Peter A. Stauffer
Stephen G. Wright

Research Report 353-3F

Stability Evaluation for Earth Slopes
Research Project 3-8-83-353

conducted for

Texas State Department of Highways and
Public Transportation

in cooperation with the
U.S. Department of Transportation
Federal Highway Administration

by the

CENTER FOR TRANSPORTATION RESEARCH
BUREAU OF ENGINEERING RESEARCH
THE UNIVERSITY OF TEXAS AT AUSTIN

November 1984

The contents of this report, excepting the comments on page xi, reflect the views of the authors, who are responsible for the facts and the accuracy of the data presented herein. The contents, excepting the comments on page xi, do not necessarily reflect the official views or policies of the Federal Highway Administration. This report does not constitute a standard, specification, or regulation.

The comments on page xi reflect the views of the Federal Highway Administration, but not necessarily those of the authors or of the Center for Transportation Research.

There was no invention or discovery conceived or first actually reduced to practice in the course of or under this contract, including any art, method, process, machine, manufacture, design or composition of matter, or any new and useful improvement thereof, or any variety of plant which is or may be patentable under the patent laws of the United States of America or any foreign country.

PREFACE

Research Project 353 was undertaken with the primary objective being the development of an improved computer program for performing slope stability computations, including the necessary user documentation for the program. This was accomplished with the development of the computer program UTEXAS and the reports by Wright and Roecker (1984a, 1984b). In conjunction with the development of the computer program an effort was made to identify important slope stability problems encountered by the Texas State Department of Highways and Public Transportation to ensure that their needs would be met by the computer program and related user documentation. An earlier study by Abrams and Wright (1972) had identified a number of important slope problems in the State and, thus, the efforts of Project 353 were intended primarily to update the earlier work. However, as this study progressed it became evident that a much more severe problem existed with the stability of embankments than had been anticipated or recognized earlier. Accordingly, a significant effort was made to identify better and understand the embankment slope stability problems. The results of the examination of the slope problems in Texas and the efforts at understanding the embankment slope stability problem are presented in this report.

ABSTRACT

Slope stability problems encountered by the Texas State Department of Highways and Public Transportatin have been identified and examined. Problems have been encountered with cut and natural slopes, embankment foundations, and the embankment slopes themselves. The most frequent problems encountered occur with the embankment side slopes themselves and occur in embankments constructed of soils having liquid limits generally exceeding 50. Slope failures typically occur in such embankments a number of years after construction and involve relatively shallow slides. Effective stress ("drained") shear strength parameters were back-calculated from the observed slides and compared with corresponding laboratory values. The laboratory strengths were significantly higher than the back-calculated values and suggest that conventional laboratory tests and procedures may be inappropriate for use in design.

SUMMARY

A number of slope stability problems encountered by the Texas State Department of Highways and Public Transportation have been identified and examined. The problems include slope failures in cut and natural slopes, embankment foundations, and embankment slopes themselves. Failures in cut and natural slopes were not examined in detail but still continue to be a problem. Embankment foundation failures do not occur frequently, but when they do occur they are often costly. Simplified procedures, based on classical bearing capacity equations, have been examined to compute the factor of safety for embankment foundations. The results from calculations performed using the simplified procedures have been compared with results obtained by using more conventional slope stability approaches in this report.

Embankment failures in which sliding occurs entirely within the embankment slope represent the most significant type of slope stability problem examined in this study. Most of the embankment slope failures observed occurred in embankments which were constructed of soils with liquid limits generally in excess of 50 and plasticity indices generally in excess of 30. The failures were observed to have occurred a number of years after construction, and the sliding surfaces appeared to be relatively shallow. Stability calculations were performed to back-calculate "long-term," effective stress shear strength parameters from the slope

and slide geometry, and a series of relatively simple charts were developed to facilitate the computations. The shear strengths which were back-calculated were significantly less than those measured in conventional consolidated-drained laboratory tests. Factors of safety calculated using laboratory strength values were greater than 2.0 for slopes which actually failed.

IMPLEMENTATION STATEMENT

The results of this study show that in several Districts of the Texas SDHPT (1, 12, 13 and 14) embankments constructed of clays having liquid limits in excess of 50 and with side slopes of 3(horizontal)-to-1(vertical) or steeper are likely to experience sliding a number of years after construction. Accordingly, it appears that, in these Districts, either materials with liquid limits in excess of 50 should be excluded from use in constructin of slopes 3:1 or steeper or, if such materials are used, slopes should be flatter than 3:1.

A series of charts have been developed which can be used to back-calculate shear strength parameters from slopes which have failed. These charts can be used to develop useful information for use in future slope designs and repair. Classical bearing capacity equations have also been examined for use in computing factors of safety for embankments founded on relatively weak foundations. The classical bearing capacity equations were shown to produce what are believed to be conservative estimates for the factor of safety and are relatively simple to use. Accordingly, the bearing capacity equations, when used with the procedures outlines in Chapter Six, may be very useful for at least preliminary design of embankments.

REVIEW COMMENTS FROM FHWA

The following comments address the IMPLEMENTATION STATEMENT on page vii:

1. In some cases, side slopes of 4 (horizontal) to 1 (vertical) or flatter have also experienced sliding problems.

2. We believe the comment that "if materials with liquid limits in excess of 50 are used, slopes should be flatter than 3:1" is too restrictive and that the designer should be provided with other options. We recommend that the following design options be considered by the designer for those projects where soils likely to experience sliding problems are proposed as embankment fill material:

   (a) flatten slope
   (b) replace part of the problem soil with granular material
   (c) treat the problem soil with lime
   (d) design a "reinforced soil" slope (different reinforcement materials are currently available)

   The most "cost-effective" alternative (least cost with adequate predicted performance) should then be selected. We recommend that options (c) and (d) be designated as experimental project features so that their design, construction and performance can be documented and reported. This approach would allow the State to continue to "engineer" each project.

3. The charts developed for back-calculating shear strength parameters from slopes which have failed should <u>not</u> be used for future (new) slope designs.

4. We agree that the bearing capacity equations provide conservative estimates for the factor of safety, and are useful for preliminary design of embankments; but we strongly recommend that they never be used for final design when subsurface conditions are such that stability problems could develop.

TABLE OF CONTENTS

LIST OF TABLES

LIST OF PLATES

LIST OF FIGURES

NOMENCLATURE

A	Soil activity
B	Width of loaded area
B'	Reduced effective width
c	Cohesion
c_m	Mobilized cohesion
$\bar{c}$	Effective stress cohesion
d	Maximum depth of slide measured normal to slope face
d_c	Depth of vertical "tension" crack
D	Diameter of stone column
e	Eccentricity of resultant load
F	Factor of safety
F_L	Factor of safety with respect to load
F_S	Factor of safety with respect to shear strength
h	Height of slide
H	Height of slope
l	Length of slide measured transversely along the slope face
L	Length of slope measured transversely along the slope face
$L.I.$	Liquidity index
N	Standard penetration or cone penetration blow count
N_c	Bearing capacity factor
N_{cm}	Bearing capacity factor calculated using mobilized shear strengths
N_{cf}	Dimensionless slope stability number
N_q	Bearing capacity factor

N_γ	Bearing capacity factor
$N_{\gamma m}$	Bearing capacity factor calculated using mobilized shear strengths
q	Bearing capacity
q_a	Average applied bearing pressure
q_{ult}	Ultimate bearing capacity
q_{ult}'	Factored ultimate bearing capacity
Q	Resultant bearing load
Q_a	Applied bearing load
r_u	Pore water pressure parameter
s_u	Undrained shear strength
S	Center-to-center spacing between stone columns
w	Equivalent width of stone column
w_n	Natural water content
w_{LL}	Liquid limit
w_{PL}	Plastic limit
X_c	Horizontal distance from toe of slope to center of critical circle
Y_c	Vertical distance from toe of slope to center of critical circle
z	Height of fill above original ground surface
β	Inclination of slope
γ	Total unit weight of soil
θ	Slope angle of original ground surface beneath fill
$\lambda_{c\phi}$	Dimensionless slope parameter
σ	Normal stress
τ	Shear stress
ϕ	Angle of internal friction

ϕ_m Mobilized angle of internal friction

$\bar{\phi}$ Effective stress angle of internal friction

CHAPTER ONE. INTRODUCTION

Slope stability problems have been encountered in conjunction with the design, construction and maintenance of Texas highways for many years. A number of these problems were identified approximately ten years ago in a study by Abrams and Wright (1972) for the Texas State Department of Highways and Public Transportation. Abrams and Wright found that many of the slope failures which had been experienced occurred in excavated slopes in heavily overconsolidated clays and shales. In 1982 a new study was initiated to determine if the nature of slope problems encountered by the Department had changed significantly and to define typical problems which the Department currently encounters. The results of the new study are presented in this report.

As part of this study a number of sites in Texas where slope failures occurred have been visited, and numerous soil samples have been taken to identify the type of materials which caused problems. Field measurements have been made of the slope and slide geometry for slopes which have failed. Laboratory tests have been performed on the soil samples to identify the index properties and water contents in slide areas.

Stability calculations have been performed for a number of the slopes which have failed. The calculations were performed either to back-calculate the shear strength of the soil at the time of the slide or to compute the factor of safety using shear strength properties determined from back-calculation or from laboratory tests. Most of the sta-

bility calculations were performed using the computer program UTEXAS, which was developed as part of this study and is described by Wright and Roecker (1984a, 1984b). In several cases it became evident that simpler means than using the computer could be employed for the calculations. Where shear strength parameters were being back-calculated for actual embankment slope failures, it was possible to develop a number of charts which can be used for the computations and greatly reduce the effort required.

In Chapter Two the information collected from the field inspection of slopes is presented. Data were collected for a number of embankment slope failures and the shear strengths were back-caluclated for comparison with other shear strength data, as well as with index properties. The procedures used to back-calculate the shear strength, including the charts which were developed, are described in Chapter Three. A relatively large number of the slope failures examined occurred in embankment side slopes and were independent of the foundation. The soil properties, including the shear strength properties which were back-calculated for these embankments, are presented and examined in Chapter Four. Two of the embankments which failed were selected for more detailed study and analysis, including laboratory tests to measure the shear strength parameters. The more detailed study of these two embankments is presented in Chapter Five. In Chapter Six simplified procedures for calculating the stability of embankments on weak foundations are examined, and in Chapter Seven analyses are presented for an actual

embankment foundation failure. A summary and conclusions are presented in Chapter Eight, the final chapter.

CHAPTER TWO. INVESTIGATION OF EARTH SLOPE FAILURES

INTRODUCTION

One of the principal objectives of this study was to identify the significant types of slope stability problems which the Texas State Department of Highways and Public Transportation is presently experiencing. Consequently, a number of slope failures were examined by field inspection of the sites during which various types of information were collected, including field measurements of the slope and slide geometry, and retrieval of soil samples for laboratory testing. Three types of slope failures were examined in this study: 1) cut and natural slope failures, 2) embankment foundation failures, and 3) embankment slope failures. The three types of failures are described in this chapter. Observations made during field inspections, procedures used to make field measurements and to collect soil samples, and a summary of the field measurements obtained for embankment slope failures are also presented.

CUT AND NATURAL SLOPE FAILURES

Only two cut slope failures were observed during this study, although more probably exist. The first occurred on a slope at the SH 225 and SH 146 Interchange near Houston, in District 12. The soil in the cut slope was probably similar to material which was used to construct two embankments at this interchange. Numerous failures have occurred on these embankments slopes; three of these failures are considered later in this chapter in the section titled "Embankment Slope Failures." The cut slope failure differed from the embankment slope failures in that the failure surface in the cut slope intersected the top of the slope, and the failure surface was noticably deeper. A sheet pile wall was used to repair this slide. The second cut slope failure examined occurred near the intersection of U.S. 21 with the Middle Yegua Creek in District 14. The slope was cut at about 2(horizontal)-to-1(vertical) and was about 23 feet high. The failure surface at this site was obscurred by heavy weed growth and was barely discernable.

Only one failure in a natural slope was observed. This failure was located on SH 105 at the Brazos River crossing southwest of Navasota in District 17. One of the bridge piers on the southwest side of the river crossing is located in a slide mass which has recently been moving downslope, toward the river. The movement appears to be related to erosion of material along the toe of the slope by the river and to a relatively shallow water table near the ground surface in and above the slide

area. The slope has been modified by excavation of material at the head of the slide and is continuing to be monitored at this time (1984).

EMBANKMENT FOUNDATION FAILURES

One embankment foundation failure was examined in this study. This failure occurred during the construction of a new approach embankment on the west side of SH 358 at the Oso Bay crossing near Corpus Christi in District 16. Failure was due to the presence of a weak underlying foundation material through which the failure surface passed. The slope was stabilized using "stone columns" which extended through the weak foundation material to firmer material. This slope failure is considered in greater detail in Chapter Seven.

EMBANKMENT SLOPE FAILURES

During the course of this research project a total of twenty-eight slides in embankment slopes were examined. These embankments were located in Districts 12 (Houston), 14 (Austin), 13 (Yoakum), and 1 (Paris), as shown in Fig. 2.1. Project personnel were informed of these slides by Texas SDHPT personnel and it was possible to conduct field trips to examine many sites. During the field inspections, measurements of slope geometry and slide dimensions were made and soil samples were taken. The measurements taken, the quantities which were

Fig. 2.1. Texas State map showing Districts where embankment slope failures were examined.

subsequently calculated, and the soil sampling procedures are described in this section. A brief description of remedial measures observed in connection with embankment slope failures is also presented.

Measurement of Slope Geometry and Slide Dimensions

For each embankment slide inspected an attempt was made to obtain information on the geometry of the slope and slide surface. The specific items which were measured were the slope angle, the length of the slope (from the toe of the slope to the top of the slope), and the length of the slide (from the head of the slide scarp to the estimated location of the lower intersection of the sliding surface with the original slope surface). The depth of the slide normal to the slope was estimated. Quantities which were calculated from these values included the height of the embankment, the height of the slide, and a "slide depth ratio." A description of each of these quantities is given below.

A typical cross-section of an embankment where failure has occurred is shown in Fig. 2.2. This cross-section represents an actual embankment slope failure which occurred at the northeast quadrant of the intersection of IH 610 and Scott Street in Houston. The cross-section as viewed in the field is shown in Fig. 2.2a, which shows how the slope and slide appeared at the time of the field inspection. The position of the failure surface was estimated from an examination of the slope and the slide mass geometry. The idealized cross-section is shown in Fig. 2.2b, which illustrates what was estimated to be the original embankment slope

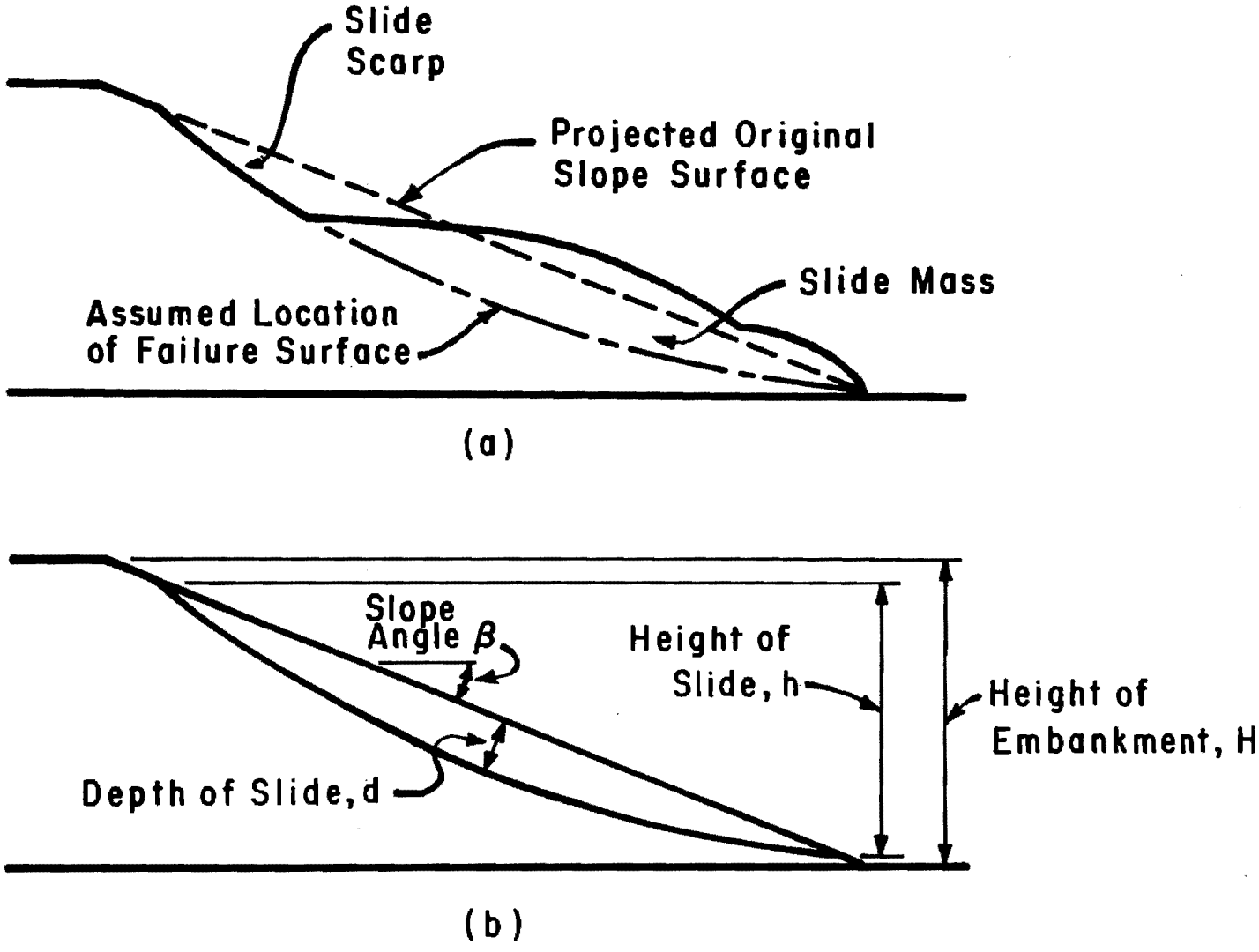

Fig. 2.2. Cross-sections of embankment slope failure at IH 610 and Scott Street, District 12: (a) cross-section as viewed in field; (b) idealized cross-section and parameters used to define slope and slide geometry.

with the assumed failure surface drawn in. Variables used to define the slope and slide geometry are labelled on the cross-section in Fig. 2.2b.

Measurements Made During the Field Inspection: During the field inspections measurements were taken of the slope angle, the length of the slope, and the length of the slide, and the depth of the slide was estimated. Details of the measurements and estimate are described below.

Slope Angle: The slope angle, β, was measured using a device called a "pantometer," which is illustrated in Fig. 2.3. The pantometer consists of a parallelogram shaped framework constructed of four wood segments connected at four hinge points spaced at 4 feet parallel to the surface of the slope and 3.5 feet vertically. A clear Plexiglas plate is fixed to one of the vertical wood segments near the upper hinge point, and the plate is etched so that the slope angle may be read off in degrees. A level bubble is fixed to the clear Plexiglas plate and oriented such that, when the bubble is level, the vertical wood segments of the pantometer are exactly vertical in the plane of the level vial. The clear Plexiglas plate is positioned such that angles may be measured by a wire sight built into the adjacent wood segment. In order to measure the angle of a slope, the pantometer is set on the slope as shown in Fig. 2.3, and the level bubble is used to position the vertical segments upright. The slope angle, measured from horizontal, is then read off the clear Plexiglas gauge. The slope angle, β, is illustrated in Fig. 2.2 for a typical embankment slope.

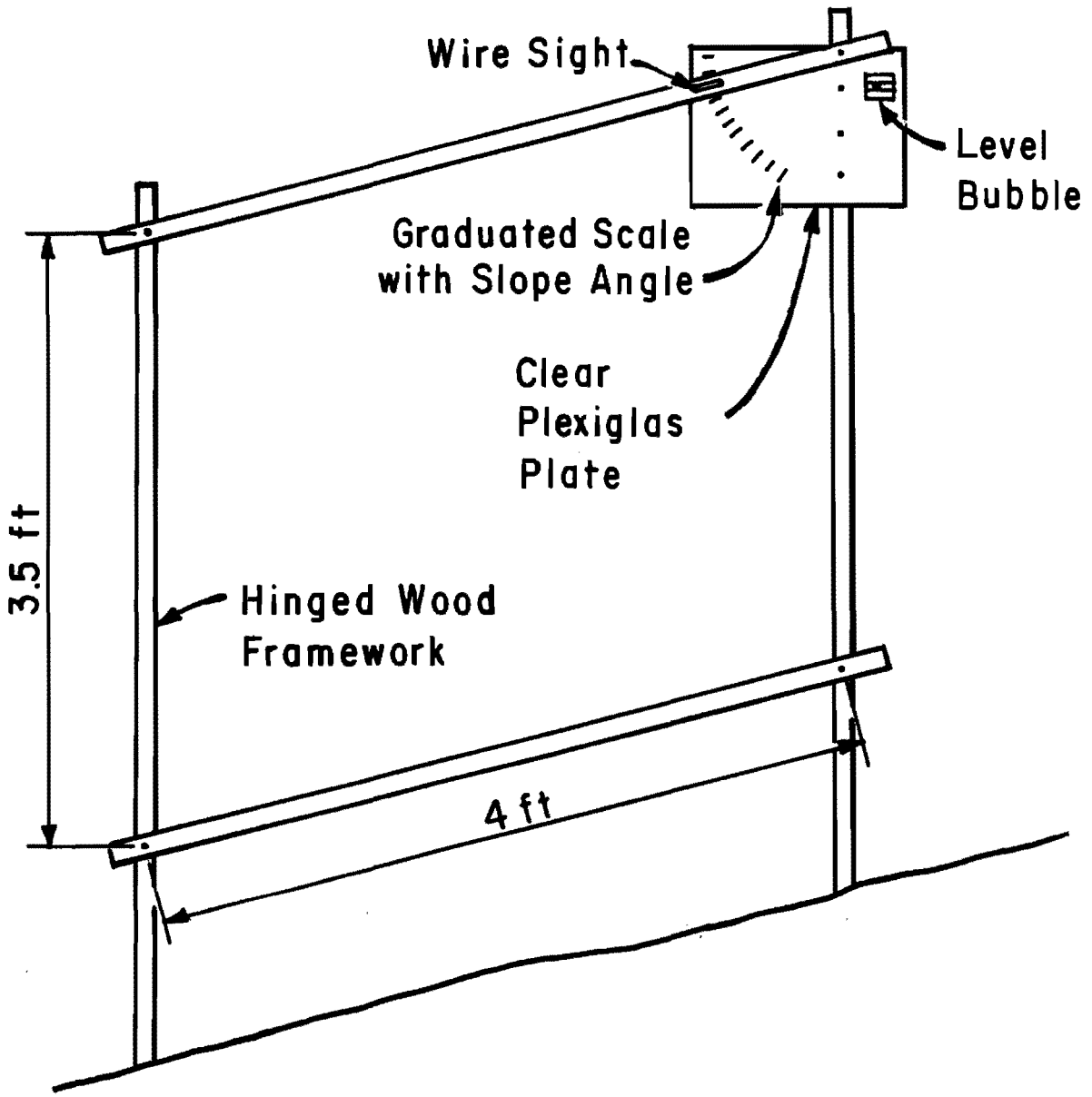

Fig. 2.3. Pantometer used to measure slope angles.

The pantometer was not used to measure the slope angles for those slides examined in District 1; instead, an alternate approach was used. A person would stand on the slope, facing upslope, and use a hand level to locate the point on the slope at the same elevation as the hand level, directly upslope from the point where the individual was standing. The distance along the face of the slope between the point sited to with the level and the point where the individual was standing was measured using a steel tape. This distance, "a," corresponds to the hypotenuse of a right triangle formed by the surface of the slope, the horizontal line of sight through the hand level, and the vertical line formed by the individual standing on the slope. The height of the individual (from the ground surface to the elevation of the hand level), "b," was measured. The slope angle, β, was then calculated as

$$\beta = \arcsin\left(\frac{b}{a}\right) \tag{2.1}$$

Slope angle measurements were usually taken at several locations surrounding the slide for each slope examined. In most instances it was possible to obtain measurements at different elevations on both sides of the slide. Often there were only small variations among these measurements. For such cases, the average of these measurements was used to represent the slope angle prior to failure. The cotangent of the slope angle, $\cot\beta$, was computed from the slope angle, β. The cotangent of the slope angle corresponds to the ratio of horizontal-run-to-vertical-rise

and was chosen to represent the slope inclination in the tabulated results and subsequent presentations.

Five of the twenty-eight embankment failures examined occurred near the abutment (end) section of the embankment. In such cases the slope angle generally varied from one side of the slide to the other around the corner of the embankment. The embankment slope typically varied from about 3:1 on the side slope to about 2:1 beneath the bridge deck. Thus, the geometry of slides occurring near the abutment was distinctly different from that of those occurring on the side slopes. Those which are reported in the subsequent data presentation are identified as "failure at abutment." The slope angle used for the slides in the abutment area is an average angle based on the measurements taken from both sides of the slide.

In addition to the variations in slope angle from one side of the slide to the other, there were sometimes variations observed in measurements taken from the base to the top of the slope. These variations may be due in part to the swelling of embankment materials near the surface of the slope, occurring with time after construction. In most instances the variation in slope angle from bottom to top was not more than one or two degrees. The procedure used for defining slope inclination where the slope angle varied from the bottom to the top of the slope was to average the slope angle measurements taken on the slope outside the slide mass at elevations near the center of the original position of the slide mass.

Length of the Slope: The distance measured along the slope face from the toe of the slope to the top of the slope at the center of the slide is

referred to as the "length of the slope" and is designated by the symbol L. This distance (L) was measured typically with a 50-foot metal tape.

Length of the Slide: The distance measured along the slope face from the head of the slide scarp to a point corresponding to the estimated lower intersection of the failure surface with the original slope surface at the center of the slide is referred to as the "length of the slide" and is designated by the symbol l. The length of the slide (l) was measured at the center of the slide, typically with a 50-foot metal tape.

Depth of the Slide: The depth of the slide, d, was not measured directly, but was estimated. Additional field measurements of the position of the slide scarp and the depth of the slide scarp, relative to the original surface of the slope, were made during the field inspection of the first four embankment slides. Using the slope and slide geometry data, including these additional measurements, a cross-section was constructed and the scarp was accurately plotted on this cross-section. The location of the failure surface was estimated and was drawn on the cross-section. The depth of the slide was then scaled off. This effort proved to be time consuming. It did, however, confirm field estimates of the depth of the slide such that what was judged to be a reasonably accurate estimate could be made by careful observation. Thus, for the majority of the slides inspected, the depth of the slide, d, was estimated directly from field observations. The depth of the slide (d) is illustrated in Fig. 2.2.

Quantities Calculated from Field Measurements: Three quantities were calculated from the field measurements for each embankment slide examined. These quantities were the embankment height, the height of the slide, and the slide depth ratio. A description of each is given below.

Embankment Height: The embankment height, H, was calculated from the field measurement of the length of the slope, L, and the slope angle, β. The embankment height was computed from the equation

$$H = L \cdot \sin\beta \tag{2.2}$$

The embankment height (H) is illustrated in Fig. 2.2.

Height of Slide: The height of the slide, h, was calculated from field measurements of the length of the slide, l, and the slope angle, β. The height of the slide was computed from the equation

$$h = l \cdot \sin\beta \tag{2.3}$$

The height of the slide (h) is also illustrated in Fig. 2.2.

Slide Depth Ratio: "Slide depth ratio" was defined as the ratio of the depth of the slide, d, to the height of the slide, h. The slide depth

ratio was computed from the equation

$$\text{slide depth ratio} = \frac{d}{h} \tag{2.4}$$

Slope Geometry and Slide Dimension Data

Slope geometry and slide dimension data for the twenty-eight embankment slope failures examined in this study are summarized in Table 2.1. In addition to the data for the twenty-eight embankment slope failures, data for one embankment slope which was stable are also presented in Table 2.1. This slope is located northwest of the intersection of U.S. Highway 79 and Carlos G. Parker Boulevard near Taylor in District 14. The embankment slopes summarized in Table 2.1 are listed in approximate chronological order of inspection with those inspected earliest listed first.

Referring to the data presented in Table 2.1, it can be seen that the embankment heights, H, for embankments which failed ranged from approximately 10 to 39 feet. The range in the height of the slides, h, is identical (10 to 39 feet) although for specific cases the height of the embankment and the height of the slide were generally not the same. The mean height of embankments which failed is 21.5 feet while the mean value for the height of the slides is 19.0 feet. The slope ratios for embankments which failed, as summarized in Table 2.1, range from 2.1:1 to 3.4:1, with a mean value of 2.7:1. The estimated depth of the slides

TABLE 2.1. SUMMARY OF GEOMETRY DATA FOR EMBANKMENT SLIDES

Slope Location	District	Emb. Height, H (ft)	Slope Ratio, cot β	Height of Slide, h (ft)	Depth of Slide, d (ft)	Depth Ratio, d/h	Comments
IH 610 @ Scott St., NE quadrant, Harris Co.	12	19.0	2.6	17.0	3.5	0.21	Large bag samples taken
SH 225 @ SH 146, SW quadrant, Harris Co.	12	15.0	3.0	13.0	4.3	0.33	Large bag samples taken. Had been repaired when visited 11/26/83
SH 225 @ SH 146, NW quadrant, Harris Co.	12	17.6	3.1	14.0	2.4	0.17	Large bag samples taken. Had been repaired when visited 11/26/83
SH 225 @ SH 146, NE quadrant, Harris Co.	12	13.5	3.4	13.5	3.5	0.26	Had been repaired when visited 11/26/83
SH 225 @ Southern Pacific RR Overpass, SE quadrant, Harris Co.	12	26.5 19.2	2.6 3.1	21.0 12.0	4.0 3.0	0.19 0.25	West slide East slide

(continued)

TABLE 2.1. (Continued)

Slope Location	District	Emb. Height, H (ft)	Slope Ratio, cot β	Height of Slide, h (ft)	Depth of Slide, d (ft)	Depth Ratio, d/h	Comments
SH 225 @ Southern Pacific RR Overpass, SW quadrant, Harris Co.	12	23.5	2.4	23.5	5.0	0.21	
SH 225 @ Southern Pacific RR Overpass, NW quadrant, Harris Co.	12	10.2	3.1	10.2	2.5	0.25	
SH 225 @ Scarborough, SE quadrant, Harris Co.	12	19.0	2.1	19.0	3.0	0.26	Failure at abutment
IH 610 @ SH 225, SE quadrant, Harris Co.	12	17.4	2.7	12.0	2.0	0.17	
IH 610 @ Richmond St., SW quadrant, Harris Co.	12	25.7	2.7	22.0	5.0	0.23	
IH 10 @ Crosby-Lynchburg, NW quadrant, Harris Co.	12	25.1	2.6	19.0	5.0	0.26	

(continued)

TABLE 2.1. (Continued)

Slope Location	District	Emb. Height, H (ft)	Slope Ratio, cot β	Height of Slide, h (ft)	Depth of Slide, d (ft)	Depth Ratio, d/h	Comments
IH 45 @ SH 146, SE quadrant, Harris Co.	12	>15.5	3.0	15.0	3.0	0.20	
IH 45 @ SH 146, south side, Harris Co.	12	14.8	3.1	13.0	3.5	0.27	
IH 45 @ FM 2351, NE quadrant, Harris Co.	12	17.2	2.5	15.0	2.5	0.17	
IH 45 @ College St., NE quadrant, Harris Co.	12	11.4	3.0	11.4	2.0	0.18	Slope was first repaired in 1977
U.S. 59 @ FM 525, NE quadrant, Harris Co.	12	16.4	2.4	16.4	3.0	0.18	
U.S. 59 @ Shepard St., SE quadrant, Harris Co.	12	13.3	3.1	13.3	3.5	0.26	

(continued)

TABLE 2.1. (Continued)

Slope Location	District	Emb. Height, H (ft)	Slope Ratio, cot β	Height of Slide, h (ft)	Depth of Slide, d (ft)	Depth Ratio, d/h	Comments
U.S. 79 @ Carlos G. Parker Blvd., NW quadrant, Williamson Co.	14	30.0	2.2	--	--	--	Slope was stable 10/18/83
U.S. 79 @ U.S. 95, SE quadrant, Williamson Co.	14	39.0	2.3	39.0	6.0	0.15	Failure at abutment. Slope had been repaired (lime treatment) when visited 10/18/83
U.S. 77 @ SH 21, SW quadrant, Lee Co.	14	26.0	3.4	20.0	4.0	0.20	Slope was being repaired (lime treatment) when visited 12/13/83
U.S. 77 @ SH 21, NW quadrant, Lee Co.	14	26.0	2.9	16.0	3.0	0.19	Slope was being repaired (lime treatment) when visited 12/13/83
U.S. 290 ~ 5 miles east of IH 35, NW quadrant, Travis Co.	14	38.0	2.5	38.0	6.0	0.16	Failure at abutment

(continued)

TABLE 2.1. (Continued)

Slope Location	District	Emb. Height, H (ft)	Slope Ratio, cot β	Height of Slide, h (ft)	Depth of Slide, d (ft)	Depth Ratio, d/h	Comments
U.S. 87 @ Loop 175, NW quadrant, Victoria Co.	13	30.7	2.2	30.7	5.0	0.16	Failure at abutment
Loop 286 @ SH 271 Interchange, NW quadrant, Lamar Co.	1	14.1	2.5	14.1	4.0	0.29	
Loop 286 @ Missouri Pacific RR Overpass, SW quadrant, Lamar Co.	1	27.0	2.9	15.0	8.0	0.53	Slide occurred in lower portion of embankment slope, north slide
		29.6	2.8	26.2	6.0	0.23	South slide
Loop 286 @ Missouri Pacific RR Overpass, NW quadrant, Lamar Co.	1	27.4	2.7	27.4	10.0	0.36	Width of slide along embankment was about 500 ft
Loop 286 @ FM 79, SW quadrant, Lamar Co.	1	23.9	2.3	23.9	4.0	0.17	Failure at abutment

ranges from 2.0 feet to 10.0 feet, with a mean value of 4.2 feet; the corresponding slide depth ratios range from 0.15 to 0.55 with a mean value of 0.23.

The one stable slope included in Table 2.1, U.S. Highway 79 and Carlos G. Parker Boulevard, is an embankment with a height of 30 feet and a slope ratio of 2.2:1. This slope is therefore one of the highest and steepest of those examined and was included in the table because it represents either an anomoly or a candidate for future sliding. Further consideration of this slope is given in Chapter Four.

Those slides which occurred near the abutment, on the curved portion of the embankment, are noted as "failure at abutment" in the comments column. Some of the embankment slides had been repaired following the initial inspection. Embankment slides which had been repaired or which were being repaired during subsequent inspections are also noted in the comments column.

Age of Slope at Failure

The date each embankment was constructed, the date failure occurred, and the resulting age at failure for each of the embankment slides are summarized in Table 2.2. The dates of construction of the embankments shown in Table 2.2 were obtained from Texas SDHPT personnel in each of the respective District offices. Two of the failures on the southern slopes of the embankments at SH 225 and the Southern Pacific Railroad Overpass in District 12, according to Texas SDHPT personnel,

TABLE 2.2. SUMMARY OF TIME TO FAILURE DATA FOR EMBANKMENT SLIDES

Slope Location	District	Date of Construction	Date Failure Observed	Age at Failure (years)
IH 610 @ Scott St., NE quadrant, Harris Co.	12	1966	1983	17
SH 225 @ SH 146, SW quadrant, Harris Co.	12	1952	1983	31
SH 225 @ SH 146, NW quadrant, Harris Co.	12	1952	1983	31
SH 225 @ SH 146, NE quadrant, Harris Co.	12	1952	1983	31
SH 225 @ Southern Pacific RR Overpass, SE, SW, and NW quadrants, Harris Co.	12	1963	1983	20
SH 225 @ Scarborough, SE quadrant, Harris Co.	12	1966	1983	17
IH 610 @ SH 225, SE quadrant, Harris Co.	12	1964	1983	19
IH 610 @ Richmond St., SW quadrant, Harris Co.	12	1965	1983	18
IH 10 @ Crosby-Lynchburg, NW quadrant, Harris Co.	12	1958	1983	25

(continued)

TABLE 2.2. (Continued)

Slope Location	District	Date of Construction	Date Failure Observed	Age at Failure (years)
IH 45 @ SH 146, both SE quadrant and south side, Harris Co.	12	1969	1983	14
IH 45 @ FM 2351, NE quadrant, Harris Co.	12	1971	1983	12
IH 45 @ College St., NE quadrant, Harris Co.	12	1959	1977	18
U.S. 59 @ FM 525, NE quadrant, Harris Co.	12	1959	1983	24
U.S. 59 @ Shepard St., SE quadrant, Harris Co.	12	1961	1983	22
U.S. 79 @ U.S. 95, SE quadrant, Harris Co.	14	1972	1983	11
U.S. 77 @ SH 21, SW and NW quadrants, Lee Co.	14	1964	1983	19
U.S. 290 ~ 5 miles east of IH 35, NW quadrant, Travis Co.	14	1967	1983	16
U.S. 87 @ Loop 175, NW quadrant, Victoria Co.	13	1964	1983	19

(continued)

TABLE 2.2. (Continued)

Slope Location	District	Date of Construction	Date Failure Observed	Age at Failure (years)
Loop 286 @ SH 271 Interchange, NW quadrant, Lamar Co.	1	1969	1983	14
Loop 286 @ Missouri Pacific RR Overpass, SW and NW quadrants, Lamar Co.	1	1965	1983	18
Loop 286 @ FM 79, SW quadrant, Lamar Co.	1	1964	1983	19

had occurred as a result of, and therefore probably shortly after, the passing of Hurricane Alica on August 18, 1983. However, for the majority of the embankment slides examined the date failure occurred was not known except that it was sometime prior to inspection in 1983, probably within one or two years. For the purposes of this study, the date failure occurred for these slides is assumed to be 1983. The age at failure values shown in Table 2.2 ranges from 11 to 31 years, with a mean value of 19.4 years.

Annual Precipitation Data for Houston

The annual precipitation in Houston for the years 1940 to 1982 is shown on a bar graph in Fig. 2.4. The annual precipitation appears to be generally increasing from about the year 1954 to 1982; however, there do not appear to be any years from 1974 to 1982 where the precipitation was exceptionally high, nor is there a sustained high annual precipitation over these recent years. Thus, annual precipitation records for Houston do not appear to correlate with the recent occurrence of numerous embankment slides in the Houston area.

Analysis of Embankment Slope Failure Data

In this section the data summarized in Tables 2.1 and 2.2 are

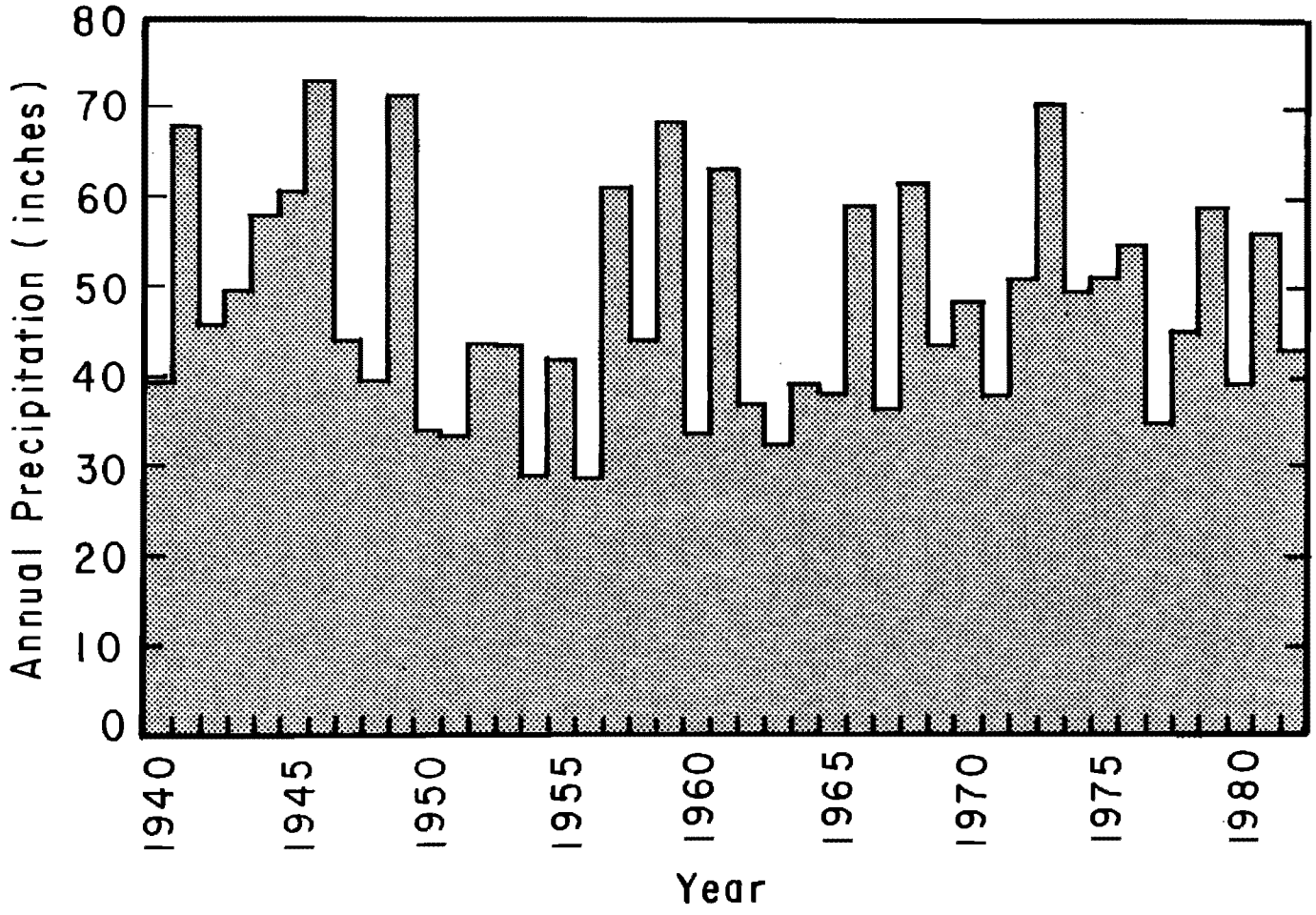

Fig. 2.4. Annual precipitation in Houston for the years 1940 to 1982 (from Gale Research Company, 1981 and National Oceanic and Atmospheric Administration, 1979 to 1982).

examined to determine if any relationships exist between various quantities presented in these tables. The embankment height, slope ratio, and age at failure for each embankment slide are plotted versus one another in order that relationships within these data may be more easily recognized.

The embankment height is plotted versus the slope ratio ($\cot\beta$) for each embankment slide in Fig. 2.5. Examining the data shown in Fig. 2.5, it appears that slides on steeper slopes (corresponding to lower values of the slope ratio) generally occur on higher embankments. This may be an indication that higher embankments are typically constructed with steeper slopes, perhaps due to right-of-way considerations which would be more restrictive for higher embankments, or perhaps due to higher costs which would result from the additional fill required when high embankments are constructed with flatter slopes.

The age at failure is plotted versus the embankment height in Fig. 2.6. Examining the data shown in Fig. 2.6, there does not appear to be any relationship between the age at failure and the embankment height, i.e., embankment slope failures do not tend to occur on higher embankments before or after they occur on lower embankments.

The age at failure is plotted versus the slope ratio ($\cot\beta$) in Fig. 2.7. The straight line shown on Fig. 2.7 represents the best fit line, which was calculated by the method of least squares. Examining the data shown in Fig. 2.7, it appears that embankment slope failures generally tend to occur on steeper slopes before they occur on flatter slopes.

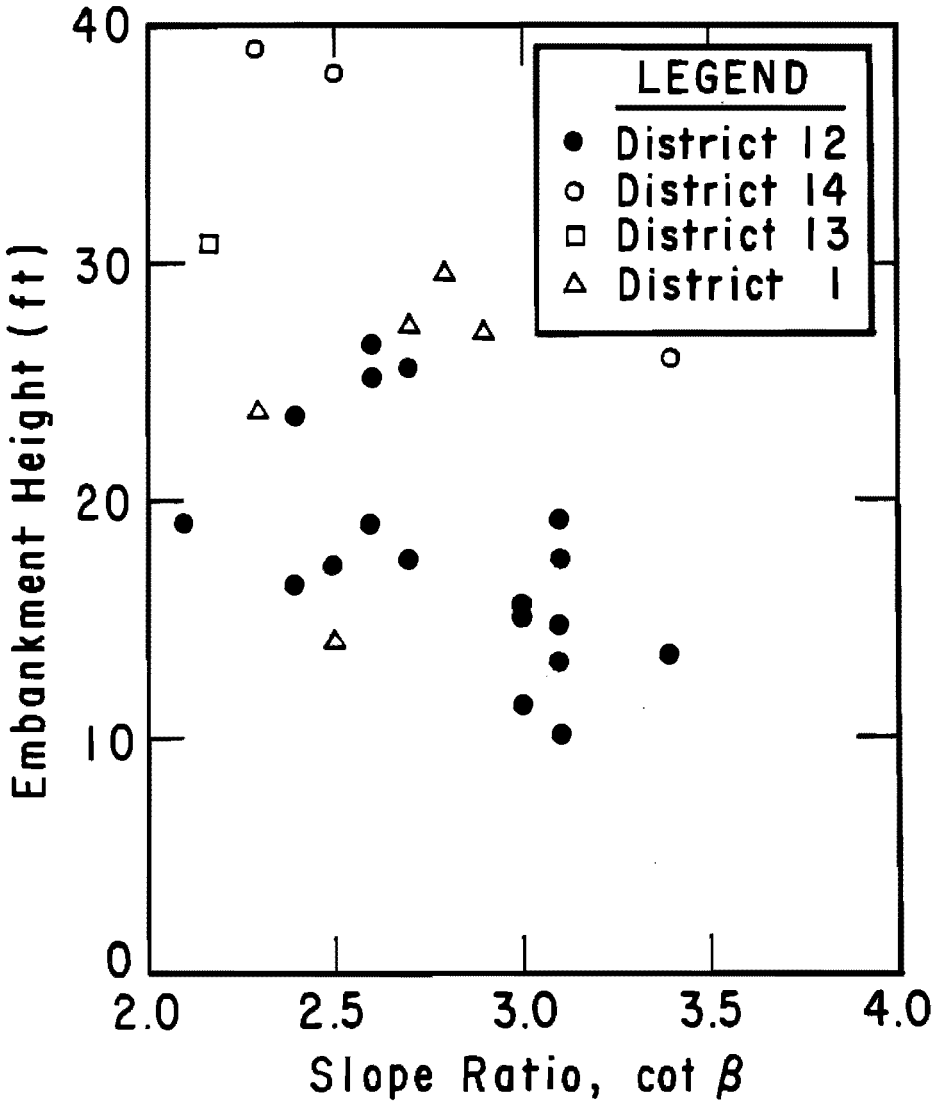

Fig. 2.5. Variation of embankment height with slope ratio (cot β) for embankments which failed in Districts 1, 12, 13, and 14.

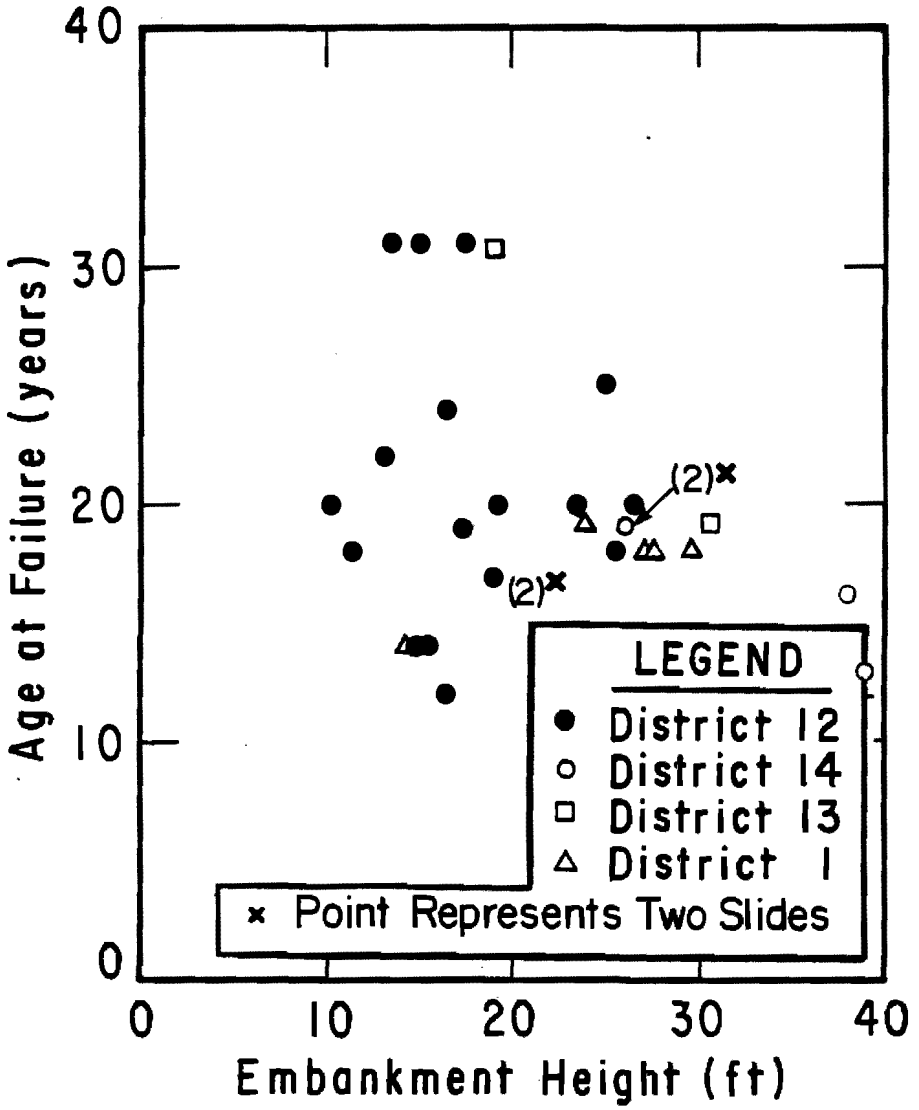

Fig. 2.6. Variation of age at failure with embankment height for embankments which failed in Districts 1, 12, 13, and 14.

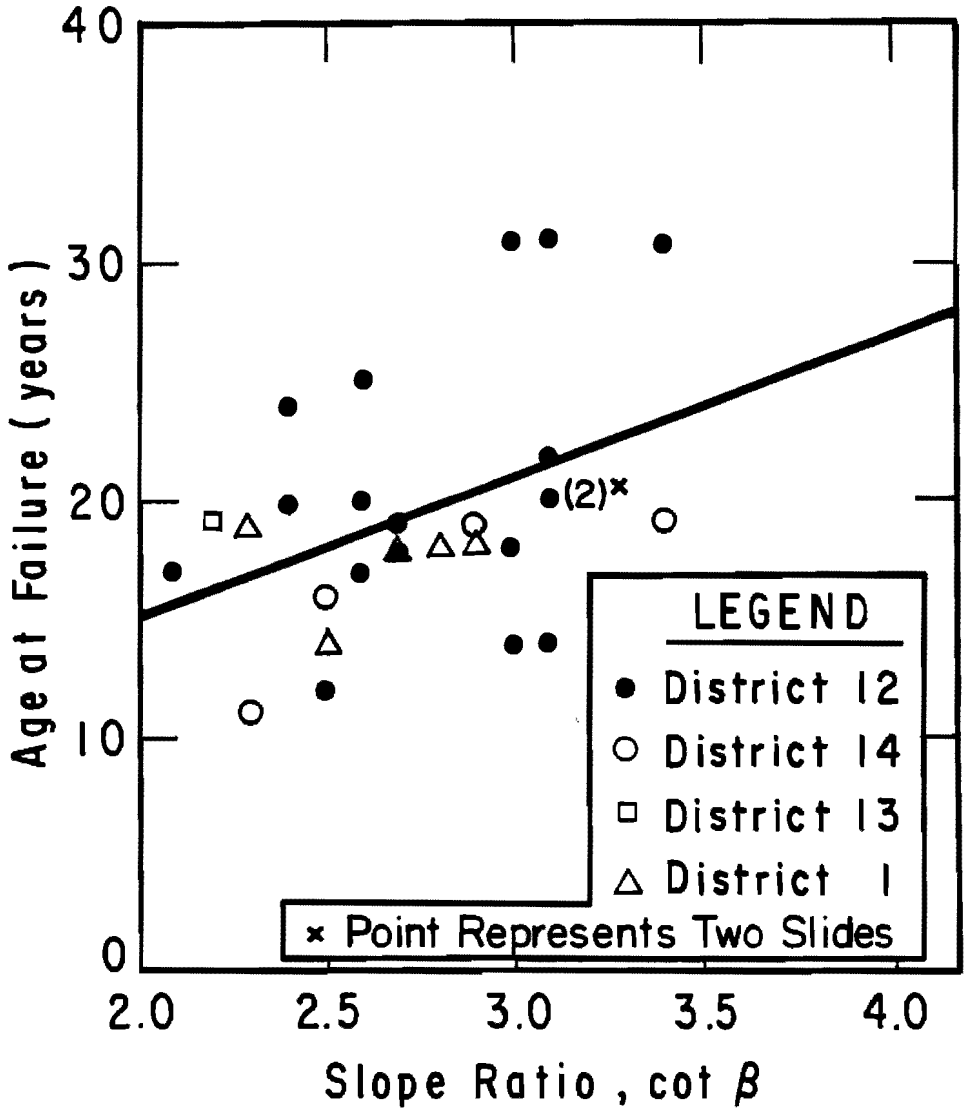

Fig. 2.7. Variation of age at failure with slope ratio (cot β) for embankments which failed in Districts 1, 12, 13, and 14.

This trend would be expected, especially if the soil is swelling and gradually losing strength with time.

Soil Sampling

Soil samples were obtained for each embankment slope studied. By examining soil samples from a large number of failures it was felt that properties common to these soils might be identified, and that the conditions common to these failures could be established. The majority of the embankments examined were found to be relatively nonhomogeneous. Accordingly, for each embankment examined, several soil samples were typically taken and tested. Soil properties as determined for these soils are presented in Chapter Four.

Preliminary Sampling: The type of soil samples taken, as well as the extent of the sampling, varied from site to site. The type of samples taken consisted of disturbed bag samples from excavations near the surface, from hand excavated test pits at moderate depth (1 to 4 feet), and from hand auger cuttings. In addition, two hand driven 3-inch-diameter Shelby tube samples were taken from an embankment slope at IH 10 and Crosby-Lynchburg Road in District 12.

Bag samples from excavations near the surface were commonly taken of material from the slide mass or of material exposed in the slide scarp. A shovel was most often used to excavate through material on the surface and to obtain a sample at about 0.5 to 1.0 foot depth. These

samples were not necessarily kept in sealed bags since the moisture content of soils near the ground surface was highly variable and depended on current environmental conditions. All bag samples taken at depths greater than about 1 foot, however, were sealed by double bagging the soil using "Ziploc" bags. Air was expelled from the bags prior to sealing them and two bags were used for protection against moisture loss.

Bag samples from hand excavated test pits were taken at depths of about 1 foot to about 4 feet as the test pit was excavated. Test pits were typically located near the center of the slide mass.

The hand auger borings were excavated using either a 2-inch or a 4-inch diameter, clam-shell-type hand auger. Samples were obtained at approximately 1 foot intervals, or wherever a significant change of material was observed. Care was taken to avoid mixing soils from different depths. The maximum sampling depth was about 3.5 feet. Two hand auger holes were excavated at a number of the sites. One was located in the slide mass area, preferably such that it penetrated the failure surface, and the second was located on the stable slope adjacent to the slide. Where only one hole was excavated at a site, it was located in the slide mass.

Two hand driven 3-inch-diameter Shelby tube samples were obtained from a slope failure in the northwest quadrant at IH 10 and Crosby-Lynchburg in District 12. One was taken in the slide mass and the other was taken on the adjacent, stable slope. The top 0.5 foot of material was excavated by hand, and the Shelby tube was then driven to obtain

about 0.5 foot of material. Upon their return to the laboratory, both ends of each tube were sealed with wax.

More Extensive Sampling: During the early stages of this study a limited quantity of Atterberg limit data had been acquired by Texas SDHPT personnel. Samples had been obtained from near the surface of several embankment slopes which had failed in the Houston area. These data, combined with observations made during an inspection tour on February 16, 1983, were used to select three embankments for more extensive sampling. The three sites selected were:

1. IH 610 at Scott Street, northeast quadrant,

2. State Highways 225 and 146, southwest quadrant, and

3. State Highways 225 and 146, northwest quadrant.

These sites were selected over others for the following reasons: 1) no concrete slope protection had been used and, thus, soil sampling was possible, 2) the slides at the time of consideration were essentially undisturbed and, thus, measurement of slope geometry and slide dimensions was possible, and 3) the preliminary Atterberg limit data showed that the embankments contained soils which encompassed the extreme values of liquid limits and plasticity indices which had thus far been measured.

At each of the three sites, eight large bag samples, approximately 50 pounds each, were obtained from the slide mass by hand exca-

vation of test pits. The test pits were about 4 feet deep and were located at about the center of the slide mass. The soil obtained was to be used in performing laboratory tests to measure the shear strength of recompacted specimens. Preliminary results of laboratory testing are presented by Gourlay and Wright (1984) and are used in Chapter Five to analyze the failure at IH 610 and Scott Street.

Observations Regarding Remedial Measures

A number of the slopes which were examined had been repaired. Although the emphasis in this study was on the failures rather than remedial measures, observations made during the field inspections regarding these remedial measures are described herein. The remedial measures which were observed included lime stabilization, restraint structures, concrete rip-rap, and "pushing and recompacting." In addition, efforts were sometimes made to control surface runoff.

The western embankment at the intersection of U.S. 77 and SH 21 in District 14 failed on both side slopes (slope and slide geometry data for these failures are presented in Table 2.1). The failures in both side slopes were repaired using lime stabilization. The construction procedure used at this site consisted of first excavating a strip of the slide material, parallel to the roadway, starting at the toe of the slope. The excavated material was stockpiled near the embankment. Lime was added and mixed into the material which was then placed in lifts back into the recently excavated area. Compaction was performed using a rub-

ber tired roller and other construction equipment. Construction proceeded as the excavation-replacement process described above proceeded upslope from the base to the top of the embankment slope.

For two of the embankment slides examined, it appeared that lime treatment had been used unsuccessfully. The embankment failure in the northwest quadrant of the SH 225 and SH 146 Interchange near Houston appeared to have been previously stabilized using lime treatment. During the initial field inspection of the abutment slope failure in the southeast quadrant at the intersection of U.S. 79 and U.S. 95 near Taylor, it was observed that the slope had been repaired previously using lime treatment and then subsequently slid. In addition, steel H-piles located just upslope from the head of the scarp had apparently been used to prevent regression of the slide. In October, 1983, the slide was repaired a second time using lime treatment. Material comprising the slide mass was removed to where firm, drier material was encountered. Lime was added and the treated material was replaced. Concrete rip-rap adjacent to the slide, and a concrete lined channel at the toe of the slope, which had been damaged by the slide, were also repaired.

An embankment slope in the southwest quadrant at the intersection of IH 610 and Westpark in District 12 had been repaired in 1980 using concrete rip-rap. One year later the slope had failed again. Holes were opened near the base of the rip-rap to relieve water pressures; however, this apparently did not stop the slope movement. The slope was repaired again, this time using a combination of a "Doublewal" precast retaining wall system (Doublewal, 1982), slope flattening and

concrete rip-rap. Sheet piling was driven near the top of the slope to provide temporary support for the shoulder of IH 610 until the permanent remedial measures described above were constructed.

Records of embankent slope failures in District 12 show that pushing and recompacting has often been used for the repair of embankment slope failures. The method involves replacing the material which has slid, typically using a bulldozer. Compaction is typically achieved by rolling with the dozer. For many of the embankment slides reported in District 12, pushing and recompacting was the initial repair method used. Reoccurrence of the slide is common, though it is uncertain how much time has passed between failures. In one case it appears that as much as five years transpired between failures; however, in many instances it has been reported that failures occurred again within a year of repair.

SUMMARY AND CONCLUSIONS

A number of earth slope failures were investigated as part of this research project. Slope failures investigated fell into three categories: 1) cut and natural slope failures, 2) embankment foundation failures, and 3) embankment slope failures. Only two failures were observed in cut slopes, and one failure was observed in a natural slope, where the toe of the slope was being removed by river erosion. One embankment foundation failure was examined and is considered in greater detail in Chapter Seven.

Most of the slope failures observed in this study occurred in embankment side slopes. Twenty-eight embankment slope failures were examined. These embankments were located in Districts 12 (Houston), 14 (Austin), 13 (Yoakum), and 1 (Paris). Slope geometry and slide dimension data for the twenty-eight embankment slope failures are presented and show that failures occur on embankments ranging in height from about 10 to 39 feet and on slopes ranging from about 2.1:1 to 3.4:1.

When the embankment slope failures examined in this study are considered together the following common characteristics are noted:

1. Embankment slides typically occur 15 to 25 years after construction of the embankment. Embankment slides on steeper slopes generally occur sooner after construction of the embankment than embankment slides on flatter slopes, which tend to occur a longer time after construction of the embankment.

2. The occurrence of an embankment slide is not significantly related to the embankment height; slides do not necessarily occur on the portion of the embankment with the greatest height, nor do they typically involve the full height of the slope. One slide was observed on a portion of the embankment slope where the height of the embankment was only 10 feet.

3. The failure surface is shallow and is generally restricted to the slope face. None of the failure surfaces extended into the foundation material.

Each of these characteristics is an indication that embankment slope failures occur under long-term conditions. The soil near the slope surface is losing strength with time, and eventually failure occurs. This loss of strength appears to be associated with the infiltration of water and subsequent swelling of the embankment soils.

A variety of types of soil samples were taken during the field inspections of embankment slides; these included: bag samples of near surface soils, of soils from test pits, and of soils from hand auger borings, and 3-inch-diameter Shelby tubes. Soil properties were determined for many of the soils sampled and are presented and discussed in Chapter Four. In addition, laboratory strength tests have been performed on soils from the IH 610 and Scott Street site. Preliminary results of these tests are presented in a recent report by Gourlay and Wright (1984) and are used in Chapter Five to perform detailed slope stability calculations for the IH 610 and Scott Street site.

CHAPTER THREE. CHARTS AND PROCEDURES FOR BACK-CALCULATING SHEAR STRENGTH PARAMETERS

INTRODUCTION

Field investigations of a number of embankment slope failures were discussed in Chapter Two. The information collected from these failures included measurements of the slope angle, height of the slope, and height of the slide. In addition, the depth of slide was estimated for each of the slopes examined. This information on the slope and slide geometry was used to back-calculate shear strengths for the soils involved in each failure by performing a series of slope stability calculations as described in this chapter.

Abrams and Wright (1972) previously used the approach of back-calculating shear strengths from slope and slide geometry data and developed a relatively simple chart which could be used to back-calculate both cohesion and friction angle values for the soil at the time of the slide. The procedures and chart which Abrams and Wright developed were based on the assumption that the soil was homogeneous. Accordingly, the critical surface of sliding always intersected the crest of the slope as shown in Fig. 3.1a. A number of the slides which were examined in this study were restricted to the face of the slope, as shown in Fig. 3.1b, and it is not clear that the chart developed by Abrams and Wright is applicable to such cases. In addition, Abrams and Wright considered

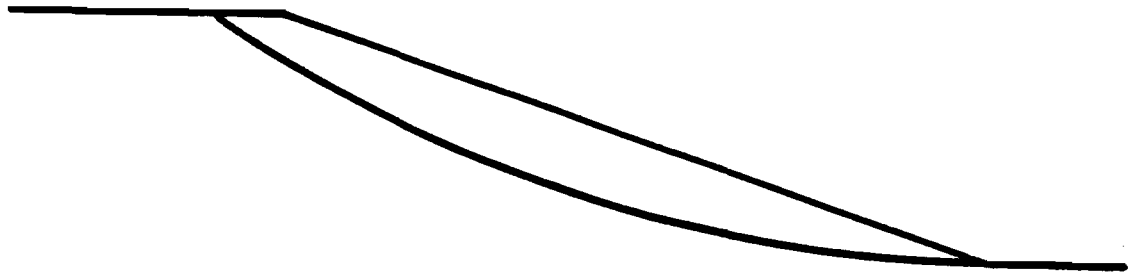

"Slope" Failure

(a)

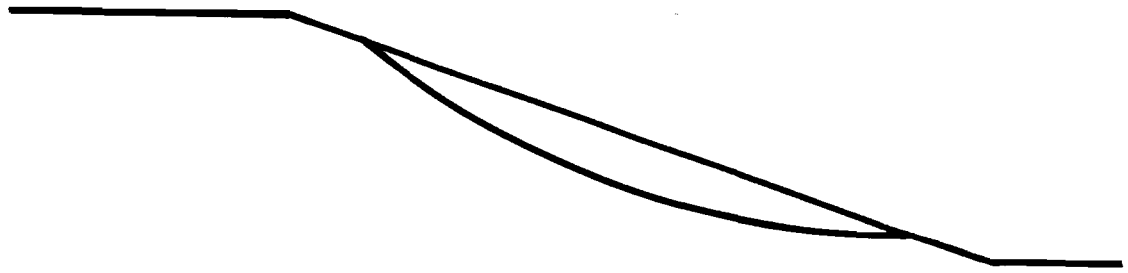

"Face" Failure

(b)

Fig. 3.1. Examples of slide surfaces for (a) "slope" and (b) "face" failures.

only total stresses, rather than effective stresses, and, thus, they did not consider pore water pressures in their analyses and chart.

As part of the research presented in this report a series of new charts have been developed which extend the work of Abrams and Wright to the case of slides which are confined entirely to the face of the slope, and to the case of effective as well as total stress analyses. Thus, the charts developed in this study are applicable to both short-term and long-term slope problems and to a wider range of practical cases including many of those which were observed. The developement of the charts for back-calculating the shear strength parameters from observed slope failures, and procedures for using these charts, are described in this chapter.

DIMENSIONLESS SLOPE PARAMETERS

In order to develop simple charts for the purpose of back-calculating the shear strength parameters, it is convenient to make use of several sets of dimensionless quantities and the relationships which exist among these quantities. In the case of a homogeneous slope, and

using total stresses, the factor of safety can be expressed by a dimensionless ratio, N_{cf}, defined as

$$N_{cf} = \frac{F}{c/\gamma H} \tag{3.1}$$

where F is the factor of safety, c is the cohesion value for the soil determined using total stresses to plot the Mohr-Coulomb failure envelope, γ is the total unit weight of the soil, and H is the height of the slope. The dimensionless quantity N_{cf} is termed a stability number and is uniquely related to the slope angle, β, and a second dimensionless quantity, $\lambda_{c\phi}$, which is defined as

$$\lambda_{c\phi} = \frac{\tan\phi}{c/\gamma H} \tag{3.2}$$

where ϕ is the friction angle for the soil determined using total stresses to plot the Mohr-Coulomb failure envelope. For a given value of $\lambda_{c\phi}$ and slope angle, β, there is a single unique value for N_{cf}.

In the case of homogeneous slopes, such as the ones considered by Abrams and Wright and assumed for the purpose of back-calculating shear strength parameters, it is reasonable to assume that the most critical sliding surface is circular. It can then be shown that for given values of the dimensionless parameter $\lambda_{c\phi}$ and the slope angle, β, there is a unique critical circular shear (sliding) surface corresponding to the minimum factor of safety. The critical circle has coordinates located as shown in Fig. 3.2, where X_c and Y_c represent the horizontal and vertical

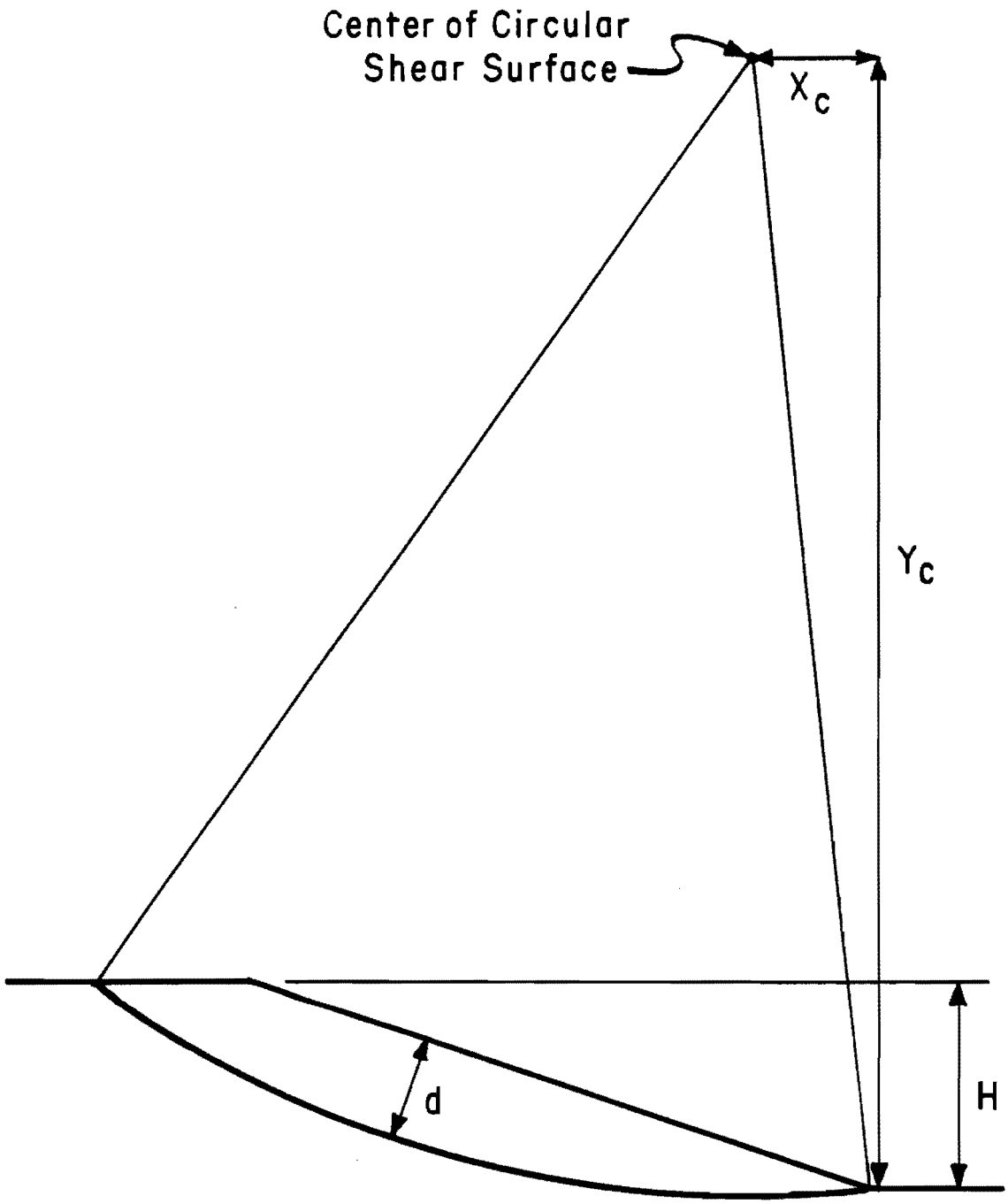

Fig. 3.2. Quantities which define the shear surface for "slope" failures.

distances, respectively, from the toe of the slope to the center of the critical circle. The height of the slope, H, and the depth of the critical circle normal to the slope surface, d, are also shown in Fig. 3.2. The dimensionless ratios X_c/H and Y_c/H are uniquely dependent on the dimensionless parameter $\lambda_{c\phi}$ and the slope angle, β. Similarly, there will be a unique value for the ratio of the slide depth-to-slope height, d/H, which depends only on β and $\lambda_{c\phi}$. Thus, for a given slope angle and value of $\lambda_{c\phi}$ there will be a unique value for both the dimensionless parameter, N_{cf}, and the ratio, d/H. Expressed in another way, there will be unique values for $\lambda_{c\phi}$ and N_{cf} for a given slope angle and slide depth ratio, d/H.

Abrams and Wright (1972) based their chart for back-calculating shear strength parameters on the unique relationship which exists for a given slope angle among the slide depth ratio, d/H, and the parameters $\lambda_{c\phi}$ and N_{cf}. For a given slope angle and slide depth ratio, d/H, there is a unique value of N_{cf}. Thus, if a slide has occurred in a slope with a given inclination, and the depth ratio is determined, a unique value of N_{cf} can be determined. Since the factor of safety is unity for a slope which has failed, Eq. 3.1 can be written as

$$N_{cf} = \frac{1.0}{c/\gamma H} \tag{3.3}$$

which can be rearranged to give

$$c = \frac{\gamma H}{N_{cf}} \tag{3.4}$$

Once the appropriate value for N_{cf} is determined, Eq. 3.4 can be used to calculate the cohesion value since the total unit weight of soil, γ, and the slope height, H, are considered to be known. The angle of internal friction, ϕ, associated with the cohesion calculated from Eq. 3.4, is calculated from the value of the parameter, $\lambda_{c\phi}$. A unique value of $\lambda_{c\phi}$ will exist for the given slope angle, β, and slide depth ratio, d/H. Thus, from Eq. 3.2 it follows that the friction angle, ϕ, can be calculated as

$$\phi = \arctan\left(\lambda_{c\phi} \cdot c/\gamma H\right) \tag{3.5}$$

Abrams and Wright (1972) developed a chart from which the values of $c/\gamma H$ and $\tan\phi$ corresponding to a factor of safety of unity could be determined directly, given the slope angle and slide depth ratio. Their chart has been redrawn and is shown in Fig. 3.3. The chart covers slope inclinations ranging from 2:1 to 4:1, and slide depth ratios, d/H, ranging from about 0.2 to about 1.0.

"SLOPE" VERSUS "FACE" FAILURES

The chart developed by Abrams and Wright considered the slope to

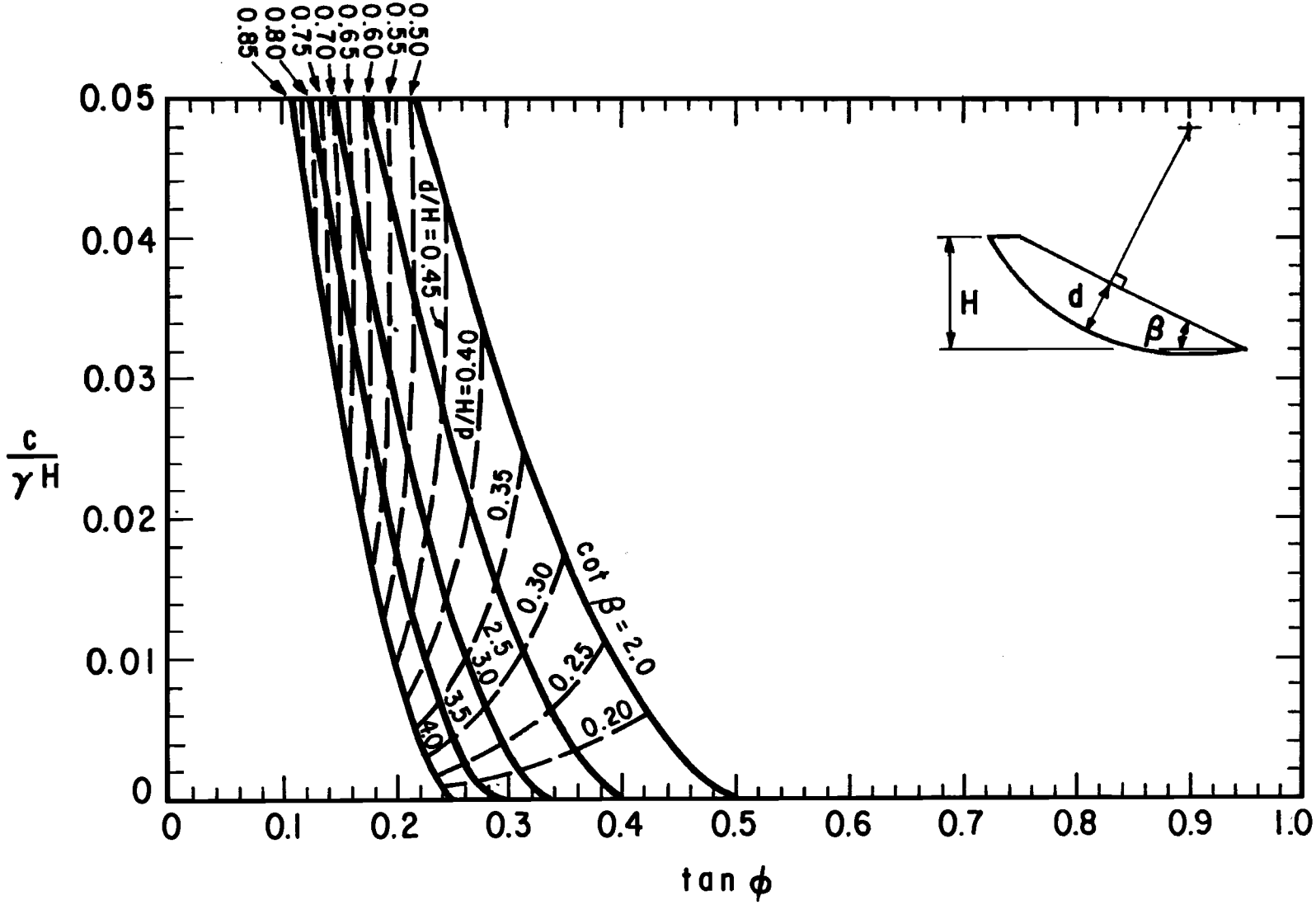

Fig. 3.3. Chart developed by Abrams and Wright (1972) for back-calculating shear strength parameters (c and ϕ) from slide information: "Slope" Failures - No Pore Water Pressures.

be homogeneous and, thus, the sliding surface would be similar to the one shown in Fig. 3.1a. In the case of homogeneous slopes the critical shear surface intersects the top of the slope some distance back from the face of the slope, as shown in these figures. However, many of the slides observed in this study involved only the face of the slope, as illustrated in Fig. 3.1b. Such slides have been termed "face" failures for the purposes of this study, while slides involving the entire slope, as shown in Fig. 3.1a, have been termed "slope" failures.

Separate charts from the ones developed for slope failures are necessary for the case of face failures. As part of this study various dimensionless relationships were examined for the case of face failures. It was found that if the slide depth ratio was defined as d/h, where d is the depth of the slide as defined previously and h is the "height" of slide as shown in Fig. 3.4, then, for a given slope angle, β, and slide depth ratio, d/h, unique values will exist for cohesion and friction angle, expressed by dimensionless ratios $c/\gamma h$ and $\tan\phi$, respectively.

The companion chart to the one developed by Abrams and Wright is shown in Fig. 3.5 for the case of face failures. This chart can be used to determine values of cohesion and friction angle, c and ϕ, respectively, corresponding to a Mohr-Coulomb envelope expressed in terms of total stresses and a factor of safety of unity for various slope angles, β, and slide depth ratios, d/h.

The values of the strength parameters, c and ϕ, which are determined for a face failure represent the values corresponding to a critical shear surface which is restricted to the face of the slope over a height,

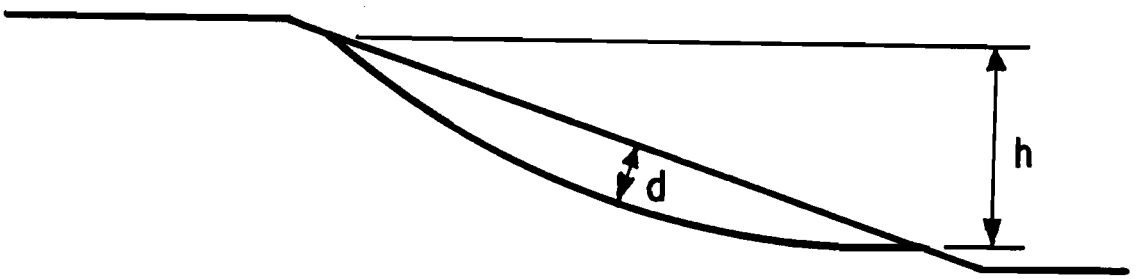

Fig. 3.4. Quantities which define the shear surface for "face" failures.

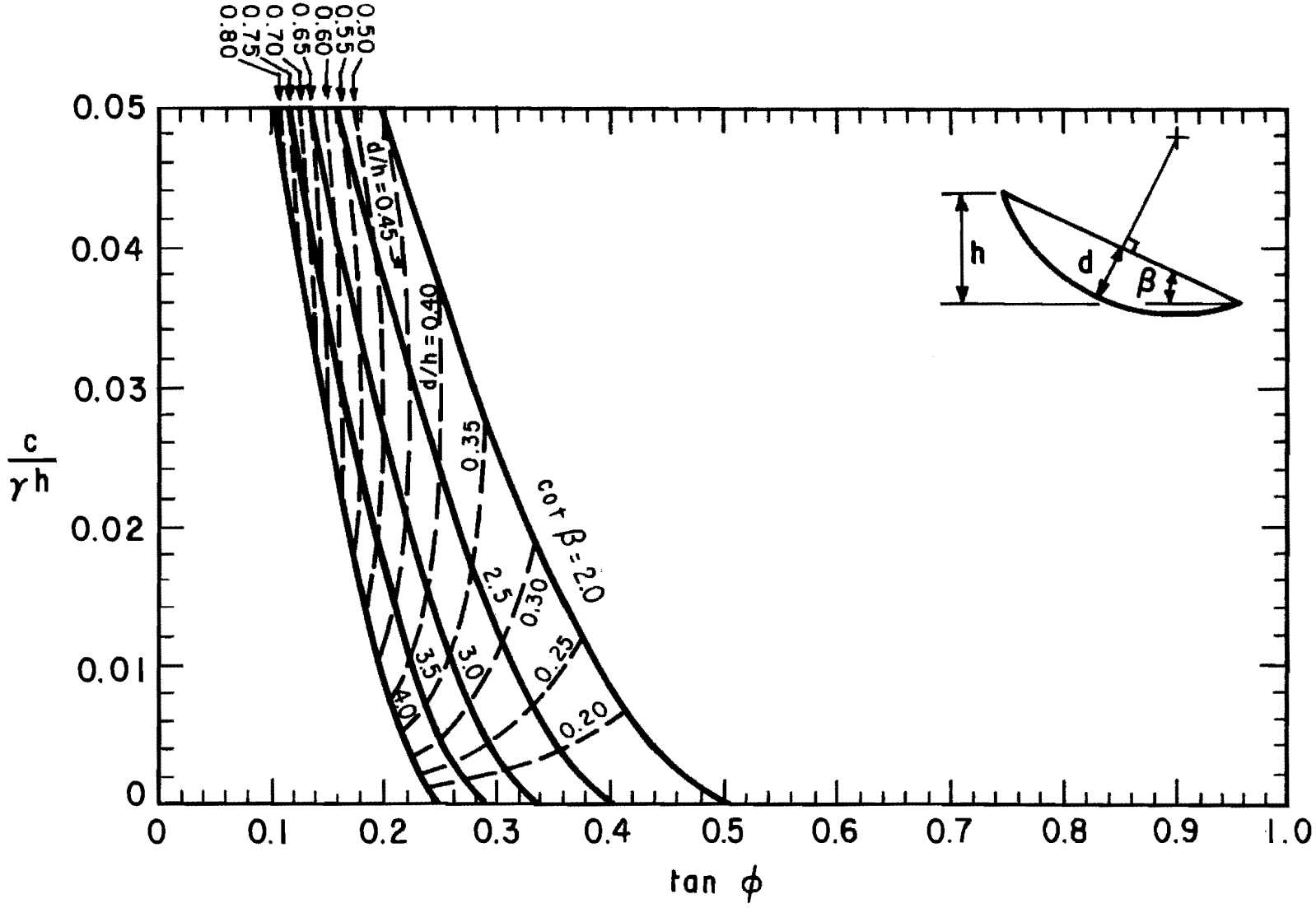

Fig. 3.5. Chart for back-calculating shear strength parameters (c and ϕ) from slide information: "Face" Failures - No Pore Water Pressures.

h, only. The occurrence of a face failure implies that nonhomogenities exist within the slope. If the shear strength parameters determined for a face failure were applied to the entire slope, the critical shear surface would intersect the top of the slope as shown in Fig. 3.1a and the factor of safety would be somewhat less than unity.

EFFECTIVE STRESS ANALYSES

The calculations and charts described up to this point were developed using total stresses, rather than effective stresses, to characterize the shear strength of the soil. Total stresses are usually used to characterize the shear strength for short-term stability computations where negligible drainage occurs during construction. Accordingly, the charts presented earlier are considered to be appropriate for use in back-calculating shear strengths applicable to slides which occur during or very shortly after construction. However, most of the slope failures which were observed and reported in this study occurred a number of years after construction. In the case of such "long-term" slope failures, shear strengths are usually expressed in terms of effective stresses. "Drained" shear strengths, such as those measured in consolidated-drained (CD, S) shear tests, are deemed appropriate for slope stability analyses, and such shear strengths are always expressed in terms of effective stresses. Thus, for long-term slides, such as those observed in this study, it is more appropriate to calculate shear strength parameters in terms of effective stresses.

In the case of effective stresses, the shear strength parameters are expressed by an effective stress cohesion value, $\bar{c}$, and an effective stress friction angle value, $\bar{\phi}$, where the "bars" ($\bar{}$) denote effective stress values. Stability calculations are performed in a manner similar to the way in which stability calculations are performed using total stresses, except that c and ϕ are replaced by $\bar{c}$ and $\bar{\phi}$, and pore water pressures are included in the computations. Where the pore water pressure is zero, the charts presented in Figs. 3.3 and 3.5 can be used for effective stress analyses by replacing c and ϕ with c and ϕ and keeping everything else as before. However, if the pore water pressures are not equal to zero, the charts in Figs. 3.3 and 3.5 cannot be used; other charts are required.

In order to develop charts for back-calculating shear strength parameters using effective stresses with other than zero pore water pressures, it is convieient to introduce the pore pressure parameter, r_u, defined by Bishop and Morgenstern (1960) as

$$r_u = \frac{u}{\gamma \cdot z} \tag{3.6}$$

where u is the pore water pressure at a point, γ is the total unit weight of soil overlying the point, and z is the depth from the ground surface to the point of interest. If the value of r_u is constant, then charts similar to those developed previously for zero pore water pressures can be developed for various selected values of r_u. For the present study, charts were developed for values of r_u of 0, 0.2 and 0.4. Separate

charts were developed for "slope" and "face" failures. The charts for slope failures are presented in Figs. 3.3, 3.6, and 3.7; the charts for face failures are presented in Figs. 3.5, 3.8, and 3.9. Each chart shown in these figures corresponds to a particular value of r_u. Depending on the particular value of r_u, charts bracketing the value estimated in the field may be used, and linear interpolation may be employed to obtain the shear strength parameters for the actual value of r_u.

The charts developed for effective stress analyses with pore water pressures greater than zero are all based on the assumption that r_u is constant in the area of interest, i.e., in the vicinity of the slide. In cases where r_u is not constant, it may be necessary to perform detailed stability calculations using a computer program such as the one described by Wright and Roecker (1984a). However, it appears that the charts can also be used for cases where r_u is not constant by using a representative average value for r_u. Bishop and Morgenstern (1960) describe a procedure to be used to estimate an appropriate average value for r_u in such cases, where the value varies. Their procedure is recommended for use with the charts developed in this study.

APPLICATION OF CHARTS

Average values for cohesion and friction angle may be determined from an earth slope failure using the charts illustrated in Figs. 3.3, and 3.5 through 3.9. The step-by-step procedures for using the charts to back-calculate shear strength parameters are given in Plates 3.1 through

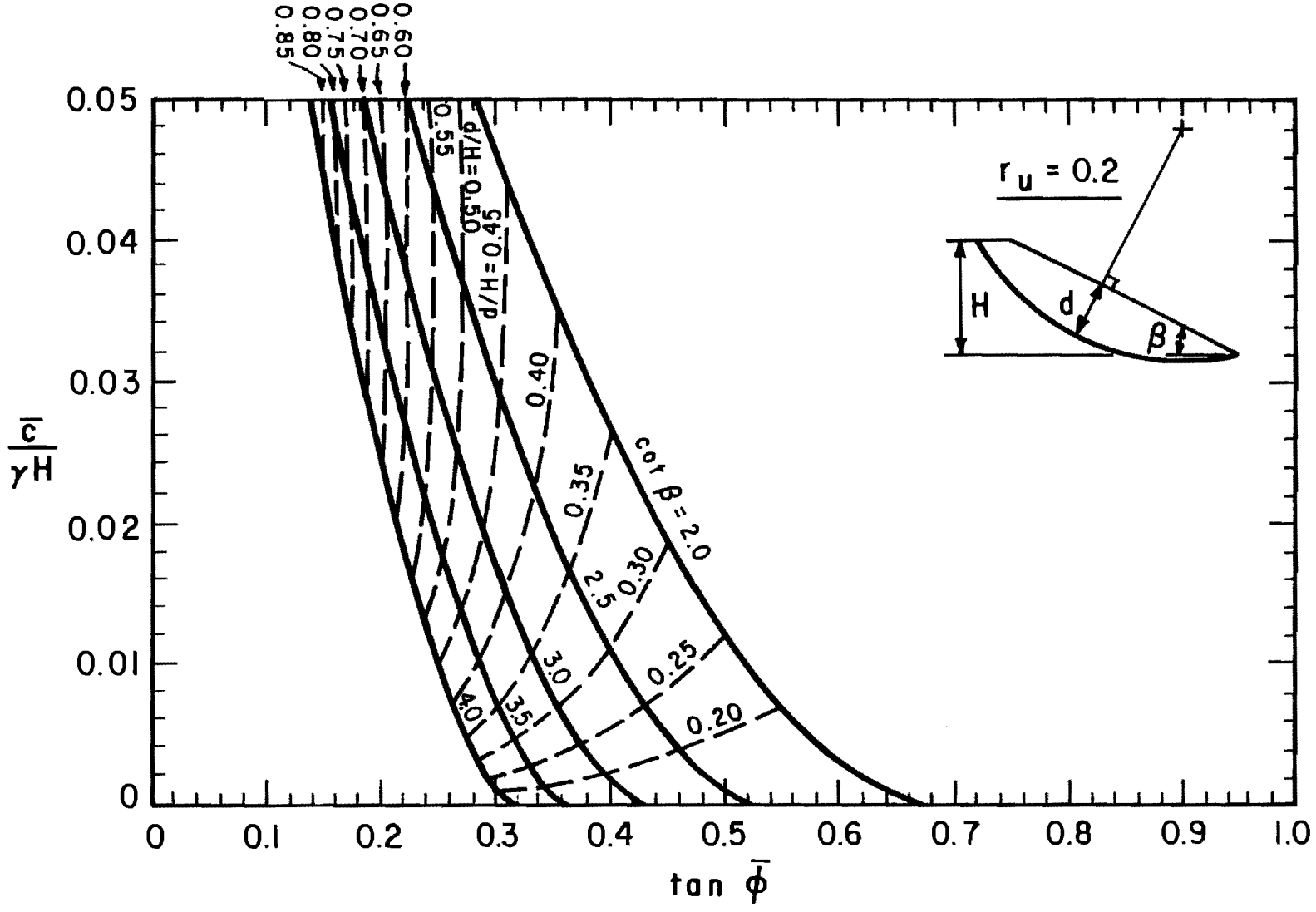

Fig. 3.6. Chart for back-calculating effective stress shear strength parameters ($\bar{c}$ and $\bar{\phi}$) from slide information: "Slope" Failures - r_u = 0.2.

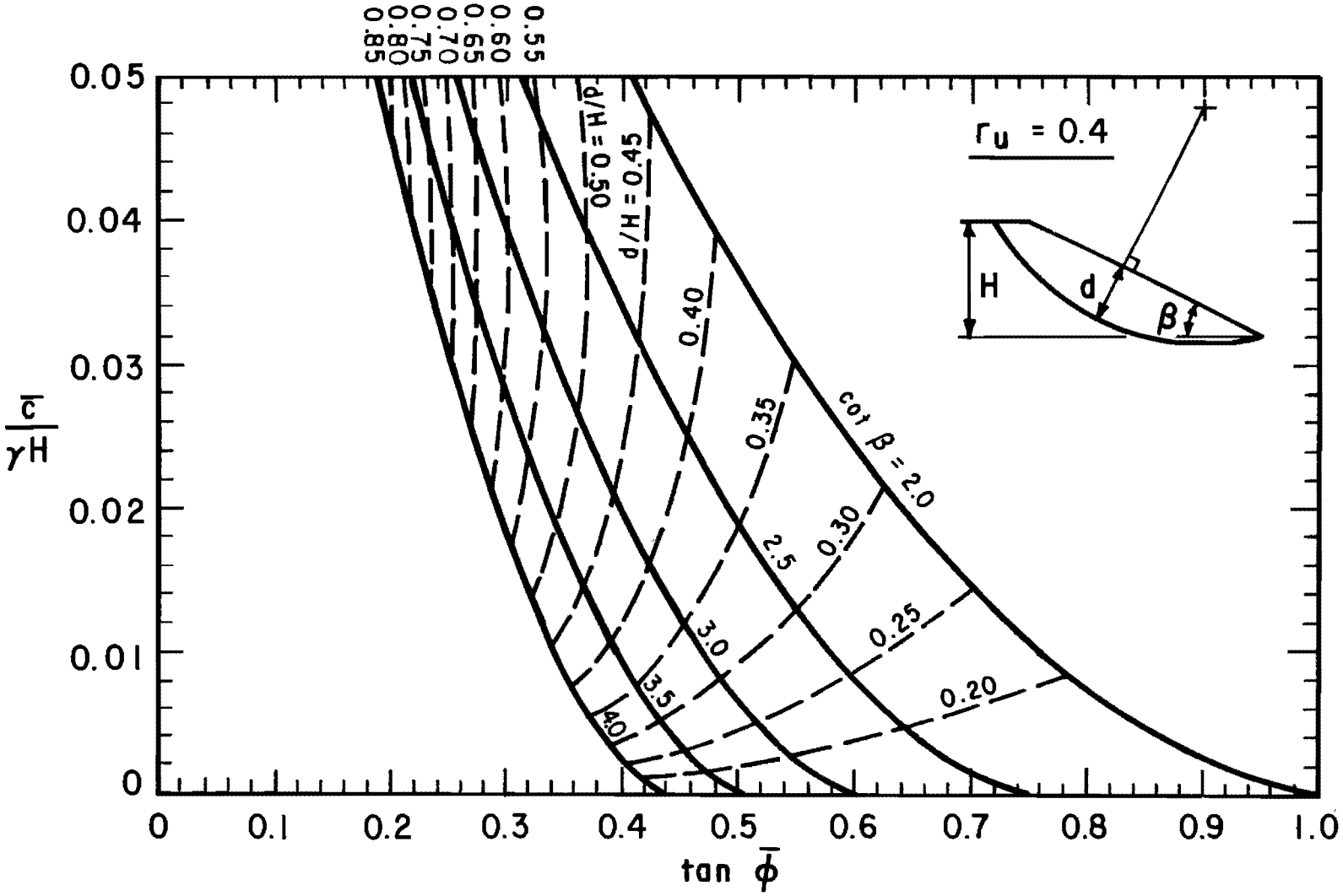

Fig. 3.7. Chart for back-calculating effective stress shear strength parameters ($\bar{c}$ and $\bar{\phi}$) from slide information: "Slope" Failures - r_u = 0.4.

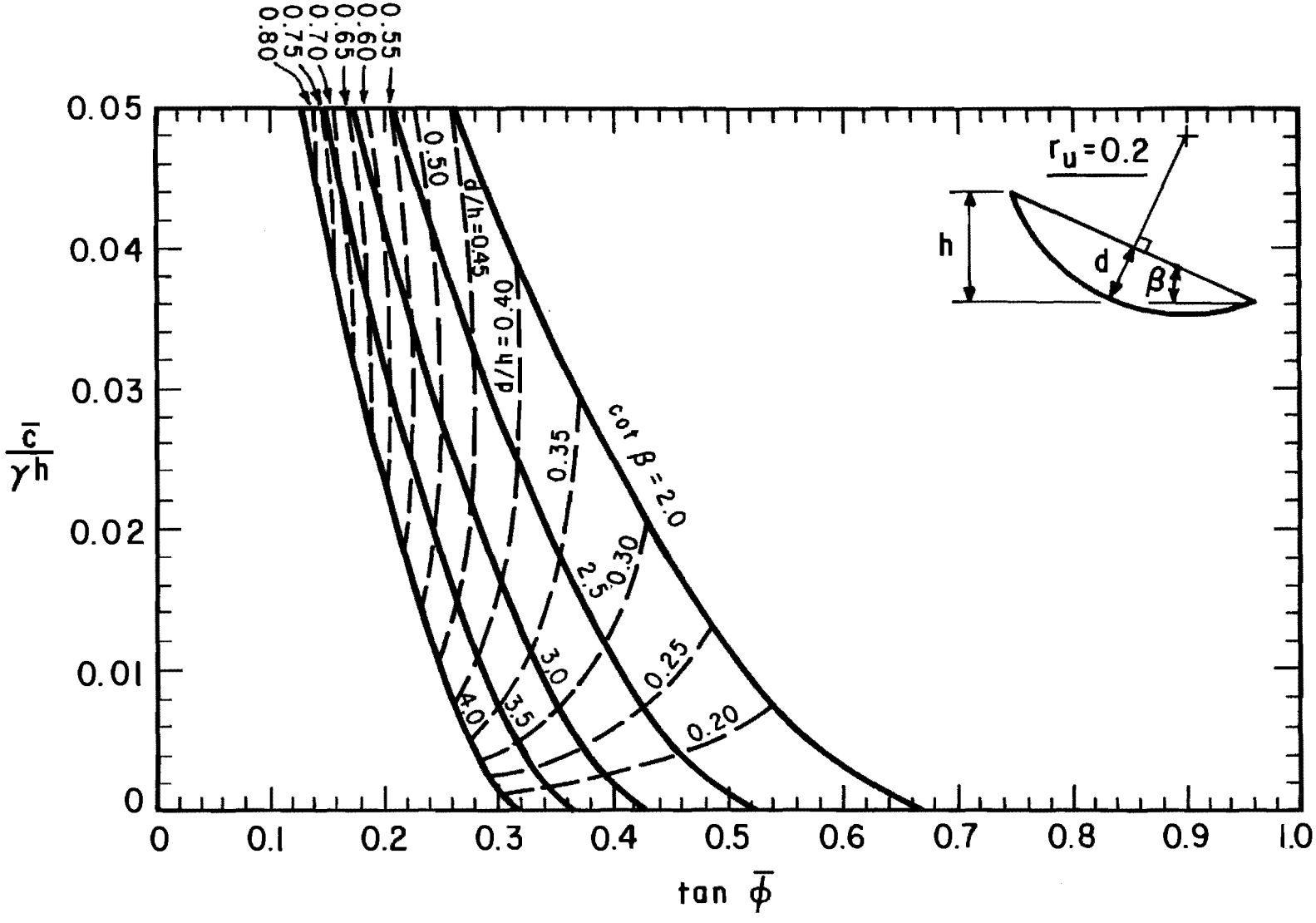

Fig. 3.8. Chart for back-calculating effective stress shear strength parameters ($\bar{c}$ and $\bar{\phi}$) from slide information: "Face" Failures - r_u = 0.2.

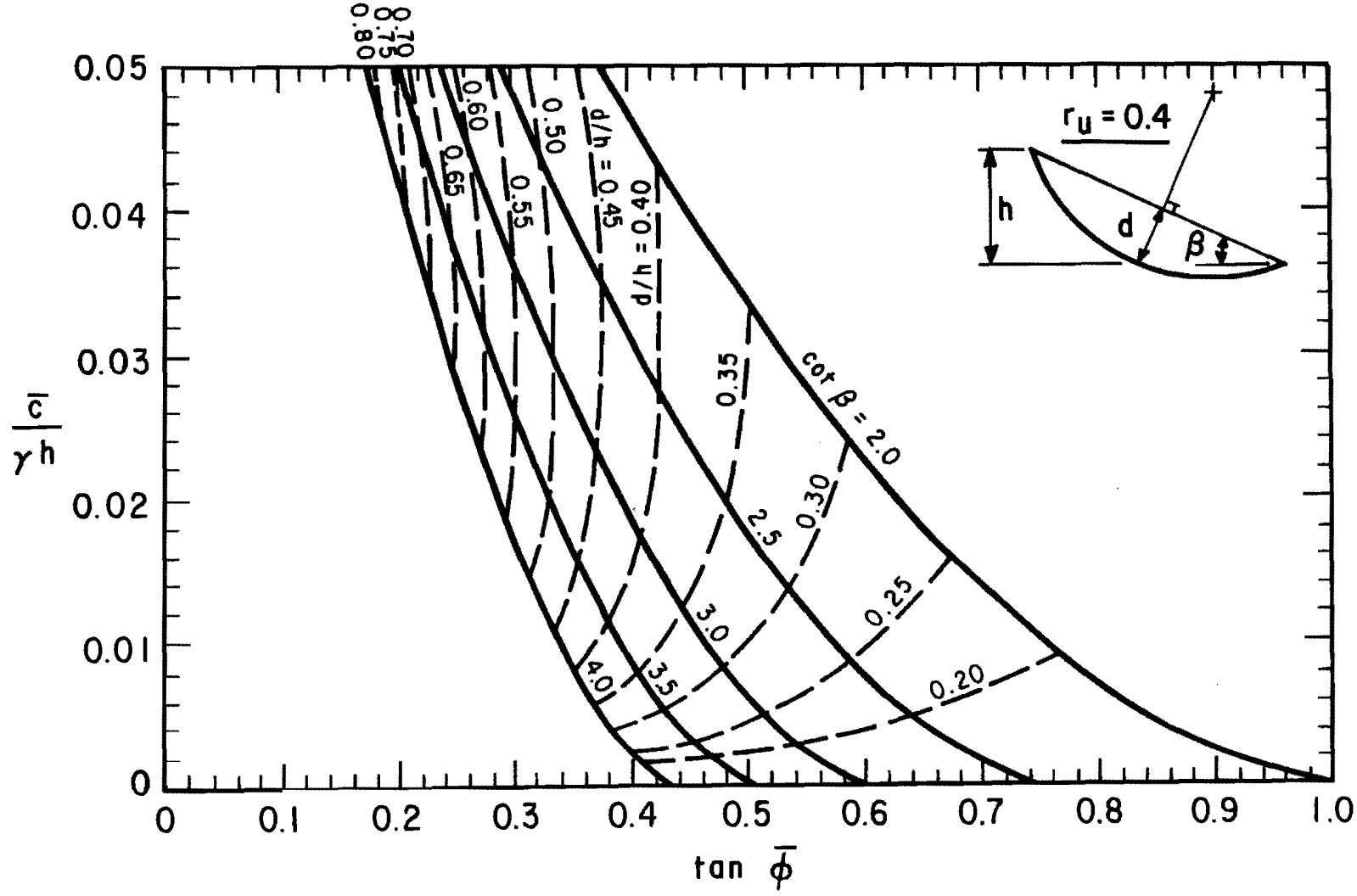

Fig. 3.9. Chart for back-calculating effective stress shear strength parameters ($\bar{c}$ and $\bar{\phi}$) from slide information: "Face" Failures - $r_u = 0.4$.

3.4. Procedures which apply to "slope" failures are given in Plates 3.1 and 3.2; Plate 3.1 is applicable to total stress analyses, and Plate 3.2 is applicable to effective stress analyses. Procedures which apply to "face" failures are given in Plates 3.3 and 3.4; Plate 3.3 is applicable to total stress analyses, and Plate 3.4 is applicable to effective stress analyses.

A series of sample calculations has been performed to illustrate the use of the charts and procedures for back-calculating shear strength parameters. The embankment slope failure at IH 610 and Scott Street in District 12, which was described in Chapter Two, was selected for the sample calculations. Sample calculations were performed for both total and effective stress shear strength parameters.

Slope geometry and slide dimension data for the IH 610 and Scott Street slide are as follows:

Embankment height, $H = 19.0$ ft.

Slope ratio, $\cot\beta = 2.6$

Height of slide, $h = 17.0$ ft.

Depth of slide, $d = 3.5$ ft.

Plate 3.1: Back-Calculation Procedure

"Slope" Failure - Total Stress ("Undrained") Analyses

1. Based on an examination of the slide geometry estimate the following quantities (see Fig. 3.2):
   (a) "Height" of slide, H (measured vertically)
   (b) Depth of slide, d (measured perpendicular to the slope)
   (c) Slope angle, β (measured from the horizontal); or cotangent of the slope angle, "cotβ" (corresponds to run-over-rise ratio).
2. Calculate a value for the dimensionless ratio, d/H, using the values of d and H estimated from Step 1.
3. Estimate from experience or measurements the total unit weight of soil, γ (total weight divided by total volume).
4. From the chart shown in Fig. 3.3, determine values of the dimensionless quantities "$c/\gamma H$" and "tanϕ" corresponding to the values of β and d/H estimated in Steps 1 and 2.
5. (a) Calculate a value of cohesion, c, as follows:

$$c = [c/\gamma H] \cdot \gamma H$$

   where the term, $c/\gamma H$, in brackets, [ ], represents the value determined in Step 4, H represents the "height" of slide estimated in Step 1, and γ represents the total unit weight of soil estimated from Step 3.

   (b) Calculate a value of friction angle, ϕ, from:

$$\phi = \text{arctangent } [\tan\phi]$$

   where the term, $\tan\phi$, in brackets, [ ], represents the value determined in Step 4.

Plate 3.2: Back-Calculation Procedure

"Slope" Failure - Effective Stress ("Drained") Analyses

1. Based on examination of the slide geometry estimate the following quantities (see Fig. 3.2):
   (a) "Height" of slide, H (measured vertically)
   (b) Depth of slide, d (measured perpendicular to the slope)
   (c) Slope angle, β (measured from the horizontal); or cotangent of the slope angle, "cotβ" (corresponds to run-over-rise ratio).
2. Calculate a value for the dimensionless ratio, d/H, using the values of d and H estimated from Step 1.
3. Estimate from experience or measurements the following quantities:
   (a) Total unit weight of soil, γ (total weight divided by total volume)
   (b) Pore water pressure parameter, r_u.
4. From the appropriate chart (Fig. 3.3, 3.6 or 3.7) determine values of the dimensionless quantities, "$\bar{c}/\gamma H$" and "tan$\bar{\phi}$" corresponding to the values of β and d/H estimated in Steps 1 and 2.
5. (a) Calculate a value of cohesion, $\bar{c}$, as follows:

$$\bar{c} = [\bar{c}/\gamma H] \cdot \gamma H$$

   where the term, $\bar{c}/\gamma H$, in brackets, [ ], represents the value determined in Step 4, H represents the "height" of slide estimated in Step 1, and γ represents the total unit weight of soil estimated from Step 3.

   (b) Calculate a value of friction angle, $\bar{\phi}$, from:

$$\bar{\phi} = \text{arctangent } [\tan\bar{\phi}]$$

   where the term, $\tan\bar{\phi}$, in brackets, [ ], represents the value determined in Step 4.

Plate 3.3: Back-Calculation Procedure

"Face" Failure - Total Stress ("Undrained") Analyses

1. Based on an examination of the slide geometry estimate the following quantities (see Fig. 3.4):
   (a) "Height" of slide, h (measured vertically)
   (b) Depth of slide, d (measured perpendicular to the slope)
   (c) Slope angle, β (measured from the horizontal); or cotangent of the slope angle, "$\cot\beta$" (corresponds to run-over-rise ratio).
2. Calculate a value for the dimensionless ratio, d/h, using the values of d and h estimated from Step 1.
3. Estimate from experience or measurements the total unit weight of soil, γ (total weight divided by total volume).
4. From the chart shown in Fig. 3.5 determine values of the dimensionless quantities, "$c/\gamma h$" and "$\tan\phi$" corresponding to the values of β and d/h estimated from Steps 1 and 2.
5. (a) Calculate a value of cohesion, c, as follows:

$$c = [c/\gamma h] \cdot \gamma h$$

   where the term, $c/\gamma h$, in brackets, [ ], represents the value determined in Step 4, h represents the "height" of slide estimated in Step 1, and γ represents the total unit weight of soil estimated from Step 3.

   (b) Calculate a value of friction angle, ϕ, from:

$$\phi = \text{arctangent } [\tan\phi]$$

   where the term, $\tan\phi$, in brackets, [ ], represents the value determined in Step 4.

Plate 3.4: Back-Calculation Procedure

"Face" Failure - Effective Stress ("Drained") Analyses

1. Based on examination of the slide geometry estimate the following quantities (see Fig. 3.4):
   (a) "Height" of slide, h (measured vertically)
   (b) Depth of slide, d (measured perpendicular to the slope)
   (c) Slope angle, β (measured from the horizontal); or cotangent of the slope angle, "$\cot\beta$" (corresponds to run-over-rise ratio).
2. Calculate a value for the dimensionless ratio, d/h, using the values of d and h estimated from Step 1.
3. Estimate from experience or measurements the following quantities:
   (a) Total unit weight of soil, γ (total weight divided by total volume)
   (b) Pore water pressure parameter, r_u.
4. From the appropriate chart (Fig. 3.5, 3.8 or 3.9) determine values of the dimensionless quantities, "$\bar{c}/\gamma h$" and "$\tan\bar{\phi}$" corresponding to the values of β and d/h estimated in Steps 1 and 2.
5. (a) Calculate a value of cohesion, $\overline{c}$, as follows:

$$\overline{c} = [\bar{c}/\gamma h] \cdot \gamma h$$

   where the term, $\bar{c}/\gamma h$, in brackets, [ ], represents the value determined in Step 4, h represents the "height" of slide estimated in Step 1, and γ represents the total unit weight of soil estimated from Step 3.

   (b) Calculate a value of friction angle, $\overline{\phi}$, from:

$$\overline{\phi} = \text{arctangent } [\tan\bar{\phi}]$$

   where the term, $\tan\bar{\phi}$, in brackets, [ ], represents the value determined in Step 4.

The slide occurred entirely within the face of the slope and is therefore classified as a "face" failure. A total unit weight, γ, of 120 pcf was assumed for the embankment material.

Back-Calculation of Total Stress Shear Strength Parameters

Total stress shear strength parameters were calculated for the IH 610 and Scott Street slide using the step-by-step procedure outlined in Plate 3.3 and the chart in Fig. 3.5. The steps used to back-calculate the shear strength parameters are as follows:

Step 1: This step involves the collection of the field data, which for the present slide was described in Chapter Two and summarized in the previous section.

Step 2: Based on a slide depth of 3.5 feet and a height of slide of 17.0 feet, the slide depth ratio, d/h, was calculated to be 0.21.

Step 3: The total unit weight of soil was assumed to be 120 pcf.

Step 4: Referring to Fig. 3.5 and interpolating between the solid curves corresponding to slope ratios of 2:1 and 3:1, and interpolating between dashed lines corresponding to depth ratios of 0.20 and

0.25, the following values were obtained:

$$c/\gamma h = 0.004$$

$$\tan\phi = 0.34$$

Step 5: Using the dimensionless values obtained in Step 4, the value of cohesion is calculated as

$$c = [0.004] \cdot 120 \cdot 17.0 = 8.2 \text{ psf}$$

and the value for the angle of internal friction is

$$\phi = \arctan [0.34] = 18.8 \text{ degrees}$$

Back-Calculation of Effective Stress Shear Strength Parameters

Effective stress shear strength parameters were determined for the IH 610 and Scott Street slide using the step-by-step procedure for face failures outlined in Plate 3.4 and the chart in Fig. 3.9. The steps

used to back-calculate the shear strength parameters are as follows:

Step 1: This step involves the collection of the field data, which for the present slide was described in Chapter Two and summarized in the previous section.

Step 2: Based on a slide depth of 3.5 feet and a height of slide of 17.0 feet, the slide depth ratio, d/h, was calculated to be 0.21.

Step 3: For the purposes of this example, the pore water pressures were assumed to be represented by a value of r_u equal to 0.4. The total unit weight of soil was assumed to be 120 pcf.

Step 4: Referring to Fig. 3.9 and interpolating between the solid curves corresponding to slope ratios of 2:1 and 3:1, and interpolating between dashed lines corresponding to depth ratios of 0.20 and 0.25, the following values were obtained:

$$\bar{c}/\gamma h = 0.005$$

$$\tan\bar{\phi} = 0.61$$

Step 5: Using the dimensionless values obtained in Step 4, the value of the effective stress cohesion is calculated as

$$\bar{c} = [0.005] \cdot 120 \cdot 17.0 = 10.2 \text{ psf}$$

and the value of the effective stress angle of internal friction is calculated as

$$\bar{\phi} = \arctan [0.61] = 31.4 \text{ degrees}$$

The pore water pressures assumed for this example ($r_u = 0.4$) are probably much higher than those that actually existed in the field. The pore water pressures for this slide were thought to be negligible as discussed later in Chapter Four. For the case of zero pore water pressures the chart in Fig. 3.5 would be used and the values obtained for the effective stress shear strength parameters would be identical to the total stress shear strength parameters obtained in the previous example, that is, $\bar{c}$ = 8.2 psf and $\bar{\phi}$ = 18.8 degrees.

SUMMARY

Charts and procedures have been presented for back-calculating shear strength parameters from earth slopes which have failed. The charts which have been developed represent an extension of charts developed by Abrams and Wright (1972) and extend the charts to the case of

slides which are confined to the face of the slope, and to the case of effective stress as well as total stress analyses.

Slope failures provide an excellent opportunity for determining the probable values of shear strength parameters which exist at the time of failure. In many cases no other shear strength information is available; the back-calculated values are all that are available for redesign of the slope. However, some caution must be used to ensure that the pore pressure conditions which are assumed and the shear strength parameters which are back-calculated are appropriate for use in redesign. In the next chapter strengths are back-calculated for a number of embankment slope failures in Texas and the reasonableness of the back-calculated values for use in design is examined.

CHAPTER FOUR. EMBANKMENT MATERIAL PROPERTIES

INTRODUCTION

A variety of soil properties were determined for the embankments described in Chapter Two. Atterberg limits, grain size distributions, and water contents were determined for many of the soil samples taken during field investigations. In addition, the types of clay minerals present in two of the soils were determined by X-ray diffraction analysis. Although no laboratory shear tests were performed in this study, shear strength parameters were back-calculated for each of the embankment slides examined using procedures described in Chapter Three and the slope geometry and slide dimension data presented in Chapter Two. All of the soil properties which were either measured or back-calculated are presented and discussed in this chapter. In addition, soil property data are examined to determine if any relationships exist between the measured and back-calculated soil properties, and the slope geometry and slide dimensions.

INDEX PROPERTIES

Atterberg limits and grain size distributions were determined for soils obtained from each of the twenty-nine embankment slopes examined in this study. All tests were carried out to ASTM specifications (ASTM, 1982, D423 for the liquid limit, D424 for the plastic limit, and D422 for the grain size analysis by hydrometer). Data are summarized in Table 4.1. Specific tests and data are discussed in detail in the following sections.

Selection of Soil

Several procedures were used to select soils for index property tests depending on the variability of the soils within a slope, and the amount of material available. Where the samples obtained from a site indicated that the embankment was relatively homogeneous, the sample selected for testing was one which was judged to best represent the soils encountered. If possible, samples taken near the estimated location of the failure surface were selected.

Where the samples obtained from a site indicated nonhomogeniety of the embankment materials, it was often necessary to test more than one soil. Variations among soil samples were recognized by examining the soil color, grain size, including estimated sand content, and plasticity. When it was clear which of the soils encountered at a site was the most highly plastic and, thus, potentially the most expansive, this was

TABLE 4.1. SUMMARY OF INDEX PROPERTY DATA FOR SOILS FROM EMBANKMENT SLIDES

Slope Location	District	Soil Description	Atterberg Limits (percent)		Grain Size (percent by weight passing)		Activity
			Liquid Limit	Plasticity Index	No. 200 Sieve	2 microns	
IH 610 @ Scott St., NE quadrant, Harris Co.	12	Grey clay (1st sampling)	53.8	39.2	83.6	49.2	0.80
		Grey clay (2nd sampling)	55.2	37.2	85.5	49.7	0.75
		Red clay (1st sampling)	71.4	51.7	95.4	68.0	0.76
		Red clay (2nd sampling)	72.7	51.6	95.3	69.1	0.75
SH 225 @ SH 146, SW quadrant, Harris Co.	12	Brown clay	70.4	49.2	91.6	63.3	0.78
SH 225 @ SH 146, NW quadrant, Harris Co.	12	Red clay	63.2	40.6	97.6	75.0	0.54
		Tan clay	57.4	38.7	93.2	55.2	0.70
SH 225 @ SH 146, NE quadrant, Harris Co.	12	Grey clay	62.8	42.1	90.0	65.5	0.64

(continued)

TABLE 4.1. (Continued)

Slope Location	District	Soil Description	Atterberg Limits (percent)		Grain Size (percent by weight passing)		Activity
			Liquid Limit	Plasticity Index	No. 200 Sieve	2 microns	
SH 225 @ Southern Pacific RR Overpass, SE quadrant, Harris Co.	12	Grey clay	53.8	35.8	86.9	53.6	0.67
SH 225 @ Southern Pacific RR Overpass, SW quadrant, Harris Co.	12	Grey clay	49.3	33.0	85.9	48.5	0.68
		Grey clay w/ some red	60.0	39.7	91.1	62.5	0.64
		Tan clay	97.0	67.4	97.7	86.4	0.78
SH 225 @ Southern Pacific RR Overpass, NW quadrant, Harris Co.	12	Brown/tan clay	71.2	54.6	93.1	61.2	0.89
SH 225 @ Scarborough, SE quadrant, Harris Co.	12	Dark grey clay	70.9	52.7	87.5	60.0	0.88

(continued)

TABLE 4.1. (Continued)

Slope Location	District	Soil Description	Atterberg Limits (percent)		Grain Size (percent by weight passing)		Activity
			Liquid Limit	Plas-ticity Index	No. 200 Sieve	2 microns	
IH 610 @ SH 225, SE quadrant, Harris Co.	12	Dark grey clay	58.1	42.2	87.7	46.9	0.90
IH 610 @ Richmond St., SW quadrant, Harris Co.	12	Grey clay	53.7	38.2	83.2	45.5	0.84
IH 10 @ Crosby-Lynchburg, NW quadrant, Harris Co.	12	Tan clay	61.2	45.2	90.7	53.2	0.85
IH 45 @ SH 146, SE quadrant, Harris Co.	12	Red/brown clay	68.7	49.8	95.2	57.8	0.86
IH 45 @ SH 146, south side, Harris Co.	12	Brown/grey clay	56.7	40.2	86.7	48.3	0.83

(continued)

TABLE 4.1. (Continued)

Slope Location	District	Soil Description	Atterberg Limits (percent)		Grain Size (percent by weight passing)		Activity
			Liquid Limit	Plasticity Index	No. 200 Sieve	2 microns	
IH 45 @ FM 2351, NE quadrant, Harris Co.	12	Red/brown clay	67.8	48.8	95.2	59.4	0.82
IH 45 @ College St., NE quadrant, Harris Co.	12	Grey/olive clay	88.8	70.9	95.6	67.4	1.05
U.S. 59 @ FM 525, NE quadrant, Harris Co.	12	Light tan clay	42.0	30.7	72.0	40.1	0.77
U.S. 59 @ Shepard St., SE quadrant, Harris Co.	12	Tan clay	45.4	32.3	80.9	37.0	0.87
U.S. 79 @ Carlos G. Parker Blvd., NW quadrant, Williamson Co.	14	Tan clay w/ some white & gold	62.1	43.7	>92.8	50.7	0.87

(continued)

TABLE 4.1. (Continued)

Slope Location	District	Soil Description	Atterberg Limits (percent)		Grain Size (percent by weight passing)		Activity
			Liquid Limit	Plasticity Index	No. 200 Sieve	2 microns	
U.S. 79 @ U.S. 95, SE quadrant, Williamson Co.	14	Tan clay	92.7	69.6	99.0	76.4	0.91
U.S. 77 @ SH 21, SW quadrant, Lee Co.	14	Brown clay	64.4	37.2	>71.7	52.7	0.71
		Gold/tan clay	82.6	56.1	89.0	71.4	0.79
U.S. 77 @ SH 21, NW quadrant, Lee Co.	14	Tan clay	89.7	61.9	97.0	81.5	0.76
		Gold/brown clay	86.7	53.5	86.5	75.5	0.71
U.S. 290 ~ 5 miles east of IH 35, NW quadrant, Travis Co.	14	Grey clay	62.5	39.3	95.8	61.8	0.64
		Light tan clay	65.9	45.0	94.2	66.7	0.68
U.S. 87 @ Loop 175, NW quadrant, Victoria Co.	13	Dark grey/black clay	60.0	40.6	86.0	60.1	0.68
		Tan clay	76.1	55.9	93.7	65.9	0.85

(continued)

TABLE 4.1. (Continued)

Slope Location	District	Soil Description	Atterberg Limits (percent)		Grain Size (percent by weight passing)		Activity
			Liquid Limit	Plasticity Index	No. 200 Sieve	2 microns	
Loop 286 @ SH 271 Interchange, NW quadrant, Lamar Co.	1	Light brown clay	58.1	39.3	80.7	55.3	0.71
Loop 286 @ Missouri Pacific RR Overpass, SW quadrant (north slide), Lamar Co.	1	Grey clay	48.3	29.9	93.7	43.2	0.69
Loop 286 @ Missouri Pacific RR Overpass, SW quadrant (south slide), Lamar Co.	1	Tan clay	75.8	48.3	98.0	69.9	0.69
Loop 286 @ Missouri Pacific RR Overpass, NW quadrant, Lamar Co.	1	Grey clay	71.0	46.2	95.8	67.1	0.69
		Tan clay	81.0	54.4	97.7	72.9	0.75
Loop 286 @ FM 79, SW quadrant, Lamar Co.	1	Tan clay	73.8	48.6	90.6	68.7	0.71

the only soil tested and is hence referred to as the "problem" soil. Where there was some uncertainty as to which soil might be the most highly plastic, those soils in question were tested to determine which one was the "problem" soil. The criteria used to determine the "problem" soil are described below under "Atterberg Limits."

In most instances the soil tested came from one sample, which was selected as described above. However, when there was not enough of the desired soil available from one sample, additional soil obtained from a similar sample taken at the site was added.

Selective combination of soils from more than one sample was used for the examination of the embankment slide at IH 610 and Scott Street in District 12. Soil samples obtained from this embankment indicated that two distinctly different soils were present. The most predominant was a red clay which was slightly sandy and highly plastic. The other soil encountered was a grey clay with a higher sand content and a slightly lower plasticity. Also present in lesser quantities was a dark grey-to-black sandy clay which appeared to be topsoil. In order to perform strength tests for the red clay and the grey clay, a large quantity of each was needed. Thus, the red and grey clay contained in each of the large bag samples obtained from test pit excavation was separated, combined, and mixed to obtain a large quantity of each. The soil tested for this site came from these quantities.

Atterberg Limits

Atterberg limits were determined for from one to three soils for each of the sites examined in this study. Liquid and plastic limits were determined using the fraction of each of these soils passing the No. 40 sieve after air-drying, pulverizing, and grinding in a mortar with a rubber-covered pestle. Plasticity indices were also calculated. The liquid limit and the plasticity index for each soil tested are presented in Table 4.1.

As discussed in the previous section, the intent was to identify and test the "problem" soil at each site. The soil with the highest plasticity index was chosen and defined as the "problem" soil. The data shown in Table 4.1 reveal that the problem soil also generally had the highest liquid limit.

The color of each soil sample tested is included in Table 4.1. Where there was more than one soil tested at a site, and where one of these soils was grey in color, the grey soil was found to have the lowest plasticity index. Color alone is generally not used to identify soils since there can be a difference in color due to the oxidation of elements which are present in minute proportions and which do not themselves affect the engineering properties of the soil. However, for the soils encountered in this study, the presence of the color grey appears to be a helpful deteminant in identifying clays of lower plasticity.

The results from Atterberg limit tests for the soils which were identified as the problem soil from each embankment slide have been plot-

ted on a plasticity chart in Fig. 4.1. The liquid limits for these soils ranged from 42 to 97 percent, and the plasticity indices ranged from 30 to 71 percent. All but three of the soils represented in Fig. 4.1 are classified as highly plastic clays, CH, under the Unified Soil Classification System. The other three soils have liquid limits less than 50 percent and would be classified as clays with low to medium plasticity, CL.

The liquid limit of the worst soil from the stable slope at U.S. Highway 79 and Carlos G. Parker Boulevard in District 14 (not shown in Fig. 4.1) was 62 percent, and the corresponding plasticity index was 44 percent. These values would plot in the midregion of the values shown in Fig. 4.1. This soil is classified as a highly plastic clay, CH, under the Unified Soil Classification System.

An examination of Fig. 4.1 reveals no distinct grouping of soils from any given District. It should also be pointed out that although efforts were made to sample the "problem" soil at each site, it is certainly possible that the problem soil, the soil primarily responsible for failure, was not always sampled.

The soils from District 12, shown in Fig. 4.1, were obtained from embankments in the Houston area. These soils probably originate from the Beaumont Formation, a Pleistocene deposit which extends along the Gulf Coast. Vijayvergia and Sullivan (1973) presented the Atterberg limits for a total of 184 samples of Beaumont clay which were collected and tested. Their samples were obtained along the Gulf Coast, predominantly from the Houston area. The plasticity index and liquid limit for these

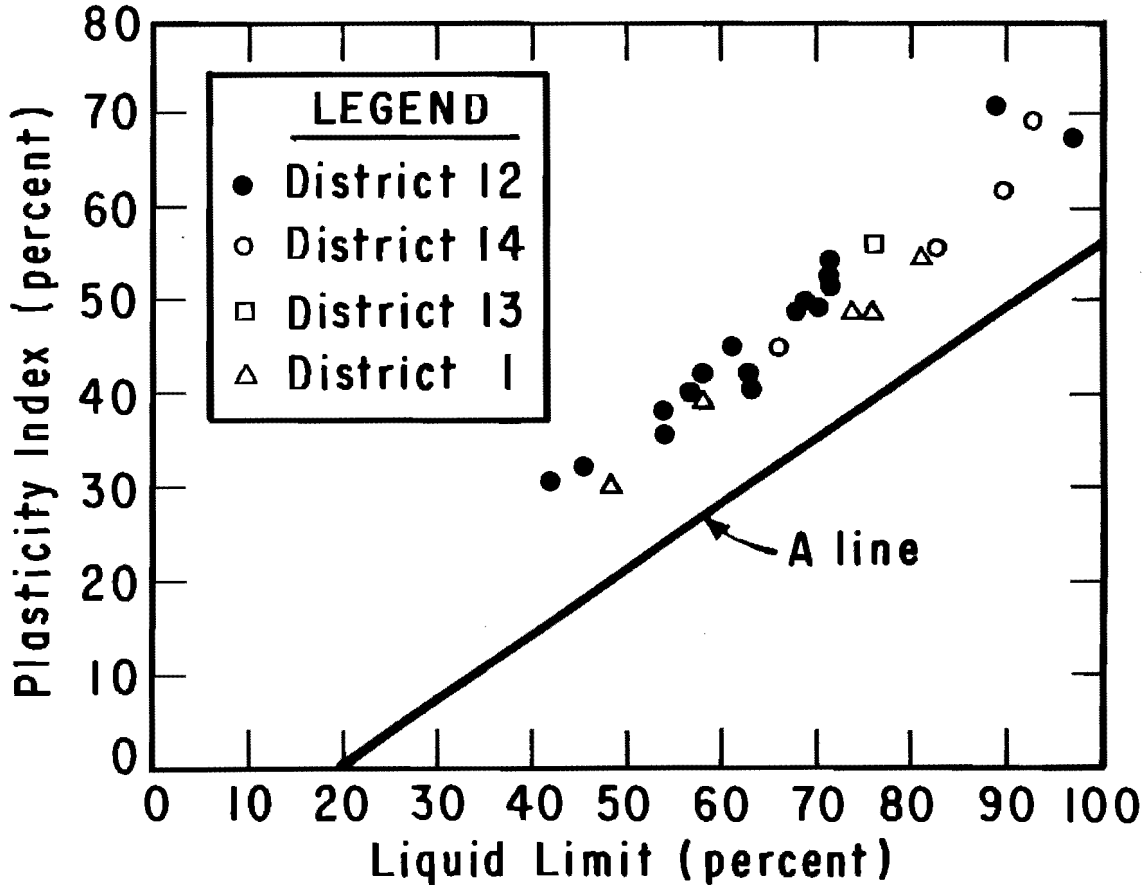

Fig. 4.1. Plasticity chart with Atterberg limits for soils from embankments which failed in Districts 1, 12, 13, and 14.

soils are plotted on a plasticity chart in Fig. 4.2. The liquid limits for these soils ranged from 33 to 76 percent, and the plasticity indices ranged from 18 to 55 percent. All but two of the problem soils from District 12 tested in this study have Atterberg limits which fall within the ranges reported by Vijayvergia and Sullivan. The two soils outside the range reported by Vijayvergia and Sullivan have liquid limits (97 and 89 percent) and plasticity indices (67 and 71 percent) which are significantly higher than any reported by Vijayvergia and Sullivan.

Grain Size Distributions

Hydrometer tests were performed to determine the grain size distributions for each of the soils represented in Table 4.1. In accordance with standard practice (ASTM D422), only the fraction of air-dried soil passing the No. 10 sieve was used. The amount of material retained on the No. 10 sieve was typically small and consisted of either hardened lumps of clay or small shell fragments. At the end of the hydrometer tests, the portion of the soil retained on a No. 200 sieve was determined by performing a wet sieve analysis. The percent by weight finer than the No. 200 sieve and the percent by weight finer than 2 microns, for each of the soils tested, are shown in Table 4.1.

Grain size distribution curves for the problem soils are presented in Fig. 4.3 for District 12, Fig. 4.4 for District 14, Fig. 4.5 for District 13, Fig. 4.6 for District 1, and Fig. 4.7 for the stable embankment slope in District 14. The shaded region shown in each of

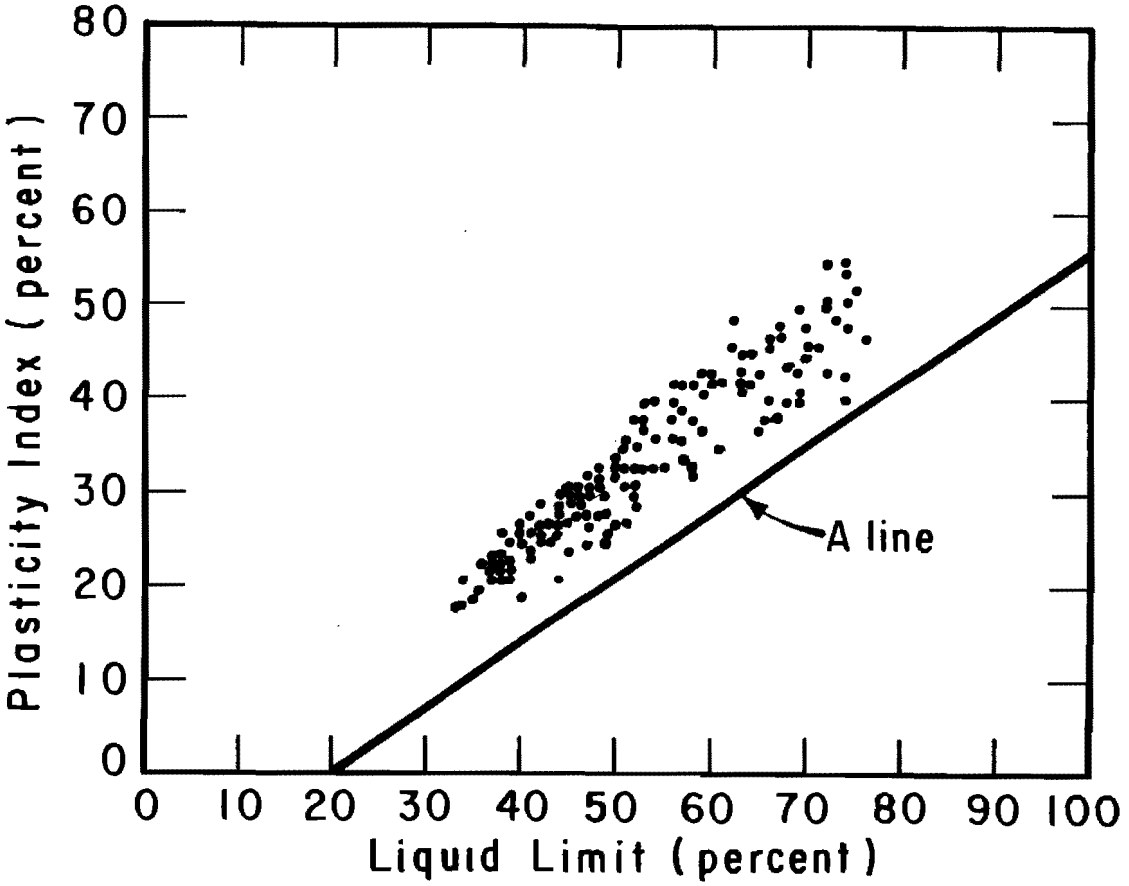

Fig. 4.2. Plasticity chart with Atterberg limits for Beaumont clay as reported by Vijayvergiya and Sullivan (1973).

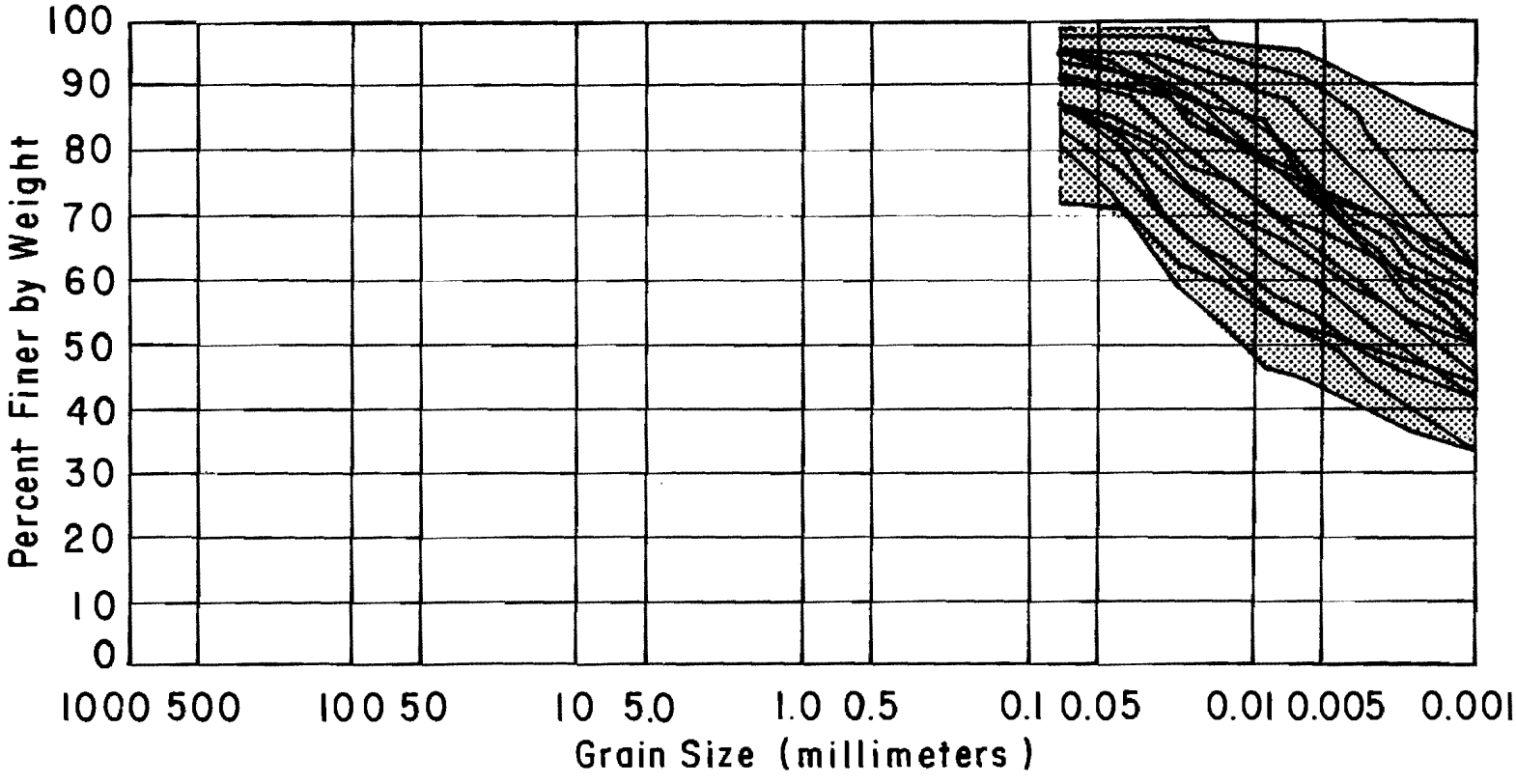

Fig. 4.3. Grain size distribution curves for problem soils from embankment slope failures in District 12.

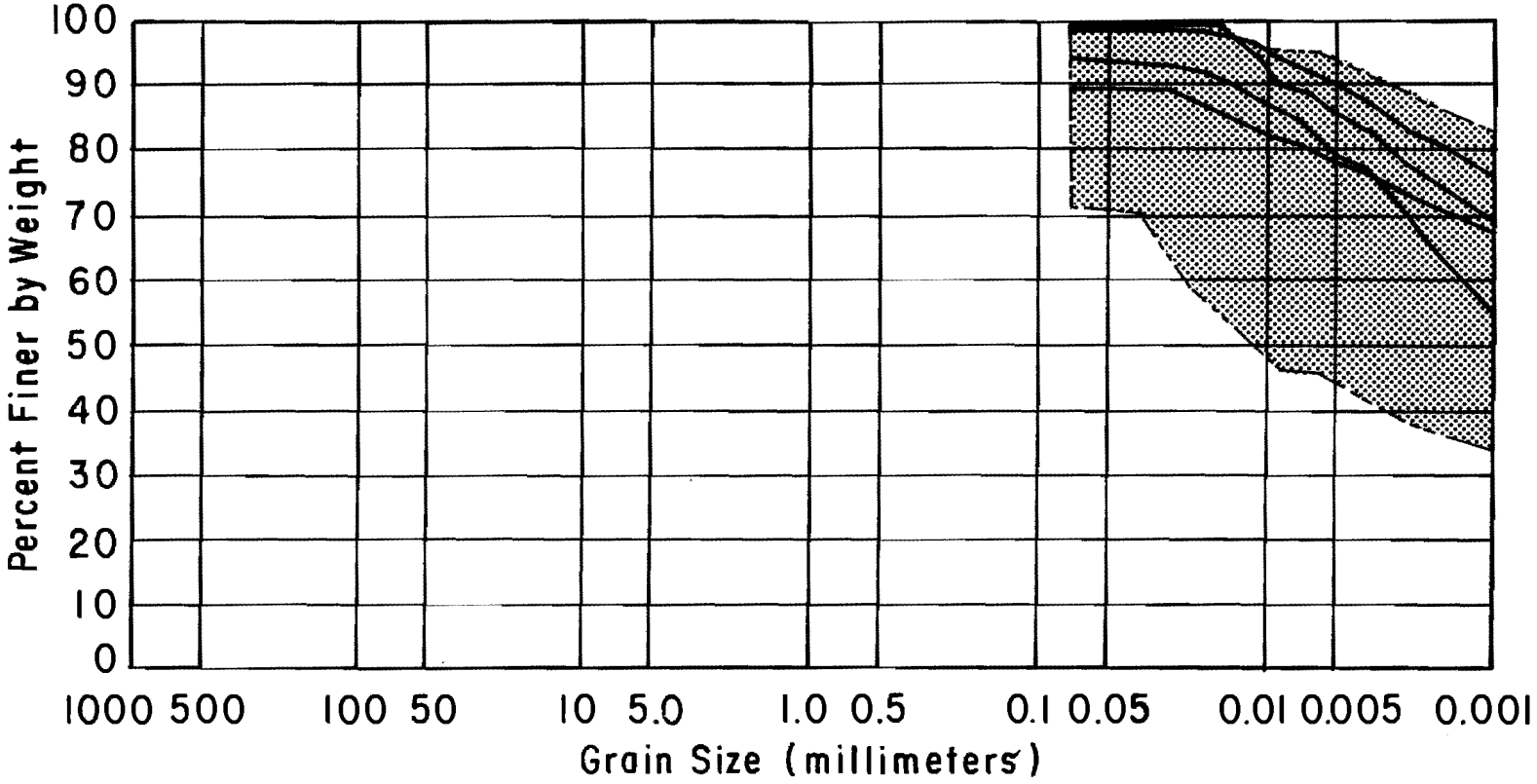

Fig. 4.4. Grain size distribution curves for problem soils from embankment slope failures in District 14.

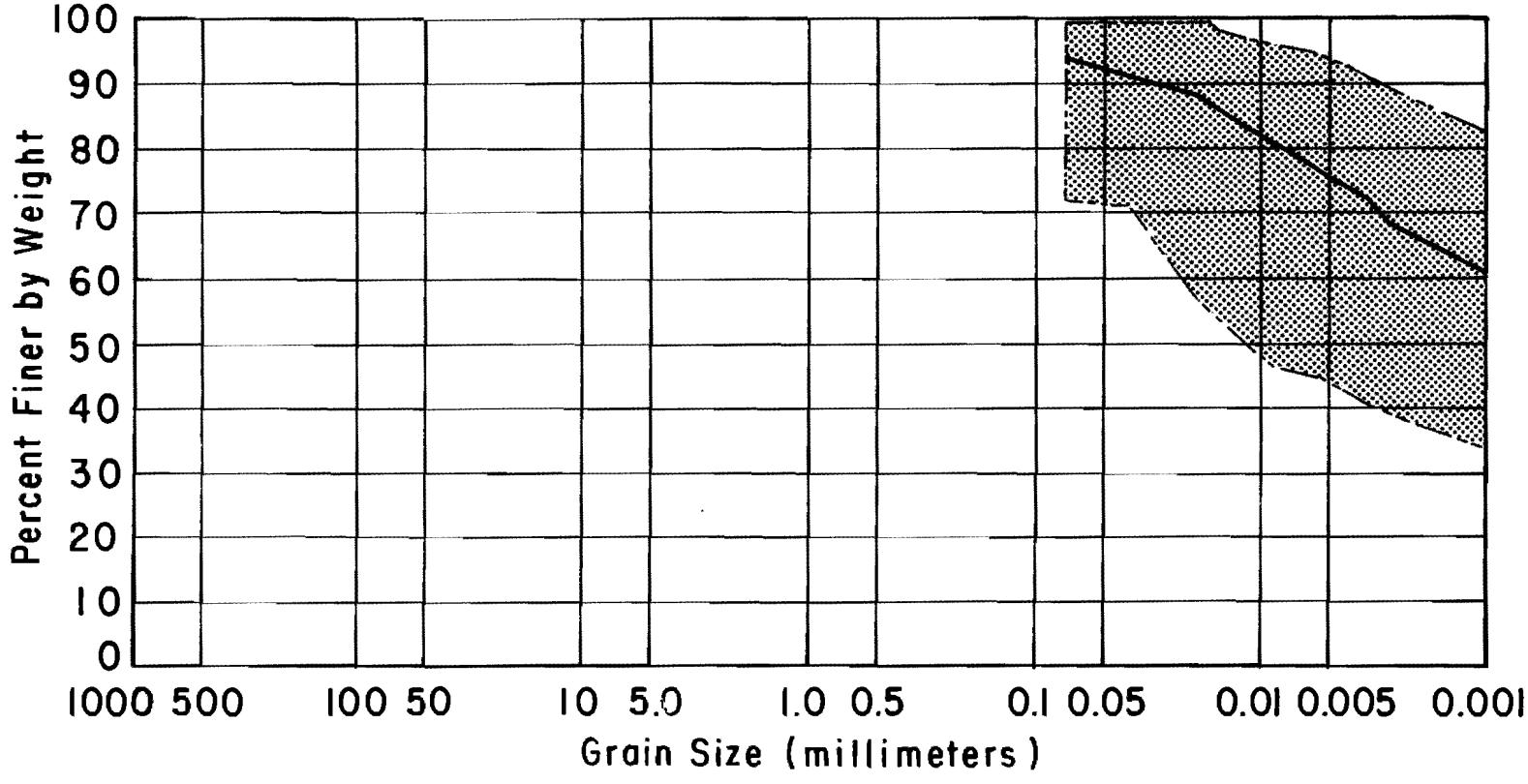

Fig. 4.5. Grain size distribution curve for problem soil from the embankment slipe failure in District 13.

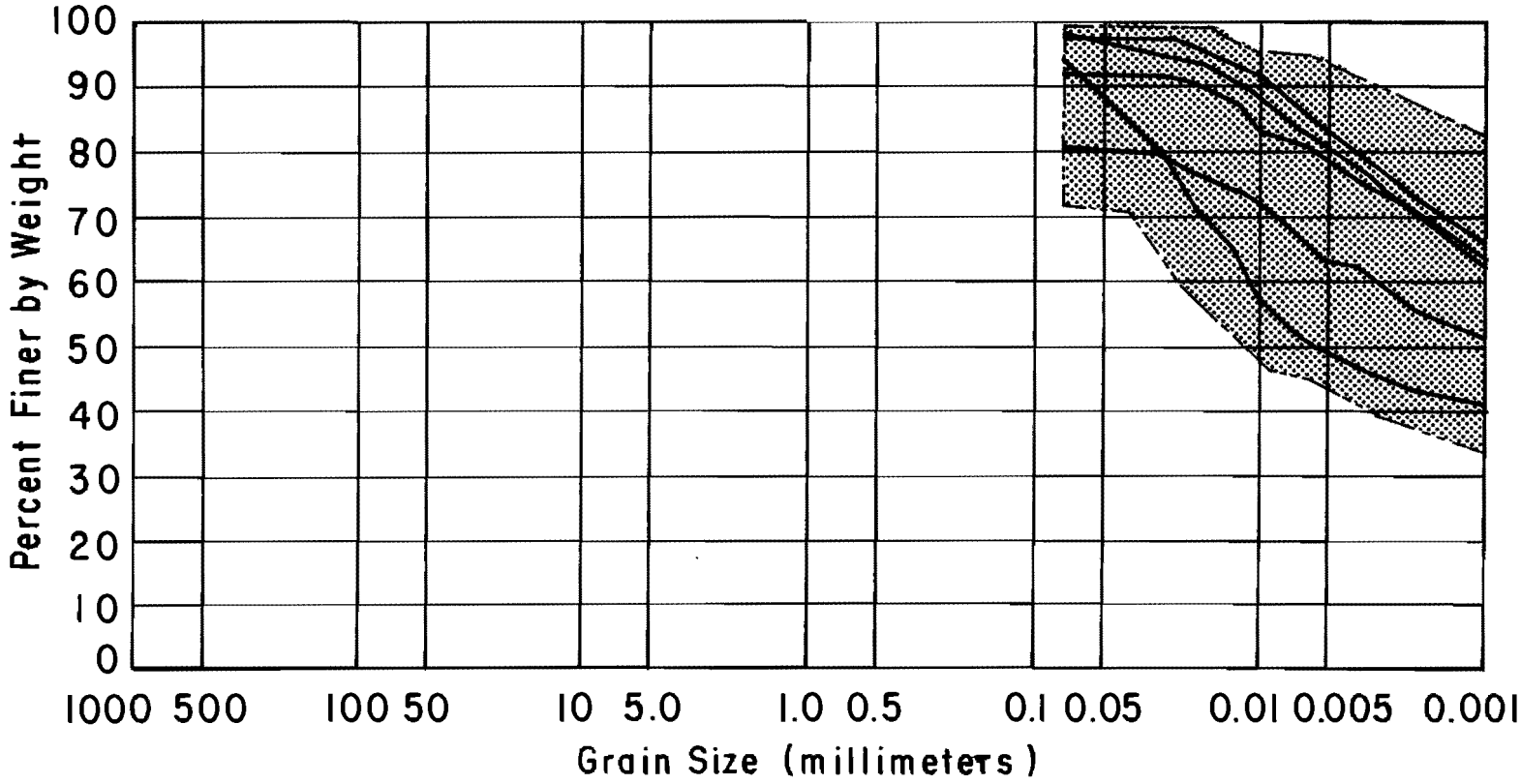

Fig. 4.6. Grain size distribution curves for problem soils from embankment slope failure in District 1.

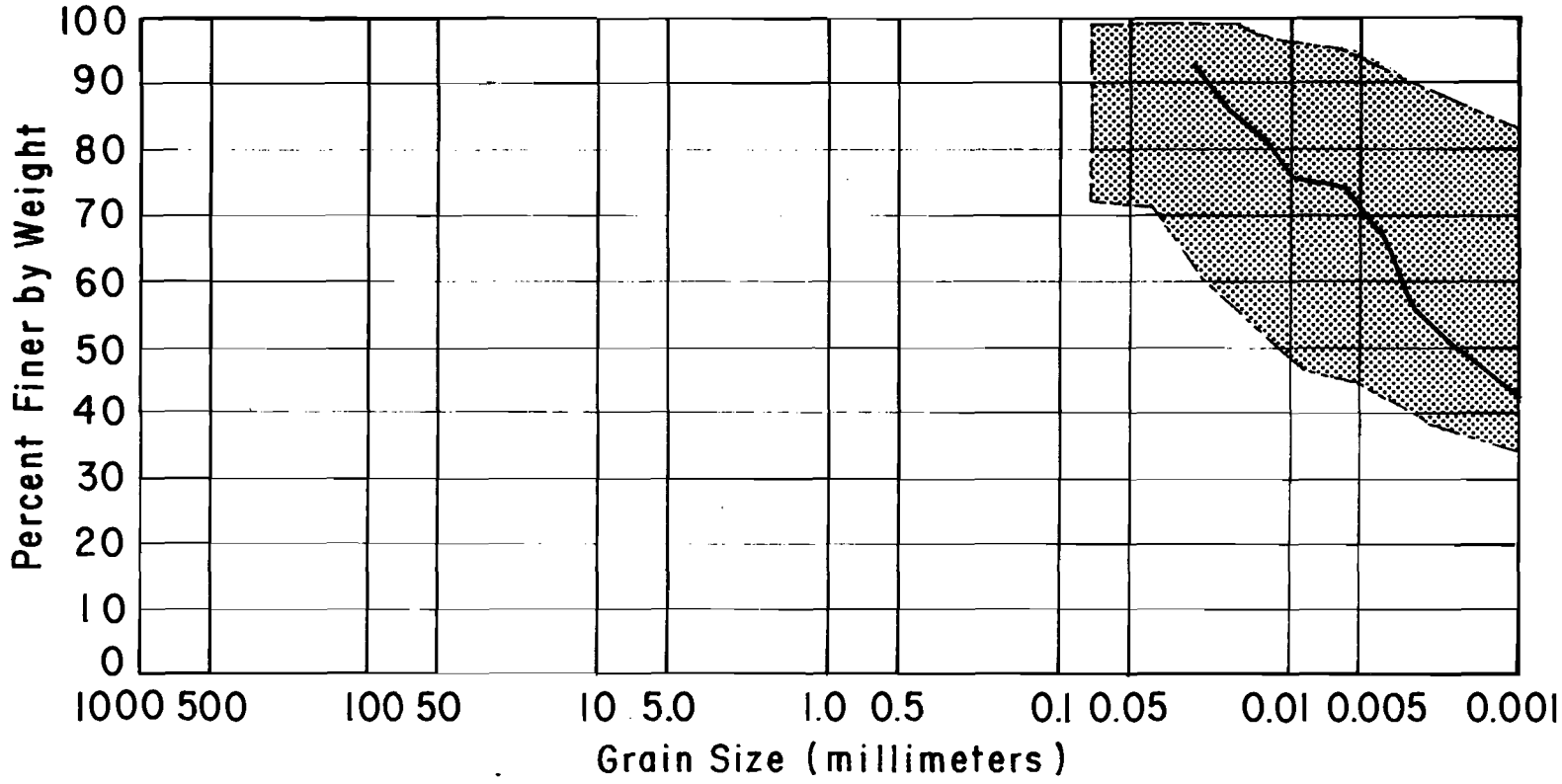

Fig. 4.7. Grain size distribution curve for worst soil from the stable slope near U.S. 79 and Carlos G. Parker Blvd. in District 14.

these figures represents the total range of grain size distribution curves for all twenty-eight problem soils from all four Districts. For these problem soils, the percent by weight finer than the No. 200 sieve ranged from 72 to 99, and the percent by weight finer than 2 microns ranged from 37 to 86. The grain size distribution curves for problem soils from District 12 ,shown in Fig. 4.3, encompass almost the entire range of gradation curves shown by the shaded region. The curves for problem soils from District 12 appear to be about evenly distributed throughout the shaded region. The grain size distribution curves for problem soils from District 14, shown in Fig. 4.4, lie in the upper portion of the shaded region, indicating that these soils tend to be finer grained. The grain size distribution curve for the problem soil from District 13, shown in Fig. 4.5, falls approximately in the middle of the shaded region. Grain size distribution curves for problem soils from District 1, shown in Fig. 4.6, range from the upper to the lower portions of the shaded region and appear to be about evenly distributed within this region.

The grain size distribution curve for the worst soil from the stable slope at U.S. Highway 79 and Carlos G. Parker Boulevard in District 14 is shown in Fig. 4.7. This curve plots about in the middle of the shaded region.

Activity

The activity, A, of a soil as defined by Skempton (1953) is obtained by dividing the plastity index (in percent) by the percent by weight of soil finer than 2 microns, as follows:

$$\text{Activity, A} = \frac{\text{Plasticity Index}}{\text{percent by weight finer than 2 microns}} \quad (4.1)$$

The activities for the various soils collected from embankment slopes are shown in Table 4.1.

In Fig. 4.8, the plasticity index is plotted versus the clay fraction (percent by weight finer than 2 microns) for the problem soils from each of the embankment slides. By plotting the plasticity index against the clay fraction, soils with similar activities will fall on straight lines radiating from the origin. The dashed lines on Fig. 4.8 represent the locus of points for activities equal to 0.50, 0.75, and 1.00. Activities for the problem soils shown in Fig. 4.8 range from 0.54 to 1.05, the mean value is 0.79 and the standard deviation is 0.10. While there is a wide range in both the plasticity index and the clay fraction, the activities do not vary significantly. The problem soils from District 12 have slightly higher activities (the mean value is 0.81) while the problem soils from District 1 have slightly lower activities (the mean value is 0.71). The activity for the problem soil from District 13 was 0.85. Problem soils from District 14 have high plasticity indices and high clay fractions. Thus, the data for problem soils from District

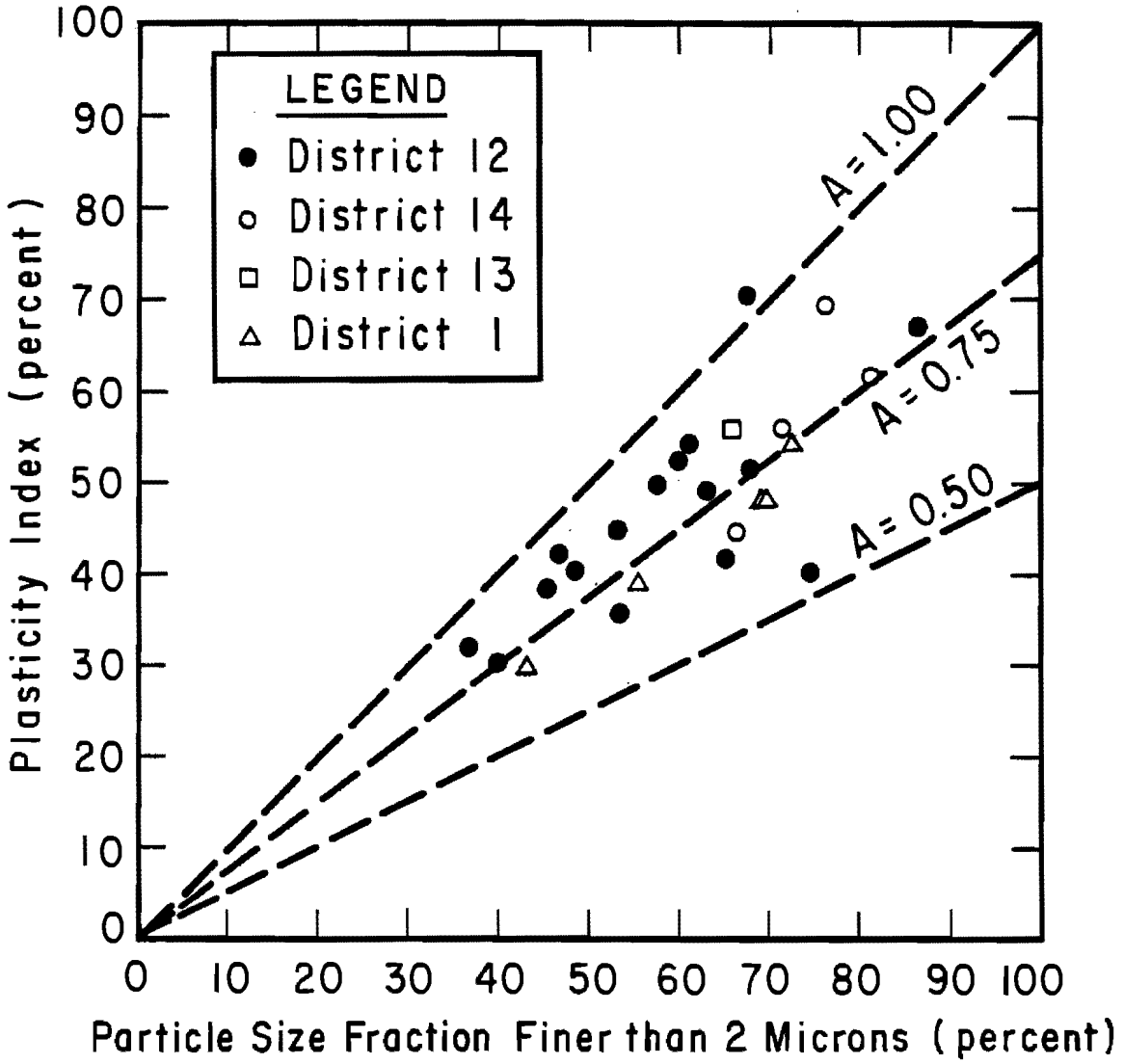

Fig. 4.8. Variation of plasticity index with particle size fraction finer than 2 microns for soils from embankments which failed in Districts 1, 12, 13, and 14.

14 plot in the upper region of Fig. 4.8; however, the mean value for the activities of these soils is 0.79, which is identical to the overall mean value for all of the problem soils. For the soils examined and presented in Fig. 4.8 there does not appear to be any significant grouping or variation from one District to the next.

CLAY MINERALOGY

A limited number of X-ray diffraction analyses was performed to identify the type of clay minerals present in two of the soils. The soils selected for this purpose were the red and grey clays from the embankment slide at IH 610 and Scott Street in District 12. The X-ray diffraction analyses were performed using the facilities of the Geology Department at The University of Texas at Austin. From these analyses, the presence of calcium montmorillonite, illite, kaolinite, quartz, and calcite were detected for the red clay. For the grey clay, calcium montmorillonite, kaolinite, and quartz were detected. This is in agreement with the findings of Vijayvergia and Sullivan (1973). For Beaumont clay they cited montmorillonite and illite as the clay minerals with non-clay minerals of quartz and feldspar.

WATER CONTENTS

Water contents were measured for each of the bag samples

obtained from hand auger borings and test pit excavations. The water content was not measured for bag samples from excavations near the surface because these soils were believed to experience extreme variations in moisture content due to environmental changes. In addition, many of the near surface samples were not sealed adequately when sampled and, therefore, reliable determination of the water content was not possible.

A summary of water content data is presented in Table 4.2. Included in this summary for each water content measured are 1) a note describing whether the sample was obtained from the slide mass or from the adjacent, stable slope, 2) the type of sample, 3) the depth below the ground surface where the sample was taken, 4) the color of the material sampled, and 5) the measured water content. Measured water contents ranged from 14.0 to 40.6 percent. The mean water content measured was 29.7 percent with a standard deviation of 5.3 percent.

Variation in Water Content with Depth

Water content data obtained from hand auger boring samples taken at various depths show how the water content varied with depth. The hand auger borings were located either in the slide mass, generally near the center of this mass, or in the adjacent, stable slope at about midheight of the slope. Water content data from within and outside the slide area are considered separately in the following presentation. It should also be noted that water content versus depth data are available for embankment slides only in District 12.

TABLE 4.2. SUMMARY OF WATER CONTENT DATA FOR EMBANKMENT SLIDES

Slope Location	District	Site ID	Location of Sample	Type of Sample	Depth of Sample (ft)	Description of Material	Water Content (percent)
IH 610 @ Scott St., NE quadrant, Harris Co.	12	A	Slide scarp	Hand auger	2.0	Red w/ grey	34.3
			" "	" "	3.5	Red w/ grey	36.3
			Adjacent to slide	" "	1.5	Red w/ grey	34.1
			" " "	" "	2.5	Tan w/ red	30.4
			" " "	" "	3.5	Red w/ grey	29.7
			Slide mass	Test pit	--	Red w/ grey	32.4
			" "	" "	--	Black/dark grey	30.9
SH 225 @ SH 146, SW quadrant, Harris Co.	12	B	Slide mass	Hand auger	1.5	Grey w/ red	28.8
			" "	" "	2.5	Grey w/ red	27.0
			" "	" "	3.5	Grey/brown	29.6
			Adjacent to slide	" "	1.2	Grey/brown	32.0
			" " "	" "	2.5	Grey w/ red	31.2
			" " "	" "	3.5	Grey w/ red	27.7
			Slide mass	Test pit	--	Grey/brown	34.5
			" "	" "	--	Black/dark grey	31.6

(continued)

TABLE 4.2. (Continued)

Slope Location	Dis-trict	Site ID	Location of Sample	Type of Sample	Depth of Sample (ft)	Description of Material	Water Content (percent)
SH 225 @ SH 146, NW quadrant, Harris Co.	12	C	Slide mass	Hand auger	1.5	Grey w/ red	28.9
			" "	" "	2.5	Grey w/ red	30.0
			" "	" "	3.5	Grey w/ red	31.8
			Adjacent to slide	" "	1.5	Red/brown w/ grey	38.3
			" " "	" "	2.5	Grey w/ red	32.3
			" " "	" "	3.5	Grey w/ red	25.8
			Slide mass	Test pit	2.5	Grey w/ brown	27.8
			" "	" "	2.8	Grey w/ red	28.9
			" "	" "	4.0	Grey w/ red	30.0
			" "	" "	--	Black/dark grey	29.2
SH 225 @ SH 146, NE quadrant, Harris Co.	12	D	Slide mass	Hand auger	1.5	Grey	36.0
			" "	" "	2.5	Grey	33.1
			" "	" "	3.5	Grey w/ red	24.4

(continued)

TABLE 4.2. (Continued)

Slope Location	District	Site ID	Location of Sample	Type of Sample	Depth of Sample (ft)	Description of Material	Water Content (percent)
SH 225 @ Southern Pacific RR Overpass, SE quadrant, Harris Co.	12	E	Slide mass (west)	Hand auger	1.5	Grey	23.1
			" " "	" "	2.3	Tan	38.1
			Slide mass (east)	" "	1.7	Grey	26.7
			" " "	" "	3.3	Grey	29.9
			Between slide masses	" "	0.8	Grey	24.3
			" " "	" "	2.0	Grey	27.0
			" " "	" "	3.5	Grey	31.7
			" " "	" "	4.0	Grey	25.0
SH 225 @ Southern Pacific RR Overpass, SW quadrant, Harris Co.	12	F	Slide mass	Hand auger	0.8	Brown/red/grey	38.6
			" "	" "	1.5	Brown/red/grey	39.8
			" "	" "	2.0	Brown/red/grey	40.6
			" "	" "	3.0	Grey	33.2
			Adjacent to slide	" "	1.0	Tan/grey	27.2
			" " "	" "	2.0	Grey	29.4
			" " "	" "	3.0	Grey	31.7
			" " "	" "	3.5	Tan	36.4

(continued)

TABLE 4.2. (Continued)

Slope Location	Dis-trict	Site ID	Location of Sample	Type of Sample	Depth of Sample (ft)	Description of Material	Water Content (percent)
SH 225 @ Southern Pacific RR Overpass, NW quadrant, Harris Co.	12	G	Slide mass	Hand auger	1.5	Grey w/ tan	35.7
			" "	" "	2.0	Grey w/ tan	35.9
			" "	" "	2.5	Dark grey w/ red	21.3
SH 225 @ Scarborough, SE quadrant, Harris Co.	12	H	Slide mass	Hand auger	2.0	Grey	27.8
IH 610 @ SH 225, SE quadrant, Harris Co.	12	I	Slide mass	Hand auger	0.8	Grey	14.0
			" "	" "	2.3	Grey	26.3
			" "	" "	3.0	Grey w/ red	25.0
IH 610 @ Richmond St., SW quadrant, Harris Co.	12	J	Slide mass	Hand auger	1.5	Grey	27.8
			" "	" "	2.3	Grey w/ tan	28.5
			" "	" "	2.5	Grey/white/tan	23.9
			" "	" "	3.5	Grey w/ red	25.2

(continued)

TABLE 4.2. (Continued)

Slope Location	District	Site ID	Location of Sample	Type of Sample	Depth of Sample (ft)	Description of Material	Water Content (percent)
IH 10 @ Crosby-Lynchburg, NW quadrant, Harris Co.	12	K	Slide scarp	Test pit	0.3	Grey/brown	29.2
			" "	" "	0.3	Grey/brown	25.6
			Slide mass	Hand auger	1.0	Grey/brown	27.9
			" "	" "	2.0	Grey/brown	23.0
			" "	" "	3.5	Grey/brown	27.4
			Adjacent to slide	" "	1.5	Grey/brown	27.9
			" " "	" "	2.5	Grey/brown	31.5
			" " "	" "	3.5	Grey	23.1
IH 45 @ SH 146, SE quadrant, Harris Co.	12	L	Slide mass	Hand auger	0.8	Grey	22.1
			" "	" "	1.3	Red w/ grey	34.2
			" "	" "	2.7	Red	26.6
IH 45 @ SH 146, south side, Harris Co.	12	M	Slide mass	Hand auger	1.3	Red w/ grey	30.1
			" "	" "	2.0	Red w/ grey	32.2
			" "	" "	3.0	Red w/ grey	32.9

(continued)

TABLE 4.2. (Continued)

Slope Location	Dis-trict	Site ID	Location of Sample	Type of Sample	Depth of Sample (ft)	Description of Material	Water Content (percent)
IH 45 @ FM 2351, NE quadrant, Harris Co.	12	N	Slide mass	Hand auger	0.8	Red	28.3
			" "	" "	1.5	Light grey w/ red	25.1
			" "	" "	2.2	Grey/red	28.2
			" "	" "	2.7	Grey w/ red	23.5
IH 45 @ College St., NE quadrant, Harris Co.	12	O	Slide mass	Hand auger	0.8	Grey	37.5
			" "	" "	1.8	Tan	33.9
U.S. 59 @ FM 525, NE quadrant, Harris Co.	12	P	Slide mass	Hand auger	1.3	Grey w/ tan	19.3
			" "	" "	2.5	Tan w/ grey	23.8
			" "	" "	3.3	Dark grey	17.4
U.S. 59 @ Shepard St., SE quadrant, Harris Co.	12	Q	Slide mass	Hand auger	1.8	Grey w/ tan	31.4
			" "	" "	2.0	Grey w/ tan	29.9
			" "	" "	2.5	Tan	30.7
			" "	" "	3.5	Tan	26.1

(continued)

TABLE 4.2. (Continued)

Slope Location	Dis-trict	Site ID	Location of Sample	Type of Sample	Depth of Sample (ft)	Description of Material	Water Content (percent)
Loop 286 @ SH 271 Interchange, NW quadrant, Lamar Co.	1	R	Slide mass	Test pit	1.5	Light brown	33.2
Loop 286 @ Missouri Pacific RR Overpass, SW quadrant (north slide), Lamar Co.	1	S	Slide mass	Test pit	1.5	Grey	24.7
Loop 286 @ Missouri Pacific RR Overpass, SW quadrant (south slide), Lamar Co.	1	T	Slide mass	Test pit	2.5	Tan	40.6
Loop 286 @ Missouri Pacific RR Overpass, NW quadrant, Lamar Co.	1	U	Slide mass	Test pit	1.5	Grey & tan	40.3
Loop 286 @ FM 79, SW quadrant, Lamar Co.	1	V	Slide mass	Test pit	1.5	Tan	38.4

The variation in water content with depth determined from samples obtained from hand auger borings within the area of the slide mass are shown in Fig. 4.9. The data points from each boring are connected by straight lines. There does not appear to be any consistent variation of water content with depth. Most of the water contents fall within the range of from 20 to 40 percent. It is not known if the water contents shown in Fig. 4.9 are representative of the values which existed at the time of failure. Changes in the topography of the slide area following the occurrence of the failure, combined with environmental factors, may affect the degree to which the measured water contents, shown in Fig. 4.9, represent conditions which existed at the time of failure.

The variation in water content with depth determined from samples obtained from hand auger borings outside the slide area are illustrated on Fig. 4.10. Once again, there does not appear to be any consistent variation of water content with depth. Most of the water contents fall within the range of from 25 to 35 percent.

The considerable variation in water content with depth which is illustrated in Figs. 4.9 and 4.10 may be due to the combination of environmental factors and variations in the soil type over the relatively shallow depths explored (0 to about 3.5 feet). Environmental factors will have a greater effect on the water content of soils near the slope surface than on soils at depth. The depth to which environmental flucuations will influence water contents is not known and is perhaps itself dependant on numerous factors. Undisturbed Shelby tube samples have recently been obtained from the IH 610 and Scott Street site in District

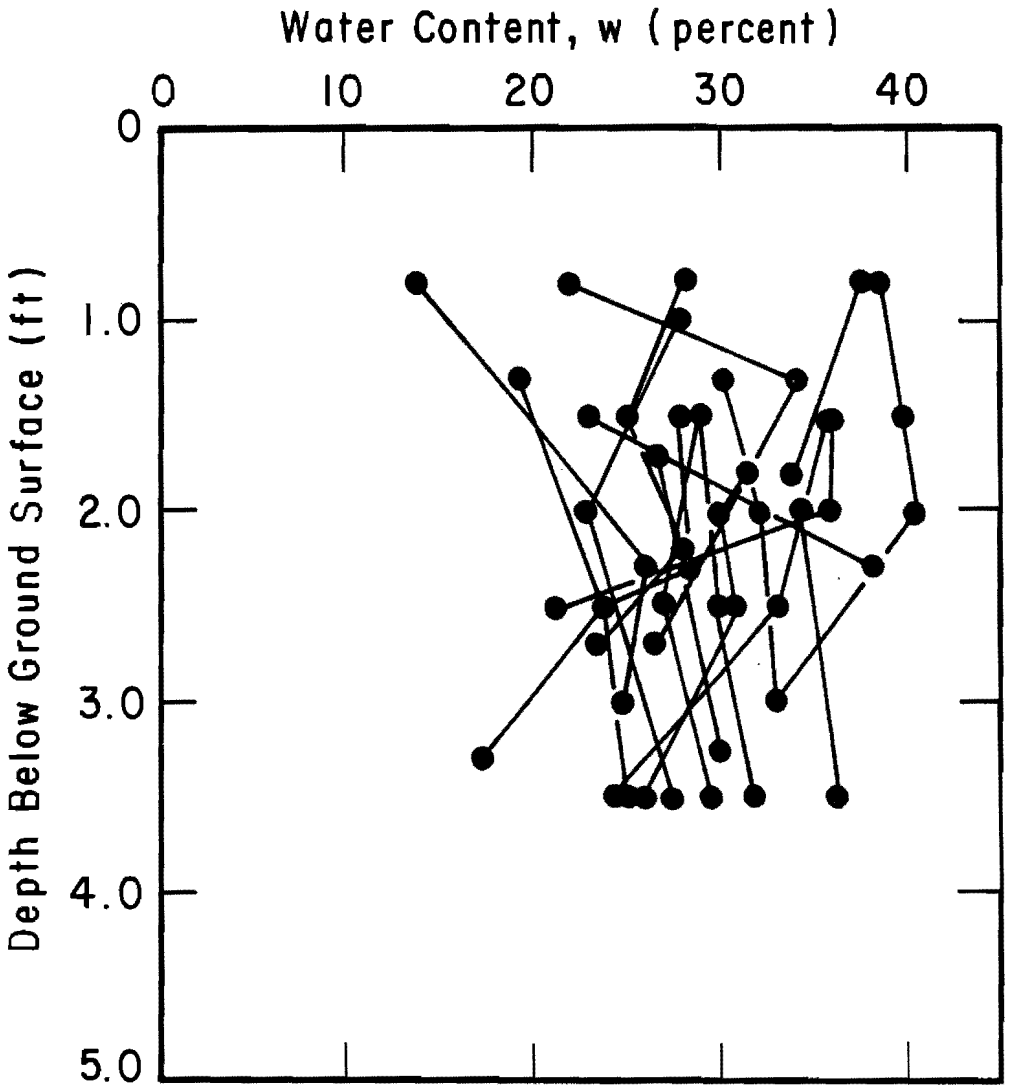

Fig. 4.9. Variation in water content with depth obtained for samples from borings in the slide mass.

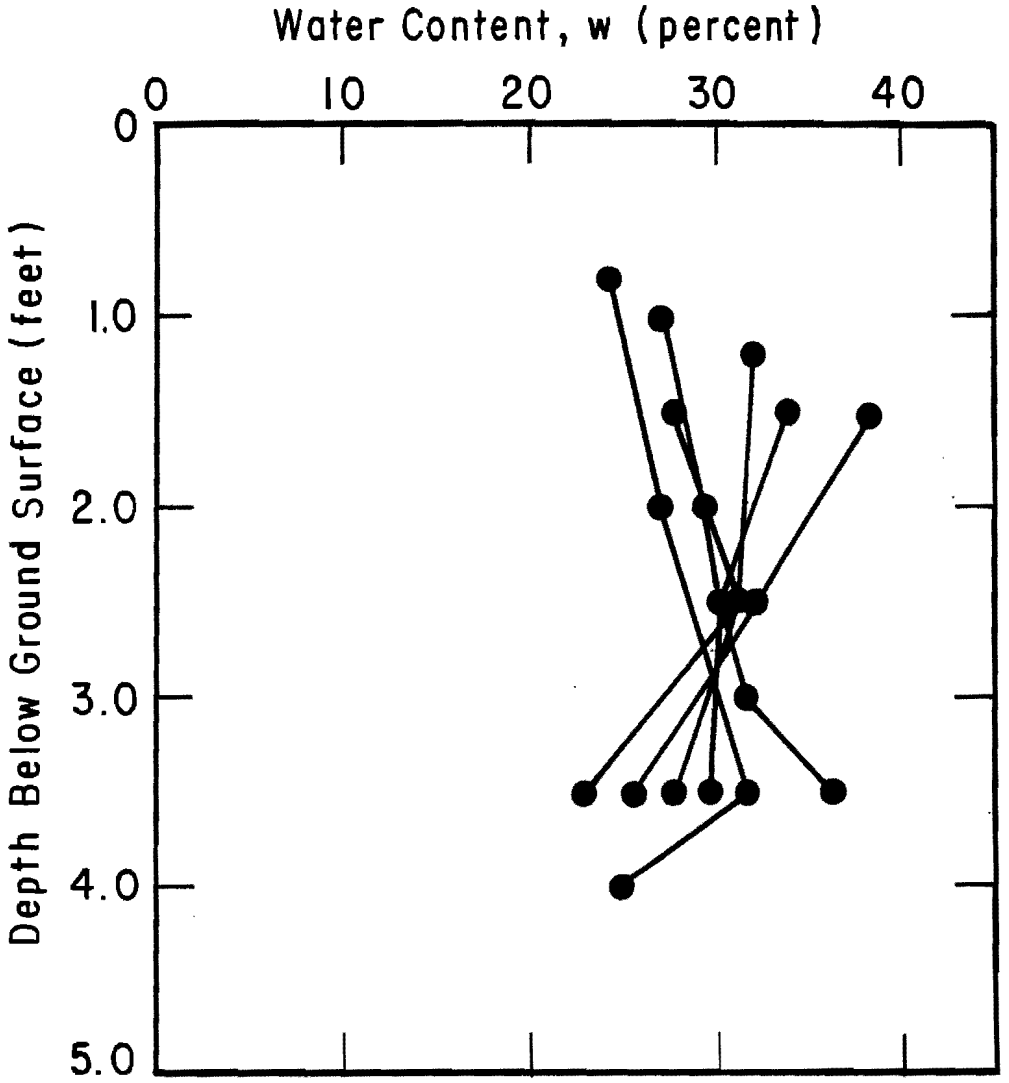

Fig. 4.10. Variation in water content with depth obtained for samples from borings adjacent to embankment slide.

12 as part of a continuing laboratory testing program. Preliminary water content data from these samples indicate that water contents for the more highly plastic red clay are generally greater than for the grey clay.

Liquidity Indices

Liquidity indices were calculated for each of the sites where water content data were available. The liquidity indices are defined by and were calculated from the following equation:

$$\text{Liquidity Index, L.I.} = \frac{\omega_n - \omega_{PL}}{\omega_{LL} - \omega_{PL}} \qquad (4.2)$$

where w_n is the natural water content, w_{PL} is the plastic limit, and w_{LL} is the liquid limit. The liquidity indices calculated are summarized in Fig. 4.11, along with the corresponding water contents and Atterberg limit values used to compute the liquidity indices. The site ID corresponds to the slope location as shown in Table 4.2. In Fig. 4.11, the upper and lower horizontal bars represent the liquid and plastic limits, respectively, while the length of the vertical line connecting these marks represents the plasticity index for the problem soil. The symbols represent water contents. Where a range of water contents was measured at a site, this range is shown by a heavy vertical line connecting a pair of symbols. The liquidity index shown at the top of Fig. 4.11 was determined using the highest water content measured at each site. The highest water content measured was not always measured for the sample which was

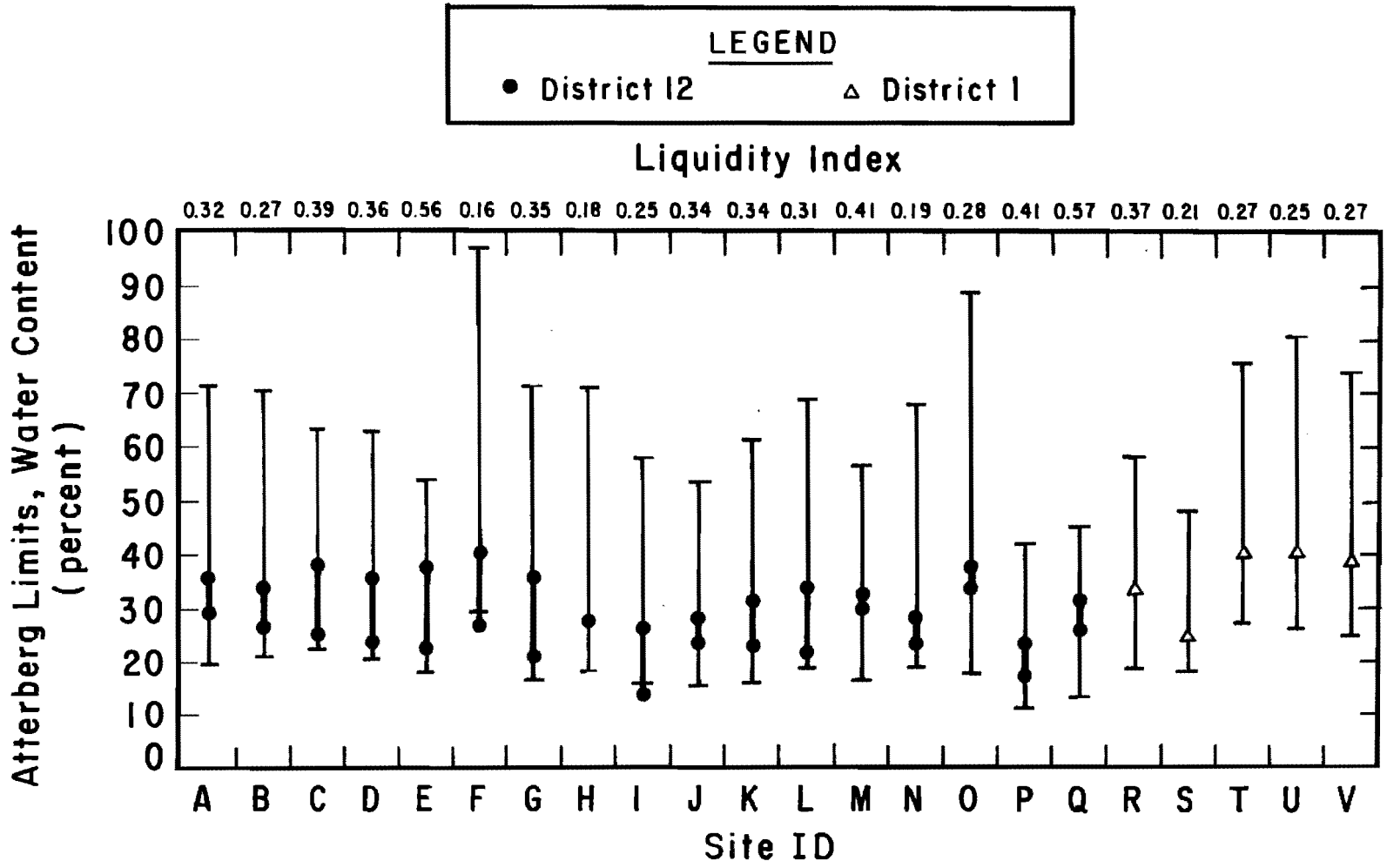

Fig. 4.11. Summary of Atterberg limits, water contents and liquidity indices for soils from embankments which failed in Districts 1 and 12.

identified as the problem soil and, therefore, the liquidity indices were in some instances calculated using Atterberg limit values and water contents determined for different soils.

Values of the liquidity index range from 0.16 to 0.57. The mean value is 0.32, and the standard deviation is 0.11. Sowers (1979) states that, based on limited data, little swell will occur after a soil reaches a liquidity index of about 0.25. Based on this, the majority of the soils shown in Fig. 4.11 would appear to be in the vicinity of their fully swelled condition.

The liquidity index is plotted versus the slope ratio for embankment slides in Districts 12 and 1 in Fig. 4.12. Examining the data shown in Fig. 4.12, it appears that failure generally occurred on steeper slopes at lower liquidity indices and on flatter slopes at higher liquidity indices. Thus, failure may have occurred on some of the steeper slopes prior to their reaching a fully swelled, "long-term" condition. It appears that the data in Fig. 4.12 define a stability "envelope" shown approximately by the dashed line in Fig. 4.12. Most slopes with liquidity indices and slope ratios which plot below the line defining this envelope would be expected to remain stable while slopes which would plot above this line may fail. The scatter of points above the stability envelope line shown in Fig. 4.12 may be due to nonhomogenieties within the embankment slopes. The presence of stronger materials within the slopes might restrict failure, whereas, if the embankment slopes were homogeneous, consisting of the problem soil, they would have failed at lower liquidity indices.

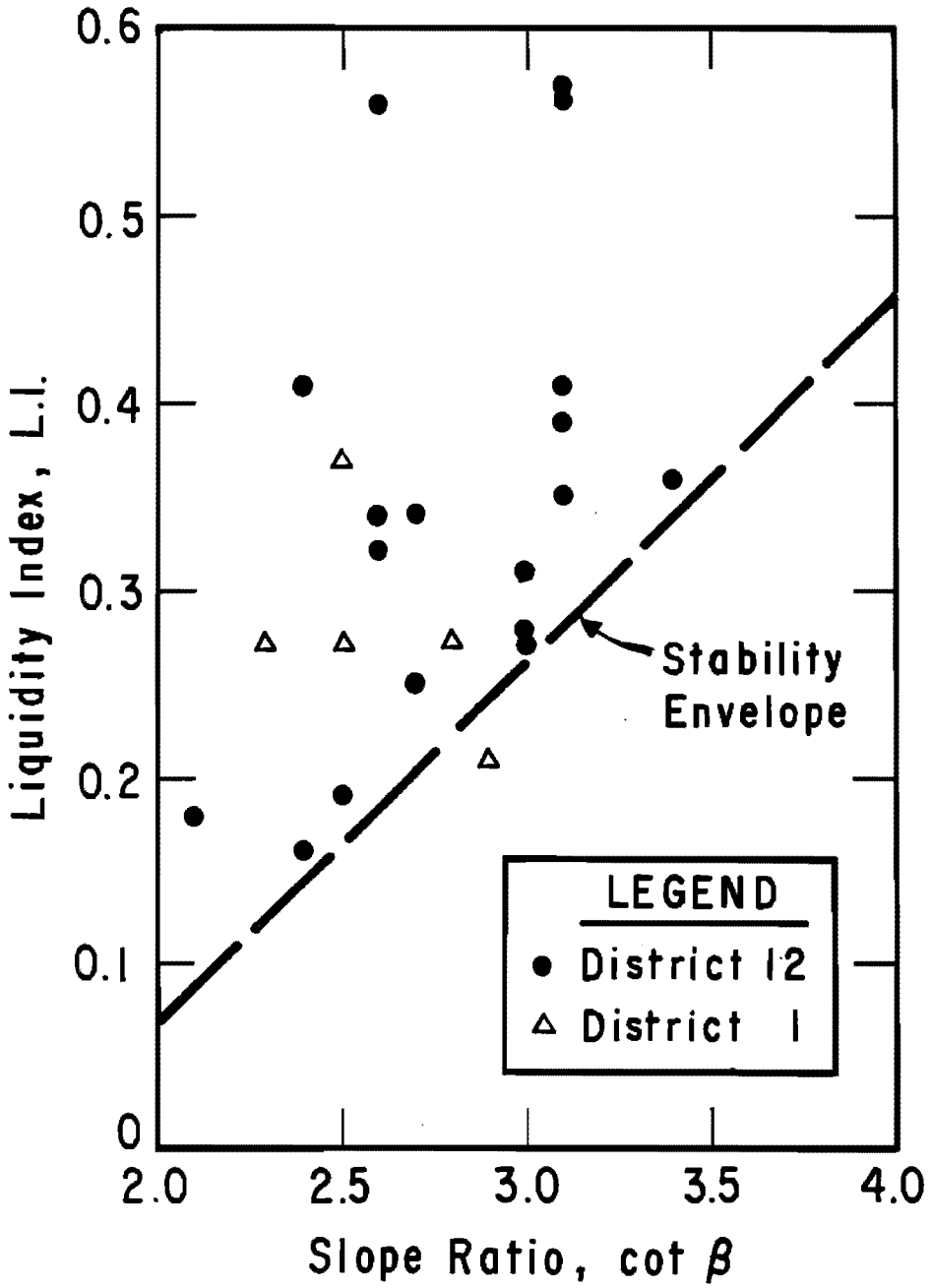

Fig. 4.12. Variation of liquidity index with slope ratio (cot β) for soils from embankments which failed in Districts 1 and 12.

BACK-CALCULATED SHEAR STRENGTH PARAMETERS

No direct measurements of shear strength properties were made as part of this study. However, the slope geometry and slide dimension data presented in Chapter Two were used to back-calculate shear strength parameter values following the procedures outlined in Chapter Three. These back-calculated shear strength parameters were then examined in order to establish if any correlations exist with the index properties presented earlier in this chapter. In addition, the back-calculated friction angles are examined to determine if they agree with values which are typically obtained for these materials.

Selection of Parameters and Summary of Values

The slope geometry and slide dimension data used to back-calculate shear strength parameters are summarized on Table 4.3. The sliding surfaces for most of the embankment slides examined were restricted to the face of the slope, rather than intersecting the top, flatter portion of the embankment slope. Thus, the charts developed in Chapter Three for face failures (Figs. 3.5, 3.8 and 3.9) were used to back-calculate the shear strength parameters presented here.

Values for the effective stress cohesion, $\bar{c}$, and angle of internal friction, $\bar{\phi}$, were back-calculated using pore pressure ratios, r_u, of zero, 0.2, and 0.4 for each of the embankment slides. An assumed total unit weight of soil, γ, of 120 pcf was used for back-calculation in all

TABLE 4.3. SUMMARY OF BACK-CALCULATED SHEAR STRENGTH PARAMETERS FOR EMBANKMENT SLIDES

Slope Location	District	Height of Slide, h (ft)	Slope Ratio, cot β	Depth Ratio, d/h	Back-Calculated Shear Strength Parameters (Face Failure)					
					$r_u = 0$		$r_u = 0.2$		$r_u = 0.4$	
					$\bar{c}$ (psf)	$\bar{\phi}$ (degrees)	$\bar{c}$ (psf)	$\bar{\phi}$ (degrees)	$\bar{c}$ (psf)	$\bar{\phi}$ (degrees)
IH 610 @ Scott St., NE quadrant, Harris Co.	12	17.0	2.6	0.21	8.2	18.8	8.8	23.8	10.2	31.4
SH 225 @ SH 146, SW quadrant, Harris Co.	12	13.0	3.0	0.33	15.0	14.7	15.3	18.6	17.0	24.6
SH 225 @ SH 146, NW quadrant, Harris Co.	12	14.0	3.1	0.17	2.7	17.0	2.9	21.3	3.2	28.4
SH 225 @ SH 146, NE quadrant, Harris Co.	12	13.5	3.4	0.26	5.7	14.7	5.8	18.5	6.0	24.7
SH 225 @ Southern Pacific RR Overpass, SE quadrant, Harris Co.	12	21.0	2.6	0.19	8.1	19.4	8.3	24.4	9.1	32.3
		12.0	3.1	0.25	5.8	15.9	6.1	20.0	6.5	26.7

(continued)

TABLE 4.3. (Continued)

Slope Location	District	Height of Slide, h (ft)	Slope Ratio, cot β	Depth Ratio, d/h	Back-Calculated Shear Strength Parameters (Face Failure)					
					$r_u = 0$		$r_u = 0.2$		$r_u = 0.4$	
					$\bar{c}$ (psf)	$\bar{\phi}$ (degrees)	$\bar{c}$ (psf)	$\bar{\phi}$ (degrees)	$\bar{c}$ (psf)	$\bar{\phi}$ (degrees)
SH 225 @ Southern Pacific RR Overpass, SW quadrant, Harris Co.	12	23.5	2.4	0.21	13.8	19.8	14.7	24.9	13.0	33.1
SH 225 @ Southern Pacific RR Overpass, NW quadrant, Harris Co.	12	10.2	3.1	0.25	4.9	15.9	5.2	20.0	5.5	26.7
SH 225 @ Scarborough, SE quadrant, Harris Co.	12	19.0	2.1	0.16	9.1	23.2	10.3	29.1	11.9	38.5
IH 610 @ SH 225, SE quadrant, Harris Co.	12	12.0	2.7	0.17	3.6	19.0	3.7	24.0	3.7	32.0
IH 610 @ Richmond St., SW quadrant, Harris Co.	12	22.0	2.7	0.23	13.2	18.1	13.2	22.6	15.3	30.1

(continued)

TABLE 4.3. (Continued)

Slope Location	District	Height of Slide, h (ft)	Slope Ratio, cot β	Depth Ratio, d/h	Back-Calculated Shear Strength Parameters (Face Failure)					
					$r_u = 0$		$r_u = 0.2$		$r_u = 0.4$	
					$\bar{c}$ (psf)	$\bar{\phi}$ (degrees)	$\bar{c}$ (psf)	$\bar{\phi}$ (degrees)	$\bar{c}$ (psf)	$\bar{\phi}$ (degrees)
IH 10 @ Crosby-Lynchburg, NW quadrant, Harris Co.	12	19.0	2.6	0.26	16.2	17.7	17.3	22.4	20.1	29.5
IH 45 @ SH 146, SE quadrant, Harris Co.	12	15.0	3.0	0.20	4.3	17.1	4.5	21.4	4.9	28.5
IH 45 @ SH 146, south side, Harris Co.	12	13.0	3.1	0.27	7.8	15.6	8.0	19.6	8.9	26.1
IH 45 @ FM 2351, NE quadrant, Harris Co.	12	15.0	2.5	0.17	5.0	20.1	5.4	25.2	5.9	33.6
IH 45 @ College St., NE quadrant, Harris Co.	12	11.4	3.0	0.18	2.7	17.3	2.7	21.6	3.3	28.8

(continued)

TABLE 4.3. (Continued)

Slope Location	District	Height of Slide, h (ft)	Slope Ratio, cot β	Depth Ratio, d/h	Back-Calculated Shear Strength Parameters (Face Failure)					
					$r_u = 0$		$r_u = 0.2$		$r_u = 0.4$	
					$\bar{c}$ (psf)	$\bar{\phi}$ (degrees)	$\bar{c}$ (psf)	$\bar{\phi}$ (degrees)	$\bar{c}$ (psf)	$\bar{\phi}$ (degrees)
U.S. 59 @ FM 525, NE quadrant, Harris Co.	12	16.4	2.4	0.18	7.1	20.5	7.5	25.8	8.5	34.1
U.S. 59 @ Shepard St., SE quadrant, Harris Co.	12	13.3	3.1	0.26	7.3	15.8	7.5	19.8	8.1	26.3
U.S. 79 @ U.S. 95, SE quadrant, Williamson Co.	14	39.0	2.3	0.15	14.5	21.5	14.5	27.3	15.0	36.2
U.S. 77 @ SH 21, SW quadrant, Lee Co.	14	20.0	3.4	0.20	4.3	15.4	4.3	19.3	4.8	25.8
U.S. 77 @ SH 21, NW quadrant, Lee Co.	14	16.0	2.9	0.19	4.6	17.5	4.8	22.1	5.2	29.2

(continued)

TABLE 4.3. (Continued)

Slope Location	District	Height of Slide, h (ft)	Slope Ratio, cot β	Depth Ratio, d/h	Back-Calculated Shear Strength Parameters (Face Failure)					
					$r_u = 0$		$r_u = 0.2$		$r_u = 0.4$	
					$\bar{c}$ (psf)	$\bar{\phi}$ (degrees)	$\bar{c}$ (psf)	$\bar{\phi}$ (degrees)	$\bar{c}$ (psf)	$\bar{\phi}$ (degrees)
U.S. 290 ~ 5 miles east of IH 35, NW quadrant, Travis Co.	14	38.0	2.5	0.16	11.4	20.2	11.9	25.4	13.2	33.9
U.S. 87 @ Loop 175, NW quadrant, Victoria Co.	13	30.7	2.2	0.16	13.6	22.2	14.7	28.0	16.2	37.2
Loop 286 @ SH 271 Interchange, NW quadrant, Lamar Co.	1	14.1	2.5	0.29	17.9	17.2	18.4	21.8	21.5	28.6
Loop 286 @ Missouri Pacific RR Overpass, SW quadrant, Lamar Co.	1	15.0	2.9	0.53	59.4	10.5	61.4	13.2	65.7	17.3
		26.2	2.8	0.23	14.2	17.4	14.5	22.0	16.4	29.3

(continued)

TABLE 4.3. (Continued)

Slope Location	District	Height of Slide, h (ft)	Slope Ratio, cot β	Depth Ratio, d/h	Back-Calculated Shear Strength Parameters (Face Failure)					
					$r_u = 0$		$r_u = 0.2$		$r_u = 0.4$	
					$\bar{c}$ (psf)	$\bar{\phi}$ (degrees)	$\bar{c}$ (psf)	$\bar{\phi}$ (degrees)	$\bar{c}$ (psf)	$\bar{\phi}$ (degrees)
Loop 286 @ Missouri Pacific RR Overpass, NW quadrant, Lamar Co.	1	27.4	2.7	0.36	50.6	15.0	52.6	18.6	58.2	24.8
Loop 286 @ FM 79, SW quadrant, Lamar Co.	1	23.9	2.3	0.17	10.9	21.2	11.8	26.8	13.5	35.6

cases. This value corresponds to the approximate total unit weight of specimens of compacted clay following consolidation and saturation at low effective confining pressures as measured by Gourlay and Wright (1984). The shear strength parameters which were back-calculated are summarized in Table 4.3.

Discussion of Angle of Internal Friction

The angles of internal friction which were back-calculated were compared with the Atterberg limits, embankment slope angles, and assumed pore pressure ratio to determine if any relationship could be established between the friction angle and these other quantities. These comparisons and correlations are described in the next several sections.

Correlation with Atterberg Limits: The back-calculated angles of internal friction based on zero pore water pressures are plotted versus the plasticity index of the problem soils in Fig. 4.13 for each embankment slide. A similar plot of the back-calculated angle of internal friction versus liquid limit is shown in Fig. 4.14. The two plots do not show significantly different features since there is generally a direct relationship between the plasticity index and the liquid limit for these soils. Soils with high plasticity indices generally have high liquid limits, and soils with low plasticity indices generally have low liquid limits.

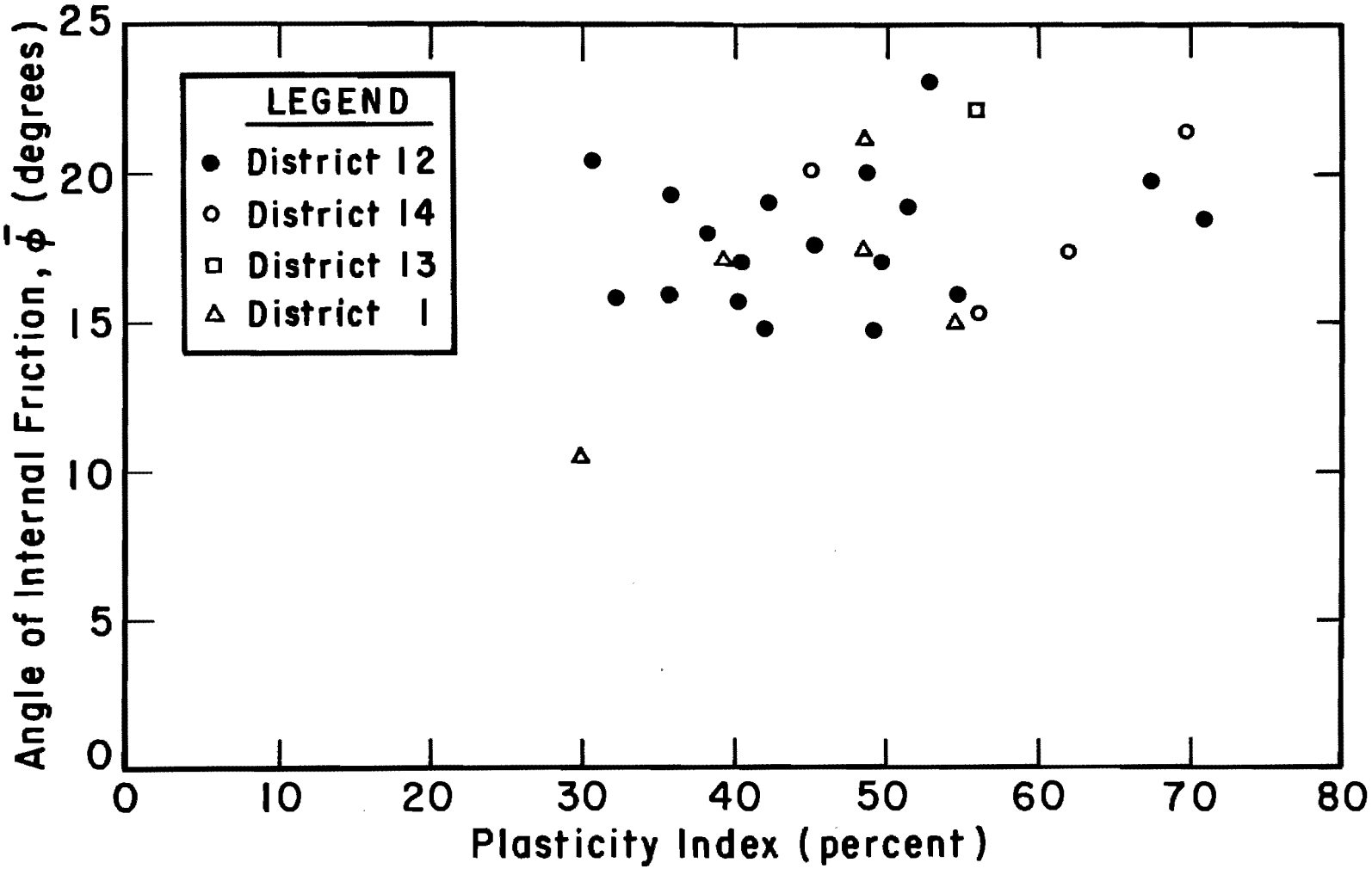

Fig. 4.13. Variation of back-calculated angles of internal friction ($\bar{\phi}$) with plasticity index of soils from embankments which failed in Districts 1, 12, 13, and 14 - zero pore water pressures assumed.

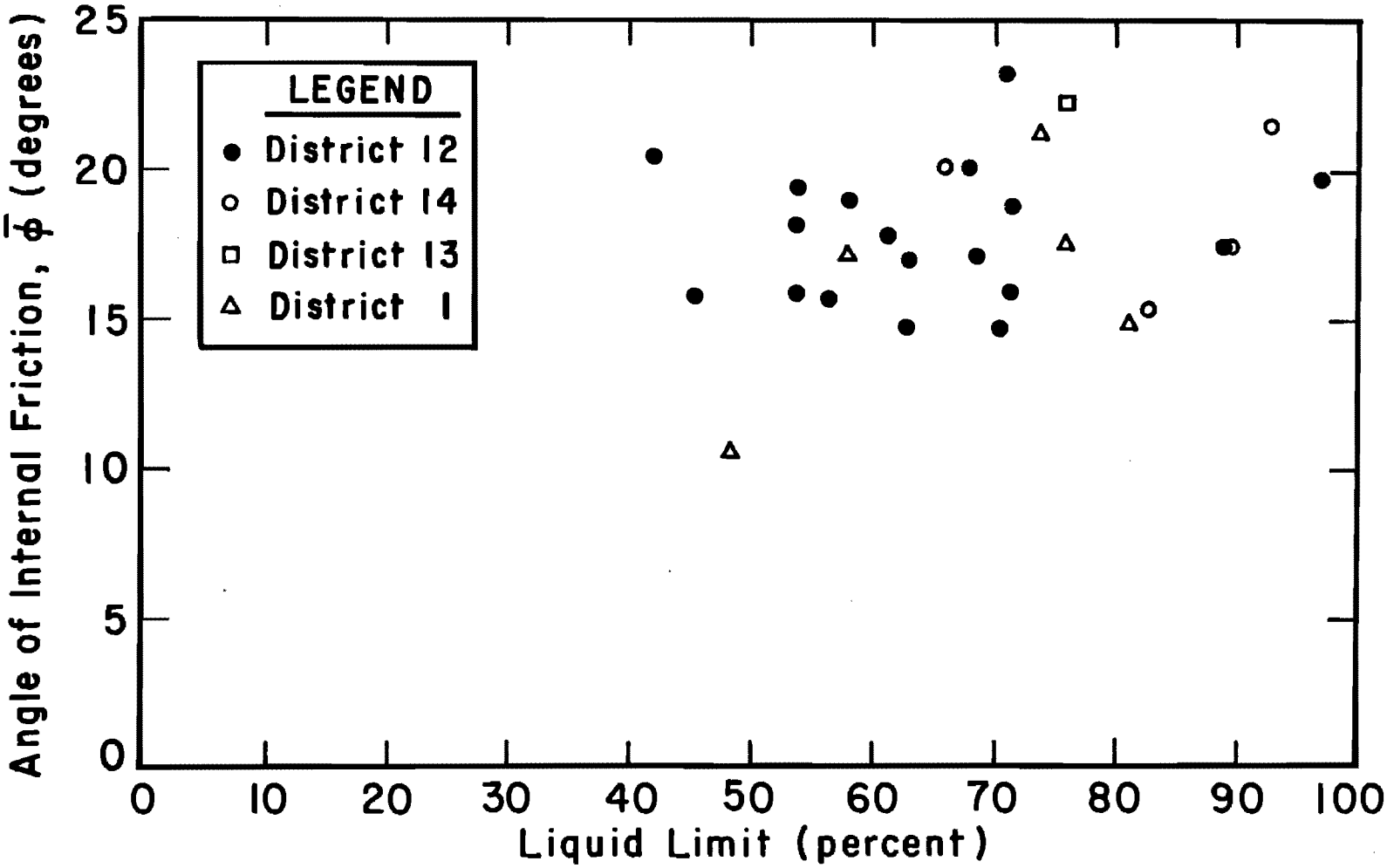

Fig. 4.14. Variation of back-calculated angles of internal friction ($\bar{\phi}$) with liquid limit of soils from embankments which failed in Districts 1, 12, 13, and 14 - zero pore water pressures assumed.

The data in Figs. 4.13 and 4.14 show no distinct relationship between the friction angle and either the plasticity index or the liquid limit. Other researchers have found a general trend of decreasing effective stress angle of internal friction with increasing plasticity index, as shown in Fig. 4.15, which illustrates some of the relationships which have been developed for various soils. The trends shown in Fig. 4.15 are not observed for the data shown in Figs. 4.13 and 4.14.

Influence of the Embankment Slope Angle: The back-calculated angles of internal friction based on zero pore water pressures are plotted versus the cotangent of the slope angle in Fig. 4.16. The variation of the angle of internal friction is found to be related to the slope angle for these failures. Steeper slopes, with smaller values of cotβ, have higher back-calculated friction angles, whereas the flatter slopes have lower back-calculated friction angles.

The lowest value of the back-calculated friction angle shown in Fig. 4.16, 10.5 degrees, corresponds to a very deep failure which occurred in District 1. The depth ratio for this slide is 0.53, the highest value of any of the slides examined. The highest values for the friction angles shown in Fig. 4.16 correspond to failures which occurred near the abutment and were therefore generally the steepest slopes. The mean value of the back-calculated friction angle for failures near the abutment was 21.7 degrees, and the standard deviation, 1.1 degrees. The mean value of the back-calculated friction angle for failures on side slopes was 17.0 degrees, and the standard deviation, 2.2 degrees.

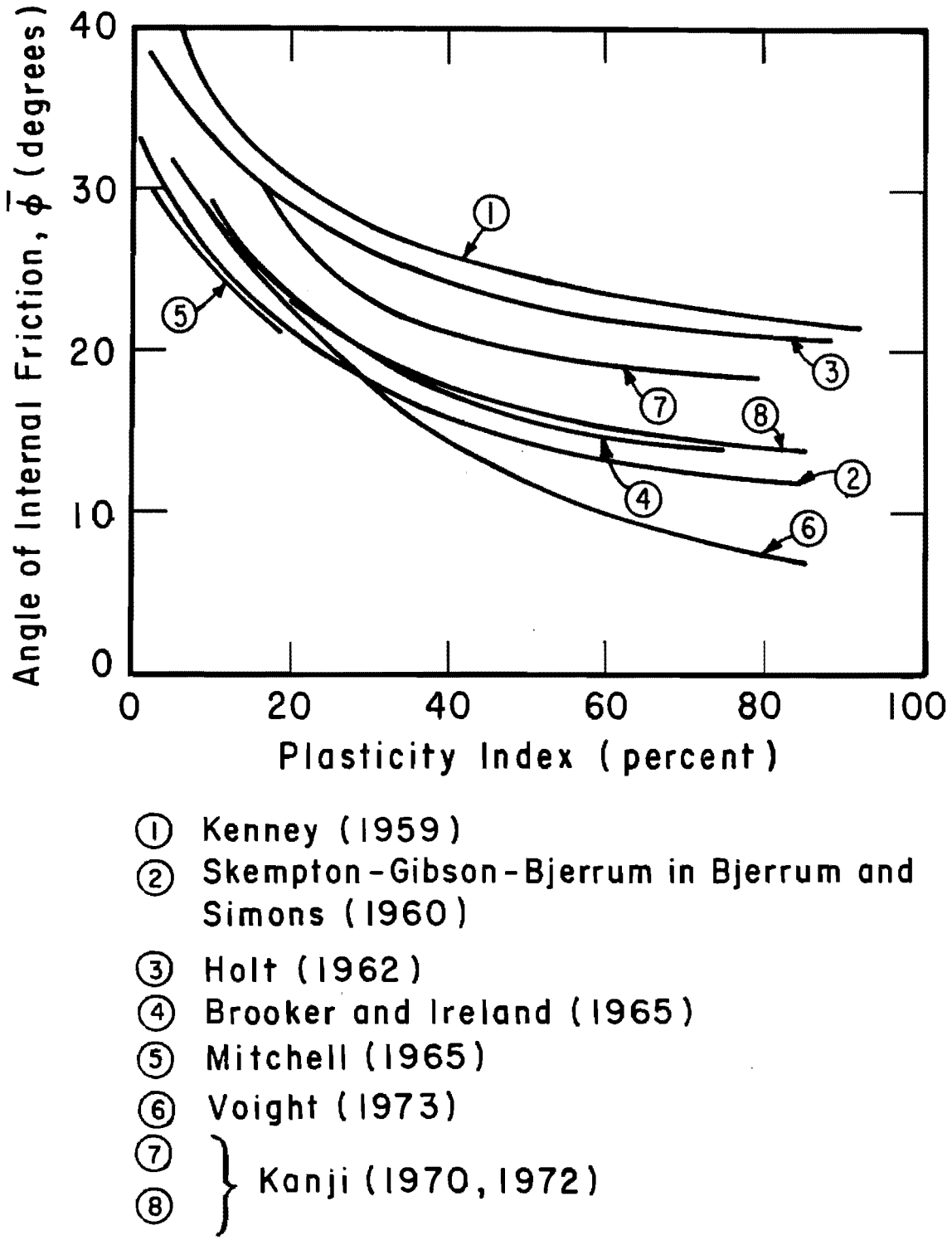

Fig. 4.15. Variations in friction angle ($\bar{\phi}$) with plasticity index as determined by various investigators (after Kanji, 1974).

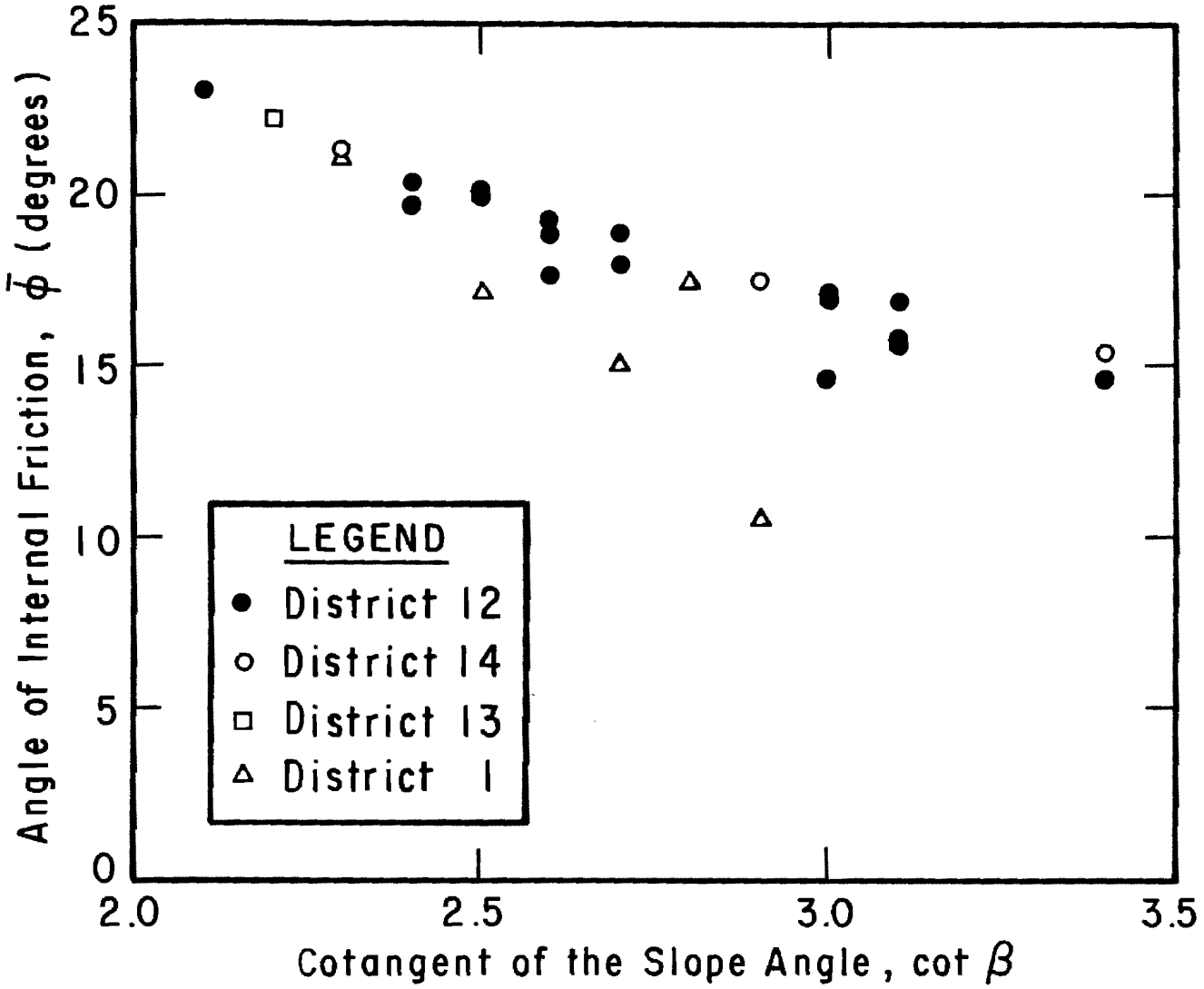

Fig. 4.16. Variation of back-calculated angle of internal friction ($\bar{\phi}$) with the cotangent of the slope angle (cot β).

If the soils in abutment failures had not reached a similar, fully swelled condition as soils from side slope failures at the time of failure, as was suggested earlier, in the section titled "Liquidity Indices," it follows that the pore pressure conditions within these slopes differ. This may explain why the friction angles which were back-calculated for the slides at the abutment are consistently higher than for the slides in the side slope (a 21.7 degree average for slides at the abutment versus a 17.0 degree average for slides in the side slope). A second possible explanation for the differences in back-calculated friction angles is that the geometry for abutment slopes and side slopes is fundamentally different. Abutment failures occur on the curved portion of the embankment and are therefore three dimensional in nature. Side slope failures, on the other hand, more closely approximate the two dimensional, plane strain conditions which were assumed for all stability calculations.

Influence of Pore Pressure Ratio, r_u: The friction angles examined in the previous sections were back-calculated based on the assumption that the pore water pressures were zero; the friction angles varied from 10.5 to 23.2 degrees. When a pore pressure ratio, r_u, of 0.2 was assumed, the corresponding angle of internal friction varied from 13.2 to 29.1 degrees, and when a pore water pressure ratio of 0.4 was assumed, the angle of internal friction varied from 17.3 to 38.5 degrees, as shown in Table 4.3. From these data it is apparent that the friction angle increases as the assumed pore pressure ratio increases. This increase in friction angle is found to be consistent from one site to the next. With

only slight variation, the back-calculated friction angle increases by 26 percent when the assumed pore pressure ratio is increased from zero to 0.2 and increases by 67 percent when the assumed pore pressure ratio is increased from zero to 0.4.

Friction angles back-calculated using the three values of the pore pressure ratio were compared with the friction angle values reported by other investigators for various soils as shown in Fig. 4.15. The back-calculated friction angles based on zero pore water pressures generally fall within the bounds formed by the values shown for other soils in Fig. 4.15, whereas, for pore pressure ratios of 0.2 and 0.4, the friction angles tend to be noticably higher than those for other soils. On this basis it appears that it is reasonable to assume zero pore pressures (a pore pressure ratio, r_u, of zero) for back-calculating shear strength parameters for the embankment slides examined in this study.

Back-Calculated Cohesion

The back-calculated cohesion values are also shown in Table 4.3 for zero pore water pressure and for pore pressure ratios of 0.2 and 0.4. The cohesion values range from 2.7 to 59.4 psf for zero pore water pressure, from 2.7 to 61.4 psf for a pore pressure ratio of 0.2, and from 3.2 to 65.7 psf for a pore pressure ratio of 0.4. The effect of pore pressure on the back-calculated cohesion value appears to be relatively minor.

The back-calculated cohesion values based on zero pore water pressures are plotted against the plasticity index for the problem soil from each embankment slide in Fig. 4.17. A similar plot of the back-calculated cohesion values versus the liquid limit is shown in Fig. 4.18. The two plots do not show significantly different features.

The data in Figs. 4.17 and 4.18 show no distinct relationship between the cohesion and either the plasticity index or the liquid limit. In addition, the cohesion does not appear to be related to the slope angle as was the case for the back-calculated friction angle. It was found, instead, that any variation in the back-calculated cohesion was more closely related to variations in the slide depth ratio. The highest values of cohesion (assuming zero pore water pressure) were 50.6 and 59.4 psf for two slides which occurred in District 1. These two slides had the largest depth ratios of all slides examined. Conversely, the lowest values of the back-calculated cohesion generally correspond to the slides with the smallest depth ratios.

DISCUSSION AND SUMMARY OF RESULTS

The Atterberg limit tests performed on soils from the embankment slides examined indicated that the "problem" soils sampled at each site have plasticity indices ranging from 30 to 71 percent and liquid limits ranging from 42 to 97 percent. Under the Unified Soil Classification System all but three of these soils are classified as highly plastic clays, CH, with the remaining three being classified as low to medium

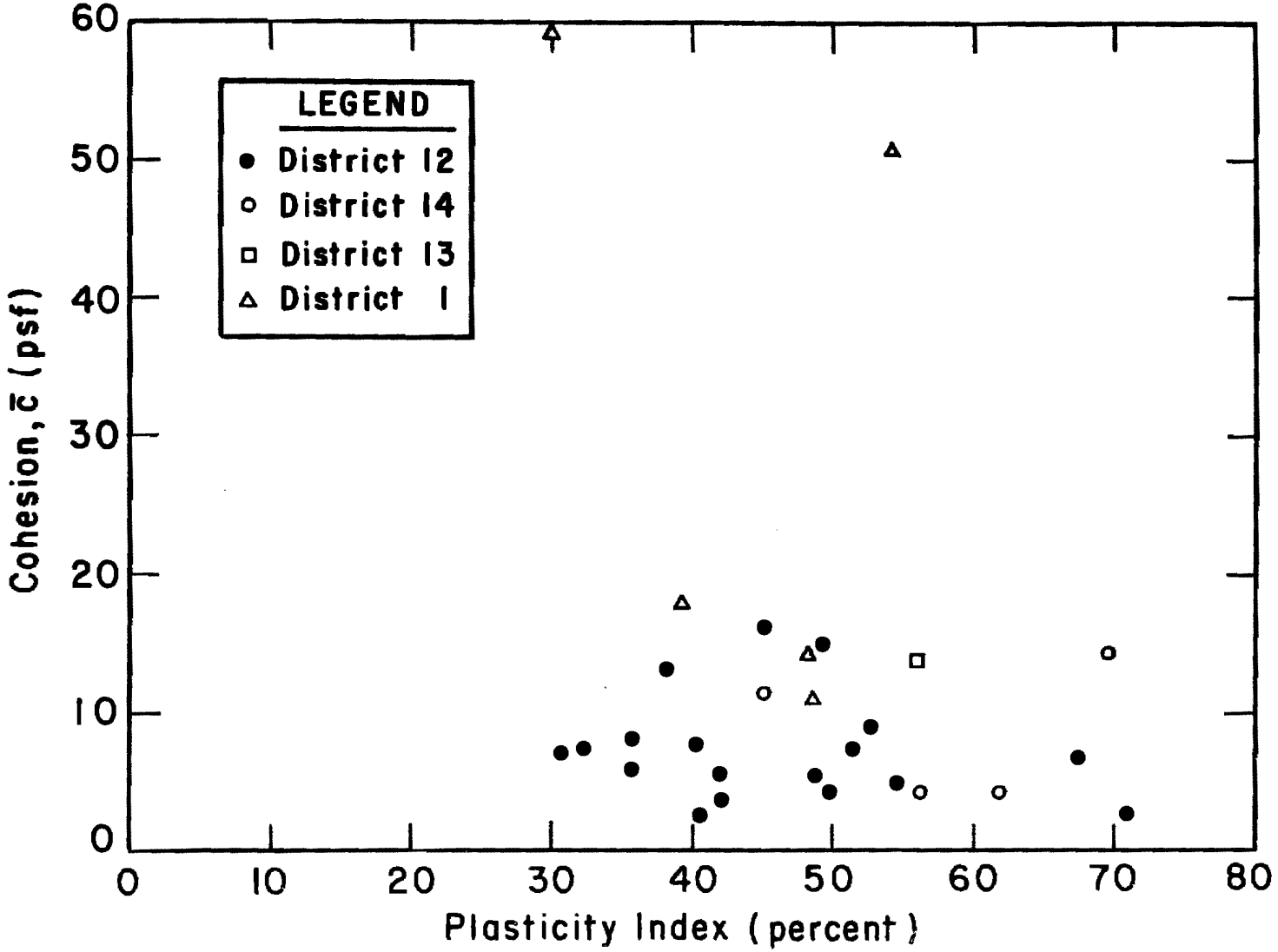

Fig. 4.17. Variation of back-calculated cohesion ($\bar{c}$) with plasticity index of soils from embankments which failed in Districts 1, 12, 13, and 14 - zero pore water pressures assumed.

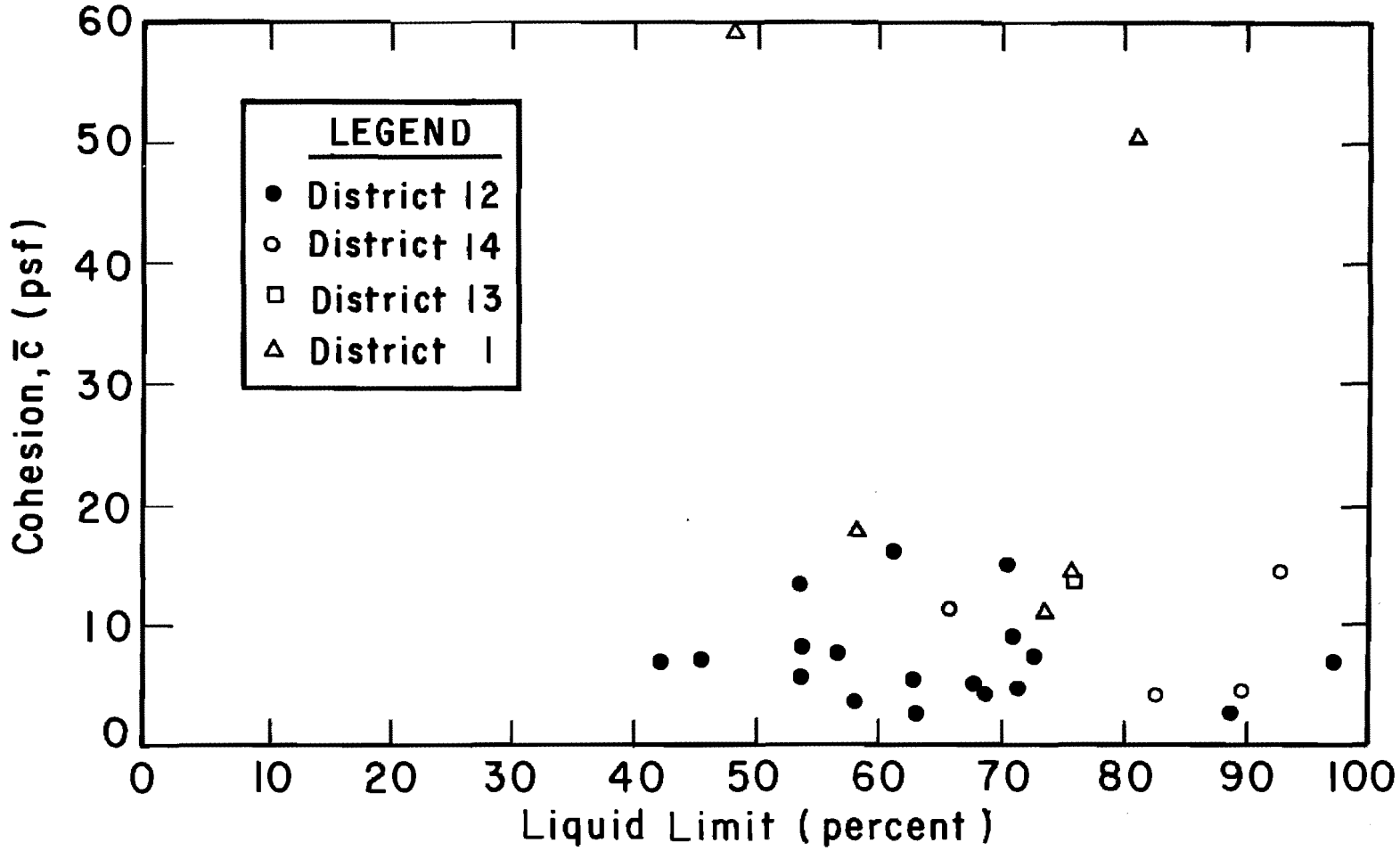

Fig. 4.18. Variation of back-calculated cohesion ($\bar{c}$) with liquid limit of soils from embankments which failed in Districts 1, 12, 13, and 14 - zero pore water pressures assumed.

plasticity clays, CL. Grain size determinations showed the soils to be fine grained with the percent by weight finer than the No. 200 sieve ranging from 72 to 99, and the percent by weight finer than 2 microns ranging from 37 to 86. Activities ranged from 0.54 to 1.05, with the mean value 0.79. X-ray diffraction analyses were performed on two of the soils, and the clay minerals found to be present included calcium montmorillinite, illite, and kaolinite.

Water contents measured for samples taken at depths greater than about one foot ranged from 14.0 to 40.6 percent, with the mean value 29.7 percent. There did not appear to be any consistent pattern of variation in water content with depth. Liquidity indices ranged from 0.16 to 0.57, with the mean value 0.32. It appears that many of the soils are at least in the vicinity of their fully swelled condition.

In addition to the twenty-eight embankment slides examined in this study, one embankment slope which was stable was examined. This slope is located northwest of the intersection of U.S. 79 and Carlos G. Parker Boulevard near Taylor in District 14. Index property data for the worst soil from this site show that there is nothing which distinguishes this soil from the problem soils tested from failure sites. The height of the embankment was determined to be 30 feet and the slope ratio was 2.2:1. Thus, this slope appears to be a likely candidate for failure. Possible reasons for the continued stability of this embankment are many. Stratification within the embankment could be such that potential failure surfaces would have to pass through materials of greater strength, i.e., sands or gravels. Another explanation is that the

"long-term" condition has not yet been reached under the prevailing environmental conditions and, thus, the potential for failure remains. On the other hand, it may be that the "long-term" condition has been reached and the slope is stable under these conditions. The "long-term" condition for an embankment slope will be a function of the prevailing environmental conditions. Given a sustained change in these conditions, the stability of an embankment may either improve or deteriorate. Thus, there exists the possibility that failure will yet occur on the embankment slope near the intersection of U.S. 79 and Carlos G. Parker, as well as on perhaps many other embankment slopes in Texas.

Soil strength parameters were back-calculated for each of the embankment slope failures using three different pore pressure assumptions. It was thought to be most reasonable to assume that the pore water pressures are zero for the purposes of back-calculating shear strength parameters from these failures. Assuming zero pore water pressures, the back-calculated effective stress angles of internal friction ranged from 10.5 to 23.2 degrees, and the back-calculated cohesion values ranged from 2.7 psf to 59.4 psf. There did not appear to be any relationship between the index properties and the back-calculated shear strength parameters.

The mean value of the back-calculated effective stress angle of internal friction for failures at the abutment is 21.7 degrees, whereas the mean value for side slope failures is 17.0 degrees. This difference may be due either to different pore pressure conditions existing at the time of failure within abutment versus side slopes or differences in the

slope geometry; for abutment failures the slope surface is curved and three dimensional, whereas, for the side slope failures, the slope surface is flat and two dimensional.

CHAPTER FIVE. DETAILED SLOPE STABILITY ANALYSIS FOR TWO EMBANKMENT SLOPE FAILURES

INTRODUCTION

Two of the embankment slope failures described earlier were selected for more detailed analysis. The two slopes selected were located at the northeast quadrant of IH 610 and Scott Street and the southwest quadrant of the SH 225 and SH 146 Interchange; both of these slopes are in the Houston area, in District 12. These sites were selected because they represented two sites where laboratory tests had been performed to measure the shear strength properties of the fill material involved. The laboratory tests to measure the shear strength were initiated through Interagency Contract (84-85) 1026 in November 1983 with Texas SDHPT District 12 in response to the recognition of problems with embankment slope stability in District 12. Results of the laboratory testing program are described by Gourlay and Wright (1984). The two slides selected for the more detailed slope stability analyses are the only two where laboratory tests have been performed to measure shear strength parameters and they provide an excellent opportunity to compare the back-calculated shear strength parameters with those which were measured with conventional laboratory tests.

IH 610 AND SCOTT STREET SITE DESCRIPTION

The first slide examined occurred on the north side slope of the east embankment where IH 610 crosses over Scott Street in south Houston. According to Texas SDHPT District 12 records, the embankment was constructed in 1966. The project was a combination of excavation and fill, and the type of embankment material was described as "Common Roadway Excavation and Fill (Clayey Soil)." Thus, the embankment was probably constructed of material from near the site. Records show that a slope failure in the quadrant of interest had been previously repaired by pushing the material back into place and recompacting the replaced material. It is uncertain if this previous failure had occurred at the location of the current failure, which was examined and is reported in this study.

A plan view of the area surrounding the intersection of IH 610 and Scott Street is shown in Fig. 5.1. The embankment east of the intersection of IH 610 and Scott Street extends between two bridges: the bridge over Scott Street at the embankment's west end, and the bridge over the Southern Pacific Railroad at the embankment's east end. An off-ramp for westbound traffic exiting IH 610 onto Scott Street is located along the north slope of the embankment. The southern curb of the off-ramp is located at the toe of the slope of interest.

The face of the slope along the north side of the east embankment is shown on a sketch in Fig. 5.2. The portion of the slope which had failed was approximately 100 feet east of the west end of the embankment. Some additional slope movement was observed between the slide and the

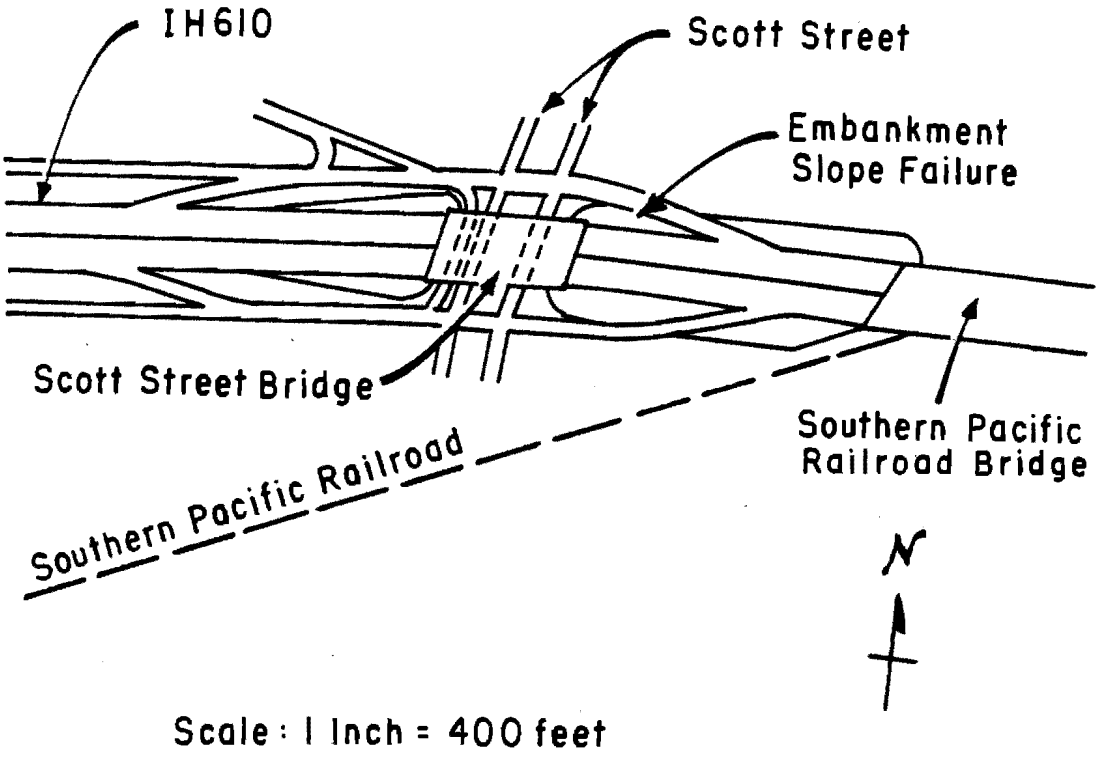

Fig. 5.1. Plan view of IH 610 and Scott Street Intersection (redrawn from Texas SDHPT Project Layout Sheet).

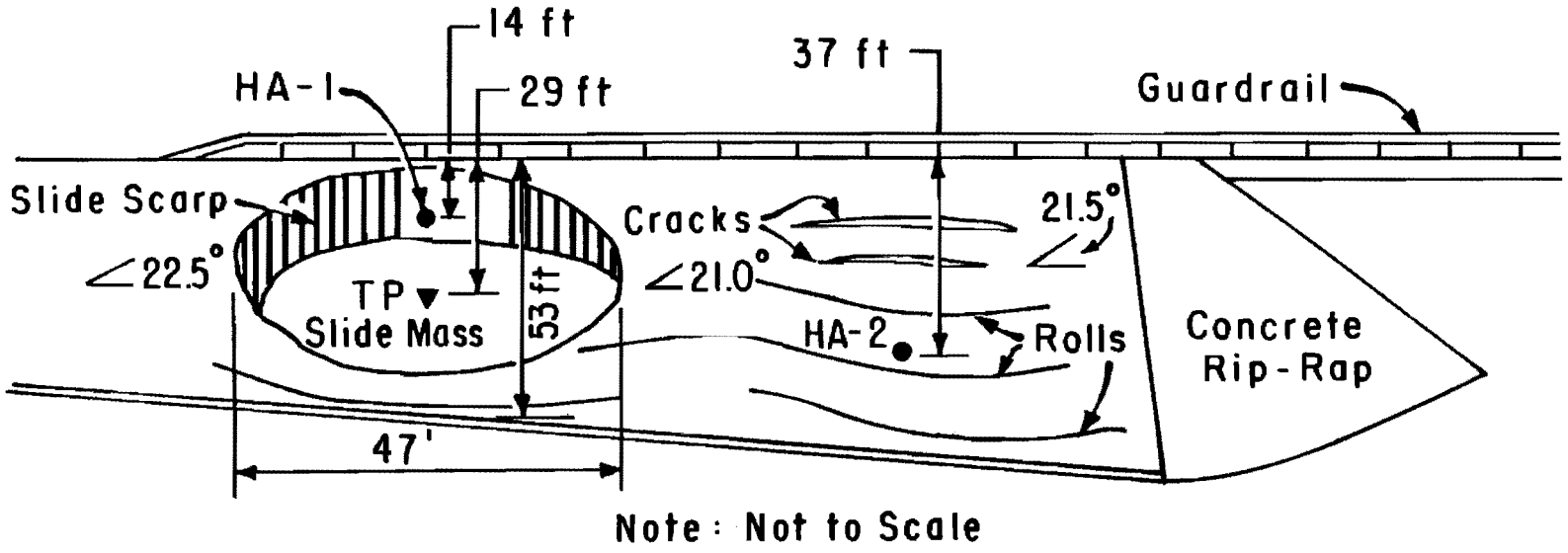

Fig. 5.2. Sketch of embankment at IH 610 and Scott Street (NE quadrant) showing extent of slope movement and sampling locations (redrawn from field sketch, 15 March 1983).

abutment (west) end of the embankment. Two cracks were observed in this area of additional movement; the cracks were located about one third of the way down from the top of the embankment. These cracks did not appear to be deeper than about one foot. Below the cracks, three rolls or ripples in the slope were observed. Additional movement of this portion of the embankment has been noted during subsequent inspections (post March 15, 1983).

The slope angle where the slides were observed varied from about 21 degrees at the west end to about 22 1/2 degrees at the east end of the failure. The length of the slope, from the top to the bottom of the face of the slope, at the location of the slide was about 53 feet. The failure surface was restricted to the slope face with the scarp of the slide located just below the top of the embankment, and the base of the failure surface appeared to be located just above the toe of the slope. The length of the slide was estimated to be about 47 feet, and the width of the slide at its widest point was also about 47 feet. Heavy weed and grass growth had developed in the vicinity of the main slide, whereas the remainder of the embankment was covered predominantly with shorter grass which appeared to have been mowed.

The slope ratio (cotangent of the slope angle) at the location of the slide varied from about 2.5:1 to 2.6:1. A slope ratio of 2.6:1 was used to represent this slide for the subsequent calculations. This slope ratio (2.6:1) corresponds to a slope angle of about 21 degrees. The height of the embankment at the location of the slide was determined to be about 19 feet. A cross-section illustrating the slope geometry at the

location of the slide is shown on Fig. 5.3. The height of the slide was determined to be about 17 feet and the depth of the slide was estimated to be 3.5 feet. The location of the slide on the slope, along with the slide dimensions, is also illustrated on the cross-section in Fig. 5.3.

GEOLOGIC CONDITIONS

The geology of the Houston area is controlled by the Gulf Coast geosyncline, which extends from Alabama to the northeastern part of Mexico. This region, referred to as the Gulf Coastal Plain, encompasses many of the areas currently experiencing embankment slope stability problems. The Gulf Coastal Plain is a sedimentary basin composed of a thick sequence (on the order of 10,000 feet) of Cenozoic sediments. The surface slopes gently from the inland boundary, at an elevation of about 500 feet, to the coast, at sea level. Bedding dips to the southeast at a very low angle, with the youngest, Pleistocene, deposits nearest the coast (including the Beaumont Formation), and the oldest, Paleocene, deposits furthest inland. The occurrence of embankment slope failures appears to be associated with the use of the fine grained, highly plastic soils of these deposits for construction of earth fills.

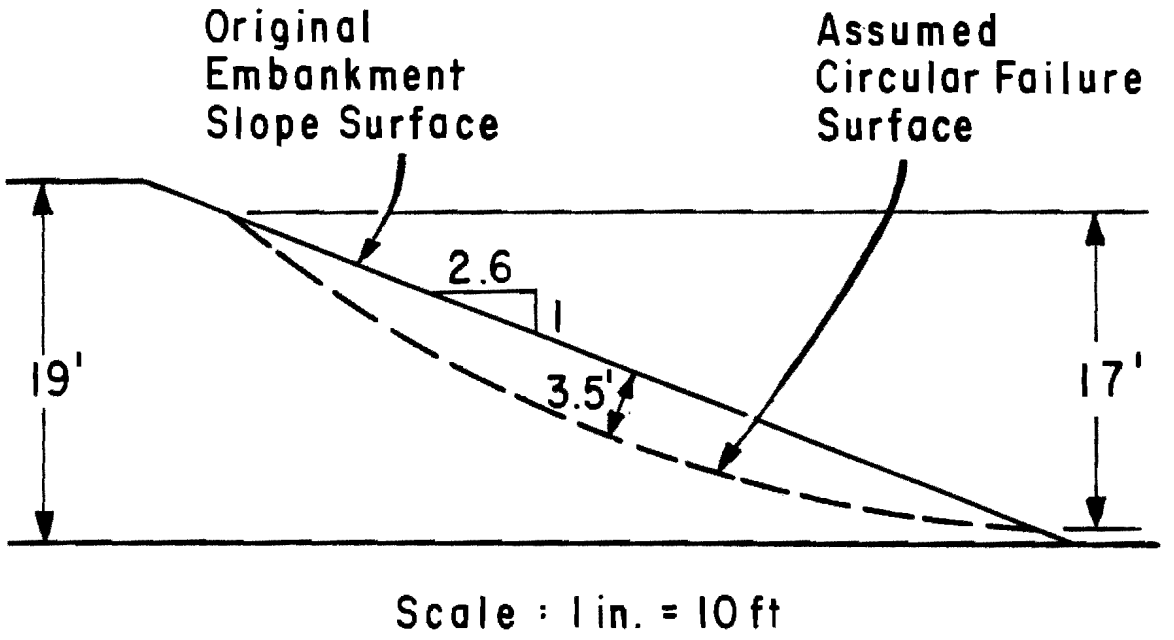

Fig. 5.3. Slope geometry and slide dimensions for the embankment slide at IH 610 and Scott Street (NE quadrant).

SOIL SAMPLING

Soil sampling at the IH 610 and Scott Street site during the initial field inspection (March 15, 1983) consisted of excavation of two hand auger borings and one test pit. The approximate locations of the borings and test pit are shown on the sketch in Fig. 5.2. Water content samples were taken from the two hand auger borings. Water content and soil profiles for these borings are shown in Fig. 5.4. There do not appear to be any consistent trends in the water content profiles. However, the average water content of those samples obtained from the boring located in the main slide scarp (HA-1) was about 35 percent, which is several percent higher than the average water content of 31 percent for samples taken from the adjacent section of the slope which was showing some slope movement (HA-2).

The test pit was excavated in the slide mass at the approximate location shown in Fig. 5.2 in order to obtain soil for the laboratory testing program. A cross-section through the slide showing the location of hand auger boring HA-1 and the test pit is presented in Fig. 5.5. The depth of the test pit was approximately 3.5 feet and does not appear to have been sufficient to penetrate the estimated location of the failure surface. The soil profile determined from the test pit is shown in Fig. 5.6. Two distinctly different clays were recognized during excavation of the test pit: a red Beaumont clay, and a grey Beaumont clay. Subsequent measurement of index properties showed that the red clay was more highly plastic and finer grained than the grey clay. The red clay was

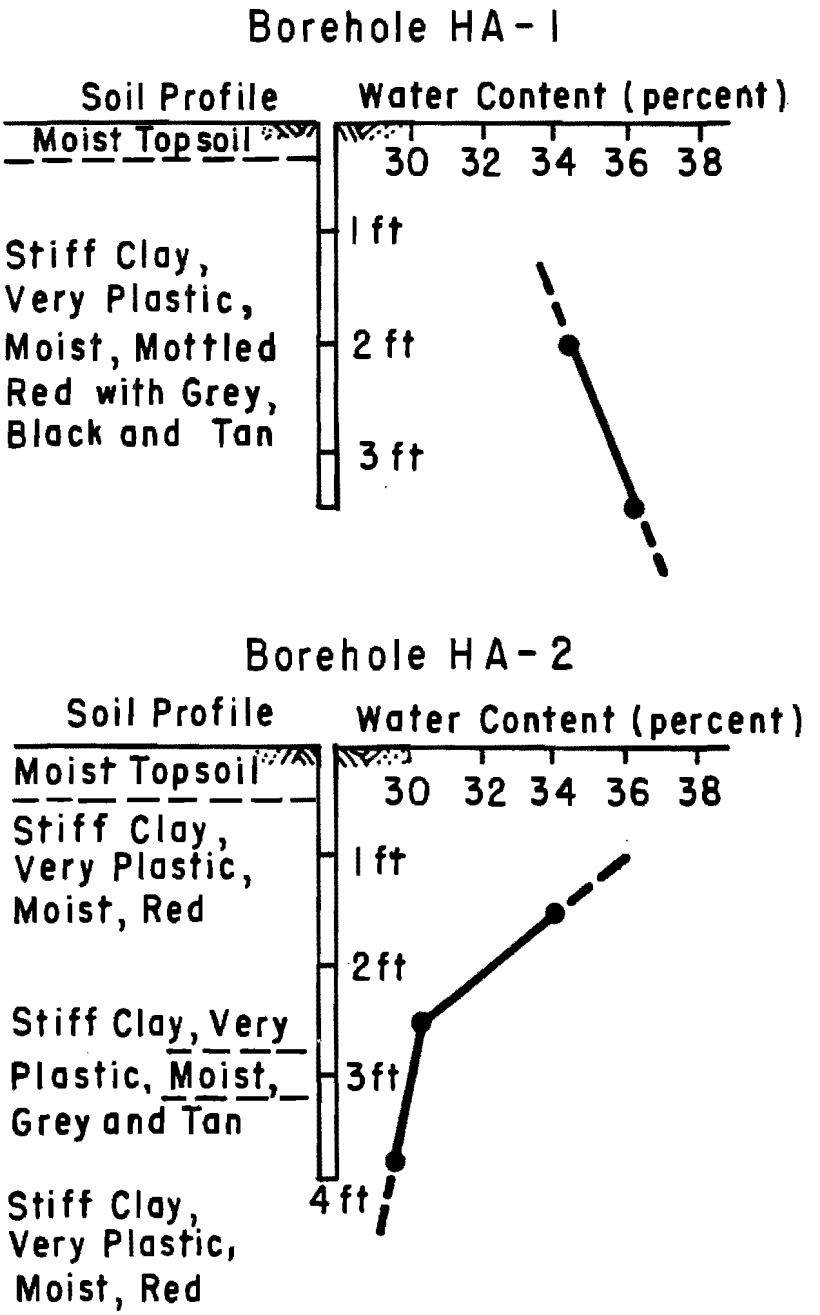

Fig. 5.4. Soil and water content profiles for two hand-augered boreholes at IH 610 and Scott Street (NE quadrant).

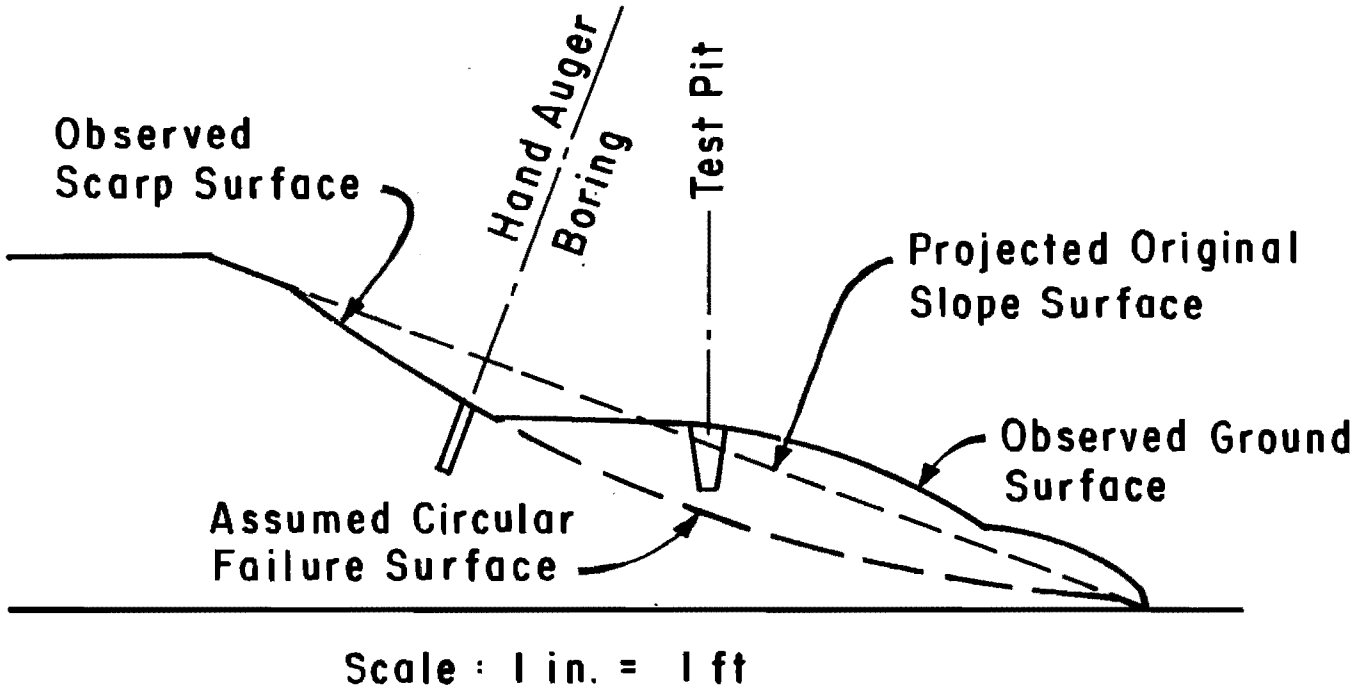

Fig. 5.5. Cross-section of embankment slide at IH 610 and Scott Street (NE quadrant) showing approximate locations of hand-augered borehole and test pit.

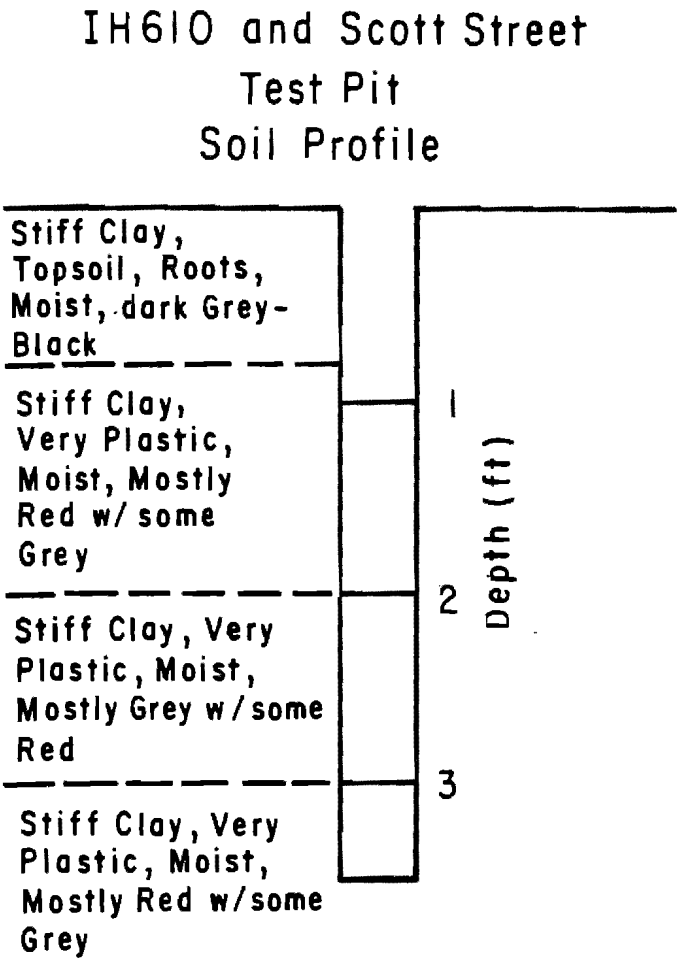

Fig. 5.6. Soil profile for the test pit at IH 610 and Scott Street (NE quadrant).

therefore identified as the "problem" soil at this site. Consolidated-undrained (CU) triaxial compression tests with pore water pressure measurements were performed on both of these soils and are described in detail in the report by Gourlay and Wright (1984).

COMPARISON OF FIELD AND LABORATORY WATER CONTENTS

The water contents measured for samples obtained from within the slope at the IH 610 and Scott Street site were compared with the compaction water contents and final water contents of laboratory prepared triaxial test specimens presented by Gourlay and Wright (1984). Gourlay and Wright performed laboratory compaction tests on the red and grey clays from the site, and a "target" water content and dry density were selected to represent probable compaction conditions for these soils at the time of placement in the field.

The water content data obtained by Gourlay and Wright are summarized in Fig. 5.7 for the red clay and in Fig. 5.8 for the grey clay and are briefly reviewed below. The circular symbols in these two figures (5.7 and 5.8) represent the final water contents of specimens after they were saturated and brought to equilibrium under selected final effective consolidation pressures. The water contents shown by these symbols are plotted versus the corresponding consolidation pressures. A solid horizontal line representing the target value of the water content selected for compaction is also shown in each of these figures. The target compaction water content for the red clay was 24 percent and for the grey

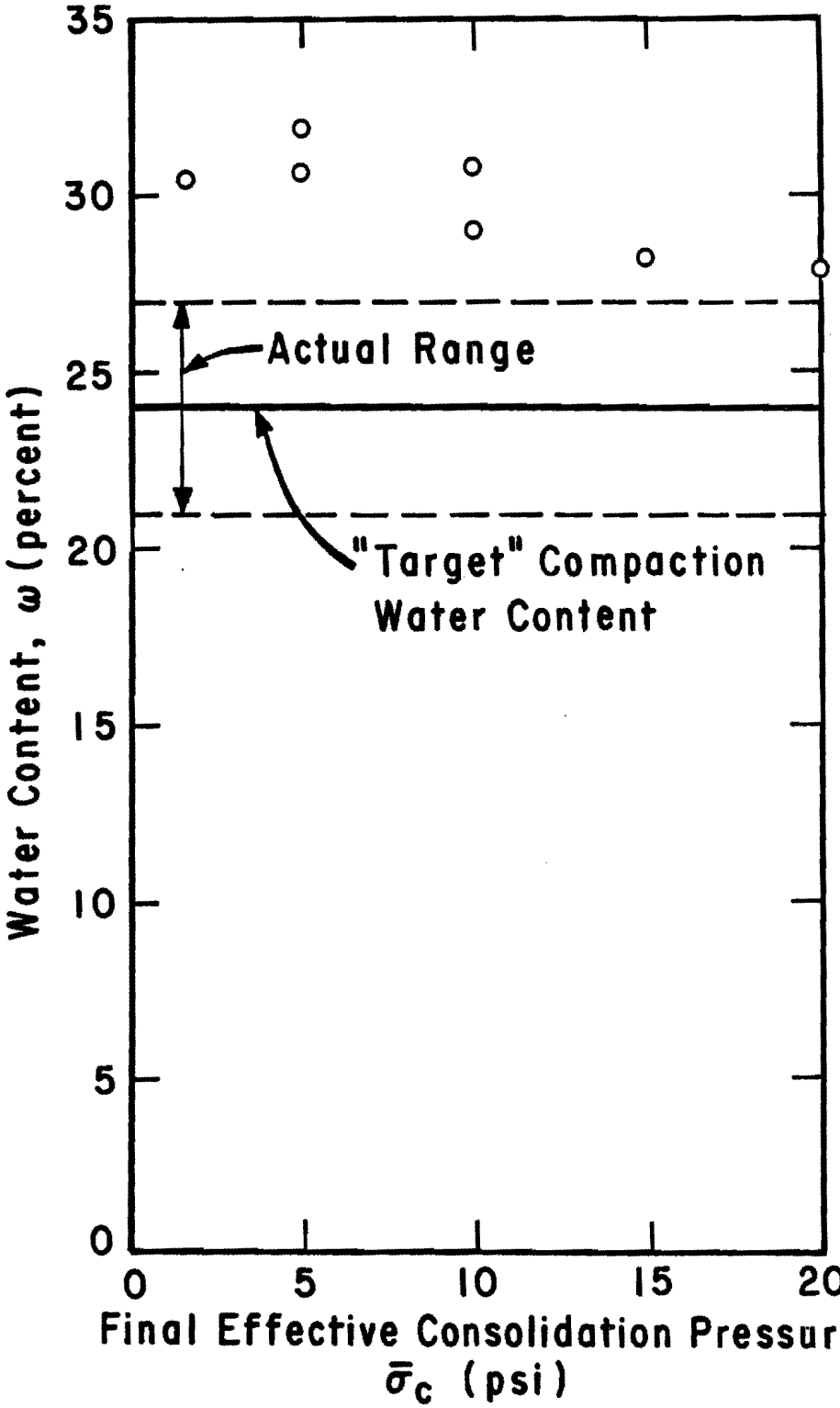

Fig. 5.7. Variation in water content with final effective consolidation pressure for laboratory compacted specimens of red clay.

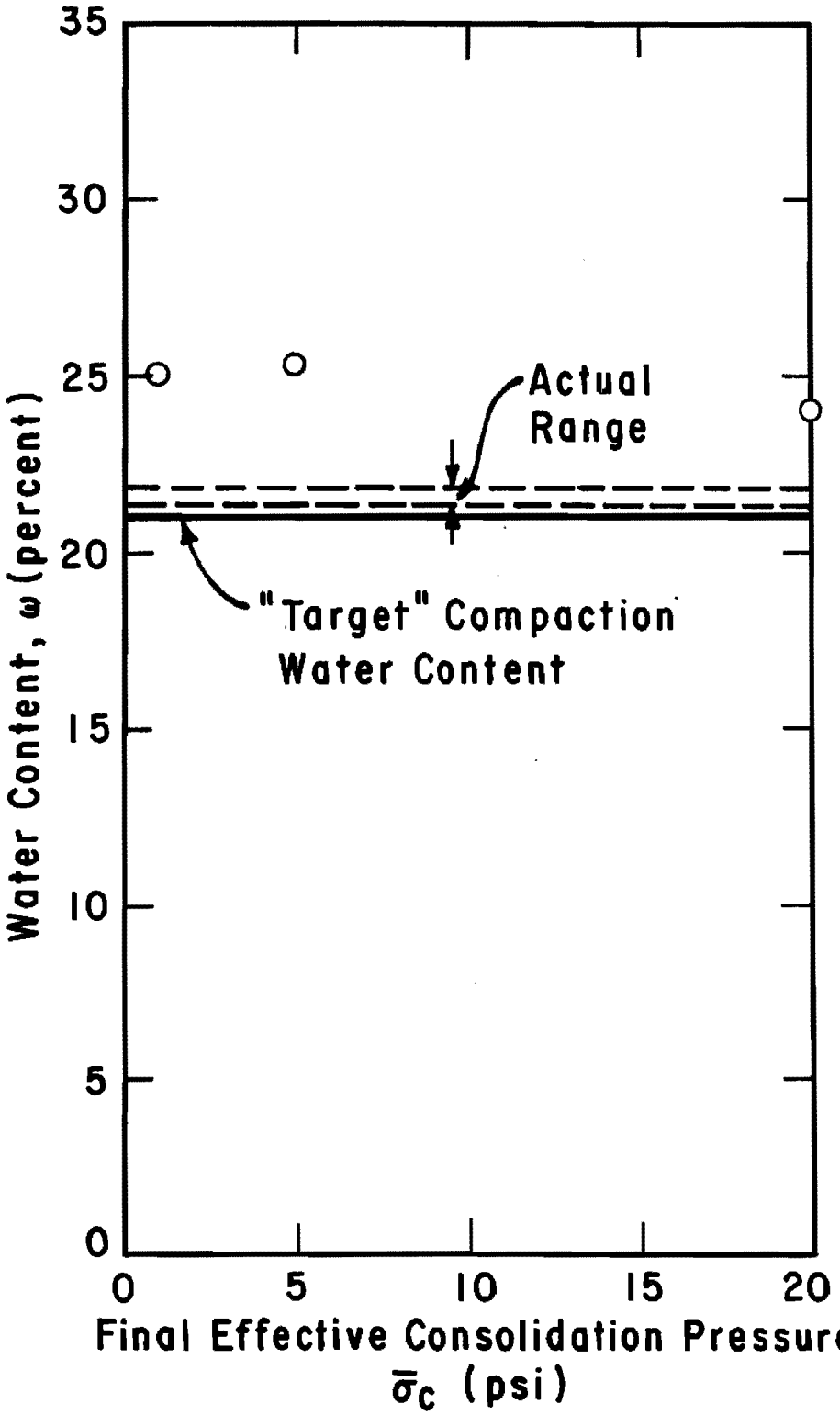

Fig. 5.8. Variation in water content with final effective consolidation pressure for laboratory compacted specimens of grey clay.

clay was 21 percent. Two broken horizontal lines representing the range in actual water contents for the specimens which were compacted in the laboratory are also shown in Figs. 5.7 and 5.8. A comparison of the compaction water contents with the water contents after saturation of the soil shows that, in all cases, the water contents increased noticebly, with the greatest increase occurring for the specimens with the lowest final effective consolidation pressures.

The water content diagrams shown in Figs. 5.7 and 5.8 have been reproduced in Fig. 5.9 along with the water contents measured from the field samples. The water contents from the field samples are plotted versus the corresponding depth of the sample. It is found that the field water contents are near, or a few percentage points greater than, the final water contents of the laboratory specimens of red clay at low effective consolidation pressures. It would be expected that the two sets of water contents (field and laboratory at low consolidation pressures) would be similar since the field samples were taken from relatively shallow depths (1.5 to 3.5 feet) which correspond to low effective confining pressures, and since the majority of the samples obtained at this site consisted predominantly of the red clay. However, it is not known why some of the field water contents are greater than the final water contents of laboratory compacted specimens of the red clay with low consolidation pressures.

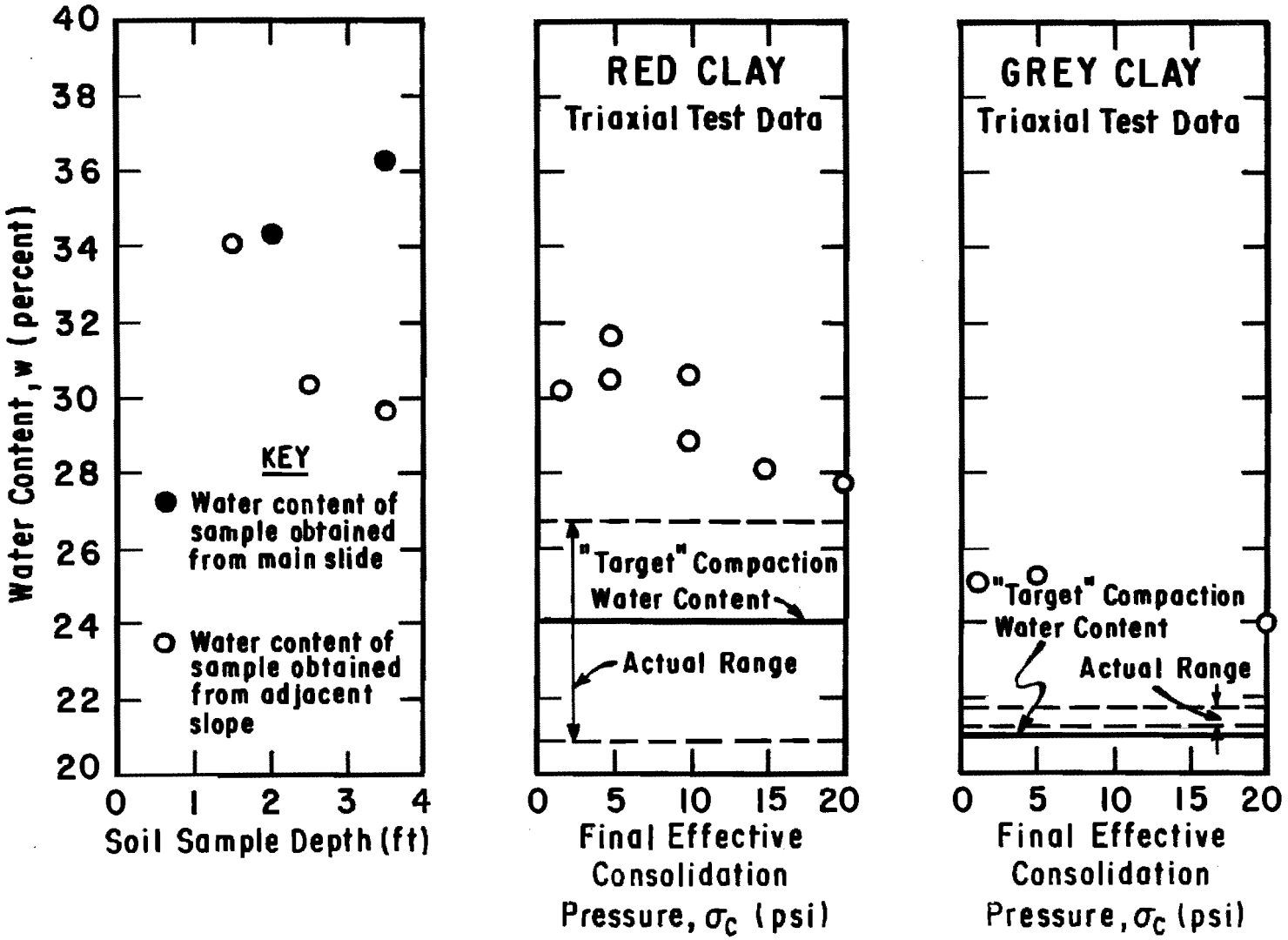

Fig. 5.9. Comparison of water contents from field samples with water contents of triaxial specimens for the IH 610 and Scott Street embankment.

SHEAR STRENGTH PARAMETERS FOR EMBANKMENT MATERIAL

Shear strength parameters for the embankment at IH 610 and Scott Street were measured in the laboratory tests reported by Gourlay and Wright (1984) and were also back-calculated from the observed failure as part of the current study. The shear strength parameters determined by these two means were subsequently used for slope stability calculations. The shear strength parameters are briefly reviewed below.

Shear Strength Parameters Measured in the Laboratory

Gourlay and Wright (1984) performed both unconfined compression tests and consolidated-undrained (CU) triaxial tests with pore water pressure measurement on soils from the IH 610 and Scott Street site. Unconfined compression tests were performed on a number of compacted specimens of red clay. Specimens compacted to conditions similar to those which probably existed at the time of fill placement (water content of about 24 percent, and dry unit weight of about 95 percent) were found to have an unconfined compressive strength of approximately 4000 psf.

Consolidated undrained triaxial shear tests with pore pressure measurement were performed on specimens of both the red and the grey Beaumont clays. However, only the data for the red Beaumont clay, which is identified as the "problem" soil, are considered. The effective stress shear strength parameters obtained for the red clay are $\bar{c}$ = 270 psf and $\bar{\phi}$ = 20 degrees.

Shear Strength Parameters From Back-Calculation

The back-calculated shear strength parameters presented in Chapter Four were obtained using the procedures outlined in Chapter Three. The slope and slide geometry determined from the failure was used to obtain shear strength parameters which existed in the embankment slope at the time of failure. Based on the examination of embankment slides presented in Chapter Four, it was judged to be reasonable to assume that the pore water pressures are zero for the purposes of back-calculating shear strength parameters. The shear strength parameters which were back-calculated for the slide at IH 610 and Scott Street are $\bar{c}$ = 8.2 psf and $\bar{\phi}$ = 18.8 degrees.

STABILITY CALCULATIONS FOR IH 610 AND SCOTT STREET EMBANKMENT

Separate sets of slope stability calculations were performed for the IH 610 and Scott Street embankment for conditions existing at the time of construction ("short-term" conditions) and for conditions existing at the time of failure ("long-term" conditions). Stability calculations were performed using a new computer program, UTEXAS, which was developed as part of this research project (Wright and Roecker, 1984a). Results obtained using the new computer program were verified using another computer program, SSTAB1 (Wright, 1982).

For all of the stability calculations the embankment was considered homogeneous, the embankment-foundation interface was assumed to be horizontal at the elevation of the toe of the slope, and the foundation material was assumed to be strong enough to prevent any failure surface from passing through the foundation. Except where noted later, pore water pressures were assumed to be zero. Finally, only circular shear surfaces were considered in these analyses.

Short-Term Stability

Stability calculations were performed to determine the short-term stability of the embankment slope at IH 610 and Scott Street. These calculations were made using a cohesion of 2000 psf for the embankment material and assuming that ϕ was equal to zero. An automatic search was used to locate the most critical circular shear (sliding) surface shown in Fig. 5.10. The minimum factor of safety corresponding to the critical circle shown in Fig. 5.10 is 8.28. In actuality ϕ would be greater than zero for the as-compacted soil and, thus, the actual factor of safety would probably be even greater than this value (8.28). In any case, the factor of safety for the as-compacted soil is very high and would indicate that the slope is stable under short-term conditions.

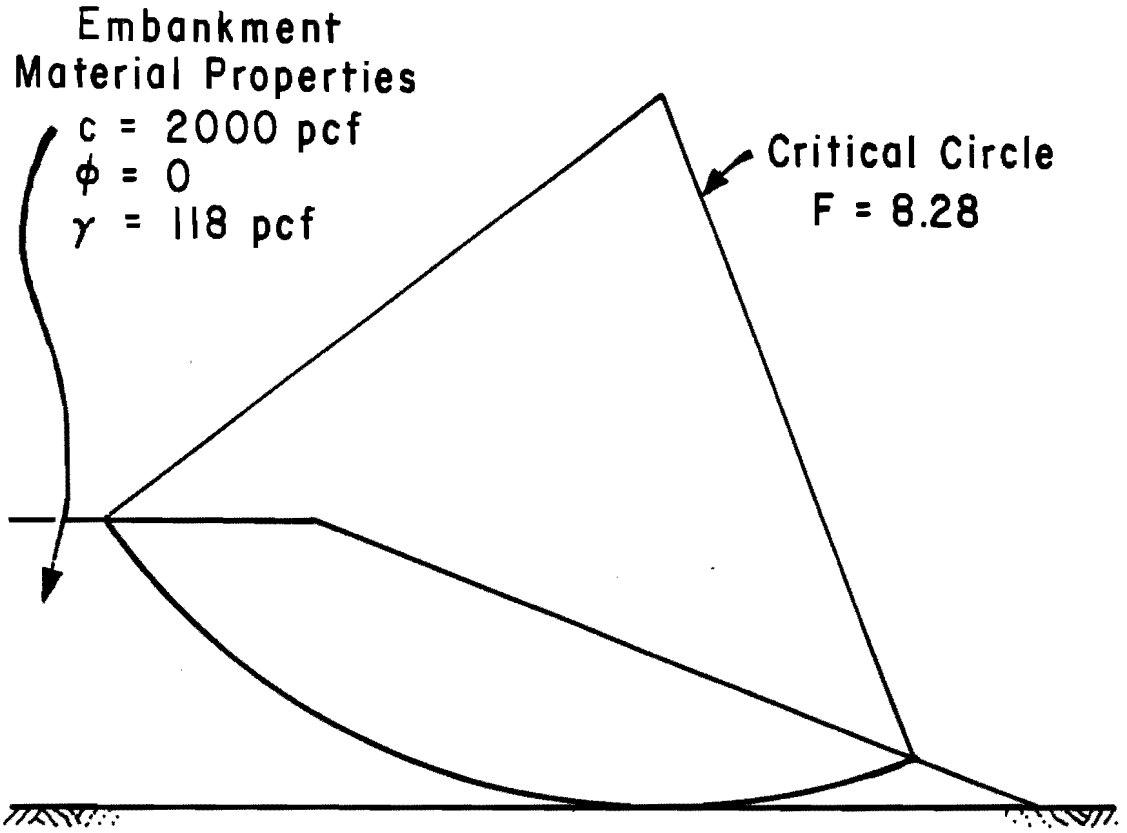

Fig. 5.10. Critical circle for embankment at IH 610 and Scott Street based on "short-term" stability calculations with shear strengths obtained from laboratory unconfined compression tests.

Long-Term Stability

Two series of calculations were performed to examine the long-term stability of the embankment slope at IH 610 and Scott Street. Shear strength parameters obtained from back-calculation and from laboratory tests were used in these calculations. Additional calculations were performed to determine the effects of pore water pressures, and of a vertical, "tension" crack, on the stability of this embankment.

Stability Calculatons Using Back-Calculated Strengths: The first series of stability calculations were performed using shear strength parameters which were back-calculated from the failure. An automatic search was performed to locate the most critical circular shear surface, which is shown in Fig. 5.11. The critical shear surface shown in Fig. 5.11 intersects the top, flat, portion of the embankment and is thus characteristic of a "slope" failure. The height of the slide formed by this critical circle is 19.0 feet, and the depth of the slide is about 4.0 feet. The observed failure surface is also shown in Fig. 5.11, as a dashed line. It is apparent that the critical circle resembles, but is not quite the same as, the observed failure surface. The minimum factor of safety corresponding to the critical circle shown in Fig. 5.11 is 0.99.

The fact that the observed failure surface is different from the critical circle shown in Fig. 5.11 is apparently due to nonhomogeneities in the actual slope which caused the failure to occur at a slightly different location from the one that would be expected for a homogeneous slope. The factor of safety for the observed failure surface is 1.0 (the

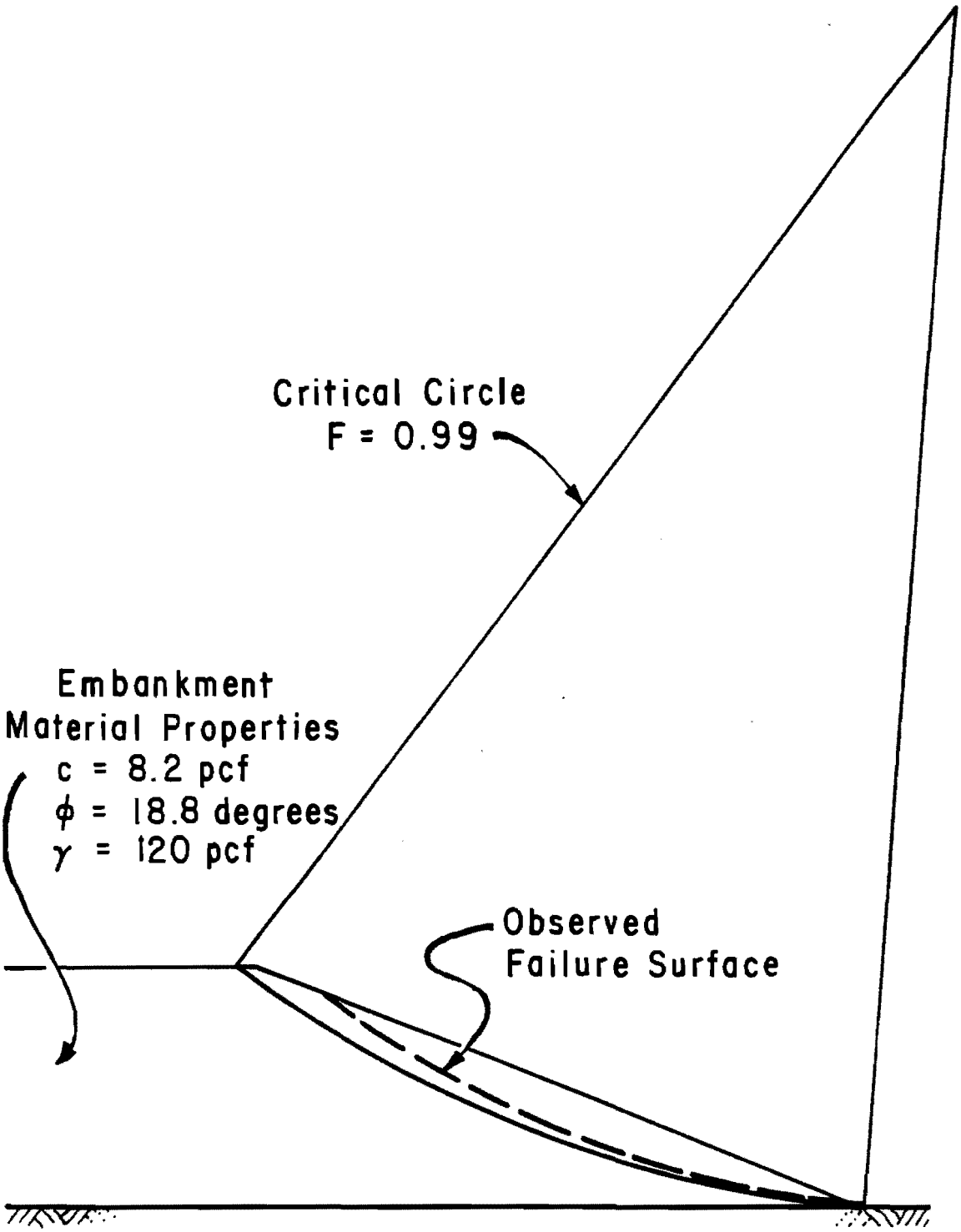

Fig. 5.11. Critical circle for embankment at IH 610 and Scott Street based on "long-term" stability calculations with back-calculated shear strength parameters - no pore water pressures.

observed failure surface was used to back-calculate the shear strength parameters used in these calculations), while the factor of safety for the most critical circle is slightly less (0.99).

Stability Calculations Using Laboratory Strengths: The second series of stability calculations were performed using shear strength parameters measured in the laboratory. An automatic search was performed to locate the most critical circular shear surface which is shown in Fig. 5.12. As was the case when back-calculated strengths were used, the shear surface shown in Fig. 5.12 intersects the top, flat, portion of the embankment and is thus characteristic of a "slope" failure. The height of the slide formed by the critical circle is about 17.4 feet, and the depth of the slide is about 9.5 feet. The observed failure surface is also shown in Fig. 5.12, as a dashed line. The depth of the slide formed by the theoretically most critical circle is about two and one-half times the depth of the actual slide. The minimum factor of safety corresponding to the critical circle shown in Fig. 5.12 is 2.37, indicating that the slope is stable.

The differences between the observed and theoretically most critical shear surfaces, as well as the relatively high calculated factor of safety (2.37) based on the laboratory shear strength parameters, indicate that the stability calculations made in this section do not closely approximate the observed slope behavior. It appears that the shear strength parameters measured in the laboratory and used in these calculations are too high. Since the back-calculated and laboratory measured values for the friction angle (18.8 and 20 degrees respectively) are

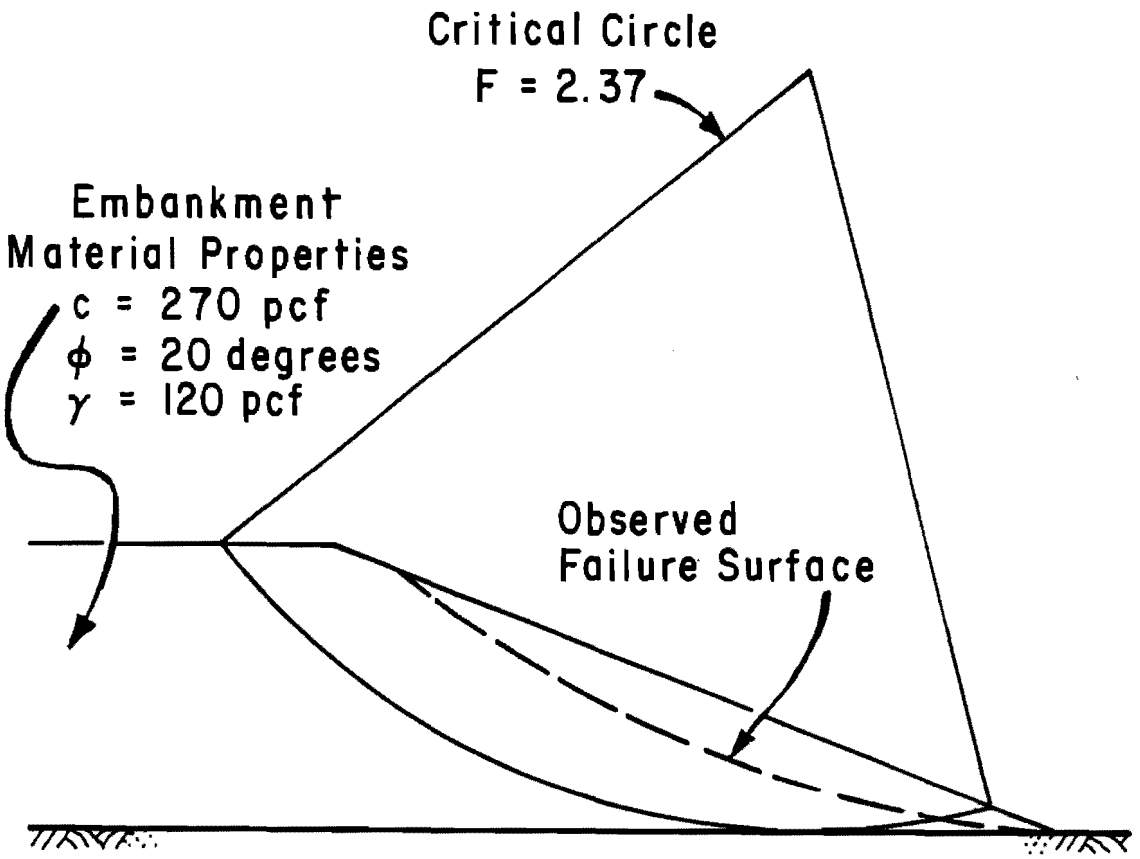

Fig. 5.12. Critical circle for embankment at IH 610 and Scott Street based on "long-term" stability calculations with shear strength parameters measured in the laboratory - no pore water pressures.

almost the same, it appears that the cohesion value measured in the laboratory (270 psf from laboratory tests versus 8.2 psf from back-calculation) is too high. Other factors possibly responsible for the discrepancy between the analyses made in this section and the observed slope behavior are investigated in the following sections.

Effect of Pore Water Pressures: Additional stability calculations were performed to investigate the effect of pore water pressures on the stability of the IH 610 and Scott Street embankment. These calculations were made using the shear strength parameters measured from laboratory tests.

For the first additional set of calculations a pore pressure ratio (r_u) of 0.4 was assumed. The location of the critical circle changed only slightly from the location found in the previous section where pore water pressures were assumed to be zero. The factor of safety decreased from 2.37 to 1.84, a decrease of approximately 22 percent.

A second additional set of calculations were made assuming a pore pressure ratio (r_u) of 0.8. The location of the critical circle again changed only slightly. The most critical circular shear surface which was located is shown in Fig. 5.13. The most critical circular shear surface located assuming zero pore water pressures is also shown in Fig. 5.13, as a dashed line.

The factor of safety calculated for the critical circle shown in Fig. 5.13 (assuming a pore pressure ratio of 0.8) is 1.29. While this

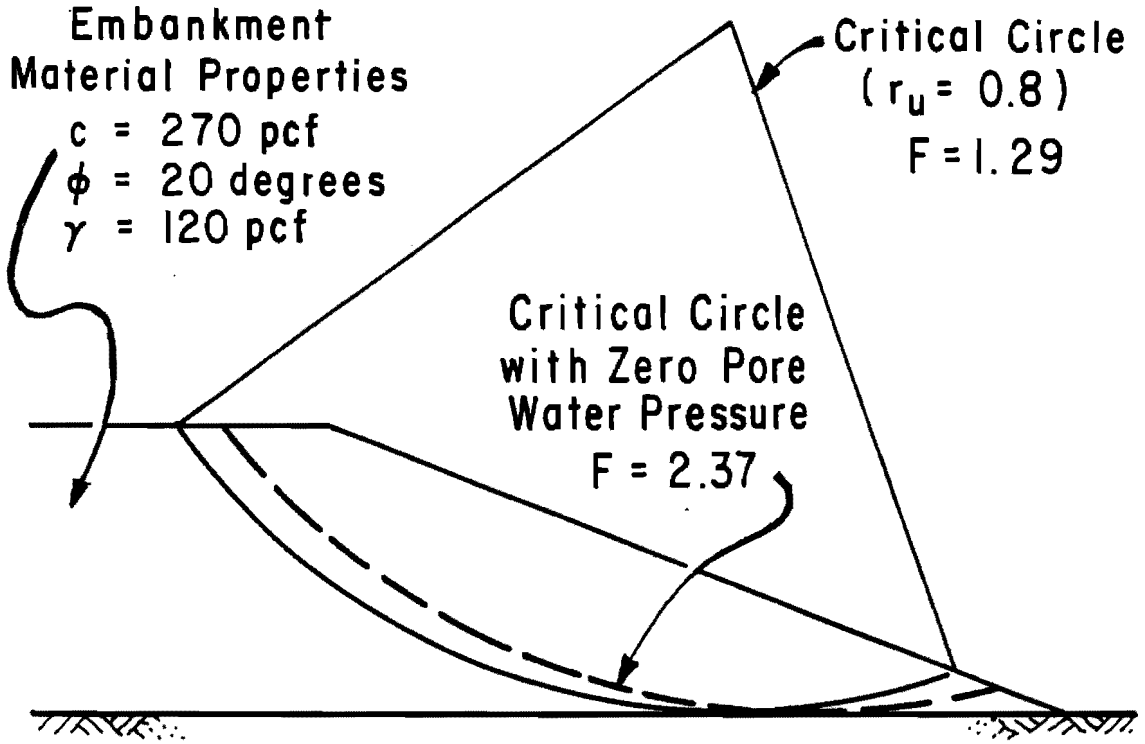

Fig. 5.13. Critical circle for embankment at IH 610 and Scott Street based on "long-term" stability calculations with shear strength parameters measured in the laboratory - pore water pressure ratio, r_u = 0.8.

value represents a considerable decrease from the value calculated when the pore water pressures are zero (2.37), it still indicates that the slope would be stable.

A pore pressure ratio of about 0.5 corresponds approximately to a case where the phreatic surface is at the slope surface. This would be considered a very extreme pore pressure condition in an embankment under normal conditions. Pore pressure ratios greater than 0.5 do not generally represent realistic conditions in embankment slopes. In light of the above calculations, it is clear that increased pore pressures would not explain the discrepancy between stablilty calculations made using laboratory strengths, and the observed slope failure.

Effect of a Vertical, "Tension" Crack: A final set of stability computations was performed to determine if a vertical crack near the crest of the slope might have a significant effect on the stability of the IH 610 and Scott Street embankment. A vertical crack filled with water was introduced and used in the stability calculations. Calculations were performed using both the shear strength parameters back-calculated from the slide and those measured in the laboratory. The depth of the crack was determined such that tensile stresses would not be developed within the slide mass. This depth was estimated to be equal to the depth of tensile stresses beneath a horizontal surface based on an active Rankine

earth pressure state. The crack depth, d_c, was estimated using the equation

$$d_c = \frac{2 \cdot c_m}{\gamma \cdot \tan (45 - \frac{\phi_m}{2})} \tag{5.1}$$

where ϕ_m and c_m represent the mobilized shear strength parameters which are calculated from the following:

$$c_m = \frac{c}{F} \tag{5.2}$$

$$\phi_m = \arctan (\frac{\tan\phi}{F}) \tag{5.3}$$

where F is the factor of safety. The vertical tension crack was assumed to be completely filled with water. A crack depth of 0.2 foot was used with the shear strength parameters obtained from back-calculation, and a crack depth of 2.3 feet was used with the shear strength parameters measured in the laboratory.

The critical circle located using back-calculated strengths with a water filled crack was the same as that located with no crack. The factor of safety corresponding to the critical circle with the crack was only slightly less than that for the critical circle without a crack: the rounded off value remained at 0.99. The critical circle located using shear strength values based on the laboratory tests with a water filled crack shifted only slightly from the critical circle located without a crack. The factor of safety corresponding to the critical circle with a

crack decreased by about 2 percent, from 2.37 to 2.32. The presence of a crack does not appear to significantly effect the stability of the embankment considered.

SLIDE AT SH 225 AND SH 146 (SOUTHWEST QUADRANT)

The second slope failure examined in further detail was one of four slides at the SH 225 and SH 146 Interchange. The embankment slope in the southwest quadrant at this location contained one well defined slide. Figure 5.14 was redrawn from field sketches, and shows the position and extent of the slide in relation to the embankment. Figure 5.15 shows an estimated cross-section through the slide mass.

Two hand auger borings were excavated in and near the slide mass at the locations shown in Fig. 5.14. The moisture content and soil profiles at these locations are presented in Fig. 5.16. The moisture content profiles do not suggest any significant variation in water content with depth.

Information was provided by the Texas SDHPT regarding the SH 225 and SH 146 interchange. This information indicates failures have occurred on both cut and fill slopes, and repairs were made by pushing and recompacting embankments with a dozer. The information also indicates that lime was added for stabilization although failure has occurred since. An inspection conducted during this study of the slide in the southwest quadrant did not indicate that the slide had been repaired previously either by lime treatment or by pushing and recom-

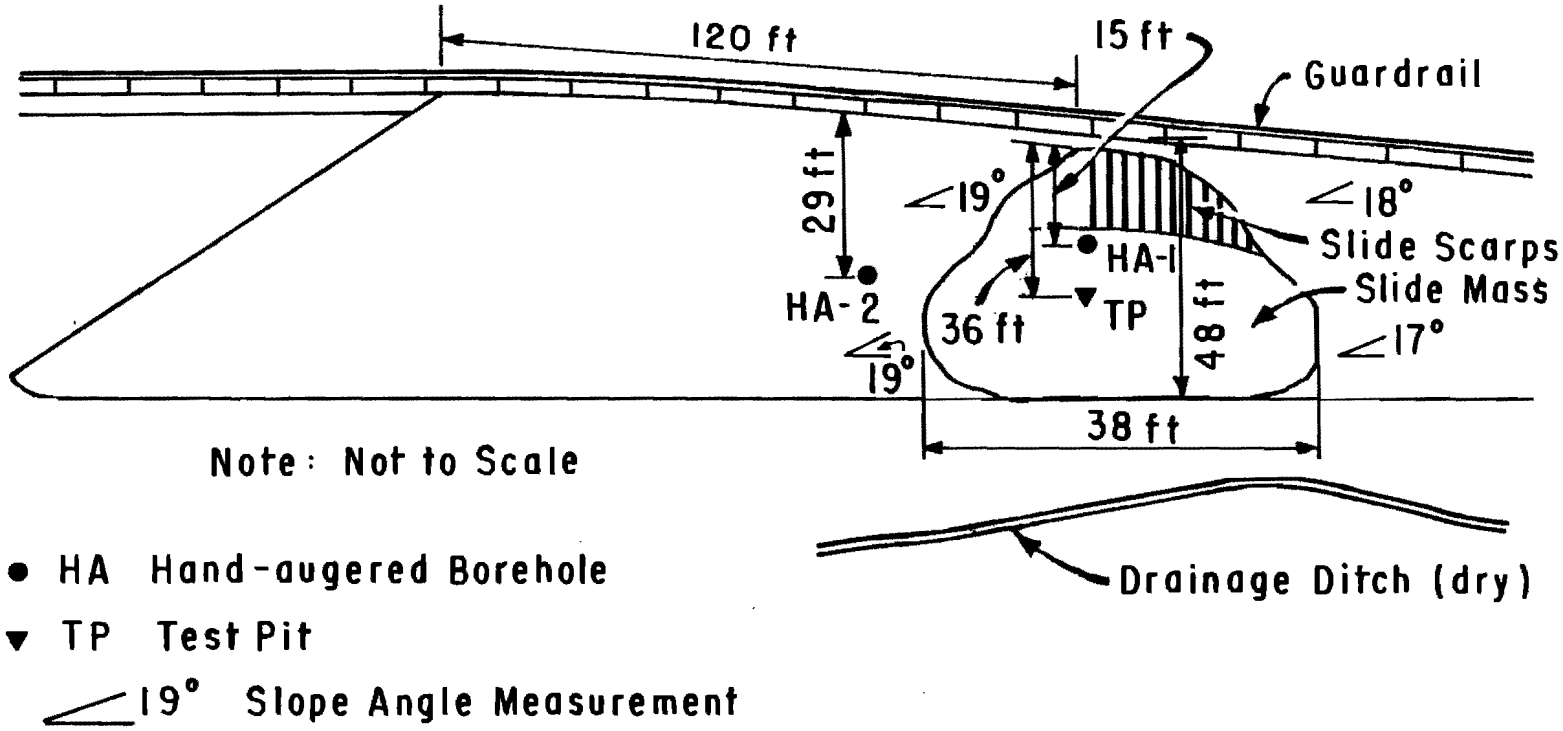

Fig. 5.14. Sketch of embankment at SH 225 and SH 146 (SW quadrant) showing extent of slope movement and sampling locations (redrawn from field sketch, 15 March 1983).

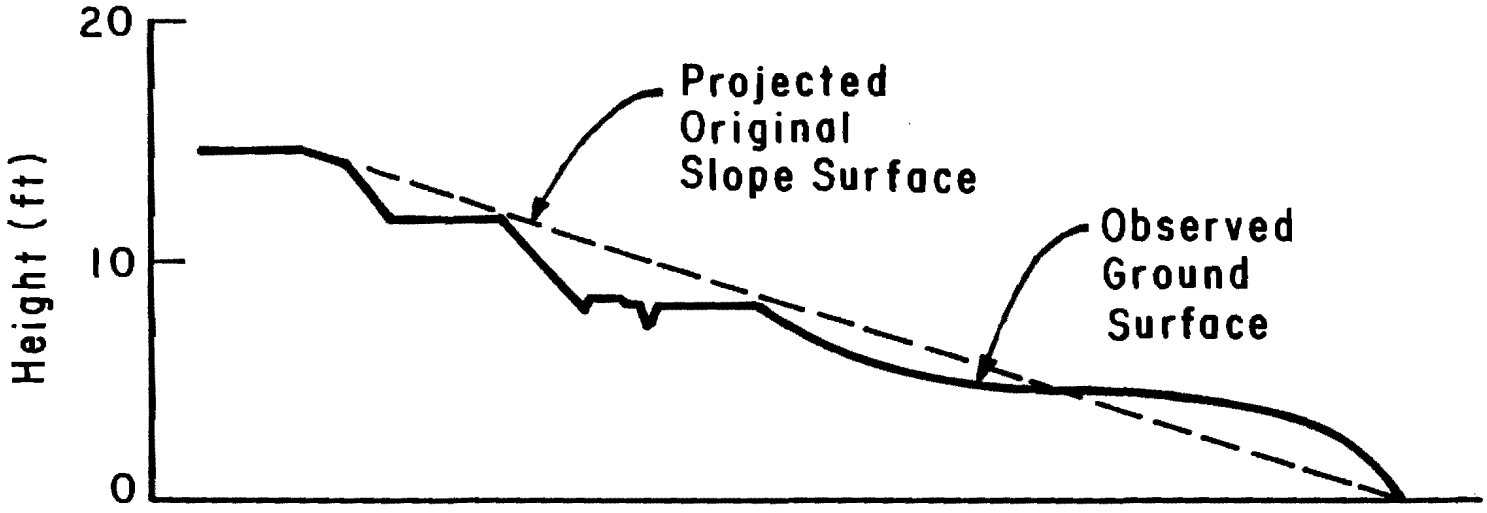

Fig. 5.15. Cross-section of embankment slide at SH 225 and SH 146 (SW quadrant).

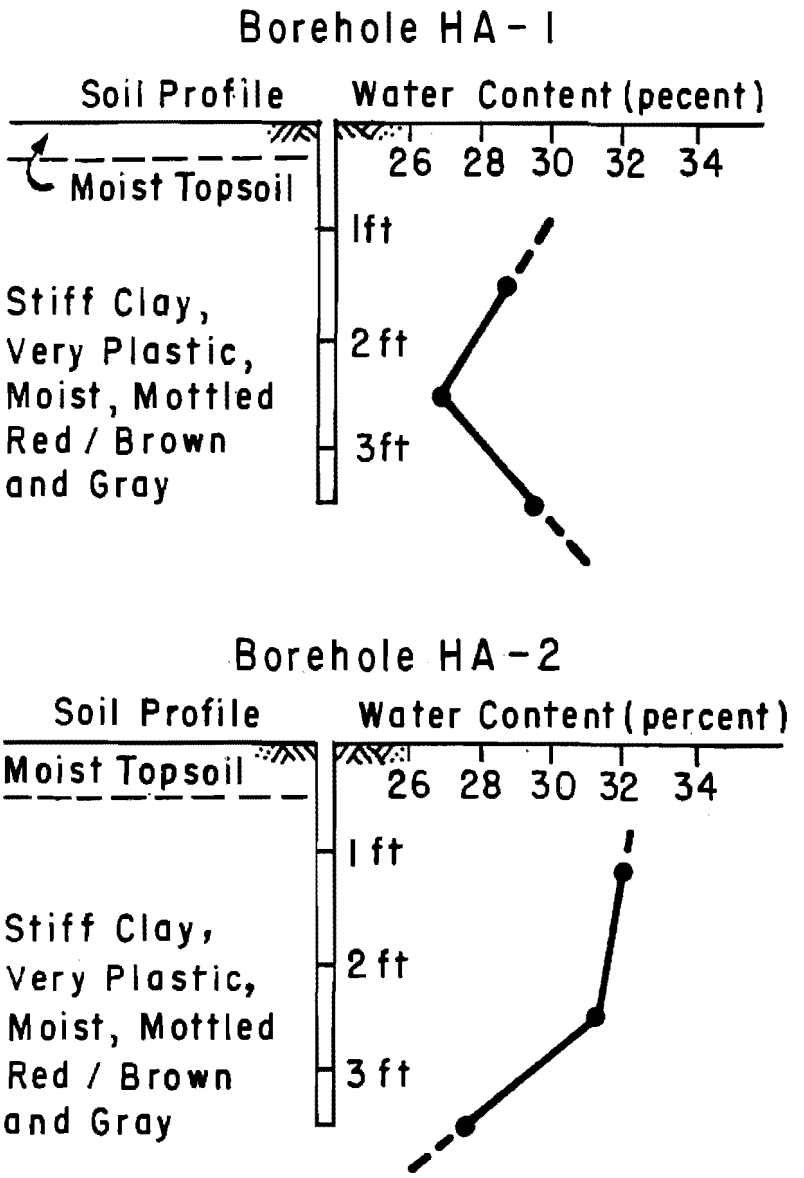

Fig. 5.16. Soil and water content profiles for two hand-augered boreholes at SH 225 and SH 146 (SW quadrant).

pacting the soil. This slide appeared to be a first time slide at this location on the embankment.

The slope ratio (cotangent of the slope angle) was determined to be 3.0:1. The height of the embankment at the slide location was determined to be about 15 feet. The height of the slide was about 13 feet, and the depth of the slide was estimated to be about 4.3 feet. Assuming a pore pressure ratio of zero, the shear strength parameters, which were back-calculated and presented in Chapter Four, are $\bar{c}$ = 15.0 psf and $\bar{\phi}$ = 14.7 degrees.

A single, consolidated-undrained triaxial shear test was performed by Gourlay and Wright (1984) on a recompacted specimen of a brown clay from the SH 225 and SH 146 southwest quadrant site. The brown clay tested was identified as the "problem" soil from this site. The results of index property tests, reported in Chapter Four, indicate that the brown clay from the SH 225 and SH 146 site was similar to the red clay from the IH 610 and Scott Street site. However, the specimen of the brown clay on which the triaxial shear test was performed had a final dry unit weight, after reaching equilibrium at the final effective consolidation pressure, that was almost 2 pcf higher than the dry unit weight of similar specimens of red clay. The higher dry unit weight was probably due to a relatively high dry unit weight to which the specimen was initially compacted. The triaxial shear test performed by Gourlay and Wright showed that the brown clay from the SH 225 and SH 146 embankment exhibited a shear strength which was slightly higher than the strength suggested by an upper-bound failure envelope developed for specimens of

the red clay. The higher strength may have been due to the higher dry unit weight. However, while it is difficult to determine, based on the results of one test, whether the brown clay has a similar or higher shear strength than the red clay, it appears that the strengths of the two clays are similar. The shear strength parameter values obtained for the red clay, as cited earlier, are $\bar{c}$ = 270 psf and $\bar{\phi}$ = 20.0 degrees and are believed to resemble or slightly underestimate the shear strength parameter values for the brown clay from the SH 225 and SH 146 embankment.

The friction angle which was back-calculated for the slide in the southwest quadrant at SH 225 and SH 146 (15.0 degrees) is slightly lower than the value based on laboratory tests (20 degrees). The cohesion value which was back-calculated (14.7 psf) is significantly less than the corresponding value based on the laboratory tests (270 psf). The differences between the two friction angle values, and perhaps some of the difference between the two cohesion values, may be explained by the fact that a complete laboratory strength envelope was not determined for the brown clay. However, this cannot in itself explain the large difference between the back-calculated and the laboratory cohesion values.

Stability calculations similar to those presented in this chapter for the slide at IH 610 and Scott Street were made for the slide in the southwest quadrant of the SH 225 and SH 146 Interchange. Stability calculations based on the shear strength parameters obtained from back-calculation showed that the most critical circle resembled the observed failure surface. The factor of safety corresponding to the critical cir-

cle found using back-calculated shear strength parameters was 0.97. Similar calculations based on shear strength parameters measured in the laboratory produced a critical circle which extended much deeper into the embankment. The factor of safety corresponding to that circle was 2.95. Thus, the results of stability calculations made for the SH 225 and SH 146 southwest quadrant site are similar to results presented earlier for the IH 610 and Scott Street site. The significance of the high cohesion value measured in laboratory tests is once again shown.

EMBANKMENT SLOPE STABILITY PROBLEMS IN SASKATCHEWAN, CANADA

A review of available literature regarding embankment slope stability shows that little consideration has been given to the long-term stability of compacted fills of highly plastic clays. One region where such slope problems have been examined is the Regina area of Saskatchewan, Canada (Widger and Fredlund, 1979). Reportedly, cut and fill slopes have failed 4 to 6 years after construction. Soils involved in these failures appear to be similar to those which have been examined in connection with embankment slides in Texas, i.e., fine grained, highly plastic clays. Failure surfaces are generally shallow and "essentially circular." Frost penetration, which can be as deep as about 7 feet, may play a significant role in the occurrence of these failures. Widger and Fredlund (1979) performed a number of laboratory tests to determine shear strength parameters for use in assessing the stability of embank-

ments at the time of constuction and at the time of failure. Stability calculations made for conditions at the time of failure, using shear strength parameters measured from triaxial tests and using a phreatic surface at the ground surface (corresponding to a pore pressure ratio of 0.54), produced factors of safety near unity. The critical circular shear surface, however, extended deeper into the embankment than the estimated position of the observed failure. Considering the results of stability calculations presented earlier in this chapter for the embankment slide at IH 610 and Scott Street, it appears that the disagreement between the critical shear surface and the observed failure surface for the embankment slide examined by Widger and Fredlund may be explained by 1) an assumed pore pressure ratio which is too high and/or 2) a cohesion value, as measured in laboratory tests and used in the stability calculations, which is too high.

SUMMARY AND CONCLUSIONS

Factors of safety calculated for the IH 610 and Scott Street slide using shear strength parameters obtained from laboratory triaxial shear tests do not agree either with the factors of safety calculated using the shear strength parameters which were back-calculated or with the observed slope behavior. The most critical circle located based on the laboratory strengths is about two and one-half times deeper than the observed failure surface. The minimum factor of safety corresponding to the most critical shear surface based on laboratory measured shear

strengths was 2.37, indicating that the slope is stable, whereas the slope is known to have failed. Additional calculations made to investigate the effect of increased pore water pressures and cracks on the stability of the slope indicate that neither high pore water pressures or a crack can explain the disagreement between the results of the stability calculations based on laboratory strengths, and observed slope behavior.

Water contents measured for field samples were compared with the final water contents of laboratory compacted specimens after they were saturated and brought to equilibrium under final effective consolidation pressures selected to produce conditions similar to those existing in the slope. In some instances it was found that the field water contents were greater than the laboratory water contents. It is not known why these differences exist, or if these differences are an indication that the conditions produced in the laboratory do not accurately model conditions existing in the slope.

Although it is uncertain whether the slide at IH 610 and Scott Street was a first time slide or had been repaired previously by pushing and recompacting the soil, this does not appear likely to have affected the observed discrepancies between field and laboratory shear strength values. Even if the original slide had a geometry different from the one observed, the back-calculated shear strength parameters would not have agreed with the laboratory values. In addition, regardless of when a slide first occurred in the slope, such a slide would not have been expected based on the shear strength values determined from the laboratory tests.

The second slide selected for more detailed analysis occurred in the southwest quadrant at the SH 225 and SH 146 Interchange and is believed to be a first time slide. Shear strength parameters obtained from back-calculation and from laboratory tests were compared, and discrepancies similar to those for the IH 610 and Scott Street site were observed. Stability calculations made for the SH 225 and SH 146 site also produced results similar to those for the Scott Street site. As before, shear strength parameters measured in the laboratory do not agree with those strengths which exist in the slope at failure. It appears that the cohesion values thus far measured in the laboratory are unreasonably high.

CHAPTER 6. PROCEDURES FOR CALCULATION OF EMBANKMENT FOUNDATION STABILITY

INTRODUCTION

While most embankment failures observed in this study occurred entirely within the embankment side slope, a few were observed which developed in the foundation. It was recognized that a potential exists in Texas, especially in the Gulf Coast region, for occasionally severe embankment foundation failure problems. Examples of such problems were observed in Texas SDHPT Districts 12, 16, and 20 during the course of the present study. While the frequency of embankment foundation failures is not as great as that of embankment "slope" failures, the consequences of failure are often much more severe and expensive. Embankment foundation failures are seldom repaired by simply pushing the fill material back into place.

Embankment foundation failures usually occur as a result of a foundation which is considerably weaker than the embankment material. In cases of a relatively weak foundation, stability computations are often performed by treating the embankment as a surcharge and the shear strength of the embankment material is ignored. This approach has been used, for example, in District 12 of the Texas SDHPT. By treating the embankment as a surcharge, the problem is reduced to essentially a classical bearing capacity problem, and conventional bearing capacity

equations can be used to calculate a factor of safety. However, several approaches may actually be used and the corresponding values obtained for the factor of safety may differ considerably. In this chapter, three of the more commonly used approaches for calculating the factor of safety using bearing capacity approaches are examined and results obtained by the various procedures are compared.

SHEAR STRENGTH CONSIDERATIONS

Most embankment foundation failures occur during construction and, thus, can be considered as "short-term" failures. Such foundation failures in most clay soils are assumed to be "undrained" with the exception of those cases where wick or sand drains are installed to expedite drainage. Although there have been some arguments that embankment foundations are seldom completely without at least some drainage (Leroueil, Tavenas, Mieussens, and Peignaud, 1978), it continues to be the practice to consider the embankment foundation as undrained during construction unless provisions are made to expedite drainage. Undrained shear strengths are determined from a variety of tests, including vane shear tests, penetration tests, unconfined compression tests, and unconsolidated-undrained tests. In the case of a saturated soil, the angle of internal friction, ϕ, would be considered to be zero, while for unsaturated soils ϕ may be greater than zero.

METHODS OF ANALYSIS

Three approaches for computing the factor of safety for embankment foundation stability have been examined and are described in the following sections. The first two approaches are based on the same general bearing capacity equations but employ different definitions for the factor of safety. The third procedure is based on procedures used for slope stability analyses and employs the slope stability computer program UTEXAS.

Bearing Capacity Approaches

The first two approaches for determining the stability of embankment foundations use the general bearing capacity equations as presented by (Meyerhof, 1951). In the case of a load on the surface of the foundation, as is the case for most embankments, the bearing capacity equation is written as

$$q = c \cdot N_c + \gamma \cdot \frac{B}{2} \cdot N_\gamma \qquad (6.1)$$

where c is the cohesion, γ is the unit weight of the foundation material, and B is the width of the loaded area. The quantities N_c and N_γ represent dimensionless bearing capacity factors which depend on the angle of internal friction of the foundation soil. The bearing capacity factors, N_c and N_γ, are defined by the equations

$$N_c = (N_q - 1) \cot\phi \tag{6.2a}$$

and

$$N_\gamma = (N_q - 1) \tan(1.4\phi) \tag{6.2b}$$

where

$$N_q = e^{\pi \tan\phi} \tan^2(45 + \tfrac{\phi}{2}) \tag{6.2c}$$

The equation for the bearing capacity factor, N_c, was derived by Prandl (1920), while the equation for N_γ was empirically derived by Meyerhof (1961).

Because the height of embankment material varies beneath the slope face, the load applied to the foundation will vary across the width of this portion of the embankment. Thus, the resultant load generated is eccentrically applied. For the case of an eccentric load Meyerhof proposed that the bearing capacity be calculated using a reduced effective

width, B', for the loaded strip, defined by

$$B' = B - 2e \tag{6.3}$$

where B is the actual width of the loaded strip, and e is the eccentricity of the resultant load. The widths, B and B', and the eccentricity, e, are illustrated in Fig. 6.1 for a typical embankment section. The resultant load, Q, is located at the centroid of the embankment area being considered. The eccentricity, e, is the horizontal distance from the resultant load to the center of the strip of width B. The reduced effective width, B', is considered to carry the resultant load, Q, as a central, vertically applied load as illustrated in the lower part of Fig. 6.1.

In the case of an eccentric load, the ultimate bearing capacity, q_{ult}, is calculated using the reduced effective width, B', in the bearing capacity equation, which is written as

$$q_{ult} = c \cdot N_c + \gamma \cdot \frac{B'}{2} \cdot N_\gamma \tag{6.4}$$

The average applied stress, q_a, which is compared to the ultimate bearing capacity, q_{ult}, to determine if the foundation is adequate, is calculated as

$$q_a = \frac{Q}{B'} \tag{6.5}$$

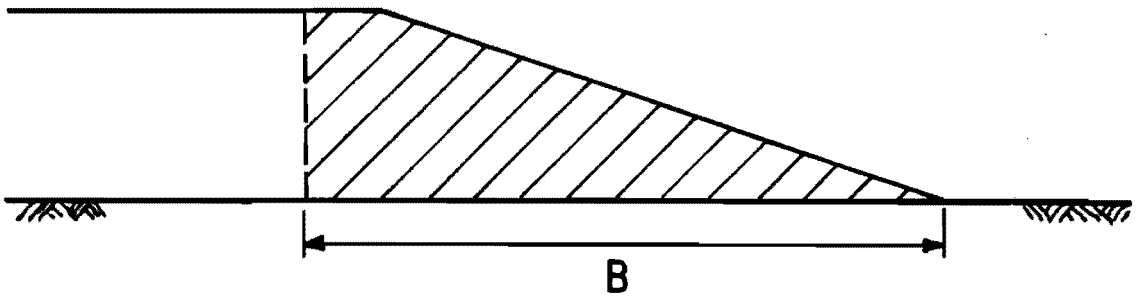

(a) Initial Assumed width of Loaded Strip

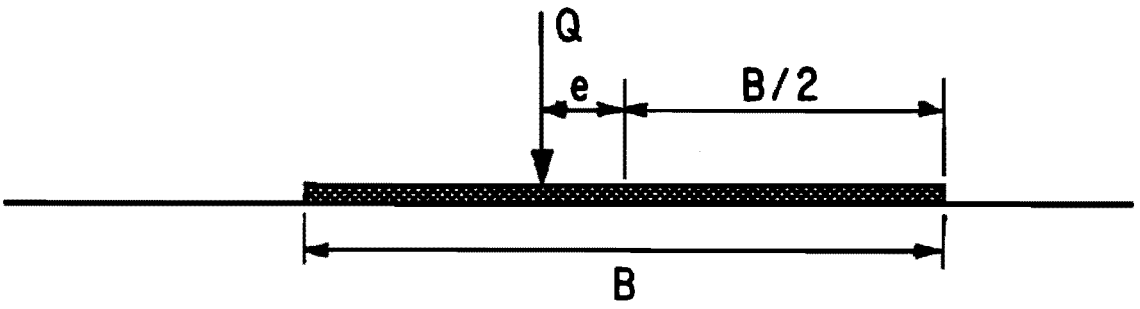

(b) Location of Resultant Load

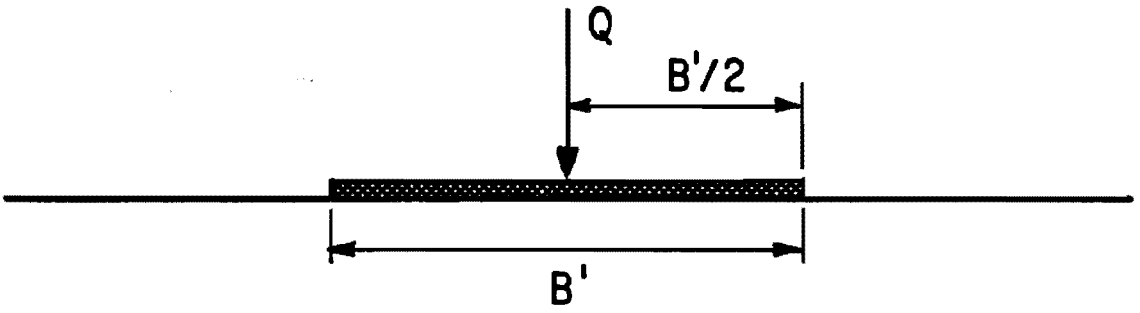

(c) Location of Resultant Load on the Strip of Reduced Effective Width, B', where $B' = B - 2e$

Fig. 6.1. Illustration of reduced effective width used in bearing capacity equations to account for eccentric loading.

For the case of an embankment, both the average applied stress, q_a, and the ultimate bearing capacity, q_{ult}, will vary with the assumed width, B, of the embankment considered. In order to find the most critical combination of q_a and q_{ult} corresponding to the minimum factor of safety, a trial and error procedure is required to find the width, B, which produces the minimum factor of safety. This width is referred to as the "critical width."

In the present study two different approaches were used with the bearing capacity equations described above to compute the factor of safety. In the first approach the factor of safety was defined with respect to load, and in the second approach the factor of safety was defined with respect to shear strength. A computer program, BEARCAP, was written and used to perform the calculations for the factor of safety using the bearing capacity equations. A trial and error procedure was used to locate the critical width, B, and the corresponding minimum factor of safety. Separate calculations were performed to compute the factor of safety with respect to load and shear strength. The two ways in which the factor of safety was defined and computed are described in the next two sections.

Factor of Safety with Respect to Load: The factor of safety with respect to load, F_L, is defined as the ratio of the ultimate bearing capacity of the foundation, q_{ult}, calculated from Eq. 6.4, to the average applied stress, q_a, calculated from Eq. 6.5. This definition of the factor of safety represents the conventional definition used for bearing capacity problems.

The trial and error procedure used to determine the critical width when the factor of safety is defined with respect to load involves six steps, as follows:

1. A trial embankment width, B, extending from the toe of the slope to a point beneath the embankment is selected for consideration.

2. The applied load, Q_a, due to the weight of the portion of the embankment which overlies the width B (chosen in Step 1) is calculated. The eccentricity of the load with respect to the center of the strip of width B is also calculated (see Fig. 6.1).

3. The effective width, B', is calculated using Eq. 6.3 with the assumed width from Step 1 and the eccentricity from Step 2.

4. The average applied stress is calculated as

$$q_a = \frac{Q_a}{B'} \tag{6.6}$$

and the ultimate bearing capacity, q_{ult}, is calculated from

$$q_{ult} = c \cdot N_c + \gamma \cdot \frac{B'}{2} \cdot N_\gamma \tag{6.7}$$

5. The factor of safety with respect to load is calculated from

$$F_L = \frac{q_{ult}}{q_a} \tag{6.8}$$

6. Finally, Steps 1 through 5 are repeated until the width giving a minimum factor of safety is located.

Factor of Safety with Respect to Strength: The factor of safety with respect to shear strength, F_S, is defined as the factor by which the foundation's shear strength must be "factored" such that the ultimate bearing capacity of the foundation is equal to the average applied stress. The "factored" shear strength is expressed in terms of "factored" shear strength parameters, c_m and ϕ_m, defined as

$$c_m = \frac{c}{F} \tag{6.9}$$

and

$$\phi_m = \arctan\left(\frac{\tan\phi}{F}\right) \tag{6.10}$$

where the subscript "m" is used to indicate that the shear strength parameters (c_m and ϕ_m) are "mobilized" values. The factored shear strength parameters are used to compute a corresponding "factored" ulti-

mate bearing capacity, q_{ult}', from the equation

$$q_{ult}' = c_m \cdot N_{cm} + \gamma \cdot \frac{B'}{2} \cdot N_{\gamma m} \qquad (6.11)$$

A trial and error procedure is used to determine the factor of safety with respect to shear strength, F_s, such that the ultimate bearing capacity, q_{ult}', calculated from Eq. 6.11, is equal to the average applied stress, q_a, calculated from Eq. 6.5. This definition of the factor of safety with respect to shear strength is equivalent to the definition of the factor of safety used in the computer program UTEXAS and for all slope stability analyses.

The trial and error procedure used to determine the critical width when the factor of safety is defined with respect to shear strength involves seven steps, as follows:

1. A trial embankment width, B, extending from the toe of the slope to a point beneath the embankment is selected for consideration.

2. The applied load, Q_a, due to the weight of the portion of the embankment which overlies the width B (chosen in Step 1) is calculated. The eccentricity of the load with respect to the center of the strip of width B is also calculated (see Fig. 6.1).

3. The effective width, B', is calculated using Eq. 6.3 with the assumed width from Step 1 and the eccentricity from Step 2.

4. The average applied stress is calculated as

$$q_a = \frac{Q_a}{B'} \tag{6.12}$$

5. A value for the factor of safety with respect to strenth, F_S, is assumed, and an "ultimate" bearing capacity, q_{ult}', is calculated from Eq. 6.11 using mobilized shear strength parameters and the effective width (calculated in Step 3). The value of the factor of safety with respect to load, F_L, determined from the first bearing capacity approach is usually used as an initial trial value for the factor of safety with respect to shear strength, F_S.

6. If the calculated value of q_{ult}' is different from the actual applied load, q_a, the value of F_S is adjusted and the calculations in Step 5 are repeated until the values of q_a and q_{ult}' are essentially the same.

7. Finally, steps 1 through 6 are repeated until the width giving a minimum factor of safety is located.

Slope Stability Approach

The third approach used to compute the factor of safety consists of using conventional slope stability analysis procedures wherein the factor of safety is defined with respect to shear strength. The factor of safety is defined in a manner identical to the way in which the factor of safety was defined in the second approach using the bearing capacity equations, as described in the previous section. For the calculations presented in this study, only circular (rather than noncircular) shear surfaces were considered. The critical shear surface corresponding to the minimum factor of safety was located using an automatic search routine in the computer program UTEXAS. The embankment was treated as a surcharge and was modeled by applying normal stresses on a horizontal surface. The "critical width" was determined based on where the critical circle intersected the horizontal ground surface as shown in Fig. 6.2.

In the extreme case where the embankment slope is vertical, the critical width was always found to be zero. This presented computational difficulties when an attempt was made to locate a critical shear surface. In order to obtain the factor of safety corresponding to zero width, the slope stability computer program was used to obtain the minimum factor of safety for critical circles which were tangent to lines at various selected depths below the ground surface. The range in depths used was 0.1 to 2.0 feet. The factor of safety was then plotted versus the corresponding depth, and the resulting plot was used to extrapolate to a mini-

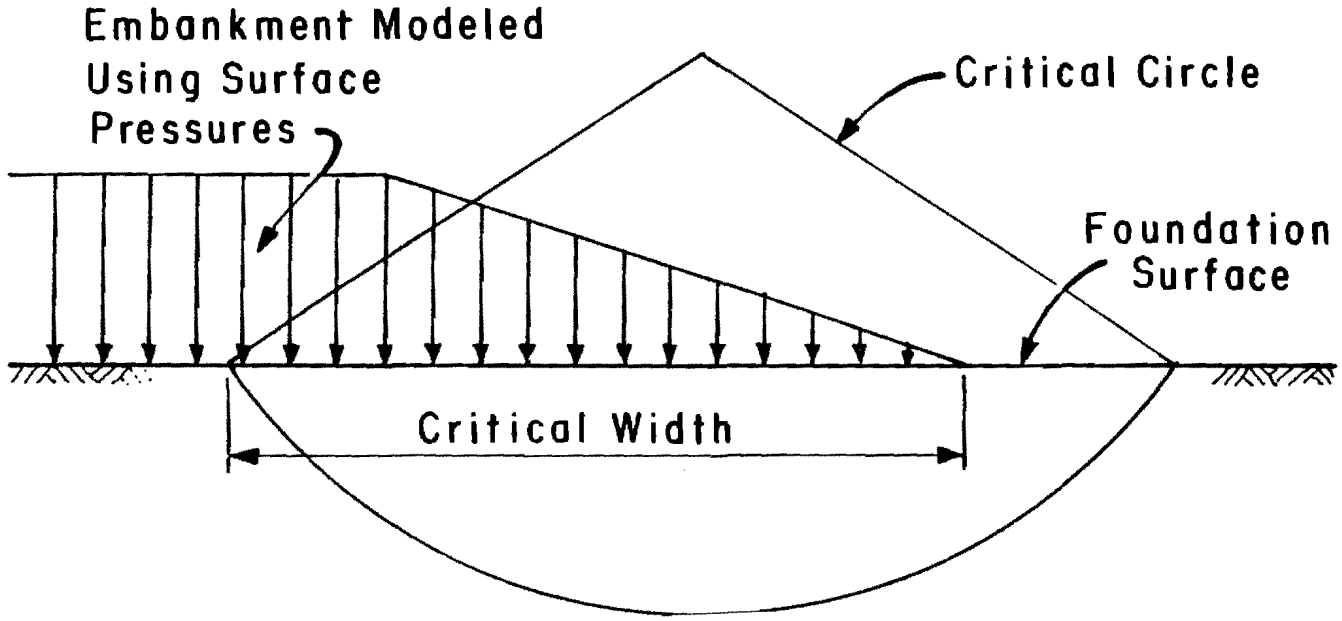

Fig. 6.2. Critical circle and resulting critical width using the slope stability approach.

mum factor of safety at zero depth, which also corresponds to an equivalent embankment width of zero.

RESULTS OF EMBANKMENT FOUNDATION STABILITY CALCULATIONS

Calculations were performed using the three approaches described above with two sets of foundation shear strength parameters. The two sets of shear strength parameters used are

Set 1: $c = 500$ psf and $\phi = 15$ degrees

Set 2: $c = 750$ psf and $\phi = 9$ degrees

These two sets of shear strength parameters had been used by the Texas SDHPT in performing bearing capacity calculations to determine potentially acceptable embankment heights at the intersections of U.S. 290 with Jones Road, Eldridge Road, and West Road in District 12. Two different embankment side slopes (vertical and 3:1) were considered for the calculations made in this chapter, as shown in Fig. 6.3. The vertical slope was considered because it represents a case where there is no eccentricity and, thus, any approximations made to account for eccentric loads would not affect the results for this case; the 3:1 slope was selected because it represents typical embankment side slopes which have been used in the past. The embankment height, H, was varied from 10 to

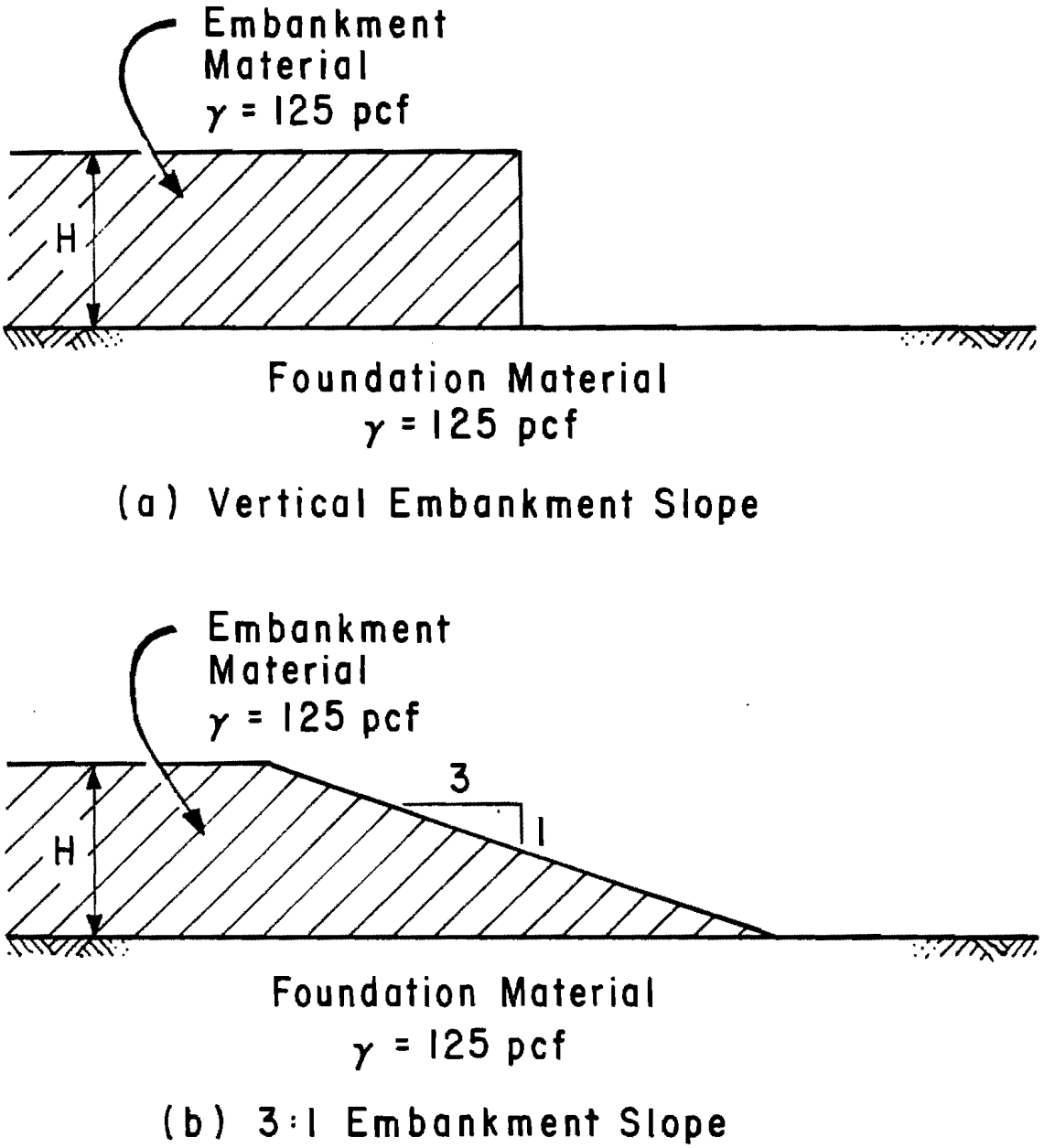

Fig. 6.3. Embankment geometries used for foundation stability computations.

50 feet. The total unit weights of both the embankment and foundation materials were assumed to be 125 pcf.

Results of calculations performed using the two bearing capacity equation approaches are considered and presented in the next section. Following this section, results based on the two approaches where the factor of safety was defined with respect to shear strength, using slope stability and bearing capacity equations, are considered. Finally, the critical widths determined for the various cases examined are presented and discussed.

Comparison of Results for Two Definitions of the Factor of Safety

The factors of safety computed using the two different definitions of the factor of safety with the bearing capacity equations are plotted versus embankment height in Fig. 6.4 for each of the embankment and soil conditions examined. The upper two figures are for the first set of soil properties (c = 500 psf and ϕ = 15 degrees), and the lower two figures are for the second set of soil properties (c = 750 psf and ϕ = 9 degrees). The two figures on the left are for vertical slopes ($\cot\beta$ = 0), and the two figures on the right are for 3:1 slopes ($\cot\beta$ = 3.0). It can be seen that the factor of safety with respect to load is always further from unity than the factor of safety with respect to strength, and that the two values for the factor of safety are equal when the factor of safety is unity. Thus, for stable slopes (factors of safety greater than

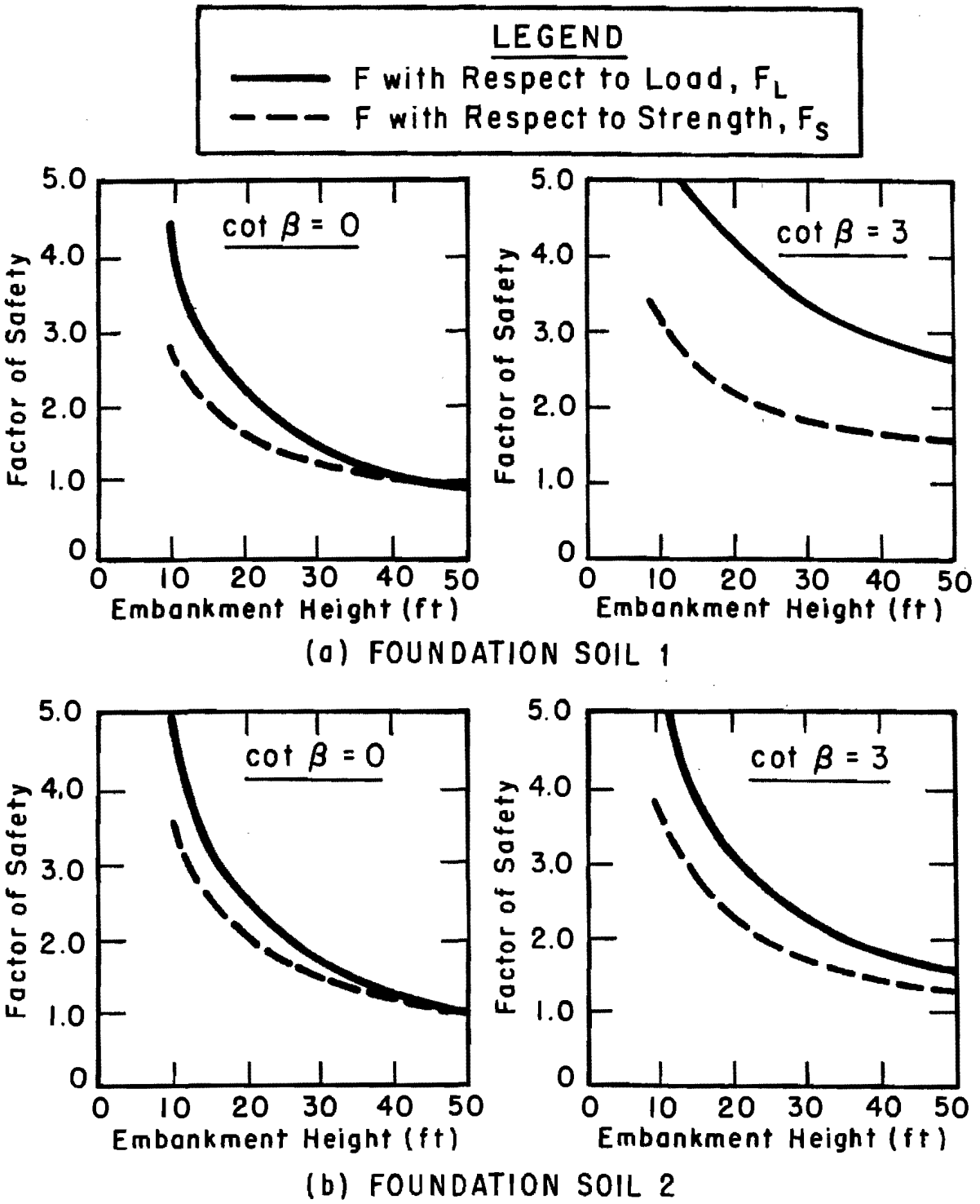

Fig. 6.4. Variation in factor of safety with embankment height, calculated using bearing capacity equations for selected slope inclinations and soil properties.

unity) the factor of safety with respect to shear strength will always be lower than the factor of safety with respect to load.

The ratio of the factor of safety with respect to load to the factor of safety with respect to shear strength is plotted versus embankment height on Fig. 6.5 for all four conditions examined. The ratio of the two factors of safety is a measure of the percentage difference between the two factors of safety and allows for easier, more meaningful comparisons between the two values. The ratio of the two factors of safety ranged between 0.96 and 2.12. It can be seen from the results shown in Fig 6.5 that the ratio of the two factors of safety was generally greatest, indicating the highest percent difference, for the flatter slope (slope ratio 3:1). The greatest differences between the ratio of the two factors of safety for the two slope ratios considered (vertical and 3:1) were found for the first set of material properties, which correspond to a greater "frictional" component of shear strength. Examining the trends shown in Fig. 6.5, it can also be seen that the ratio of the two factors of safety is greatest for embankments of lower height (corresponding to larger factors of safety).

Comparison of Results for Two Computational Approaches

The factors of safety with respect to shear strength computed using both the bearing capacity and slope stability approaches are plotted versus embankment height in Fig. 6.6 for each of the embankment and soil conditions examined. The same arrangement of diagrams is used for

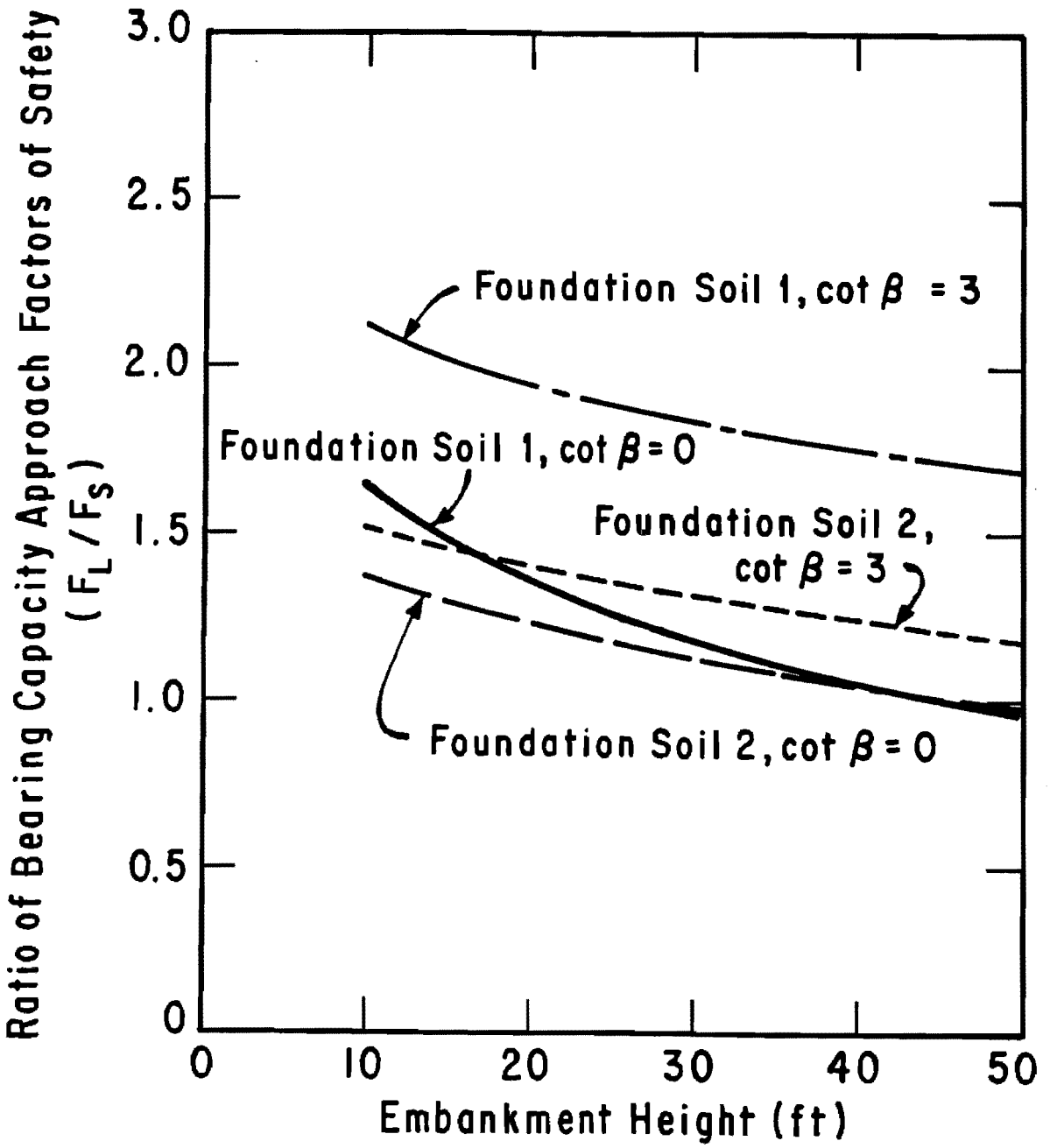

Fig. 6.5. Variation in the ratio of factors of safety with respect to load and shear strength with embankment height, calculated with bearing capacity equations for selected slope inclinations and soil properties.

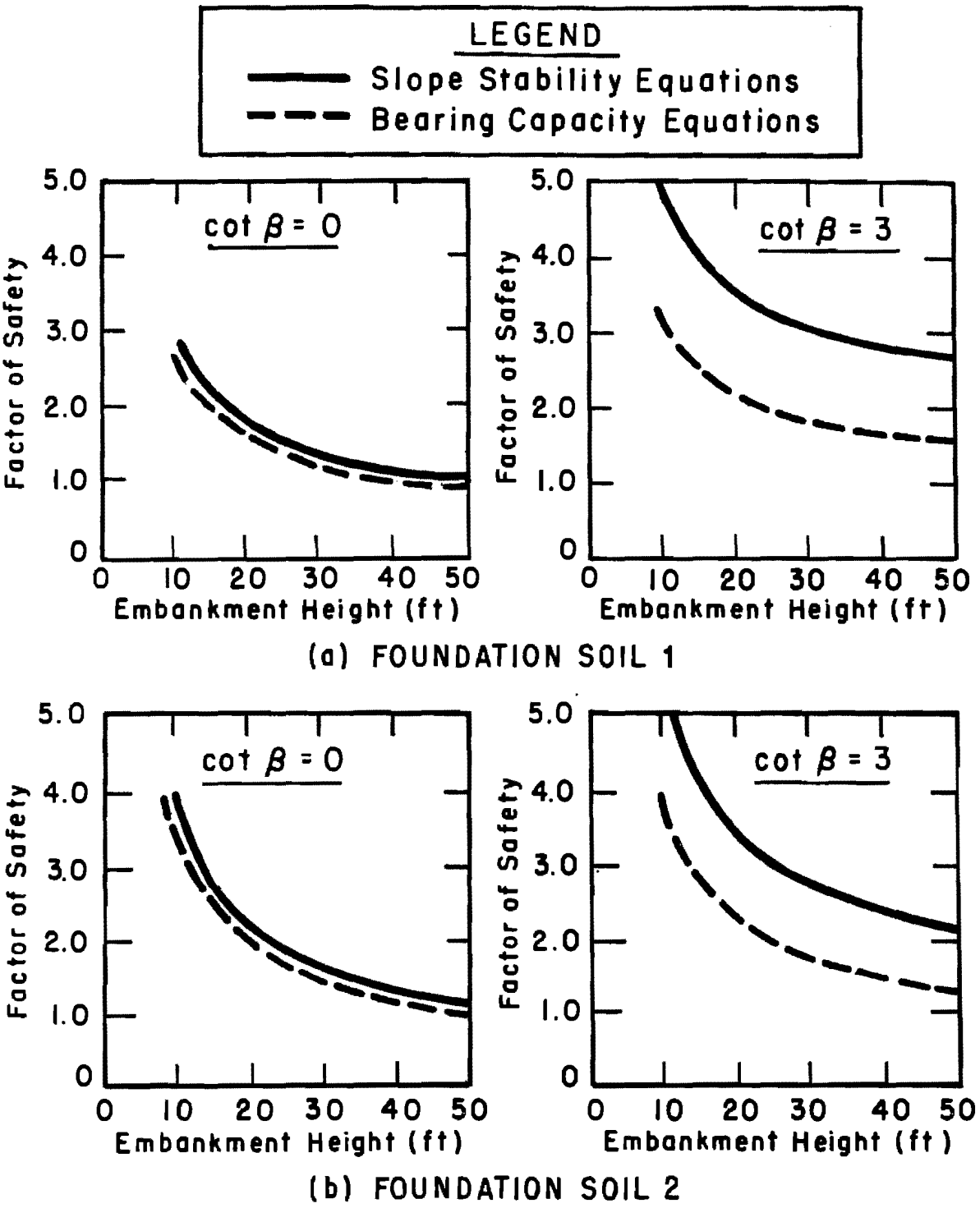

Fig. 6.6. Variation in the factor of safety with respect to strength with the embankment height, calculated by bearing capacity and slope stability equations for selected slope inclinations and soil properties.

this figure as was used for Fig. 6.4. For all embankment heights and all conditions examined it was found that the factor of safety calculated by the slope stability equations, using the computer program UTEXAS, was greater than the factor of safety calculated using the bearing capacity equations. For each of the four conditions considered it was found that the two curves representing the variation in the factor of safety with embankment height for each of the two computational approaches follow a similar trend, and the two curves appear to be essentially parallel. The differences in the two factors of safety were only about 10 percent for the vertical slope but ranged from about 50 to 70 percent for the 3:1 slope. Thus, there appears to be a significant effect of slope angle on the differences in the two factors of safety. There does not appear to be a significant effect of either soil properties or embankment height on the differences in the two factors of safety.

To illustrate the significance of the differences in the bearing capacity and slope stability approaches for computing the factor of safety, the differences in embankment heights required to provide a given factor of safety can be examined. For example, consider an embankment with a slope ratio of 3:1 and a foundation represented by the first set of soil properties, and assume that a factor of safety of 2.0 is acceptable. From the results presented in Fig. 6.6 it can be seen that the calculations based on bearing capacity equations indicate that a 24-foot embankment is allowable, whereas the calculations based on slope stability procedures would allow for embankments over 50 feet in height. Thus,

the allowable embankment heights given by the two approaches differ by a factor greater than two.

Examination of Critical Widths

The critical widths were determined by each of the three approaches used to define and calculate the factor of safety, and are plotted versus embankment height in Fig. 6.7 for the embankment with 3:1 side slopes. The diagram on the left of Fig. 6.7 represents critical widths determined for the first set of soil properties, and the diagram on the right represents critical widths determined for the second set of soil properties. In both diagrams, the lower dashed line represents the width of the face of the slope; for the case illustrated ($\cot\beta = 3.0$), the width of the slope face is three times the height of the embankment. The critical width for all three approaches considered, and for both foundation soils, is greater than the width of the slope face. The lines representing the variation in the critical width with embankment height for each approach are approximately parallel to the line representing the width of the slope face. The largest critical widths were obtained using the bearing capacity equations with the factor of safety defined with respect to shear strength, while the smallest critical widths were obtained when the slope stability procedures were used. In the case of the vertical embankment slope, the critical width was found to be zero for each of the cases examined and for each of the three approaches used to calculate the factor of safety.

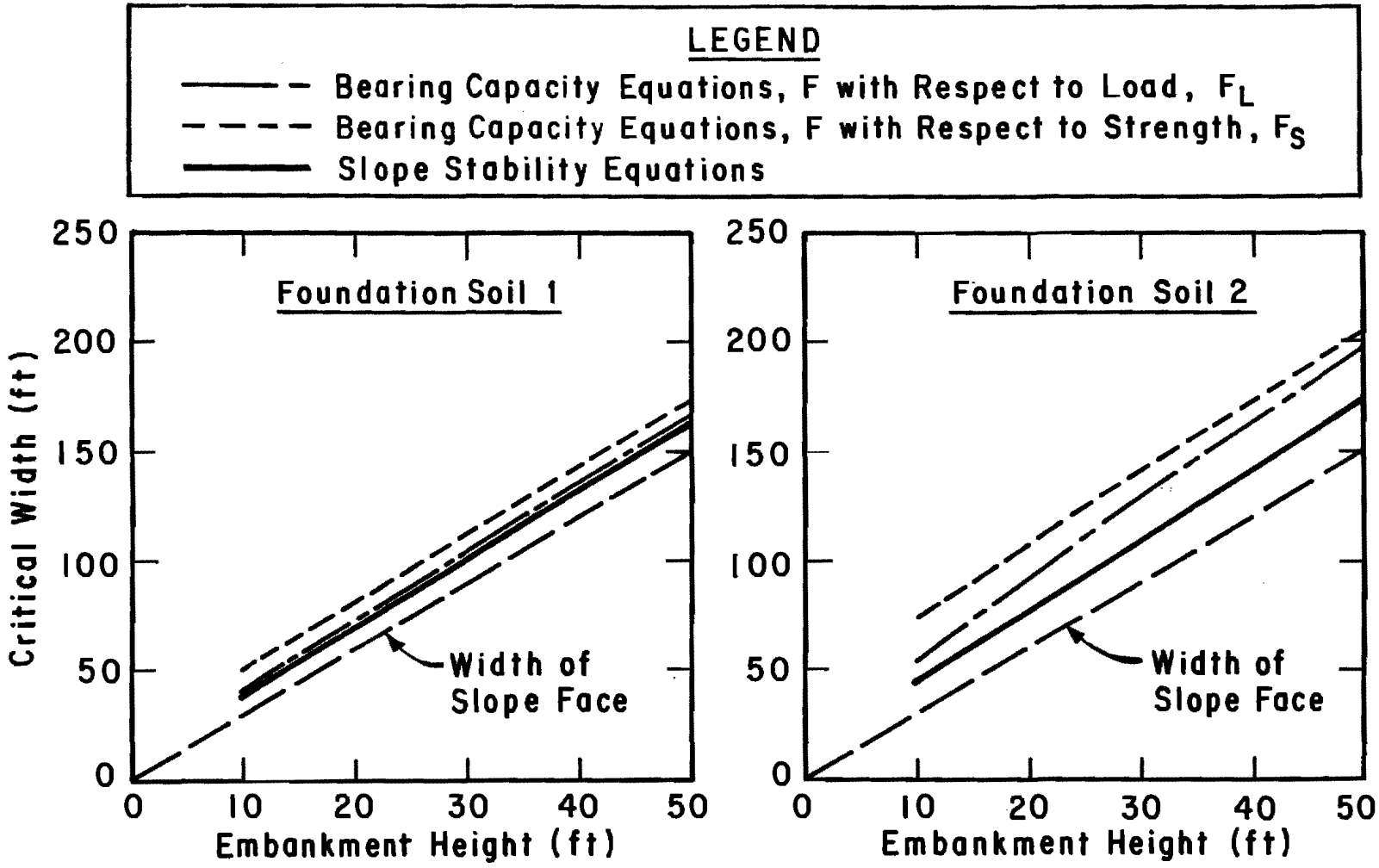

Fig. 6.7. Variation in the critical width with embankment height calculated by the various approaches for a 3:1 slope with two sets of soil properties.

SUMMARY AND CONCLUSIONS

Three simplified approaches for computing the factor of safety of embankments on weak foundations have been presented. All of these ignore the shear strength of the embankment by treating the embankment as a simple surcharge. Two of the approaches make use of the general bearing capacity equations. In one of these two approaches the factor of safety was defined with respect to load; in the other approach the factor of safety was defined with respect to shear strength. The third approach is based on conventional slope stability analysis procedures and calculations were performed using the computer program UTEXAS. These three approaches were used to compute the factor of safety for several cases.

The factors of safety determined using the bearing capacity approaches differed significantly, depending on whether the factor of safety was defined with respect to shear strength or load. For the cases considered where the slope was stable, the factor of safety with respect to load was found to be up to twice the factor of safety with respect to shear strength, although both would be equal when either the factor of safety is unity or ϕ is equal to zero.

When bearing capacity equations are to be used for embankment foundation analyses it seems most appropriate to define the factor of safety with respect to shear strength rather than with respect to the load. The greatest uncertainity lies in the shear strength of the foundation material, not in the load applied by the embankment. Definition of the factor of safety in terms of shear strength also is consistent

with the definition used in slope stability calculations. For conditions where the embankment is determined to be stable, the factor of safety defined with respect to shear strength is always lower than the factor of safety defined with respect to load.

The factors of safety defined with respect to shear strength were found to be significantly different, depending on whether bearing capacity equations or slope stability analysis procedures were used. For the cases examined in this study, the factors of safety defined with respect to shear strength using the bearing capacity equations were lower, and in some cases significantly lower, than the factors of safety computed using the slope stability approach. The differences were relatively small for cases where the slope is vertical but were much more pronounced for cases where the slope ratio was 3:1. The differences may result from several reasons. First, the bearing capacity equations were derived using different shear (failure) surfaces for the cohesive component of shear strength and for the frictional component of shear strength. Such an approximation is made for convenience, but in reality only one failure surface can exist. The approximation will lead to a "lower bound" solution for the bearing capacity, although it may not be totally realistic. The second possible reason for the differences between the factors of safety may be that in the computations by the slope stability approach the most critical shear surface may not have been used because the shear surface was assumed to be circular. Although the assumption of circular shear surfaces is often made, and appears reasonable for homogeneous soil conditions in earth slopes, the assumption

may not be entirely reasonable for the current problem and may explain, at least in part, the differences between the factors of safety calculated by the two approaches. A third possible reason for the differences in the factors of safety calculated by the bearing capacity and slope stability approaches may be due to differences in the theoretical equations used to calculate the factors of safety. The bearing capacity equations do not involve as complete a consideration of the requirements for static equilibrium as the slope stability equations do; the slope stability procedure used in this study fully satisfies the requirements for static equilibrium, while the bearing capacity equations do not. Finally, a fourth possible reason for the differences in the factors of safety may be related to the use of a reduced effective width in the bearing capacity equations. As was noted above, the differences in the two factors of safety were relatively small for cases where the slope is vertical (no reduction of the loaded width is applied in this case) but were much more pronounced for cases where the slope ratio was 3:1. It would appear that the use of the reduced effective width equation (Eq. 6.3) may introduce errors in the bearing capacity approaches.

It seems clear that the differences between the factors of safety with respect to shear strength computed using the bearing capacity and slope stability approaches are not clearly understood, and that further studies are needed. Fundamentally, the approach based on slope stability procedures appears more attractive because the factor of safety is based on a single shear surface, rather than separate surfaces for cohesion and friction, and the procedures used fully satisfy the require-

ments for static equilibrium. However, correct use of slope stability procedures requires that the most critical shear surface, whether it is circular or noncircular, be found by trial and error. It appears that the bearing capacity equations can be used to compute a conservative value for the factor of safety, and, because of the relative ease with which the bearing capacity equations can be used, they may be more attractive for some applications.

CHAPTER SEVEN. THE EMBANKMENT FOUNDATION FAILURE AT OSO BAY

INTRODUCTION

Although relatively few embankment foundation failures were observed during this study, when such failures occur, they can be costly. One such failure occurred during construction of an embankment at State Highway 358 where it crosses Oso Bay near Corpus Christi, Texas. As a result of the failure, extensive remedial measures were designed and installed. These remedial measures consisted of reinforced earth retaining walls and stone columns which improve the shear strength characteristics of the foundation. As part of the research reported on herein, slope stability analyses were performed to back-calculate the shear strengths of the foundation clays in order to establish appropriate values which might be used for redesign of the embankment and for remedial measures. Additional slope stability analyses were performed to evaluate the potential improvement in stability afforded by candidate remedial measures.

The procedures employed to back-calculate the shear strength of the foundation for the Oso Bay embankment are typical of the procedures used to back-calculate the shear strength of foundations. However, these procedures differ significantly from the procedures for back-calculating shear strengths within the slope itself, as described in Chap-

ter Three. Thus, the Oso Bay failure provides an excellent example to illustrate another type of slope failure where shear strengths are back-calculated. The slide at Oso Bay and the stability calculations performed are described in this chapter.

DESCRIPTION OF SITE AND FAILURE

The embankment of interest was being constructed as part of the expansion of State Highway 358 where it crosses Oso Bay near Corpus Christi, Texas. New approach embankments were being constructed at both east and west ends of the highway crossing. Failure occurred in June of 1983 at about Station 160 + 00 on the south side of the west embankment. Fill placement for this embankment was in progress and was near completion at the time failure occured.

A cross-section of the embankment at about Station 160 + 00 is shown in Fig. 7.1. The slope geometry shown in Fig. 7.1 had been measured by Texas SDHPT personnel shortly after failure had occurred. The soil profile shown in Fig. 7.1 was determined from test borings which are descibed in the following section.

An existing embankment for State Highway 358 where it crosses Oso Bay had been constructed in the late 1950's. This existing embankment is referred to in the following presentation as the "old embankment fill." The new embankment on the west side of the bay is shown in Fig. 7.1 and was constructed partly over the old embankment fill and partly over a deposit of soft clay "muck." The south side of the new embank-

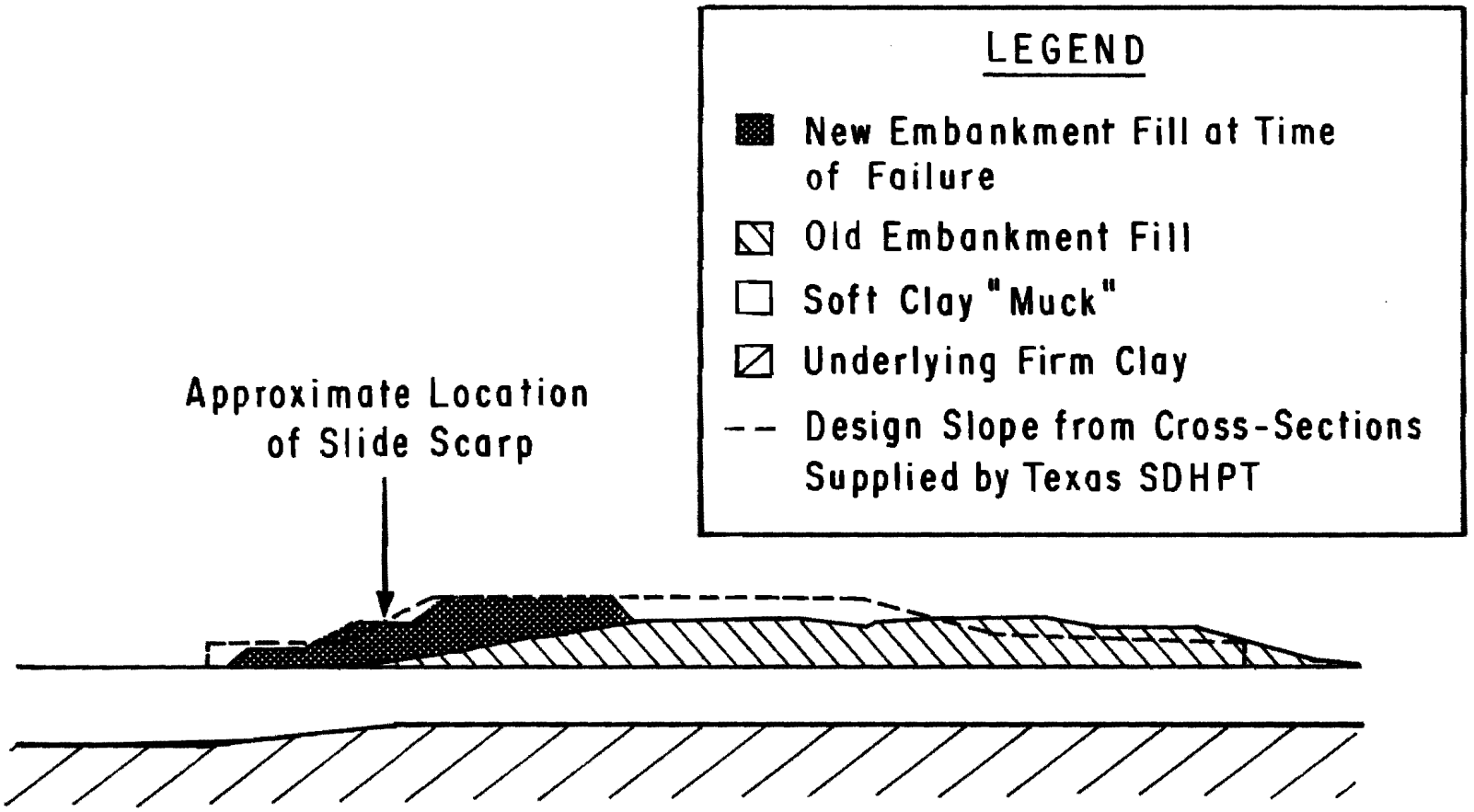

Fig. 7.1. Cross-section of SH 358 embankment near Oso Bay at Station 160 + 00 near the location of the failure.

ment, shown in the left-hand side of Fig. 7.1, extended over the muck. Placement of fill on the south side was near completion when failure occurred. The north side of the new embankment at the time of failure was located near the center of the old embankment. The northernmost portion of the new embankment had not been completed when failure occurred. The dashed line shown on Fig. 7.1 represents the design geometry which was provided by the Texas SDHPT.

The approximate location of the slide scarp is also shown in Fig. 7.1. The location and depth of the failure surface are unknown except for the approximate location of the slide scarp as shown in Fig. 7.1. The scarp was dipping nearly vertically toward the south side of the embankment. The location of the toe of the slide was obscurred by the water of Oso Bay which ponds adjacent to the toe of the embankment.

FIELD EXPLORATION

A preliminary field investigation of the Oso Bay site was conducted in 1957. During this investigation a number of exploration borings were made, some of which were in the vicinity of the failure. Soil samples were taken and standard penetration tests and in-situ vane shear tests were performed on the various materials encountered.

Following the occurrence of the embankment foundation failure in June of 1983, a number of additional test borings were made. Texas Cone Penetration tests and in-situ vane shear tests were performed. Data obtained from the 1957 and the 1983 borings were combined to obtain the

subsurface profile shown in Fig. 7.1. Fill materials shown in Fig. 7.1 include the old embankment and the new embankment; natural materials shown in Fig. 7.1 consist of a soft clayey "muck" foundation and an underlying "firm clay" stratum.

SOIL PROPERTIES

Visual descriptions of the soil from the test borings, and the results of the penetration and in-situ vane shear tests were examined to estimate probable ranges in soil properties for the materials at the site. Properties of the old and new fill materials and the soft and firm clay foundation strata are examined separately below.

New Embankment Fill Material

The nature of the material used to construct the new embankment was not clearly known and no description of this material was included in the recent, 1983, boring logs. However, it appeared to be reasonable to assume that the new fill is similar to the old fill. Soil descriptions in the 1983 boring logs refer to the old embankment fill as a stiff clay with very fine sand and silt. The clay was moist and was dark grey in color.

Texas Cone Penetrometer Test N-values were obtained in the new fill from two of the test borings excavated in the vicinity of the fail-

ure in 1983. The N-values measured ranged from 16 to 25. Undrained shear strengths were estimated from the N-values using the correlation

$$s_u = 80 \cdot N \tag{7.1}$$

where s_u is the undrained shear strength in pounds per square foot and N is the Texas Cone Penetrometer Test N-value. The correlation given by Eq. 7.1 was developed for highly plastic clay soils (The Bridge Division, Texas Highway Department, 1972). Based on this correlation and the measured N-values (16-25), the undrained shear strengths for the new embankment fill were estimated to range from 1280 to 2000 psf. However, because of the uncertainty in the shear strength of the new fill (only two penetration tests were performed), and due to the potential importance of the strength on stability computations, a range in shear strength characterizations was used in the stability computations, as discussed later.

Old Embankment Fill Material

Soil descriptions in the 1983 boring logs refer to the old embankment fill as a stiff clay with very fine sand and silt. The clay was moist and was dark grey in color. There are no field test data available for this material. For the purposes of stability calculations, the old embankment material was considered to be saturated. Thus, ϕ was assumed to be zero. A cohesion value (undrained shear

strength) of 1000 psf was used to characterize the strength of the old fill.

Soft Clay "Muck"

Soil descriptions in the 1983 boring logs refer to the soft clay "muck" as a very soft clay with very fine sand and silt and shell fragments. The clay was wet and was grey-to-black in color. In-situ vane shear tests were performed in this material during both the 1957 and the 1983 test borings. The vane test data were examined to determine the shear strength of the material, including any variation of shear strength in either the vertical or horizontal directions.

The shear strengths measured by in-situ vane tests from the 1957 and the 1983 borings are summarized in Table 7.1. The ground elevation, depth below ground elevation, elevation at the depth tested, and the vane shear strength measured are presented in Table 7.1. In addition, the thickness of fill for each of the borings, and in the case of the 1983 borings whether this was old or new fill, is included in the tabulation in Table 7.1. Vane shear strengths measured from the 1957 borings ranged from 116 to 647 psf; vane shear strengths measured from the 1983 borings ranged from 122 to 1905 psf. Bjerrum (1972) suggests multiplying the measured vane shear strength by a correction factor which is dependent on the plasticity index of the soil; however, the vane shear strengths summarized in Table 7.1 are not corrected. Application of the correction factor would reduce the vane shear strengths for soils with plasticity

TABLE 7.1. SUMMARY OF VANE SHEAR STRENGTH DATA FOR SOFT CLAY "MUCK"

1957 Borings

Boring	Ground Elev.	Depth (ft)	Elev. @ Depth	s_u from Vane (psf)	Type/Amount of Fill
6	2.8	9	- 6.2	201	5 ft fill
6	2.8	10.5	- 7.7	269	5 ft fill
6	2.8	12.5	- 9.7	647	5 ft fill
7	3.2	9	- 5.8	116	5 ft fill
7	3.2	10.5	- 7.3	229	5 ft fill

1983 Borings

Boring	Ground Elev.	Depth (ft)	Elev. @ Depth	s_u from Vane (psf)	Type/Amount of Fill
108	4.69	18	-13.3	501	3 ft New Fill
109	10.93	16.5	- 5.6	134	13 ft New Fill
109	10.93	22.0	-11.1	336	13 ft New Fill
109	10.93	26.0	-15.1	1905	13 ft New Fill
109	10.93	27.0	-16.0	885	13 ft New Fill
110	9.57	17.0	- 7.4	623	7 ft Old Fill
111	4.41	6.0	- 1.6	348	4 ft New Fill
111	4.41	16.0	-11.6	122	4 ft New Fill
112	11.01	22.0	-11.0	678	12 ft New Fill

indices greater than about 20 percent, which probably applies to the soft clay muck. The vane shear strengths are plotted versus the elevation at the depth tested in Fig. 7.2 and versus the estimated effective vertical overburden stress at the depth tested in Fig. 7.3. Examining the data shown in Figs. 7.2 and 7.3, there appears to be a general increase in strength with depth; however, there are no consistent trends observed in either of these plots. In addition, it appears that the vane shear strengths summarized in Table 7.1 do not vary in any consistent manner in the horizontal direction.

One of the principal objectives of the stability computations described in the next section was to "back-calculate" shear strengths for the soft muck. The shear strengths which were back-calculated are compared to the vane shear strength data later in this chapter.

Underlying Firm Clay Material

The underlying firm clay is described in the 1957 and 1983 boring logs as a stiff clay with streaks of sand, caliche nodules, and small pieces of quartz. The clay was moist and was cream, grey, and brown in color. Standard penetration test N-values obtained from the 1957 borings excavated in the vicinity of the failure ranged from 14 to 43. The higher N-values correspond to greater depths. According to relations suggested by Terzaghi and Peck (1967), these N-values correspond to undrained shear strengths greater than 2000 psf. N-values from Texas Cone Penetrometer tests performed during the 1983 test borings range

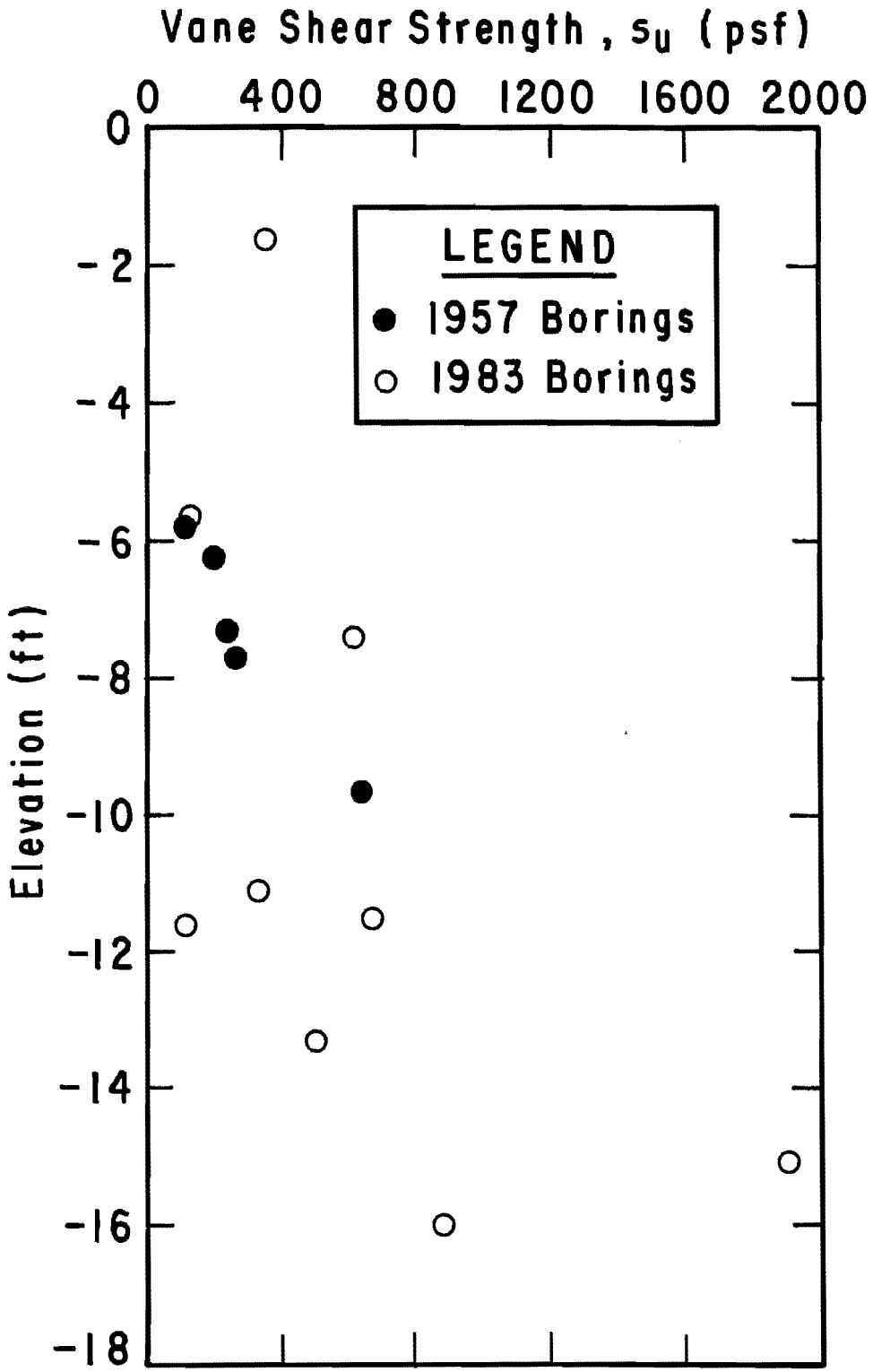

Fig. 7.2. Variation in the in-situ vane shear strength with elevation.

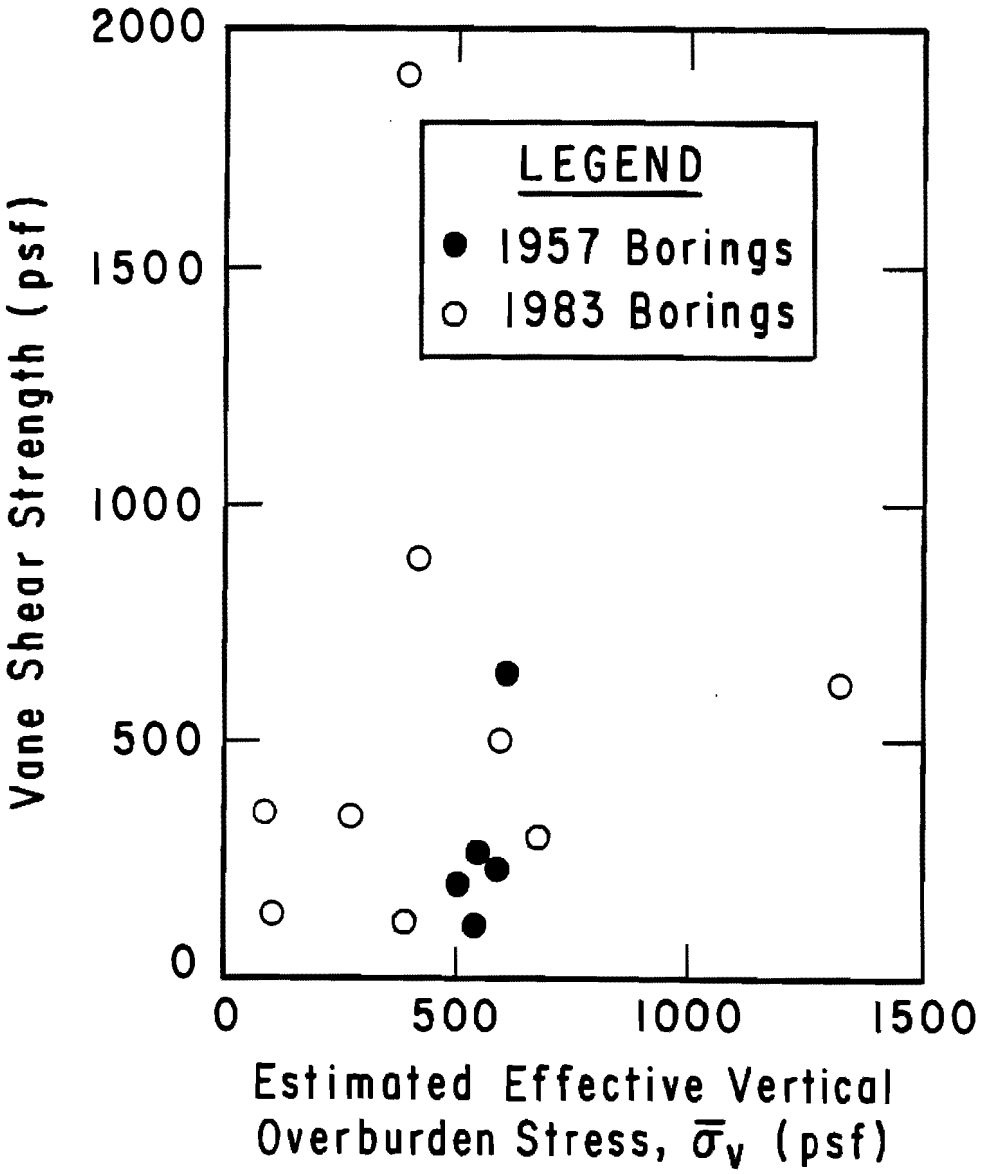

Fig. 7.3. Variation in the in-situ vane shear strength with the estimated effective vertical overburden stress.

from 15 to 23. These values were measured at depths near the contact of the firm clay with the soft clay muck. Using the previously cited correlation (Eq. 7.1), these N-values correspond to undrained shear strengths ranging from 1200 to 1840 psf. For the purposes of stability calculations, the underlying firm clay was considered to be saturated. Thus, ϕ was assumed to be zero. A cohesion value (undrained shear strength) of 1800 psf was used to characterize the strength of the underlying firm clay.

STABILITY COMPUTATION PROCEDURES

Several series of stability computations were performed for the Oso Bay embankments for conditions at the time of failure as well as for the completed embankment, both with remedial measures and without remedial measures. All of the stability calculations were performed using a new computer program, UTEXAS, which was developed as the primary goal of this research project (Wright and Roecker, 1984a). Results obtained using the new computer program were verified using another computer program, SSTAB1 (Wright, 1982). All stability computations were performed for the "short-term" condition representative of construction and immediately after construction. Therefore, all calculations were performed using total stresses rather than effective stresses. Only circular shear surfaces were considered in the analyses.

BACK-CALCULATION OF SHEAR STRENGTHS

The first several series of stability calculations were performed to back-calculate the shear strength of the soft clay muck foundation material. The procedure used to back-calculate the shear strengths involved varying the shear strength of the soft clay muck such that the shear strength corresponding to a factor of safety of unity could be determined. The slope geometry measured shortly after failure, and the soil profile shown in Fig. 7.1 were used in the stability calculations. A total unit weight of 125 pcf was assumed for all materials except for the soft clay muck which was assumed to have a total unit weight of 100 pcf.

Embankment Material Properties

Because the nature of the material used to construct the new embankment was not known, three different sets of shear strength characterizations were used for the new embankment fill in the stability calculations. For the first characterization of the new embankment fill, the material was assumed to be saturated with no drainage occurring during construction. Thus, ϕ was assumed to be zero and a cohesion value (undrained shear strength) of 1500 psf was assumed.

For the second characterization, the new fill material was assumed to drain and behave as a frictional material. The cohesion was

assumed to be zero and the shear strength was characterized by a friction angle, ϕ, of 25 degrees.

For the third characterization of the new embankment fill, the embankment was treated as a surcharge in a way similar to the way the embankment was treated in the analyses presented in Chapter Six. For the cases examined in Chapter Six, the ground surface beneath the embankment was horizontal and, thus, calculation of the surface pressure due to the embankment load was very simple: the normal stress at a point was calculated by multiplying the height of the embankment above that point by the total unit weight of the embankment fill. There are no shear stresses generated at the ground surface when the ground surface is horizontal. However, for the case of Oso Bay, a portion of the new fill was constructed over the old embankment slope such that both normal and shear stresses would be generated. The normal and shear forces were estimated assuming an infinite slope from the equations

$$\sigma = \gamma \cdot z \cdot \cos^2 \theta \tag{7.2}$$

and

$$\tau = \gamma \cdot z \cdot \sin\theta \cdot \cos\theta \tag{7.3}$$

where γ is the total unit weight of the new fill, z is the vertical distance between the point on the ground surface before placement of the new fill and the top of the new fill, and θ is the slope angle of the ground

surface before the new fill was placed. The total unit weight of the new embankment fill was assumed to be 125 pcf for all of the stability calculations.

Results of Computations

The soft muck was assumed to be saturated and, accordingly, ϕ was assumed to be zero. The cohesion value (undrained shear strength) for the muck was varied from 150 to 325 psf, and the factor of safety was calculated for each of the three characterizations of the new embankment, as described above. The factor of safety is plotted versus the assumed undrained shear strength of the muck for the three embankment characterizations in Fig. 7.4. The shear strength of the muck corresponding to a factor of safety of unity for each of the embankment characterizations was read from this figure.

For the first new embankment characterization (c = 1500 psf and ϕ = 0), the back-calculated shear strength for the muck is 188 pcf. The critical circular shear surface located for this case is shown in Fig. 7.5. For the second new embankment characterization (c = 0 and ϕ = 25 degrees), the back-calculated shear strength for the muck is 288 psf. The critical circular shear surface located for the second case is shown in Fig. 7.6. Finally, when the new embankment is treated as a surcharge, the back-calculated shear strength for the muck is 265 psf. The critical circular shear surface located with the new embankment treated as a surcharge is shown on Fig. 7.7. Additional stability calculations were per-

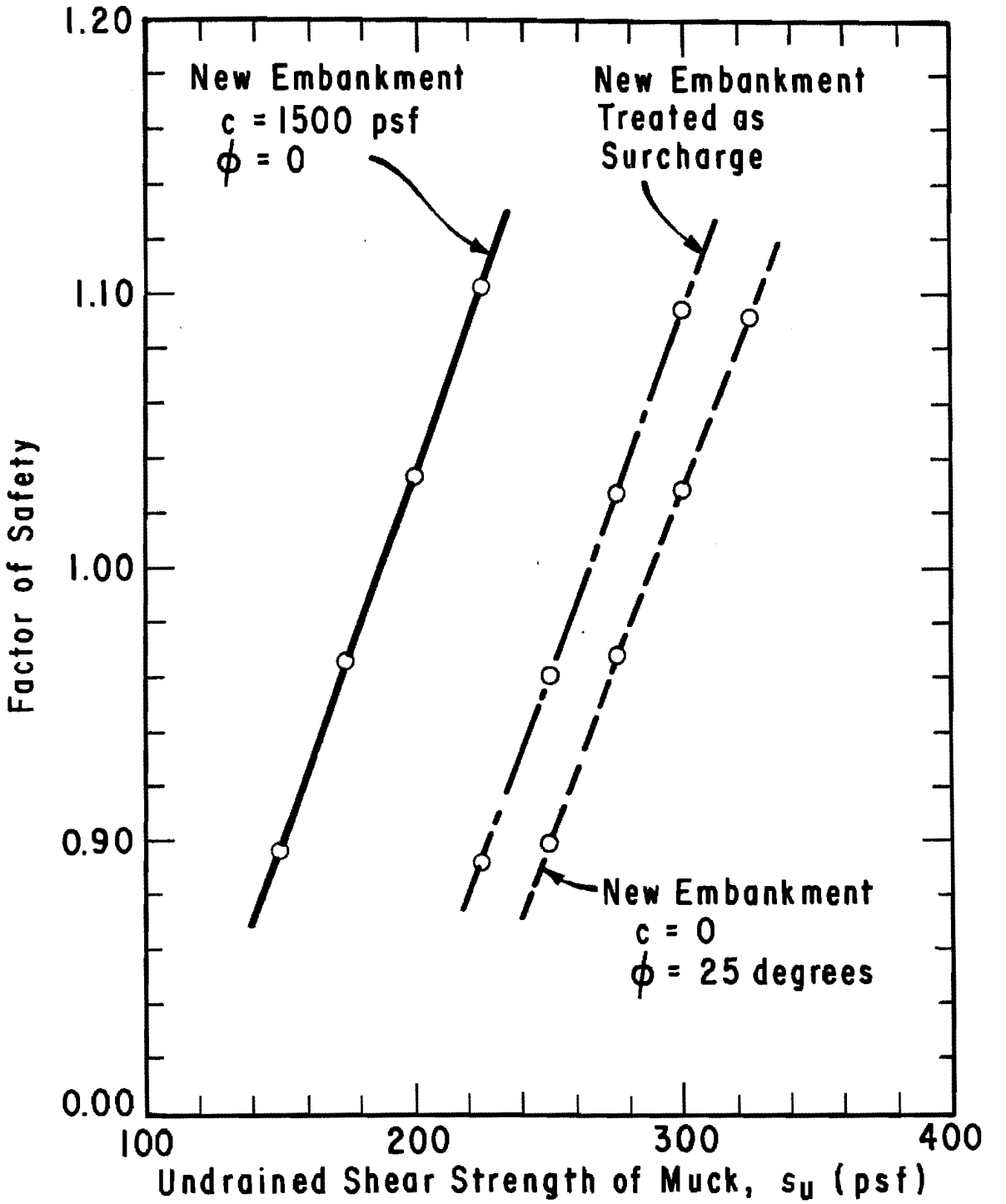

Fig. 7.4. Variation in the factor of safety with the assumed undrained shear strength of the "muck" for three characterizations of the new embankment fill.

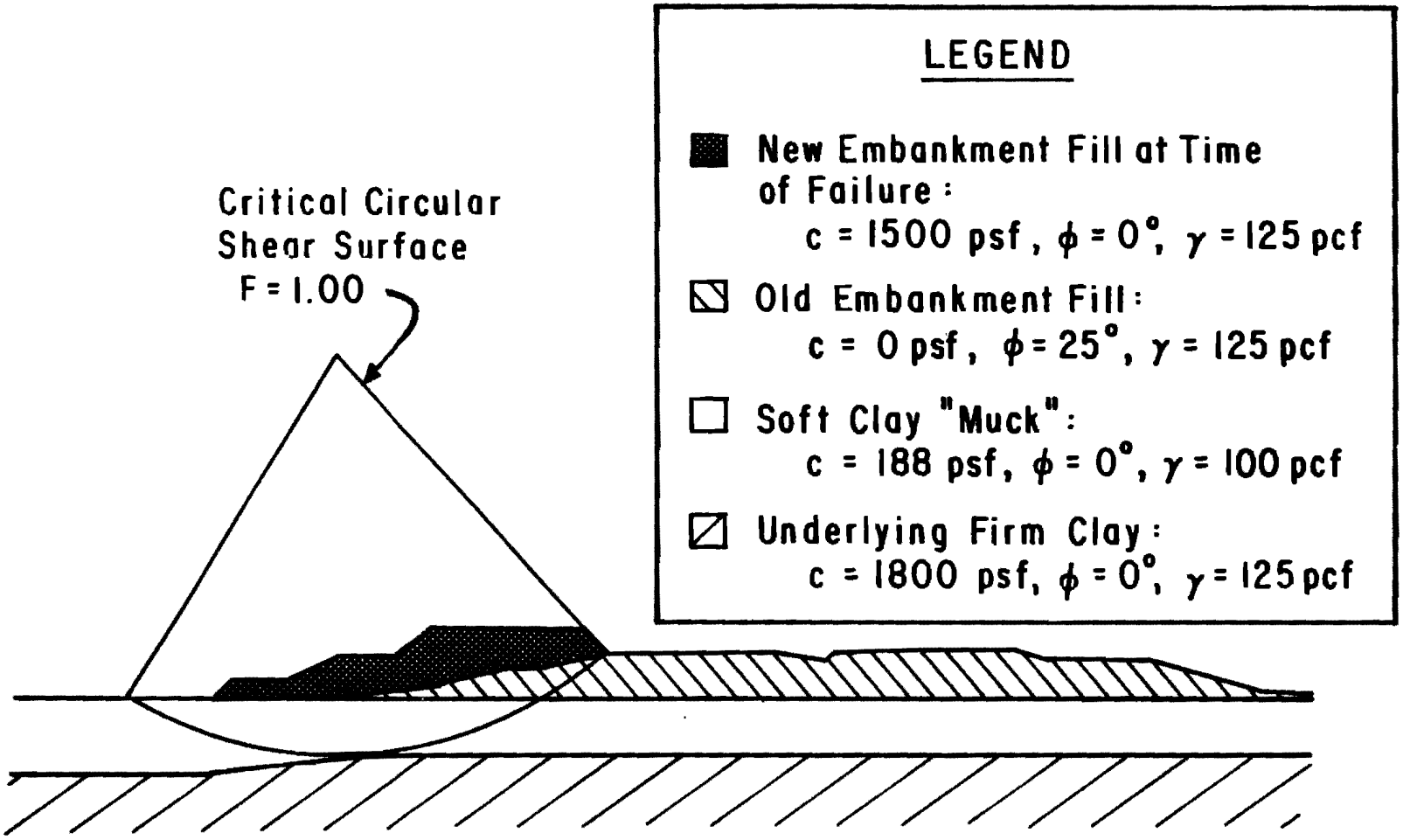

Fig. 7.5. Critical circle for Oso Bay embankment based on stability calculations for conditions at the time of failure with the new embankment characterized as a purely "cohesive" ($\phi = 0$) material.

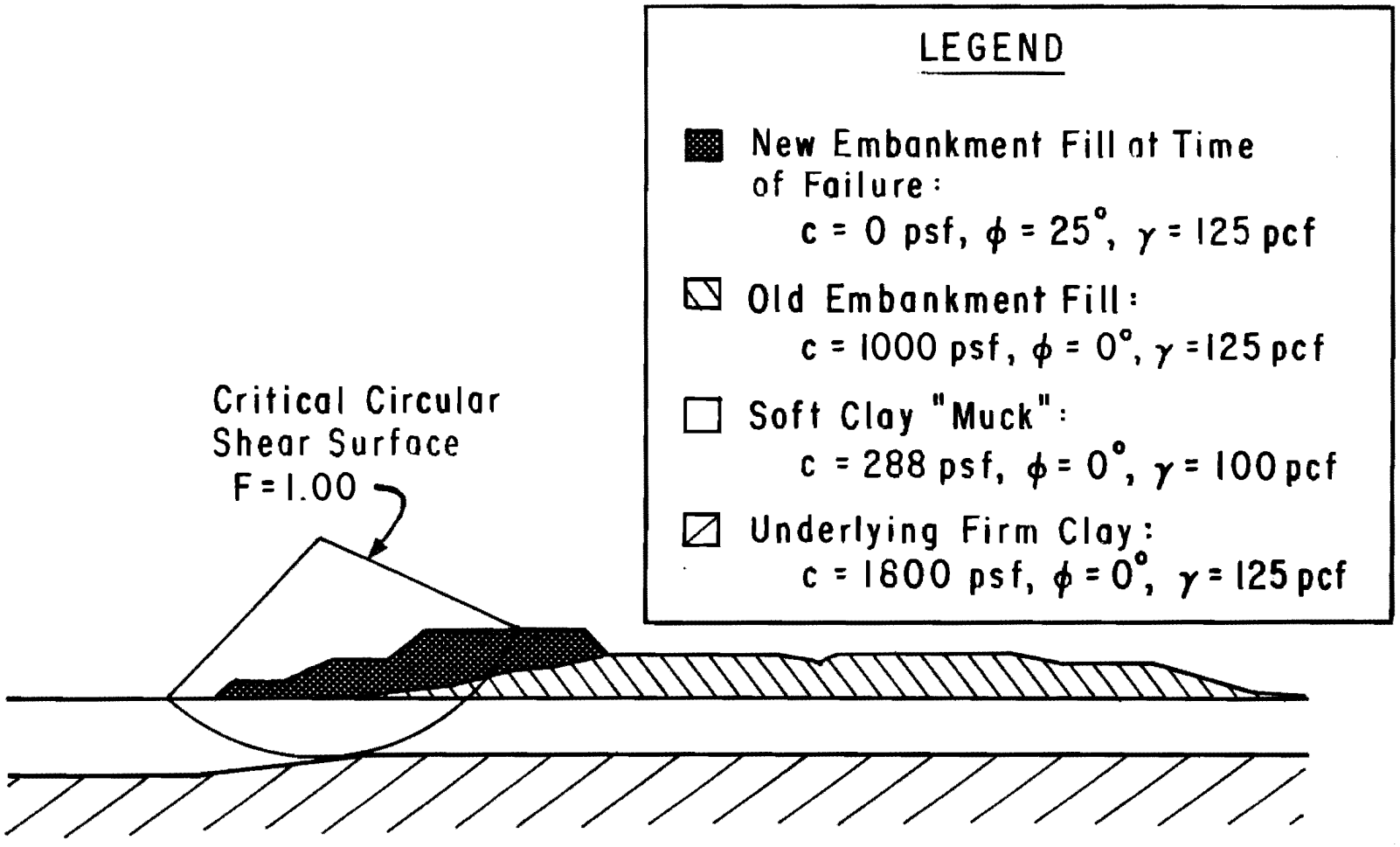

Fig. 7.6. Critical circle for Oso Bay embankment based on stability calculations for conditions at the time of failure with the new embankment characterized as a cohesionless (c = 0) material.

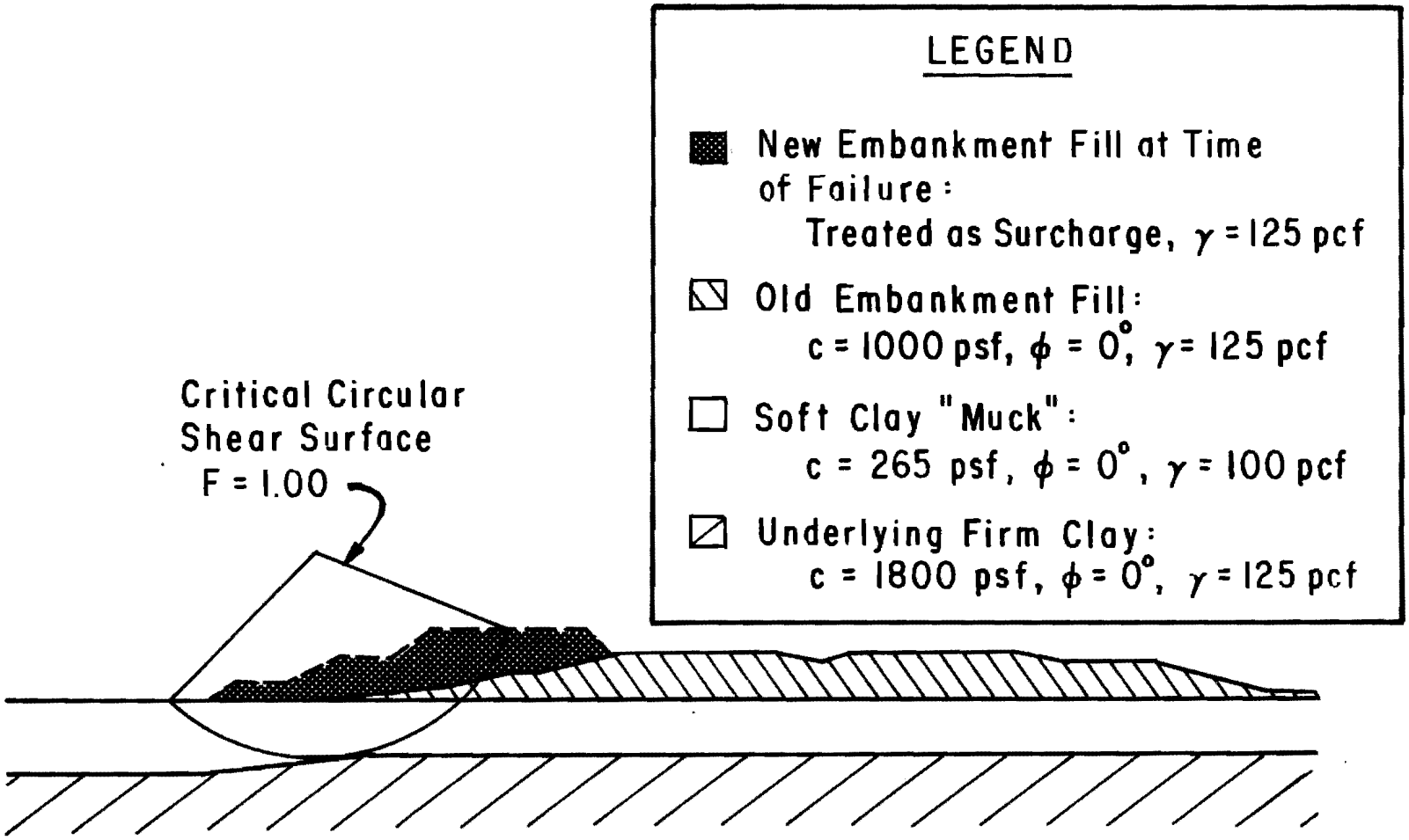

Fig. 7.7. Critical circle for Oso Bay embankment based on stability calculations for conditions at the time of failure with the new embankment characterized as a surcharge.

formed using the back-calculated values of the shear strength for the muck, as given above for each of the three embankment characterizations, to confirm the factor of safety of unity. A summary of the back-calculated shear strengths is presented in Table 7.2.

Based on the results of the stability calculations, the shear strength of the muck appears to be in the range of about 200 to 300 psf. The critical shear surfaces located for the second and third new embankment characterizations, as shown in Figs. 7.6 and 7.7, are similar and are closest to the position of the observed failure (the approximate location of the actual slide scarp is shown in Fig. 7.1). The critical circular shear surface for the first embankment characterization, as shown in Fig. 7.5, does not intersect the new embankment fill and does not resemble the observed failure surface. The shear strengths (288 and 265 psf) which were back-calculated using the second and third characterizations of the new embankment are in good agreement and compare well with the vane shear strenths measured in the field and summarized in Table 7.1. The shear strength (188 psf) which was back-calculated based on the first characterization of the new embankment fill is significantly lower and is near the low end of the range of the vane shear strengths measured in the field.

STABILITY CALCULATIONS FOR COMPLETED EMBANKMENT

Two sets of calculations were performed to evaluate the stabili-

TABLE 7.2. SUMMARY OF BACK-CALCULATED SHEAR STRENGTHS

New Embankment Fill	1st Characterization: c = 1500 psf , ϕ = 0 , γ = 125 pcf 2nd Characterization: c = 0 , ϕ = 25 degrees , γ = 125 pcf 3rd Characterization: Embankment treated as surcharge
Old Embankment Fill	c = 1000 psf ϕ = 0 γ = 125 pcf
Soft Clay "Muck" (Back-Calculated)	1st Characterization: c = 188 psf , ϕ = 0 , γ = 100 pcf 2nd Characterization: c = 288 psf , ϕ = 0 , γ = 100 pcf 3rd Characterization: c = 265 psf , ϕ = 0 , γ = 100 pcf
Underlying Firm Clay	c = 1800 psf ϕ = 0 γ = 125 pcf

ty of the completed embankment. The first set of calculations apply to a hypothetical case: the completed embankment as it would have been constructed had failure not occurred. The second set of calculations were performed using a slope geometry representing the completed embankment, including a preliminary design of the remedial measures (retaining walls and stone columns) which were employed. The material properties used in both sets of calculations were based on the characterization of the new embankment as a drained, cohesionless material and are summarized in Table 7.3.

Embankment with No Remedial Measures

The first set of stability calculations for the completed embankment were performed assuming that the embankment was constructed as originally planned, with the cross-section shown in Fig. 7.8. The slope geometry shown in Fig. 7.8 is the same as the design geometry shown by the broken line in Fig. 7.1. The critical circular shear surface which was located is shown in Fig. 7.9. The factor of safety corresponding to this surface is 0.94. This value of the factor of safety for the "completed" embankment without repair seems reasonable; the slope geometry of the "completed" embankment in the vicinity of the failure is not significantly different from the geometry of the embankment which existed when failure occurred. Hence, the minimum factor of safety for this case is near unity.

TABLE 7.3. SUMMARY OF MATERIAL PROPERTIES USED IN STABILITY CALCULATIONS FOR COMPLETED EMBANKMENT

New Embankment Fill	c = 0 ϕ = 25 degrees γ = 125 pcf
Old Embankment Fill	c = 1000 psf ϕ = 0 γ = 125 pcf
Soft Clay "Muck"	c = 288 psf ϕ = 0 γ = 100 pcf
Underlying Firm Clay	c = 1800 psf ϕ = 0 γ = 125 pcf
Stone Columns	c = 0 ϕ = 35 degrees γ = 134 pcf

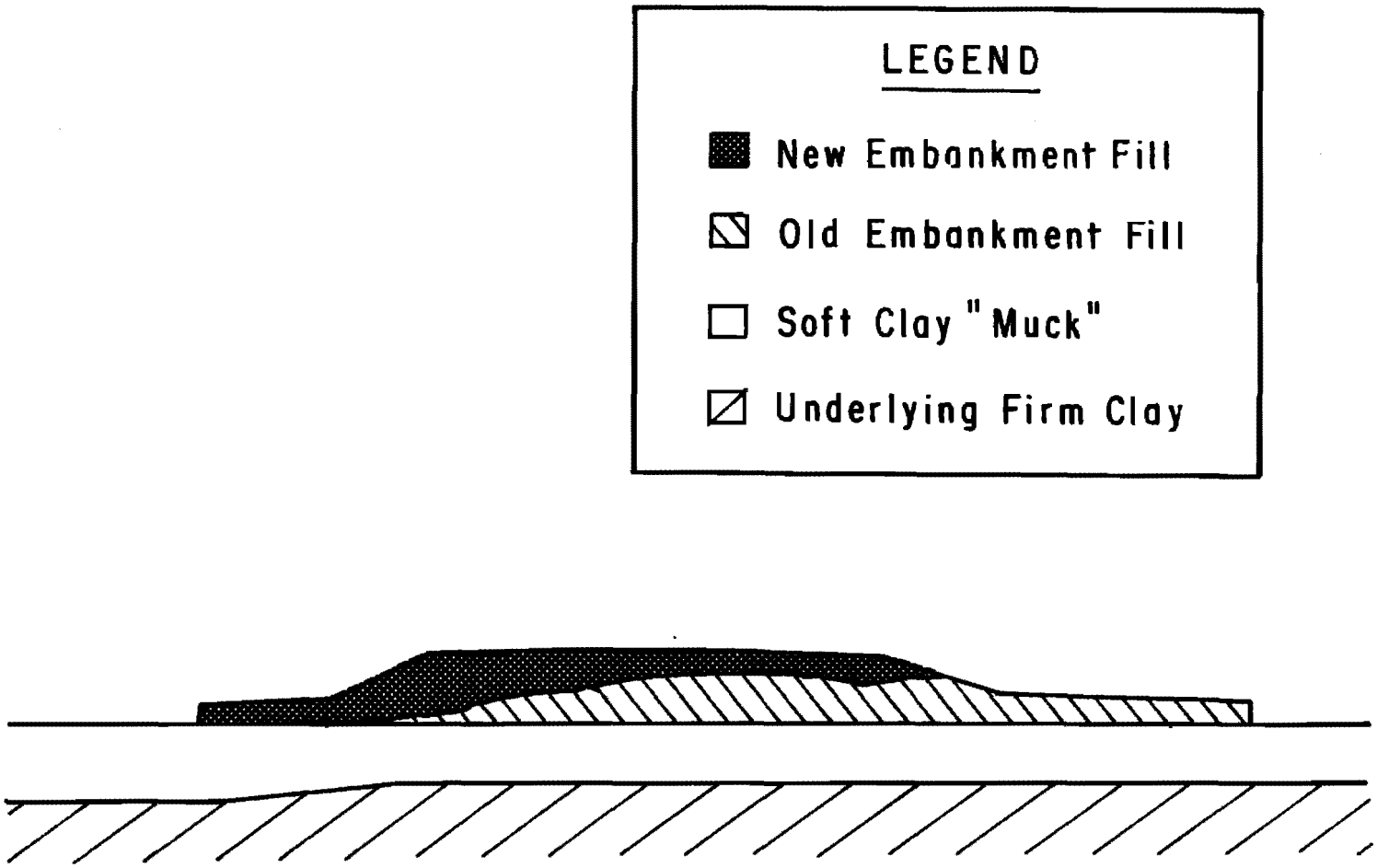

Fig. 7.8. Planned cross-section of completed Oso Bay embankment.

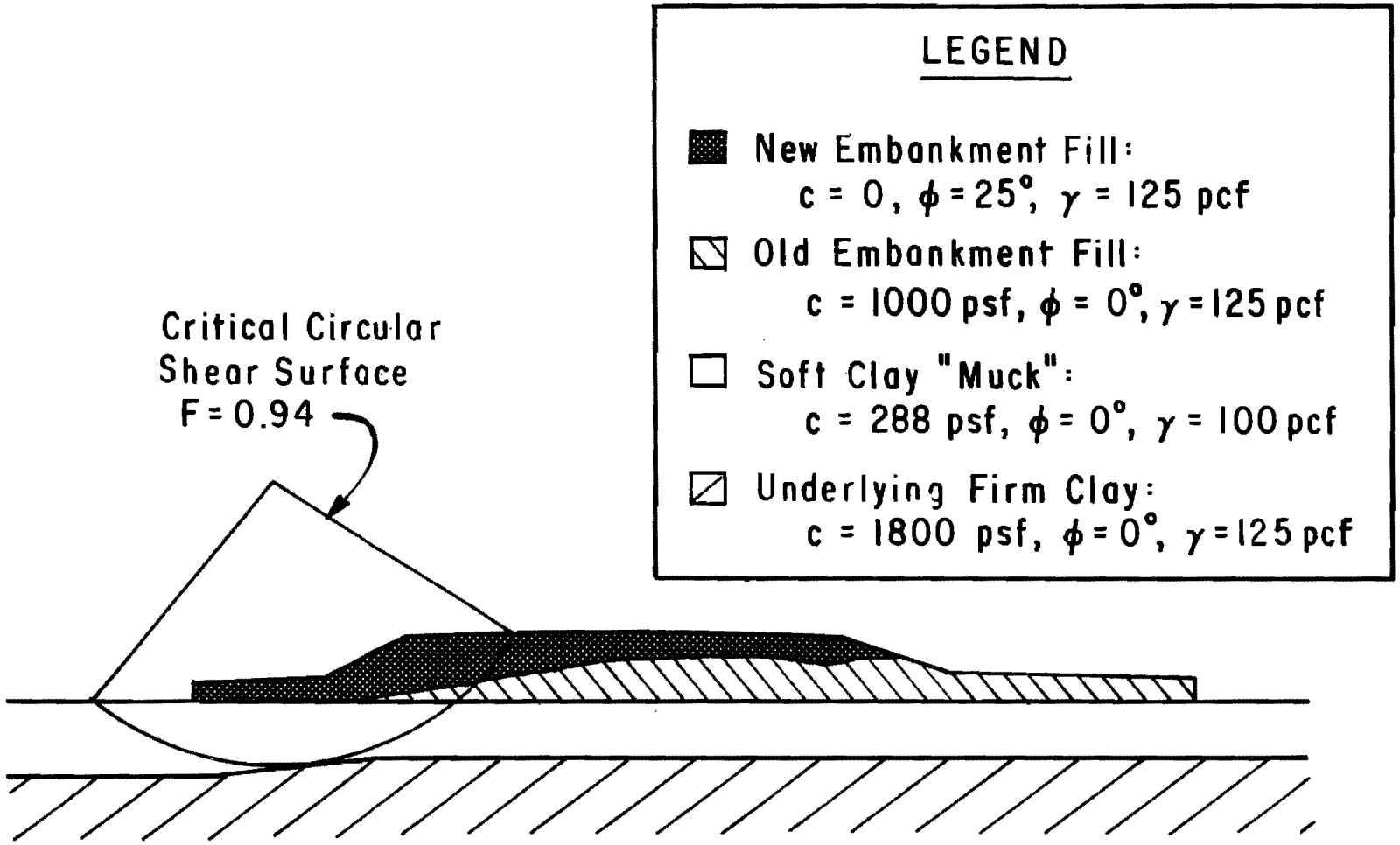

Fig. 7.9. Critical circle for Oso Bay embankment based on stability calculations for the original, planned cross-section.

Embankment with Remedial Measures

The embankment at the State Highway 358 crossing of Oso Bay was completed following the design and installation of remedial measures. The preliminary design for the repaired embankment at Station 160 + 00 is shown in cross-section on Fig. 7.10. A reinforced earth retaining wall was designed along the exterior of the frontage road on each side of the embankment. In addition, "stone columns" (Engelhardt, 1974) were to be installed. Preliminary plans for the locations of the stone columns included four rows of columns beneath the slope on the south side and two rows near the reinforced earth wall, also on the south side of the embankment, as shown in Fig. 7.10. These plans were later revised significantly for the final construction and many more stone columns were used. However, the final configuration of stone columns was not available at the time the stability calculations presented in this section were made. Thus, the computations are presented here primarily for illustrative purposes, rather than as representative of the final embankment design.

All stone columns were assumed to be 3 1/2 feet in diameter. The stone columns beneath the slope face were to be located in a triangular pattern spaced at 7 feet center-to-center, and the rows beneath the reinforced earth wall were to be located in a triangular pattern spaced at 9 feet center-to-center. For the purposes of stability calculations an "equivalent width" of the columns is calculated using the procedure described in the Appendix. For the columns spaced 7 feet center-to-cen-

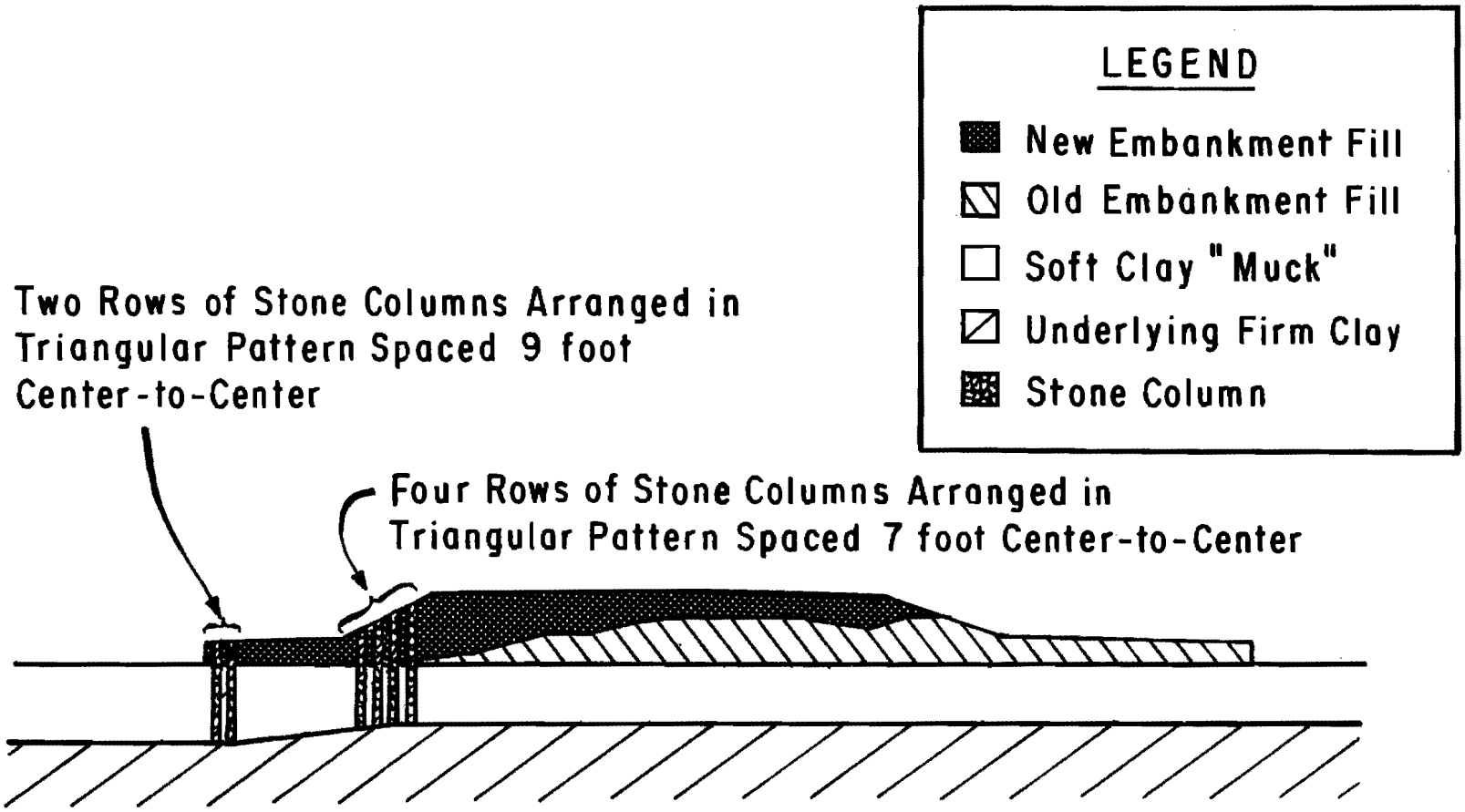

Fig. 7.10. Cross-section of Oso Bay embankment with the preliminary planned remedial measures evaluated in this study.

ter the equivalent width is 1.37 feet; for the columns spaced 9 feet center-to-center the equivalent width is 1.07 feet.

The stone columns were assumed to drain freely and, thus, "drained" shear strength parameters were used. The stone columns were assumed to be cohesionless (c = 0) and have an angle of internal friction of 35 degrees. A total unit weight of 134 pcf was assumed.

The stone columns should serve as drains and allow the muck to consolidate and become stronger with time. However, immediately after construction of the stone column, it seems reasonable to assume that no drainage will have occurred. Thus, the short term, undrained stability condition will exist and will represent the most critical condition. Since the increase in the muck strength is assumed to be minimal for short term conditions, the muck strength corresponding to the characterization of the new fill as a frictional material (c = 288 psf) was used in these computations.

The stability calculations for the "completed" embankment were made using the slope geometry and soil profile shown in Fig. 7.10. The critical circular shear surface located is shown in Fig. 7.11. The factor of safety corresponding to this surface is 1.29, which represents a 37 percent increase from the factor of safety calculated for the embankment without the stone columns (0.94), using the same material properties. While these calculations indicate that the embankment would be stable for the assumed drainage conditions, imperfections in instalation of the stone columns could lead to lower factors of safety. In addition,

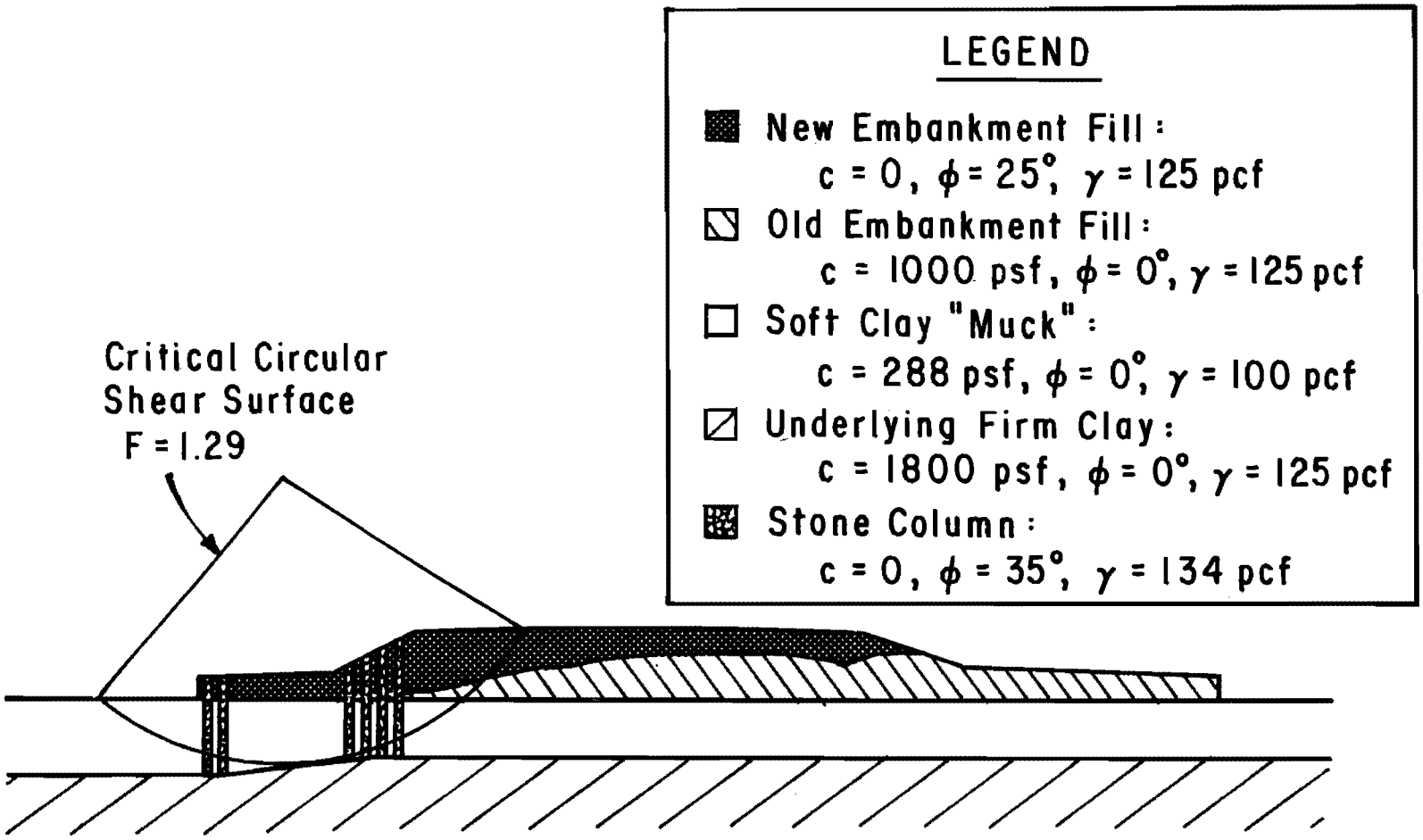

Fig. 7.11. Critical circle for Oso Bay embankment based on stability calculations with the preliminary planned remedial measures installed.

no consideration has been made for settlement, which could cause additional problems with time.

SUMMARY AND CONCLUSIONS

The embankment foundation failure on State Highway 358 where it crosses Oso Bay in Corpus Christi, Texas, provides a good example to illustrate how shear strengths may be back-calculated from an embankment foundation failure by performing a series of slope stability computations using computer programs like UTEXAS. This approach, although similar in concept, differs from the back-calculation procedures presented in Chapter Three for failures within the embankment slope itself.

Three different representations for the embankment fill material were used to back-calculate the shear strength of the soft clay foundation material. It was found that similar results were obtained when the fill was characterized as a frictional material, and when it was characterized as a surcharge with no shear strength. Both characterizations of the fill appeared to give reasonable locations of the critical shear surfaces, and the values of the shear strength back-caluclated for the soft clay foundation material agreed well with the shear strength values obtained from field vane tests. It appears that the embankment could be treated as a simple surcharge, thus lending support to the bearing capacity approaches described in Chapter Six.

The shear strength parameters back-calculated for the soft clay foundation material were used to compute the stability of the completed

embankment. The calculations were performed based on a preliminary design of the completed embankment which includes the use of stone columns as a remedial measure. The minimum factor of safety calculated for the completed embankment is 1.29, which is 37 percent greater than the factor of safety calculated for the completed embankment without stone columns. It therefore appears that the addition of a sufficient number of stone columns would adequately improve the stability of this embankment.

CHAPTER EIGHT. SUMMARY AND CONCLUSIONS

Three types of earth slope stability problems were examined in this study: 1) cut and natural slope failures, 2) embankment foundation failures, and 3) embankment slope failures. Only two failures in cut slopes were observed during this study, one in District 12, in the Houston area, and one in District 14, east of Austin. One slide was observed in a natural slope in District 17, southeast of Bryan, where the toe of the slope was being eroded by the Brazos River. Although several embankment foundation failures have occurred recently, only one such failure was examined herein. This failure occurred during the construction of an embankment in District 16 near Corpus Christi. Clearly the most significant slope problems examined in this study were those in the third category: embankment slope failures. Twenty-eight slides in embankment slopes were examined in this study. These embankments were located in Districts 12 (Houston area), 14 (east of Austin), 13 (Victoria area), and 1 (Paris). Embankment slope failures appear to be related to the gradual swelling of embankment soils and occur many years after construction.

EMBANKMENT FOUNDATION STABILITY

Three approaches were examined for computing the factor of safety for embankments on weak foundations. Two of the approaches make use of the general bearing capacity equations, while a third employs conventional slope stability analysis procedures. Two different definitions of the factor of safety were used with the bearing capacity equations, one based on load, the other based on shear strength; the factor of safety was always defined with respect to shear strength with the slope stability approach. The three different approaches were used in computations for various embankment and soil conditions. It was found that there are significant differences in the factors of safety depending on how it is defined and calculated. The approach based on slope stability procedures appears to be the most correct theoretically; however, the approaches based on bearing capacity equations are easier to use and appear to give conservative values for the factor of safety.

An embankment foundation failure at Oso Bay was examined and provided an excellent example of where shear strengths may be back-calculated from an embankment foundation failure by performing a series of computations using computer programs like UTEXAS. The shear strength which was back-calculated agreed with the shear strength measured in-situ although there was considerable scatter in the measured values. The shear strength parameters which were back-calculated were used to evaluate the stability of the completed embankment. It was found that

the remedial measures as given in a preliminary design of repairs should adequately improve the stability of the embankment.

EMBANKMENT SLOPE STABILITY

The embankment slope failures examined in this study reveal three common characteristics. First, the slides typically occur 15 to 25 years after construction, with failures tending to occur on the steeper slopes before they occur on flatter slopes. Second, the occurrence of embankment slides is not significantly related to embankment height; slides do not necessarily occur on the highest portion of the embankment, nor do they typically involve the full height of the slope. The third common characteristic observed for the embankment slope failures is that the failure surface is shallow and is generally restricted to the face of the slope.

Embankment slides were observed to occur on embankments ranging in height from about 10 to 39 feet, and on slopes ranging from about 2.1:1 to 3.4:1. The soils associated with the embankment slides are fine grained and are generally highly plastic clays. Atterberg limits were determined and showed that the "problem" soils at each site have plasticity indices ranging from 30 to 71 percent and liquid limits ranging from 42 to 97 percent.

A series of charts were developed which may be used to back-calculate shear strength parameters from embankment failures like those observed in this study. Charts were developed which may be used for

either "slope" or "face" failures, based on either total or effective stresses. Slope and slide geometry data measured for the embankment slides examined in this study were used to back-calculate effective stress shear strength parameters for each of the embankment slides. The pore water pressures were assumed to be zero for the purposes of back-calculating effective stress shear strength parameters. The friction angles, $\bar{\phi}$, which were back-calculated ranged from approximately 15 to 20 degrees, and the cohesion, $\bar{c}$, was generally less than 20 psf.

Two embankment slides were selected for more detailed investigation. Laboratory tests were performed by Gourlay and Wright (1984) to determine the effective stress shear strength parameters. For one embankment, located at IH 610 and Scott Street in District 12, the friction angles measured in the laboratory and back-calculated were found to be similar, 20.0 and 18.8 degrees, respectively, while the cohesion value measured in the laboratory (270 psf) is greater than the cohesion value which was back-calculated (8.2 psf). Stability calculations were made using both the shear strength parameters which were measured in the laboratory and the shear strength parameters which were back-calculated. Factors of safety calculated based on the shear strength measured in the laboratory were much greater than the value of unity which would be expected for a slope which has failied. For the embankment slide at IH 610 and Scott Street, the factor of safety calculated using the shear strength measured in the laboratory was approximately 2.4. Calculations made for a second embankment (located at the SH 225 and SH 146 Interchange in District 12) produced results similar to those described

above: factors of safety calculated using laboratory shear strengths were significantly greater than unity even though the slope failed.

The significant differences between the factors of safety calculated using shear strength parameters measured in the laboratory and the factors of safety which actually existed appear to result from the relatively high cohesion values measured in the laboratory. Laboratory values were several hundred psf while back-calculated cohesion values were generally less than 20 psf. Accordingly, it appears that the cohesion value which is developed by the soil over a long period of time is approaching zero and should be neglected for design.

RECOMMENDATIONS FOR FURTHER RESEARCH

The discrepancy between the factors of safety calculated using shear strengths measured in the laboratory and what has been observed in the field suggests that further research is needed to understand better the shear strength of the clays involved. Comparison of back-calculated shear strength parameters with those measured in the laboratory suggests that the "cohesion" component of shear strength is less in the field than in the laboratory and may decrease to zero with time. The possible factors contributing to the loss in "cohesion" with time warrant further attention and research. It appears that at least some of the loss in shear strength may be due to the effects of repeated wetting and drying and associated shrinkage and swelling of the soil at the shallow depths where slides occur. Until such time as the reasons for the apparently

lower strengths in the field can be established and the strengths can be predicted with appropriate laboratory tests, field evidence and experience will need to be relied upon heavily for design. Collection of the type of embankment slope data contained in this report should be continued.

None of the shear strength parameters back-calculated in this study have been correlated with regional climatic conditions, and the climatic conditions were often similar for many of the embankments investigated. However, it is likely that climate, and more specifically seasonal variations in moisture, will have a significant effect on the behavior of embankments constructed of the types of soils examined in this study. Accordingly, correlation of the performance of embankments constructed of highly plastic soils with climatic conditions is worthy of future examination.

APPENDIX

APPENDIX. CALCULATION OF EQUIVALENT WIDTH

Most slope stability calculations are performed for a two-dimensional, plane cross-section oriented in the transverse direction of the slope. In cases where piles, stone columns, or similar cylindrical elements exist in a row in the longitudinal direction of the slope, the cylindrical elements must be represented in the two-dimensional cross-section by an equivalent, continuous longitudinal strip. The equivalent width of the strip in the two-dimensional cross-section is selected to represent an amount of material (steel, concrete, or stone) which is equal to the actual amount of material in the slope. The derivation of an equivalent width is presented in this appendix.

A plan view representation of a row of stone columns is illustrated on the left hand side of Fig. A.1; the equivalent, continuous longitudinal strip used to represent the stone columns is illustrated on the right hand side of Fig. A.1. The equivalent width, w, of the strip is chosen such that the area of the strip is equal to the area of the stone columns which the strip represents. Thus, areas of the stone columns and equivalent strip are written and equated as

$$\pi\left(\frac{D}{2}\right)^2 = S \cdot \omega \qquad (A.1)$$

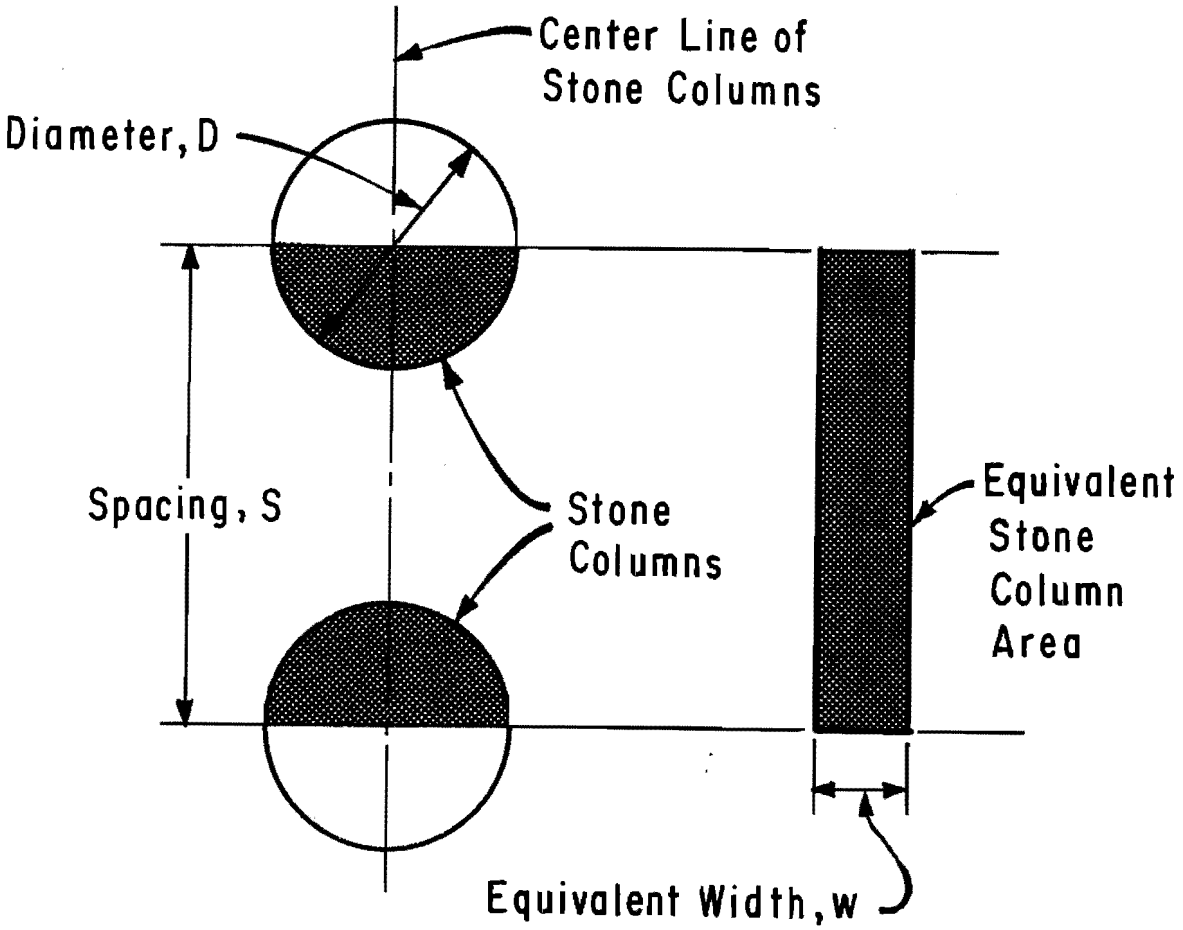

$$w = \frac{\pi (D/2)^2}{S}$$

Fig. A.1. Illustration of equivalent width used to represent cylindrical elements in two-dimensional slope stability calculations.

where D is the diameter of the stone columns and S is the center-to-center spacing between columns. Equation A.1 can then be rearranged to obtain the following expression for the equivalent width:

$$\omega = \frac{\pi(\frac{D}{2})^2}{S} \qquad (A.2)$$

BIBLIOGRAPHY

Abrams, T. G., and Stephen G. Wright (1972), "A Survey of Earth Slope Failures and Remedial Measures in Texas," Research Report No. 161-1, Center for Highway Research, The University of Texas at Austin, December, 97 pages.

ASTM (1982), 1982 Annual Book of ASTM Standards, Part 19, Natural Building Stones; Soil and Rock, Philadelphia, 710 pages.

Bishop, A. W., and Norbert Morgenstern (1960), "Stability Co-efficients for Earth Slopes," Geotechnique, The Institution of Civil Engineers, London, Vol. 10, No. 4, December, pp. 129-151.

The Bridge Division, Texas Highway Department (1972), "Foundation Exploration and Design Manual," Second Edition, pp. 5-29.

Bjerrum, Lauritis (1972), "Embankments on Soft Ground," Proceedings of the Specialty Conference on Performance of Earth and Earth-Supported Structures, Purdue University, Vol. II, June, pp. 1-54.

Doublewal (1982), Design Manual, Doublewal Interlocking Reinforced Concrete Retaining Wall Systems, Plainville, Connecticut, 51 pages.

Engelhardt, Klaus, William A. Flynn, and Albert A. Bayuk (1974), "Vibro-Replacement - A Method to Strengthen Cohesive Soils In Situ," Meeting Preprint 2281, ASCE National Structural Engineering Meeting, Cincinati, April.

Gale Research Company (1981), Weather of U.S. Cities, Detroit, Vol. 2, page 1017.

Gourlay, A. W., and Stephen G. Wright (1984), "Initial Laboratory Study of the Shear Strength Properties of Compacted, Highly Plastic Clays Used for Highway Embankment Construction in the Area of Houston, Texas," A Report on Laboratory Testing Performed Under Interagency Contract Nos. (82-83) 2187 and (84-85) 1026, Center for Transportation Research, The University of Texas at Austin, September (Preliminary Review Copy), 202 pages.

Hardin, George C. Jr. (1962), "Notes on Cenozoic Sedimentation in the Gulf Coast Geosyncline, U.S.A.," Geology of the Gulf Coast and Central Texas, Houston Geological Society, pp. 1-15.

Kanji, M. A. (1974), "The Relationship Between Drained Friction Angles and Atterberg Limits of Natural Soils," Geotechnique, The Institution of Civil Engineers, London, Vol. 24, No. 4, December, pp. 671-674.

Leroueil, S., F. Tavenas, C. Mieussens and M. Peignaud (1978), "Construction Pore Pressures in Clay Foundations Under Embankments. Part II: Generalized Behavior," Canadian Geotechnical Journal, Vol. 15, No. 1, February, pp. 66-82.

Maxwell, Ross A. (1970), "Geologic and Historic Guide to the State Parks of Texas," Guidebook 10, Bureau of Economic Geology, The University of Texas at Austin, pp. 3-12.

Meyerhof, G. G. (1951), "The Ultimate Bearing Capacity of Foundations," Geotechnique, The Institution of Civil Engineers, London, Vol. 2, No. 4, December, pp. 301-332.

Meyerhof, G. G. (1961), Discussion on Shallow Foundations, Proceedings, Fifth International Conference on Soil Mechanics and Foundation Engineering, Paris, Vol. III, July, pp. 193-194.

National Oceanic and Atmospheric Administration, Texas (1979 to 1982), "Climatological Data," Vols. 84 to 87.

Prandtl, L. (1920), "Uber die Harte plasticher Korper," Nachr. Kgl. Ges. Wiss. Gottingen, Math-Phys. Kl., pp. 74-85.

Skempton, A. W. (1953), "The Collodial Activity of Clays," Proceedings, Third International Conference on Soil Mechanics and Foundation Engineering, Switzerland, Vol. I, pp. 57-61.

Sowers, G. F. (1979), Introductory Soil Mechanics and Foundations: Geotechnical Engineering, Fourth Edition, MacMillan Publishing Co., Inc., New York, page 173.

Terzaghi, Karl, and Ralph B. Peck (1967), Soil Mechanics in Engineering Practice, Second Edition, John Wiley & Sons, page 347.

United States Department of Agriculture, Soil Conservation Service (1967), Soil Survey of Harris County, Texas.

Vijayvergiya, V. N. and Richard A. Sullivan (1973), "Simple Technique for Identifying Heave Potential," Proceedings of Workshop on Expansive Clays and Shales in Highway Design and Construction, Denver, Vol. I, pp. 275-294.

Widger, R. A., and D. G. Fredlund (1979), "Stability of Swelling Clay Embankments," Canadian Geotechnical Journal, Vol. 16, No. 1, February, pp. 140-151.

Wright, Stephen G., and James D. Roecker (1984a), "UTEXAS (University of Texas Analysis of Slopes) - A Computer Program for Slope Stability Calculations," Research Report No. 353-1, Center for Transportation Research, The University of Texas at Austin.

Wright, Stephen G., and James D. Roecker (1984b), "Example Problems for Slope Stability Computations with the Computer Program UTEXAS," Research Report No. 353-2, Center for Transportation Research, The University of Texas at Austin.

Wright, Stephen G. (1982), "Documentation for SSTAB1 - A General Computer Program for Slope Stability Analyses," Geotechnical Engineering Software GS82-1, Geotechnical Engineering Center, Bureau of Engineering Research, The University of Texas at Austin, November (Originally published as Report No. GE-74-1, August, 1974), 74 pages.